THE ORGANIC-COOLED SLOWPOKE REACTOR

Conceptual Design of an Organic-Cooled Small Nuclear Reactor to Support Energy Demands in Remote Locations in Northern Canada

LE RÉACTEUR SLOWPOKE REFROIDI PAR UNE SUBSTANCE ORGANIQUE

Design d'un Petit Réacteur Nucléaire à Caloporteur Organique pour Fournir de l'Énergie à des Endroits Éloignés du Grand Nord Canadien

A Thesis Submitted

To the Faculty of the Royal Military College of Canada

by

Colin Shannon
Lieutenant (Navy)

In Partial Fulfillment of the Requirement for the Degree of

Master of Applied Science in Nuclear Engineering

March 2018

Dedicated to Erica and Mason

ACKNOWLEDGEMENTS

First, I must acknowledge and thank my supervisors, Dr. Hugues W. Bonin and Dr. Paul K. Chan, for their tutelage and mentorship in the past two years. I would also like to thank LCdr Stéphane Paquette, Lt(N) Jason Song, and Dr. Mohamed Hussein for their support with WIMS-AECL and Lt(N) Brent Limbeek for his assistance with MCNP 6. Finally, special thanks are afforded to Dr. Tina Guenther for providing photographs of the RMCC SLOWPOKE-2.

ABSTRACT

Small nuclear reactors can offer safe, reliable, and long-lasting district heating and electrical power generation to remote locations in Northern Canada. A reactor, cooled and moderated by an organic fluid, based upon the 20 kW_{th} SLOWPOKE-2 research reactor is proposed for potential employment in Northern Canada. To achieve an uprated power of 1 MW_{th}, the conceptual design of the reactor proposes the organic coolant, HB-40, in place of the SLOWPOKE-2's light water coolant. To increase heat transfer across the reactor's core, the proposed design incorporates a coolant circulation pump below the reactor. Furthermore, the SLOWPOKE-2's dimensions are enlarged to house a greater mass of fuel and to provide a larger surface area for heat transfer. Despite these alterations, the reactor has maintained the simplicity of the SLOWPOKE-2 and early indicators suggest the design may be inherently safe. In its present state, the reactor is suitable for district heating of small installations. Operating together, multiple reactors may supply larger heat demands or even electrical power generation while providing added redundancy.

Presently, the conceptual design includes the reactor's core, annular reflector, and initial control system. At full power, the reactor's coolant circulates unpressurized at a flow rate of 7.63 kg s^{-1} from an inlet temperature of 290 ^{O}C to an outlet temperature of 340 ^{O}C. The reactor employs the same 19.89% enriched uranium dioxide as the SLOWPOKE-2 in similar, albeit longer, fuel pins. In the reactor's core, 660 fuel pins contain 8.610 kg of uranium-235 providing an approximate fuel service life of 11.5 years at full power. The annular reflector of the reactor is composed of beryllium like SLOWPOKE-2, but the annulus splits into 6 identical plates that move away from the core providing long-term regulating control. The reactor's control system is designed to provide both short-term and long-term regulating control in addition to containing sufficient negative reactivity to achieve shutdown under all circumstances. In addition to the aforementioned reflector plates, the control system is comprised of 25 hafnium control rods and 24 hafnium shutdown rods. An initial investigation of the reactor's reactivity coefficients has indicated strong potential for inherent safety due to strongly negative correlations between the reactivity and the fuel temperature, the moderator-coolant temperature, and the void fraction.

This conceptual design has been developed through simulation of the reactor's steady-state neutronics using two different computer codes. The first, Los Alamos National Laboratories' MCNP 6, employs a three-dimensional Monte Carlo-based probabilistic method to infer average particle behaviour from statistical analysis of many neutron histories. The second, Atomic Energy of Canada Limited's WIMS-AECL, numerically solves the neutron transport equations in two dimensions to determine the average particle behaviour. This initial design phase has yielded promising results that should be explored further with detailed thermal hydraulic modelling of the reactor as well as kinetic modelling of reactor in transient states. To fully achieve inherent safety in the reactor's design, a containment and shielding system are required to mitigate hazards due to escape of radiation and fission products.

RÉSUMÉ

Les petits réacteurs nucléaires peuvent fournir du chauffage urbain et de l'énergie électrique en co-génération pour des applications dans des régions éloignées du Nord du Canada. On propose un réacteur refroidi et modéré par une substance organique basé sur le concept du réacteur de recherche SLOWPOKE-2 de 20 kW_{th} pour une application potentielle dans le Nord du Canada. Afin d'obtenir une puissance de 1 MW_{th}, le design du réacteur propose l'utilisation d'un caloporteur organique, le HB-40, au lieu de l'eau ordinaire utilisée pour le réacteur SLOWPOKE-2. Dans le but d'augmenter le transfert de chaleur dans le cœur du réacteur, le design proposé inclut une pompe sous le réacteur assurant la circulation du caloporteur. De plus, les dimensions du réacteur SLOWPOKE-2 sont augmentées pour inclure une masse de combustible plus grande et pour fournir une plus grande surface pour le transfert de chaleur. Malgré tous ces changements, le réacteur conserve la simplicité du concept du SLOWPOKE-2 et les résultats calculés suggèrent que la sûreté inhérente est très possible. Dans son état présent, un réacteur peut à lui seul assurer le chauffage d'installations modestes. Cependant, un regroupement de plusieurs réacteurs semblables arrive à satisfaire de plus grandes demandes d'énergie thermique et électrique tout en assurant les bienfaits d'une redondance.

Présentement, le design inclut le cœur du réacteur, un réflecteur annulaire, et une ébauche de système de contrôle. À pleine puissance, le caloporteur du réacteur n'est pas pressurisé et circule à un débit de 7.63 kg s^{-1}, ayant des températures d'entrée et de sortie de 290 ^{O}C et de 340 ^{O}C, respectivement. Le réacteur utilise le même combustible que pour le réacteur SLOWPOKE-2, soit du bioxyde d'uranium enrichi à 19.89%, mais nécessite des crayons de combustible semblables, quoique plus longs. Le cœur du réacteur contient 660 crayons totalisant 8.610 kg d'uranium-235, ce qui assure une durée de vie utile du cœur d'environ 11.5 ans à pleine puissance. Le réflecteur annulaire du réacteur est composé de béryllium, tout comme pour le SLOWPOKE-2. Mais ici, ce réflecteur est constitué de six sections (plaques) identiques qui peuvent être positionnées plus loin du cœur du réacteur, ce qui assure un contrôle de la réactivité à long terme. Le système de contrôle du réacteur est conçu de façon à assurer la conduite du réacteur tant à court terme qu'à long terme, en plus de fournir une réactivité négative suffisante pour arrêter le réacteur dans toutes les circonstances. En plus des sections de réflecteur mentionnées ci-dessus, le système de contrôle comprend 25 barres de contrôle en hafnium et 24 barres d'arrêt aussi en hafnium. Une étude initiale visant à déterminer les coefficients de réactivité du réacteur a révélé un grand potentiel de sûreté inhérente provenant des fortes corrélations négatives entre la réactivité et la température du combustible, celle du modérateur-caloporteur et la fraction de vide.

Ce design a été réalisé par la simulation de la neutronique du réacteur en régime permanent à l'aide de deux logiciels d'ordinateur très différents. Le premier, le logiciel MCNP 6 des Laboratoires Nationaux de Los Alamos, est basé sur une méthode probabiliste dite de Monte Carlo, en trois dimensions, qui prédit le comportement moyen des particules au moyen d'une analyse statistique d'un grand nombre d'histoires de la "vie" des neutrons. Le second logiciel, WIMS-AECL d'Énergie Atomique du Canada, utilise une approche déterministe pour résoudre numériquement les équations de transport des neutrons en deux dimensions afin de déterminer en moyenne le comportement des neutrons. Cette phase initiale du design a résulté en des données très prometteuses qui devraient être étudiées davantage, à l'aide de la modélisation thermo-hydraulique du réacteur et de la simulation de la cinétique de celui-ci en régime transitoire. La sûreté inhérente du réacteur sera pleinement réalisée lorsque l'on fera le design d'un bâtiment de rétention et d'un système de blindage afin d'empêcher les rayonnements et les produits de fission de s'échapper.

Table of Contents

ABSTRACT iv
RÉSUMÉ v
List of Figures x
List of Tables xii
List of Acronyms xiii
CHAPTER 1: INTRODUCTION 1
1.0 Introductory Comments 1
1.1 The Small Modular Reactor (SMR) 1
1.2 The SLOWPOKE-2 Nuclear Research Reactor 2
1.3 The Organic Cooled and Moderated Reactor (OCR) 2
1.4 Research Goal 3
1.5 Design Constraints 3
1.5.1 Safety 3
1.5.2 Power 3
1.5.3 Coolant Selection 4
1.5.4 Reactivity Control 4
1.5.5 Fuel Enrichment 4
CHAPTER 2: LITERATURE REVIEW 5
2.1 State of the Art 5
2.1.1 The Organic Simplified Nuclear Reactor (OSNR) 5
2.1.2 The SLOWPOKE Energy System (SES) 7
2.2 Project Background 9
2.2.1 The Whiteshell Reactor 1 (WR-1) 9
2.2.2 Organic Coolants in WR-1 11
2.2.3 WR-1 Steady State Coolant Composition 11
2.2.4 HB-40 Decomposition Model in WR-1 12
2.2.5 Volatile Recycling in WR-1 13
2.2.6 Coolant Reprocessing in WR-1 13
2.2.7 Physical Properties of HB-40 15
2.2.8 Coking Control in WR-1 16
2.2.9 Research of Fouling in WR-1 16
2.3 Small Reactor Licensing in Canada 18

2.3.1 Graded Approach 18
2.3.2 Safety Analysis 18
2.3.3 Analyzed Events 18
CHAPTER 3: Design Approach 19
3.1 General Methodology 19
3.2 Preliminary Modelling 19
3.3 Core Design 19
3.4 Reflector Design 19
3.5 Control Strategy Design 20
CHAPTER 4: Theory 21
4.1 Introductory Comments 21
4.2 Neutron Diffusion Theory 21
4.3 Group Diffusion Method 21
4.4 Effective Multiplication Factor 22
4.5 The Four Factor Formula 22
4.6 Estimation of Reactor Critical Dimensions 23
4.7 Reactivity 23
4.8 Reactivity Coefficients 24
4.8.1 Temperature Coefficient of Reactivity 24
4.8.2 Void Fraction Coefficient of Reactivity 24
4.9 The Prompt Critical State 25
4.10 Fuel Burnup 25
4.11 Heat Transfer to Coolants 25
4.11.1 Thermal Resistance in Cylindrical Fuel Rods 26
4.11.2 Temperature Distributions Along Fuel Channel 27
4.12 Estimation of Organic Coolant Degradation 28
CHAPTER 5: DESIGN TOOLS 30
5.1 Introductory Comments 30
5.2 MCNP 6 30
5.2.1 The Monte Carlo Method 30
5.2.2 Error in the Monte Carlo Method 31
5.2.3 MCNP Nuclear Data Libraries 31
5.2.4 MCNP Input 31
5.2.5 MCNP Physics 32
5.3 WIMS-AECL 33

CHAPTER 6: PRELIMINARY MODELLING OF SLOWPOKE-2 34
6.1 Introductory Comments 34
6.2 MCNP 4A Model of the SLOWPOKE-2 34
6.3 Comparison of SLOWPOKE-2 Models in Excess Reactivity Calculation 38
6.4 Introducing Organic Coolant to SLOWPOKE-2 Model 39
6.5 Temperature and Void Fraction Coefficients of Reactivity for HB-40 Moderator 41
6.6 Lattice Pitch Trial for SLOWPOKE-2 with HB-40 Moderator 42
CHAPTER 7: OCSL REACTOR CORE DESIGN 44
7.1 Introductory Comments 44
7.2 Simplifications to the SLOWPOKE-2 Model and General Assumptions 44
7.3 Computation of OCSL Core Dimensions 45
7.4 Initial Thermal Hydraulic Estimation 46
7.5 Lattice Pitch Optimization 46
7.6 OCSL Reactor Core Vetting Process 48
7.7 OCSL Reactor Cores Simulated Using MCNP 49
7.8 Thermal Hydraulic Estimation of OCSL Reactor Cores 50
7.9 OCSL Reactor Cores Simulated Using WIMS 52
7.10 Burnup Analysis for OCSL Reactor Cores 54
7.11 Reactivity Coefficients for OCSL Reactor Cores 57
7.12 Summary of OCSL Reactor Core Parameters 59
CHAPTER 8: OCSL REACTOR REFLECTOR DESIGN 61
8.1 Introductory Comments 61
8.2 Reflector Material Selection 61
8.3 Effective Thickness of Reflector Materials 62
8.4 Burnup Calculations of OCSL Reactor with Various Reflectors 64
8.5 Reactivity Coefficients for Beryllium Reflected OCSL Reactor 64
8.6 Flux Distributions for the Reflected and Non-Reflected OCSL Reactor 67
8.7 OCSL Reflector with Variable Positions 70
CHAPTER 9: OCSL REACTOR CONTROL STRATEGY 72
9.1 Introductory Comments 72
9.2 The OCSL Reactor Control System 72
9.3 Absorber Rod Material Selection 73
9.4 Absorber Rod Dimensions 75
9.5 Numbering of Multiple Control Rods 76
9.6 Position and Orientation of Control Rod Clusters 78

9.7 Absorber Rod Arrangement for the OCSL Reactor 80
9.8 The Water-Gap Effect in the OCSL Reactor 84
9.9 Finalization of OCSL Reactor Absorber Rod Arrangement 86
9.10 Flux Distributions 87
9.11 Re-evaluation of OCSL Reactor Thermal Hydraulic Parameters 90
9.12 Re-evaluation of OCSL Reactor Burnup and Reactivity Coefficients 91
9.13 OCSL Reactor Start-Up Configuration 94
9.14 OCSL Reactor Start-up 97
9.15 Control Rod Sensitivity 98
9.16 Burnup Control Strategy 102
CHAPTER 10: SUMMARY AND DISCUSSION 104
10.1 General 104
10.2 Final OCSL Reactor Model (MCNP) 104
10.3 OCSL Reactor Operation 106
10.4 From SLOWPOKE-2 to OCSL 107
10.5 Organic Coolant Performance in OCSL Reactor 108
10.6 Control and Monitoring of OCSL Reactor 110
10.7 Inherent Safety in OCSL Reactor Design 111
10.8 Validity of Results 111
10.8.1 Limitations and Error of MCNP Results 112
10.8.2 Limitations and Error of WIMS Results 113
CHAPTER 11: CONCLUSION AND RECOMMENDATIONS 114
11.1 Conclusion: The OCSL Reactor 114
11.2 Recommendations for Future Design Work 115
References 117
APPENDIX A: SAMPLE MCNP 6 CODE INPUT AND OUTPUT ..... A- 1
APPENDIX B: SAMPLE WIMS-AECL CODE INPUT AND OUTPUT ..... B- 1
APPENDIX C: MATLAB® SCRIPTS ..... C- 1

List of Figures

Figure 1: Quarter Symmetric Diagrams of PWR (Left) and OSNR (Right)[14] 5
Figure 2: Outline of OSNR Plant[15] 7
Figure 3: Schematic Diagram of SES[21] 8
Figure 4: Diagram of WR-1[28] 10
Figure 5: Derivation of Terphenyl Coolants[31] 12
Figure 6: Ideal Degassing System[42] 14
Figure 7: Carbon to Hydrogen Ratio of HB-40 Coolants[49] 17
Figure 8: Monte Carlo Method Applied to an Incident Neutron[84] 30
Figure 9: Cross-section of SLOWPOKE-2[99] 35
Figure 10: SLOWPOKE-2 Fuel Layout 35
Figure 11: Control Rod Side-profile Section-cut 36
Figure 12: Side-profile Section-cut with Irradiation Sites 37
Figure 13: Critical SLOWPOKE-2 Core with HB-40 40
Figure 14: Variation of Reactivity with Moderator Temperature 41
Figure 15: Variation of Reactivity with Void Fraction 41
Figure 16: Plot of Lattice Pitch Trial 42
Figure 17: 258 Pin SLOWPOKE-2 Core with 1.25cm Lattice 42
Figure 18: Response of Effective Multiplication Factor to Increased Lattice Pitch 47
Figure 19: Iterative Process for Lattice Pitch Optimization 47
Figure 20: Temperature Distribution for Core Design 1 52
Figure 21: WIMS Concentric Arrays Applied to Original MCNP Lattice 53
Figure 22: Plotted Burnup for Cores of Minimum Cylindrical Volume 56
Figure 23: Plotted Burnup for Cores with 0.500m Length 56
Figure 24: Plotted Burnup for Cores with 0.550m Length 57
Figure 25: Variation of Excess Reactivity with Moderator Temperature for Potential OCSL Reactor Cores 58
Figure 26: Variation of Excess Reactivity with Void Fraction for Potential OCSL Reactor Cores 58
Figure 27: Cross Section View of OCSL Reactor Core 59
Figure 28: Estimated Temperature Distribution Along Fuel Channel in OCSL Reactor Core 60
Figure 29: Variation of Effective Multiplication Factor with Reflector Thickness for Potential Materials 63
Figure 30: Variation of Effective Multiplication Factor with Time for Various Reflector Options 64
Figure 31: Variation of Excess Reactivity with Moderator Temperature for Beryllium Reflected OCSL Reactor 65
Figure 32: Variation of Excess Reactivity with Void Fraction for Beryllium Reflected OCSL Reactor ... 66
Figure 33: Variation of Excess Reactivity with Fuel Temperature for Beryllium Reflected OCSL Reactor 66
Figure 34: Azimuthal Direction of Radial Neutron Flux Distribution 68
Figure 35: Two-Group Flux Distribution for OCSL Reactor Core Surrounded by HB-40 69
Figure 36: Two-Group Flux Distribution for OCSL Reactor with Beryllium Reflector 69
Figure 37: Comparison of Thermal Neutron Flux Distributions in OCSL Reactor with and without Beryllium Reflector 70
Figure 38: Various Subdivisions of the OCSL Reflector 71
Figure 39: Variation of Excess Reactivity with Displacement of Reflector Plates 71
Figure 40: Control Rods and Shutdown Rods in OCSL Reactor 73

Figure 41: Plot of Absorber Rod Dimensioning Trial 75
Figure 42: Control Rod Numbering 77
Figure 43: Effect of Central Control Rod on Radial Neutron Flux Distribution[112] 78
Figure 44: Variation of Effective Multiplication Factor with Control Rod Spacing 79
Figure 45 Control Rod Arrangement with 7b Outer Cluster 80
Figure 46: Control Rod Arrangement with 7a Outer Cluster 80
Figure 47: Absorber Rod Arrangement with Six Enlarged Shutdown Rods 83
Figure 48: Thermal Neutron Flux Comparison for OCSL Reactor with and without Absorber Rod Tubes 85
Figure 49: Final Absorber Rod Arrangement 87
Figure 50: Comparison of OCSL Normalized Flux Distributions with Baseline 88
Figure 51: Normalized Neutron Flux Distributions for OCSL Reactor with all Absorber Rods Inserted 89
Figure 52: Normalized Thermal Flux Distributions for OCSL Reactor with Absorber Rods Withdrawn and Inserted 89
Figure 53: Estimated Temperature Distributions Along OCSL Reactor Fuel Channel 91
Figure 54: Variation of Effective Multiplication Factor with Time for Baseline OCSL and OCSL Reactors 92
Figure 55: Variation of Excess Reactivity with Moderator Temperature for Baseline OCSL and OCSL Reactors 93
Figure 56: Variation of Excess Reactivity with Void Fraction for Baseline OCSL and OCSL Reactors 93
Figure 57: Variation of Excess Reactivity with Fuel Temperature for Baseline OCSL and OCSL Reactors 94
Figure 58: Withdrawing Reflector Plates from OCSL Core for Various Absorber Rod Combinations 95
Figure 59: Variation of Excess Reactivity with Reflector Position for OCSL Reactor with Central Control Rod and Cluster 11a Withdrawn 96
Figure 60: Variation of Effective Multiplication Factor with Control Rod Insertion at Start-up 97
Figure 61: OCSL Reactor Thermal Flux Distribution at Start-up 98
Figure 62: Variation of Effective Multiplication Factor with Insertion of Central Control Rod 99
Figure 63: Variation of Effective Multiplication Factor with Insertion of Cluster "5a" 100
Figure 64: Variation of Effective Multiplication Factor with Insertion of Cluster "7b" 100
Figure 65: Variation of Effective Multiplication Factor with Insertion of Cluster "10b" 101
Figure 66: Variation of Effective Multiplication Factor with Insertion of Cluster "11a" 101
Figure 67: Side Profile Section-Cut of OCSL Reactor 105
Figure 68: Cross-Sectional View of OCSL Reactor 105

List of Tables

Table 1: Comparison of Select SLOWPOKE-2 and SLOWPOKE Demonstration Reactor Specifications[2223] 9
Table 2: HB-40 Decomposition Product Classification[35] 12
Table 3: Specifications of Fuel in MCNP 4A Model[99] 35
Table 4: Comparison of SLOWPOKE-2 Models with Commissioning Data 38
Table 5: Calculation of Absorption and Scattering Cross Sections for Light Water and HB-40[101 102] 39
Table 6: Addition of Fuel to SLOWPOKE-2 Core with HB-40 40
Table 7: Lattice Pitch Trial Results – 258 Pin SLOWPOKE-2 Core 42
Table 8: Potential OCSL Reactor Cores Simulated with MCNP 6 49
Table 9: Thermal Hydraulic Estimation for OCSL Reactor Cores 51
Table 10: Comparison of MCNP and WIMS Geometries 53
Table 11: Potential OCSL Reactor Cores Simulated with WIMS 54
Table 12: Burnup Analysis for Potential OCSL Reactor Cores Using WIMS 55
Table 13: Average Reactivity Coefficients for Potential OCSL Reactor Cores 59
Table 14: General Description of OCSL Reactor Core 60
Table 15: Comparison of Reflector Material[101] 62
Table 16: Comparison of Potential OCSL Reactor Reflectors 63
Table 17: Summary of OCSL Reactor Control System 73
Table 18: Control Material [111] 74
Table 19: Absorber Rod Dimensioning Trial 76
Table 20: Trial of Various Control Rod Spacings 79
Table 21: First Round of Absorber Rod Arrangements 81
Table 22: Second Round of Absorber Rod Arrangements with Shutdown Rods Added 82
Table 23: Third Round of Absorber Rod Arrangements with Some Shutdown Rods Enlarged 83
Table 24: Water-Gap Effect Comparison for OCSL Reactor Materials [101 111] 84
Table 25: Progression of OCSL Reactor Absorber Rod Arrangements 86
Table 26: Comparative Summary of OCSL Reactor's Thermal Hydraulic Parameters 90
Table 27: Sensitivities of OCSL Reactor Control Rods 102
Table 28: Estimation of Calibrated Reflector Plate Positions 103
Table 29: Summary of OCSL Reactor Specifications 106
Table 30: Full Power Operation of OCSL Reactor 106
Table 31: Comparison of SLOWPOKE-2 and OCSL Reactors 107

List of Acronyms

AECL	Atomic Energy Canada Limited
CNSC	Canadian Nuclear Safety Commission
ÉACL	Énergie atomique du Canada limitée
HB	High Boiler
HEU	High Enriched Uranium
LEU	Low Enriched Uranium
LWR	Light Water Reactor
MCNP	Monte Carlo N-Particle Transport Version 6
OCR	Organic Cooled Reactor
OCSL	Organic-Cooled SLOWPOKE
OSNR	Organic Simplified Nuclear Reactor
PWR	Pressurized Water Reactor
RMC, RMCC	Royal Military College of Canada
SES	SLOWPOKE Energy System
SLOWPOKE-2	Safe Low Power Critical (K) Experiment 2
SMR	Small Modular Reactor
WR-1	Whiteshell Reactor 1

CHAPTER 1: INTRODUCTION

1.0 Introductory Comments

The concept and application of nuclear power are a subject that has been heavily investigated upon since the beginning of the nuclear age in the mid-twentieth Century. Specifically, electrical power generation and district heating using nuclear power have become integral to the modern world's energy industry. Subsequent developments have routinely sought to improve upon characteristics such as energy density, reliability, and safety. Recently, efforts to combat climate change have enhanced the relevance of nuclear power due to its minimal greenhouse gas emissions and sufficient energy density to compensate for the reduction in fossil fuel-based energy[1].

Regarding Canada and the Canadian Armed Forces, ensuring the Canadian sovereignty of the Arctic has become a priority in the early decades of the twenty-first century as diminished ice coverage make shipping routes in the region more accessible[2]. To this end, the infrastructure of Canada's Arctic, specifically energy, is a critical component. The remoteness of Canadian settlements in the Arctic poses a demand for safe, reliable, and self-contained electrical power generation and district heating. Currently, there are nearly 150 off-grid communities in Northern Canada that rely entirely on diesel-fuel generators for electrical power generation. This number approaches 200 when off-grid communities partially relying on diesel-fuel generators are included[3]. Cumulatively, these communities represent around 100,000 Canadians relying on exceptionally costly fossil-fuel based energy[3]. High electricity prices are largely tied to logistical difficulty in delivering the fuel to communities with limited accessibility by land and air[3]. Emerging technology in the field of small modular nuclear reactors potentially presents an alternative to costly diesel-fuel generators.

Located at the Royal Military College of Canada in Kingston, Ontario, a 20kW SLOWPOKE-2 research reactor has been operated for over thirty years. Although its output power is low in its current design, the SLOWPOKE-2 is a good example of a self-contained, reliable, and inherently safe reactor design. A reactor based on the SLOWPOKE-2 that manages to extend output power, while maintaining inherent safety, could potentially supply electrical power and district heating to remote locations. Among various uses, such a reactor could satisfy certain Canadian interests in the Arctic.

This research aims to increase the output power through the replacement of light water coolant with an organic coolant.

1.1 The Small Modular Reactor (SMR)

The concept of small modular reactors (SMRs) has gained traction in the Post-Fukushima nuclear industry[4]. In general, reactor designs of this type satisfy two definitions. First, a "small" reactor denotes a design that delivers less than 300 MW(e) equivalent electrical power. Second, the term "modular" describes the intent for the reactor to be operated within a group of reactors to meet a larger power demand[4]. Much like any nuclear reactor, the SMR concepts fall into a variety of categories such as light water reactors and molten salt reactors[4]. Among the wide array of SMR concepts, designs that feature organic liquids as coolants and/or moderators are comparatively rare[5].

1.2 The SLOWPOKE-2 Nuclear Research Reactor

The acronym "SLOWPOKE" stands for Safe Low Power Critical (K) Experiment and the number 2 indicates the improved version beyond the SLOWPOKE-1. A low enrichment uranium (LEU) fuel variant was developed in the early 1980s as an alternative to the original highly enriched uranium (HEU) fuel version. The reactor was designed by Atomic Energy of Canada Limited (AECL). Employed as a research reactor, the SLOWPOKE-2 produces 20 kW(th) and operates as a neutron source for purposes such as activation analysis and isotope production[6]. The reactor is housed in a light water filled pool that measures 6.1 m deep with a diameter of 2.5 m.

Several factors support the SLOWPOKE-2's suitability as a baseline for reactor design in this thesis. First, the SLOWPOKE was designed with simplicity of operation thoroughly incorporated[6]. Preserving this characteristic in the proposed reactor design would be integral to installation in remote locations with little existing infrastructure. Second, the use of LEU circumvents any proliferation-related concerns for the proposed reactor's fuel, because the fresh fuel enrichment is below the 20% value accepted internationally as the maximum enrichment respecting the Non-Proliferation Treaty. Finally, one of the most important characteristics of the SLOWPOKE-2 that will be maintained in the proposed reactor is that of inherent safety. The International Atomic Energy Agency defines inherent safety as[7]:

"Inherent safety refers to the achievement of safety through the elimination or exclusion of inherent hazards through the fundamental conceptual design choices made for the nuclear plant. Potential inherent hazards in a nuclear power plant include radioactive fission products and their associated decay heat, excess reactivity and its associated potential for power excursions, and energy releases due to high temperatures, high pressures and energetic chemical reactions."

In the case of the SLOWPOKE-2, its inherent safety permits licensing in Canada for unattended operation in automatic control and without automatic active shutdown devices[6]. For operation in the remote Arctic, inherent safety is essential to a reactor's design to ensure that staffing of operators is achievable. Conversely, a reactor design that is not inherently safe would face difficulty staffing highly-trained personnel in the remote locations.

1.3 The Organic Cooled and Moderated Reactor (OCR)

An organic cooled and moderated reactor (OCR) is a nuclear reactor employing an organic liquid as a coolant and moderator[5]. Like other iterations on light water reactor technology, OCRs seek to deliver higher thermal efficiency through increased operating temperatures[5]. In concept, this is accomplished naturally through organic liquids' generally higher boiling temperatures relative to light water. In the mid-Twentieth Century, several countries developed OCR designs for electrical power generation. The experiences of these reactors demonstrated a general trend of operational simplicity that suggested the OCR concept would be an appropriate fit for electrical power generating SMRs[5].

The OCR concept presents several advantages in comparison to other reactor types. Due to the low vapour pressures of the organic coolants, OCRs are capable of operation at higher temperatures without pressurization. This characteristic permits the use of lighter components while maintaining a low risk of loss of coolant accidents[5]. Furthermore, pressure vessels carry the added complexity of periodic inspections. In remote locations, the logistics of arranging these inspections would make them costly and hard to implement. Organic coolants also possess much lower corrosion potential than light water[5]. In fact, organic coolants are generally incapable of chemical reaction with the fuel. This broadens the range of possible fuels for OCRs to include high density metals and uranium carbide[8]. Concerning personnel safety, organic coolants are known to produce less activity in the primary heat transport systems than light

or heavy water. In historical cases, this permitted licensing for personnel to access more equipment during operation and ultimately enhanced maintenance efficiency[8]. Aside from these advantages, an OCR is also faced with certain disadvantages related to the organic coolant. Due to abundant hydrogen in the coolant compounds, high neutron absorption in the coolant may negatively influence the neutron economy of an OCR design[8]. Regarding thermal hydraulics, the heat transfer properties of organic coolants are poor relative to water. Thus, greater surface areas are required in heat exchangers to compensate for the deficiency[8]. Organic coolants are susceptible to degradation caused by both high temperatures and radiation. In some cases, induced polymerization of the coolant may impede its flow in the reactor and contaminate surfaces with film build-up. Volatile organic compounds also produced by coolant degradation must be dealt with to maintain safe operation of the reactor[5]. Many potential organic coolants are both toxic and flammable to some degree thus adding to safety aspects that must be addressed in an OCR design[5].

1.4 Research Goal

The primary objective of this thesis research is to design an organically cooled and moderated reactor core based upon the present SLOWPOKE-2 research reactor that extends power to support district heating and possibly electrical power generation in remote northern locations. The inherent safety characteristics of the SLOWPOKE-2 reactor must be preserved in the new reactor. Ultimately, a singular reactor or preferably, a modular group of reactors will be capable of supplying energy to Canadian Armed Forces installations, small communities, and mining operations in Northern Canada. A modular group of reactors would provide redundancy to the energy system, precluding the complete loss of energy production during the planned and unplanned shutdowns of the reactors within the group. The core will be designed and simulated using the probabilistic code MCNP 6 and the deterministic code WIMS-AECL 3.1.

1.5 Design Constraints

In this research, the organically cooled and moderated reactor must maintain the simplicity and safety of the SLOWPOKE-2 while conforming to constraints on power, coolant, reactivity control, and fuel enrichment.

1.5.1 Safety

As previously defined in Section 1.2, the reactor design must demonstrate inherent safety to meet the objective of this thesis. This characteristic is necessary for the reactor to be licensed for automatic unattended operation with limited trained personnel local to the plant. These personnel could be kept in contact with support personnel located in Southern Canada by means of a satellite communication system. For this operational scheme to be acceptable to regulatory bodies and the public, the risk of catastrophic failure due to a prompt criticality excursion must be minimized, if not completely eliminated.

1.5.2 Power

Beginning with the SLOWPOKE-2's present output of 20 kW(th), the new reactor design must extend the thermal power output to the order of 1 MW(th) to be viable for its intended use. At such an output, a realistic number of these reactors could be operated together to meet certain power demands in Northern Canada. This would present an appealing alternative to diesel-fuel generators when the reactors' simplicity of operation and reliability are weighed against the costs of transporting diesel fuel to remote locations.

1.5.3 Coolant Selection

As a starting point, HB-40 will be used as the organic coolant in the reactor design because of its proven performance in the Whiteshell Reactor 1. However, this research must eventually explore potentially suitable new coolants that have been produced in the decades since research concluded with the WR-1 reactor. To be selected for the design, a coolant must be capable of safe and stable operation at the temperatures required to sufficiently extend the reactor's power. Equally important, the selected coolant must ensure a favourable neutron economy for the reactor. The coolant's boiling temperature must exceed the required temperature to negate the need for pressurized cooling. Considering the reactor's operation in northern climates, a secondary concern will be the cloud point of the coolant because of its effects on flow and storage.

1.5.4 Reactivity Control

Within the scope of this research, reactivity in the reactor will be controlled through simple means including a central control rod and two or more control rods located in the radial reflector.

1.5.5 Fuel Enrichment

Just as in the present SLOWPOKE-2, the reactor design will utilize 20% enriched UO_2 fuel. This low maximum fuel enrichment will circumvent any issues related to compliance with the Non-Proliferation Treaty[9].

CHAPTER 2: LITERATURE REVIEW

2.1 State of the Art

As mentioned in Section 1.1, modern SMR designs featuring organic coolants are relatively rare in comparison to other concepts such as light water reactors and molten salt reactors. Consequently, a review of relevant contemporary research identified only one reactor design comparable to the concept proposed by this research; the Organic Simplified Nuclear Reactor. Outside of related OCR designs, the SLOWPOKE Energy System is a relevant reactor design that extends the SLOWPOKE-2's power to supply district heating. While similar in objective to this research, the SLOWPOKE Energy System differs by maintaining a light water coolant selection.

2.1.1 The Organic Simplified Nuclear Reactor (OSNR)

Conceived as a source for offshore underwater electrical power generation, the OSNR is a safe and simple SMR design developed by the Massachusetts Institute of Technology[10]. The OSNR utilizes organic fluid for cooling and moderation while additional moderation is provided by zirconium hydride and graphite[10]. This conceptual plant design far exceeds the power of the OCR in this research producing 500 MW(th)[11]. Presently, deployment of the OSNR would be anticipated in roughly fifteen to twenty years[12]. Similar to this research, the reactor physics analyses of the OSNR applied a dual approach with probabilistic and deterministic codes[13].

As shown in Figure 1, the OSNR core is an adaptation of a pressurized water reactor (PWR) core. The output of the original PWR was rated at 500 MW(th)[11]. Therefore, power extension was not an objective of this work. Regarding the diagram coloring, blue represents water, black represents fuel, green represents the organic coolant, red represents zirconium-hydride, and yellow represents graphite.

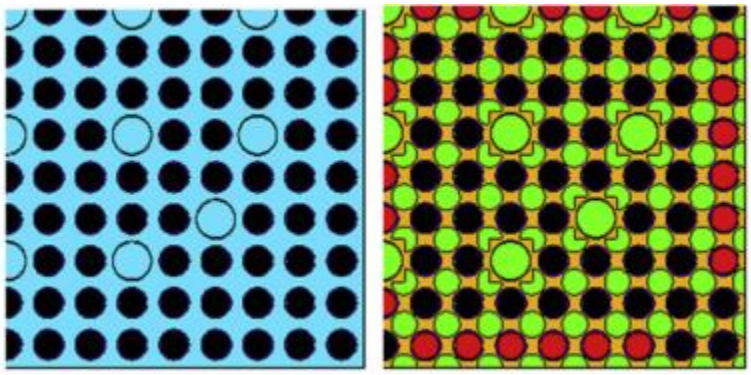

Figure 1: Quarter Symmetric Diagrams of PWR (Left) and OSNR (Right)[14]

While the OSNR differs significantly from the proposed reactor in this research, the methodology of adapting an existing reactor to employ an organic coolant is particularly relevant to this work. The steps taken in modelling the reactor physics of the OSNR informs some of the approach taken in designing the core of the OCR in this work. In the first stage, the PWR was modelled as a baseline for further modification. In subsequent models, the water coolant was swapped with organic fluid and then a portion of the coolant volume was replaced with a graphite moderator. Next, zirconium hydride rods were added in place of a portion of the fuel rods. Also, this stage of the modelling saw the dimensions of the fuel rods

altered; increasing the fuel rod diameter and decreasing the cladding thickness. Final models retained the geometry and experimented with other fuels[14].

A noteworthy portion of the OSNR research concerns the selection of an appropriate organic coolant. The task required thorough consideration because of the decades-long lapse in OCR research[13]. Several organic coolants are presented that were previously trialed in various OCRs. These coolants are terphenyl mixtures including Santowax OM, Santowax OMP and HB-40. Coolants such as these possessed desirable properties including high atmospheric boiling temperatures and proven stability against thermal and radiolytic degradation. Additionally, some terphenyl mixtures are solid at room temperatures, which can be viewed as an advantage in spills or a detriment to flow in the reactor[13]. Santowax OMP was ultimately selected for use in the OSNR models. Despite choosing an established coolant, the OSNR research also presents potential alternatives. Siloxane and perfluoropolyether are specified because of their current application in the nuclear industry as greases and lubricants. These materials are proven to possess sufficient radiation and thermal stability. From a safety perspective, they are appealing because of low flammability and less solid formation upon degradation. The key disadvantage presented is a lower neutron economy compared to terphenyl mixtures[13].

Elsewhere, the OSNR research delivers valuable insight into the implications of employing organic coolants in a plant design. A hydrocracker system is proposed as a means of compensating for coolant degradation. A general layout of the OSNR plant including the hydrocracker system and tank configuration is presented in Figure 2. By their estimates, the system could minimize the replacement of coolant by reforming more than 90% of the degraded coolant[15]. This technology would be essential to an underwater OCR or one operating in a remote location to limit storage tanks as well as the maintenance required by the plant. However, hydrocracking only addresses the replacement of degraded coolant and not the degradation itself[15]. Concerning degradation, the research contrasts organic coolants and light water by discussing the increased gamma dose received by organics. To overcome this, the OSNR utilizes solid moderators including zirconium hydride and graphite to reduce the dose received by the organic coolant[16].

The OSNR research also addresses how the use of organic coolants influences the construction of a plant. Overall, the conversion of the PWR to the OSNR saw a net reduction in plant volume. For the most part, lower operating pressures and reduced corrosion permitted thinner vessel walls and the use of less expensive alloys. On the other hand, the implementation of an organic coolant necessitated a larger steam generator to compensate for reduced heat transfer properties in organics relative to water[12]. Concerning cladding, thicknesses can generally be reduced when adapting a LWR design to an organic coolant due to reduced corrosion; however, the OSNR also had the advantage of adapting from a higher operating pressure. Reducing the cladding thickness permitted larger fuel rods. When combined with a more uranium-dense fuel, such as uranium carbide or uranium nitride, the larger fuel rods compensated for those rods that were replaced with zirconium hydride moderator[14].

Concerning safety, the OSNR research presents a limited evaluation that largely relies upon the underwater operation of the plant to mitigate certain risks. For instance, flammability of the coolant is effectively irrelevant in an underwater reactor design. Likewise, influx of water into the system would diminish the consequences of a loss of coolant accident. In such an accident, water would provide adequate moderation and coolant in place of the organic coolant. However, the operating pressure of the reactor design is notable for its safety implications. At approximately 0.6 MPa, the risk of large pressure gradients expelling coolant in the event of a rupture is minimal[12].

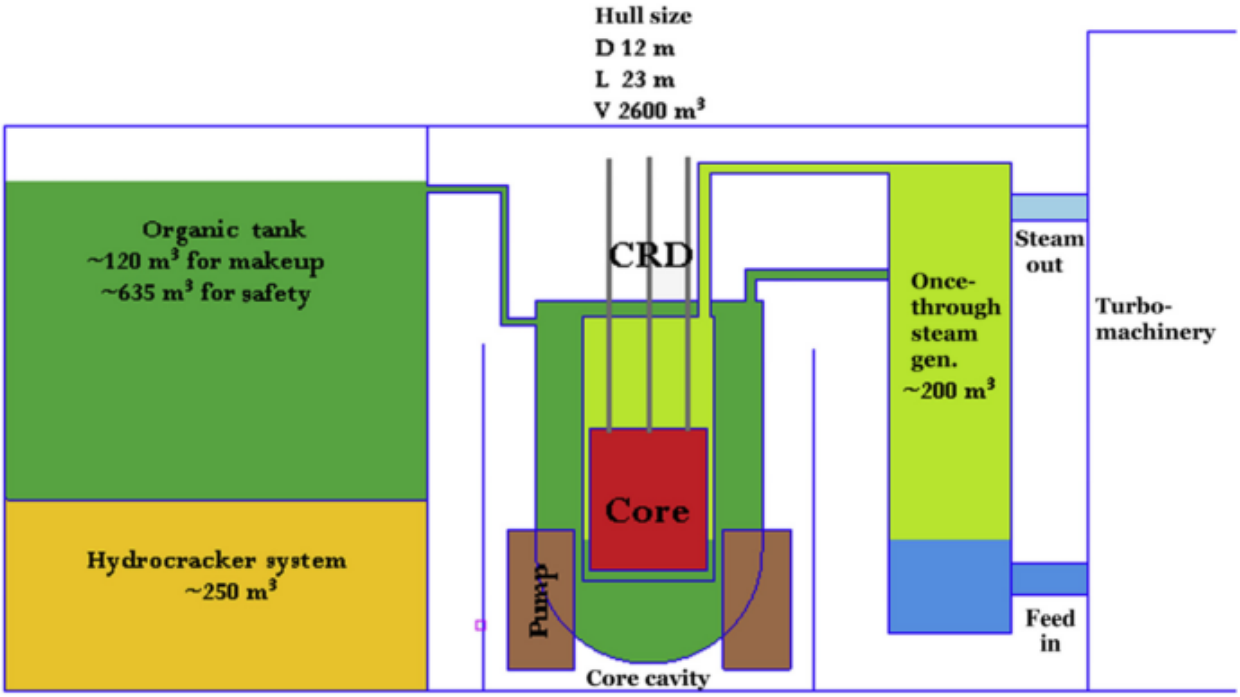

Figure 2: Outline of OSNR Plant[15]

The limitations of the OSNR research were largely tied to the selection of uranium carbide as the fuel source. The design that was modelled may not be achievable if the ongoing research and development of that fuel is unsuccessful in delivering it for application[12]. In comparison to the OCR in this research, it is important to recognize the OSNR maintained the power of the reactor it was adapting and reduced its volume to create a smaller plant for underwater use. The OSNR achieved this objective reducing hull volume by 40%[12]. In contrast, this research is extending the power of the SLOWPOKE-2 without an initial constraint on plant volume.

2.1.2 The SLOWPOKE Energy System (SES)

Developed in the 1980s by Atomic Energy of Canada Limited (AECL), the SES successfully demonstrated an extension of the SLOWPOKE-2's power, while aiming to maintain inherent safety. Many characteristics of the SLOWPOKE-2 were preserved in the SES's design including the use of light water as coolant, moderator and shielding[17].The SES was a particularly unique concept because it proposed a dedicated reactor for district heating. In this role, the SES could operate at 10 MW(th) to supply heated water at 85 ^{o}C for building heating[18]. Concerning safety, the SES was designed to permit licensing for unattended remote operation and monitoring[19]. The goal was accomplished through several facets of the engineering of the SES including negative temperature reactivity, coolant temperature and void reactivity coefficients[20].

As shown in Figure 3, the SES closely resembles the SLOWPOKE-2 Research Reactor. The SES is thoroughly self-contained with heat exchangers located in the pool with the reactor core. There are no pumps within the reactor pool as the coolant circulates naturally from the core to the heat exchangers. Like the SLOWPOKE-2, the SES pool is constructed of concrete lined with stainless steel and is unpressurized[20]. Control of the SES is engineered so that a single monitoring station could remotely operate multiple systems[17].

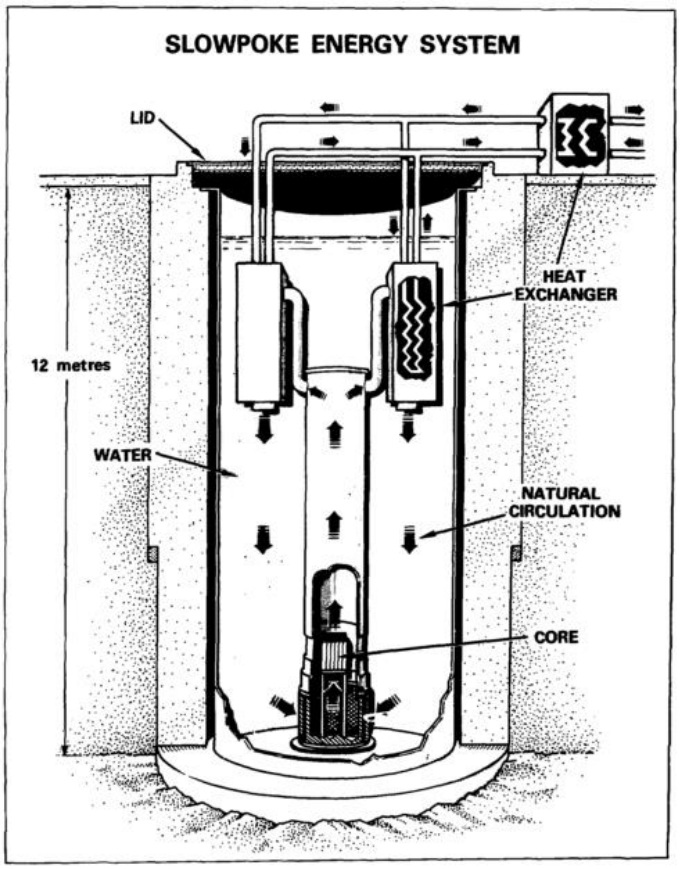

Figure 3: Schematic Diagram of SES[21]

Regarding the OCR in this research, a comparison of the SES to the original SLOWPOKE-2 is highly relevant. The demonstration reactor constructed in the late 1980s, called the SLOWPOKE Demonstration Reactor (SDR), generated 2 MW(th), which is very similar to the goal output for the OCR in this research. Table 1 presents a comparison of select specifications from the SLOWPOKE-2 and the SLOWPOKE Demonstration Reactor. The specifications of the SLOWPOKE Demonstration Reactor can provide information on the uprating of the SLOWPOKE-2 in this research. The SES's use of light water coolant is an obvious difference when comparing it to this research. Natural circulation may not be feasible for an OCR due to degradation and separation in the coolant mixture. As well, the heat transfer surface area in the SES would be insufficient for an OCR due to poorer heat transfer properties in the coolant.

Table 1: Comparison of Select SLOWPOKE-2 and SLOWPOKE Demonstration Reactor Specifications[2223]

	SLOWPOKE-2 Research Reactor	SLOWPOKE Demonstration Reactor
Thermal Power (MW(th))	0.0200	2
Pool Depth (m)	6.1	9.040
Pool Diameter (m)	2.5	4.300
Core Height (mm)	220	495
Core Length and Width (mm)		284
Core Diameter (mm)	220	
Fuel Enrichment (%)	19.9	4.9
Fuel Elements	180	196
Fuel Element Length (mm)	227	487
Fuel Element Diameter (mm)	4.19	13.1

2.2 Project Background

As stated in Section 1.5.3, the selection of an organic coolant constitutes a key design constraint in this project. Furthermore, establishing the most suitable modern-day coolant is a major secondary objective in addition to the design of the Organically Cooled SLOWPOKE Reactor. Therefore, it is necessary to explore the historical research of organic coolants; specifically, the work of the WR-1 project. In addition to that project, more recent developments in organic coolants must be reviewed.

2.2.1 The Whiteshell Reactor 1 (WR-1)

The research objectives of this project link it to several historical cases of OCR development including work by the United States, the Soviet Union as well as Canada. Of the various OCR projects, Canada's contribution, the Whiteshell Reactor 1 (WR-1), stands as the most thorough and best-documented exploration of an OCR's operation. Throughout its twenty-year operation, the WR-1 provided insight into the capabilities and limitations of organic coolants in nuclear reactors. Most importantly, the WR-1 project successfully characterized the chemical behaviour behind many of the complications experienced in early application of organic coolants[24]. In turn, the research has made OCR designs more feasible. The knowledge gained through the WR-1 project concerning organic coolants provides important information with respect to the preliminary coolant selection in this project.

Between 1965 and 1985, the WR-1 was operated by AECL at the Whiteshell Nuclear Research Establishment in Manitoba. At that time, there was interest in developing an organic-cooled variant of the CANDU reactor. Supporting this initiative, the WR-1 was commissioned to investigate the known problems associated with organic coolants as they applied to a CANDU design[25]. Although similar to American contemporary designs, the WR-1 was distinct for using an organic fluid solely for cooling purposes while employing heavy water as the moderator in the core[26]. Furthermore, WR-1 differentiated itself through the use of HB-40 coolant instead of the more commonly selected Santowax OM[27]. The WR-1 was designed to operate with an outlet coolant temperature of 375 ^{o}C producing 60 MW (th)[26]. A diagram of WR-1 is presented in Figure 4.

To produce 60 MW (th), the WR-1 core was designed to contain fuel in fifty-five sites within the calandria[26]. The WR-1 employed a uranium oxide fuel that was enriched to 2.4% by weight. Fuel was arranged into bundles of eighteen pencil elements that were assembled into eight-foot-long, five-bundle strings to occupy each site. Fuelling was conducted offline using the main building crane and shielded flasks for the fuel[27].

Three independent organic coolant circulation systems cooled the WR-1 core. Each of the three loops removed heat at 20 MW and contained its own pump, heat exchanger and surge tank. Coolant degradation produced gas in the circulation system thus necessitating a degassing system for each loop. Degassing systems consisted of vapour condensers as well as absorption columns and back-up filters. In addition to the organic coolant circulation systems, the WR-1 was outfitted with another independent circulation system containing light water[28].

The lack of control rods was a unique facet of the WR-1's design. Rather than a system of control rods, the WR-1 controlled reactivity and power output by varying the level of the heavy water moderator in the calandria. Shutdown of the reactor was achieved by rapidly draining the heavy water.

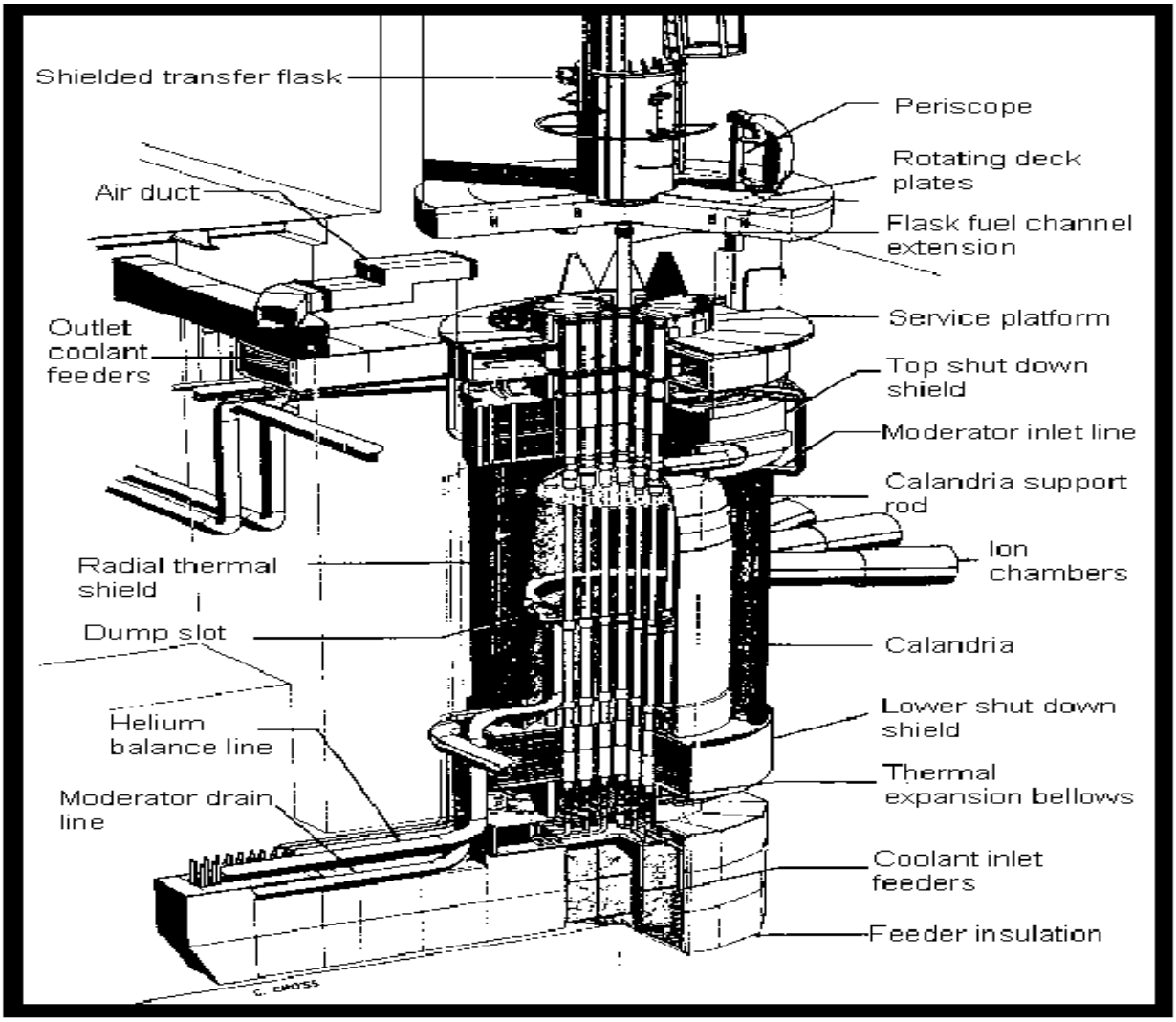

Figure 4: Diagram of WR-1[28]

2.2.2 Organic Coolants in WR-1

Prior to the WR-1 Project, organic liquids had been proposed as nuclear reactor coolants as early as 1944 in the work of Fermi and Szilard[29]. When organic coolants were investigated for practical applications by the United States Atomic Energy Commission in the mid 1950s, terphenyls were identified as the most suitable class of compounds. The selection of terphenyl coolants reflected an optimal balance of cost, availability and most importantly, chemical properties suitable for use in a reactor[29]. When terphenyl coolants were first observed in American reactor designs, such as the Piqua Reactor, the predominant complication that forced shutdown was the polymerization of the coolant in stagnant regions of the reactor[29].

The coolant selection for WR-1 began with the commercially distributed terphenyl mixtures that were employed in earlier American research. These mixtures were distributed under the name SANTOWAX and manufactured by the Monsanto Company[30]. With the pyrolysis of biphenyl from benzene, these terphenyl mixtures form as by-products. They contain ortho, meta, and para isomers of terphenyl in addition to biphenyl and high molecular weight organic compounds referred to as high boilers (HB)[31]. Figure 5 further illustrates the derivation of terphenyl coolants from benzene while also distinguishing different coolants under the SANTOWAX name. Of the coolants featured in Figure 5, SANTOWAX OMP, SANTOWAX OM and HB-40 are notable for being commercially produced and employed in OCRs[32].

Earlier American OCRs such as the failed Piqua Reactor had employed SANTOWAX OMP and SANTOWAX OM on separate occasions. SANTOWAX OMP is refined from SANTOWAX R by removing all high boilers. The presence of p-terphenyl causes SANTOWAX OMP to have a high liquidus point of 177 ^{O}C[32]. Further distillation reduces p-terphenyl content to produce SANTOWAX OM. The liquidus point of SANTOWAX OM is more practical at 65 ^{O}C but its low yield results in a more expensive coolant. Initially, the AECL OCR program identified SANTOWAX OM as its reference coolant[32]. Despite a lower liquidus point, SANTOWAX OM still carries the major disadvantage of being solid at room temperature. This complicates the storage and handling of coolant as continuous heating is required to prevent pump overload[32].

Recognizing the advantage of a liquidus point below room temperature, the WR-1 project further surveyed the available coolants to identify a replacement with a suitable range of operational temperatures. The most promising alternative was a relatively cheap coolant known as HB-40 also manufactured by the Monsanto Company. HB-40 is the product of partially hydrogenating the initial SANTOWAX R terphenyl mixture. The process results in a coolant with an ideal liquidus point of 0 ^{O}C. Confident with the results of early irradiation experiments, WR-1 commenced operation in 1965 with HB-40 as its coolant[33].

2.2.3 WR-1 Steady State Coolant Composition

Not surprisingly, the steady state composition of the coolant in an OCR varies significantly from the composition of the feed coolant. In WR-1, the influence of heat and radiation caused HB-40 to partially decompose. An increasingly black and opaque colouration of the coolant was indicative of decomposition[34]. In general, degradation of the coolant saw an increase in gases, volatile species, and high molecular weight polymers. The classes of decomposition products are defined in Table 2. The remaining weight percentage is comprised of undecomposed HB-40 feed material[35]. To maintain adequate properties of the coolant, the concentrations of certain decomposition products were controlled. Specifically, gases were maintained at a minimum and an optimum concentration of high boilers was

retained in the coolant. The presence of high boilers retard decomposition rates but excessive high boiler concentrations impede heat transfer[36].

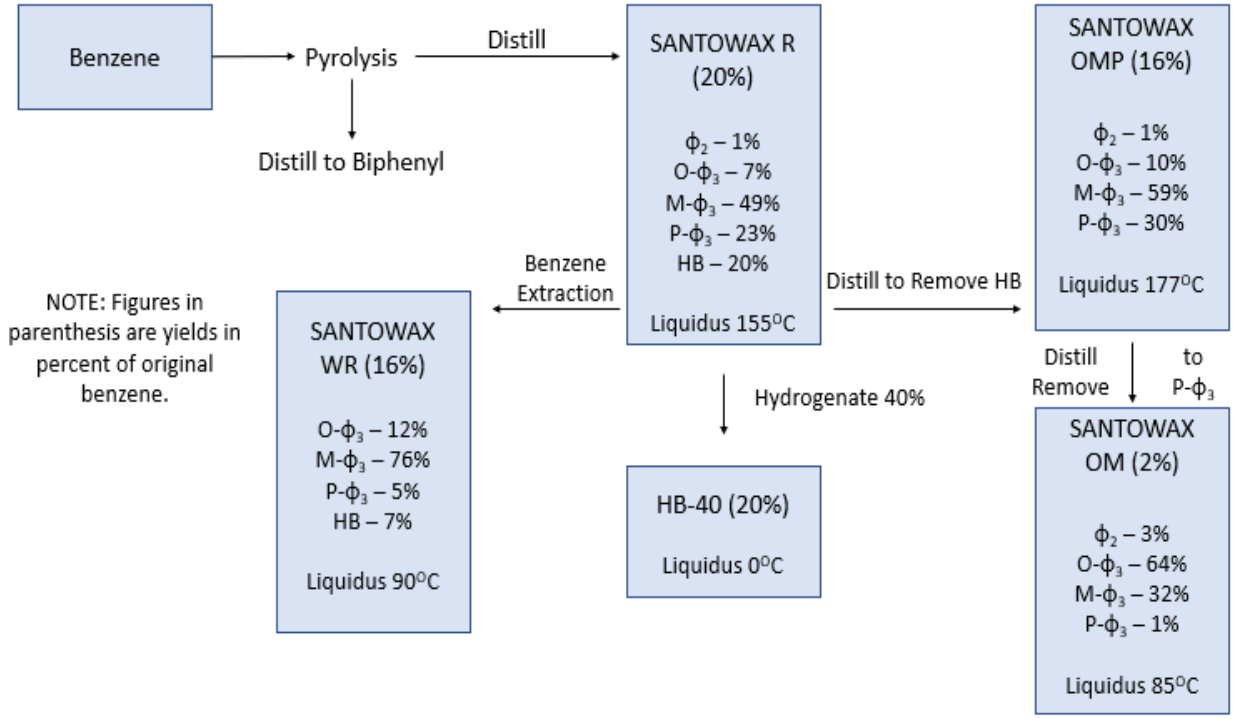

Figure 5: Derivation of Terphenyl Coolants[31]

Table 2: HB-40 Decomposition Product Classification[35]

Name	Description	Equilibrium Concentration (wt %)
Gases	Hydrogen and hydrocarbons up to C_5	1
Volatiles	Hydrocarbons C_6 to biphenyl C_{12}	3-6
Intermediates	Biphenyls to quaterphenyl	24-28
High Boilers (HB)	Volatility < quaterphenyl (> C_{24})	28-32
Undecomposed HB-40 Feed Material	Similar volatility to intermediates	35-40

2.2.4 HB-40 Decomposition Model in WR-1

The degradation of organic coolants in nuclear reactors can be described as a combination of two reactions considered to be independent below 400 °C; radiolysis and radiopyrolysis. First, radiolysis is predominantly influenced by the total ionizing radiation dose received by the coolant but is not influenced by dose rate. The radiolysis rate is relatively insensitive to the temperature and only accelerates slightly with increased temperature. In radiopyrolysis, the rates are not influenced by the dose, dose rate or radiation type. However, the reaction is predicated on a coolant that has been irradiated and contains sufficient concentrations of intermediates. Contrasting radiolysis, temperature greatly influences radiopyrolysis rates such that, at temperatures below 300 °C, the reaction becomes negligible. With

respect to untransformed coolant concentration, radiolysis is second order while radiopyrolysis is first order[37].

In hydrogenated terphenyl mixtures such as HB-40, the observed rates of decomposition are initially much faster than those in non-hydrogenated mixtures indicating a lower stability. However, the behaviour is much different at steady state. The decomposition of hydrogenated terphenyl produces less stable high boilers. These molecules subsequently decompose back into intermediate molecules and preserve the heat transfer properties of the coolant. This mechanism has the added effect of retarding gas and volatile production[38]. Regarding the effects of temperature on the mixture of decomposition products, thermal cracking reduces high boiler concentrations at higher temperatures, while increasing the concentration of gases and volatiles[39].

2.2.5 Volatile Recycling in WR-1

During extended operation in the reactor, regulating the equilibrium concentrations of gas and volatiles is important to maintaining the properties of the coolant. In addition to increasing vapour pressure, gases and volatiles were known to decrease the viscosity of the coolant in WR-1. However, a certain level of retention of these components appeared to reduce coolant decomposition rates[40]. The concentrations of these components were kept to a minimum by continuous removal through the degassing systems. Experimenting with various degas condensate recycle rates established optimum volatile equilibrium concentrations. Essentially, these results indicated the concentration where the decomposition rates were minimized but the vapour pressure was not large enough to cause excessive surface boiling of the coolant. In WR-1, the optimum volatile concentration ranged from 5 to 7 %[41].

By establishing tolerable vapour pressure limits, these experiments also presented an opportunity to reduce the coolant cost by adding lighter components such as toluene and biphenyl to the coolant. Further experiments demonstrated that this practice would not negatively affect the overall steady state composition of the coolant[41].

2.2.6 Coolant Reprocessing in WR-1

Various methods of reprocessing were required to maintain the optimal composition of the coolant in WR-1. Fundamentally, the concentrations of gases, volatiles and high boilers were controlled by ideally reprocessing them into suitable intermediate components or by removing them entirely.

As explained in Section 2.2.5, gases and volatiles were continuously separated from the coolant in the degassing systems. Figure 6 presents the idealized operation of a degassing system like those found in WR-1. In Figure 6, main system refers to the WR-1 coolant circulating system. In operation, 1 to 2% of the coolant flow in WR-1 was diverted to the degassing tanks where it was flashed at low pressure. Reusable intermediates were removed using two condensing stages. The condensate from the first stage was suitable for direct recycle to the main system. However, the second stage condensate had to pass through water separators because detrimental impurities such as HCl were known to be carried by water vapour. Once purified of water, the second stage condensate was returned to the main system under control due to it higher volatility. This stream corresponds to the volatile recycling that was discussed in Section 2.2.5. In a third condensing stage, all remaining vapour was condensed and discarded. Any remaining organic compounds in this stage were too light in molecular weight for reprocessing[42].

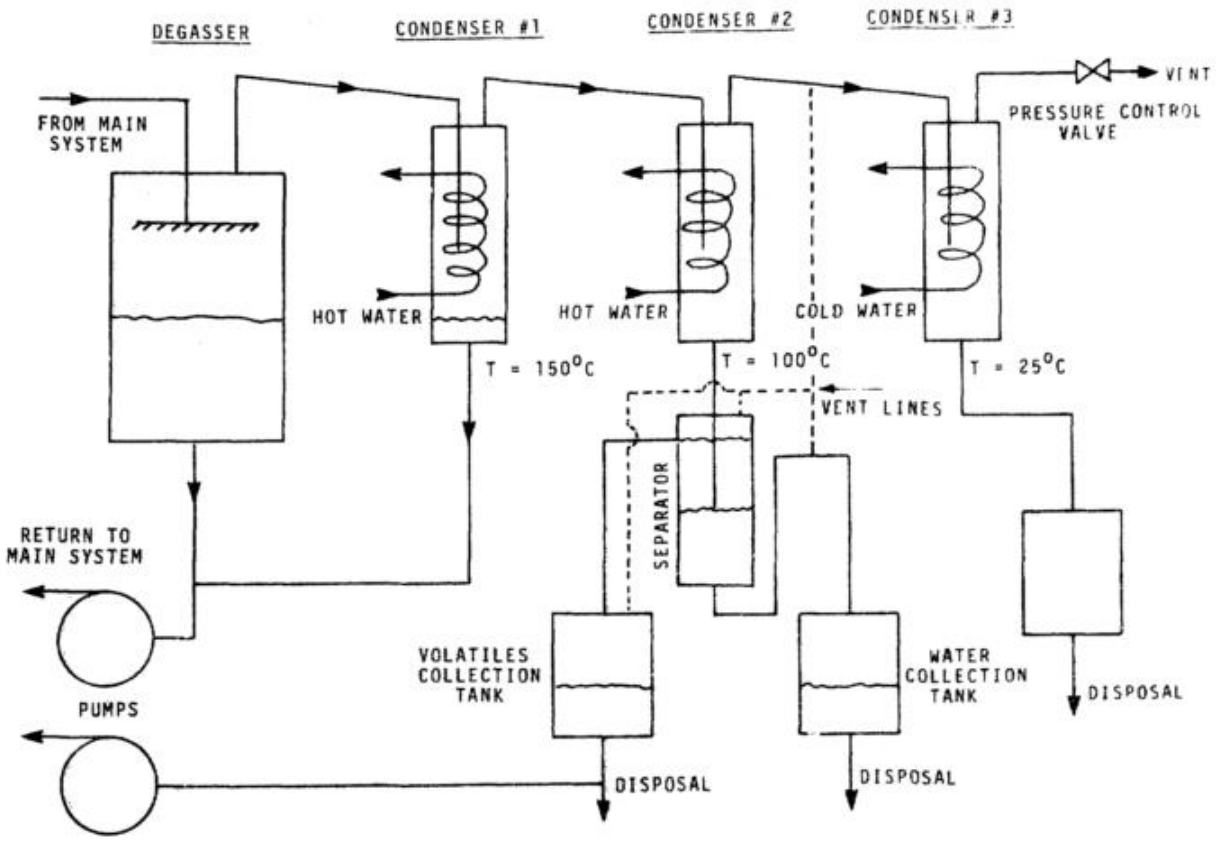

Figure 6: Ideal Degassing System[42]

In a similar fashion, high boiler concentration was maintained at an ideal 30% by removing a portion of coolant from the normal system flow. Without adequate reprocessing, this method can become costly in large reactors due to the useable intermediate components lost in the process. The WR-1 project explored several methods of removing high boilers including vacuum distillation, steam distillation and solvent extraction[43].

A vacuum distillation column was incorporated into the WR-1 design to evaluate the viability of the method. When operated, the column was held at a 7 – 15 kPa vacuum, while it continuously received a small portion of the coolant flow. Over time, the column filled with residual high boilers while useable coolant was recycled back to the main system. Once full, the high boiler concentration in the column would be approximately 80% and was subsequently discarded. Complications associated with vacuum distillation were obvious. The use of vacuums increased the probability of air entering the coolant system and raising corrosion potential. The liquidus point of the column contents greatly increased due to high molecular weight. Pumping of the waste product was difficult due to significant thickening at temperatures around 200 ^{O}C. Additionally, studies of this method noted an increase in fouling potential from the coolant returned to the system. Because of these difficulties, vacuum distillation was never employed consistently in WR-1[43].

Steam distillation was a relatively new concept that was evaluated at a small scale by the WR-1 project. In operation, injected steam acts as a carrier for the coolant and the high boiler residue collects in the column. Operating above atmospheric pressure reduced the risk of air penetrating the system and reduced the size of the distillation system. As well, many inorganic contaminants such as chlorine would

be removed from the organic coolant after passing through water separators. On the other hand, this distillation method added complexity to a plant design by requiring a steam supply and additional water separators. Also, the introduction of large amounts of steam could necessitate more expensive construction materials to reduce corrosion potential. Most importantly, the experiments with this method implied a lower retention of useable coolant. Therefore, steam distillation in WR-1 never progressed to large scale testing[44].

Solvent extraction had already been applied as a coolant reprocessing technique in American and European OCR programs. However, the WR-1 project established a simplified approach by repurposing the volatile recycle as a solvent. In previous applications, solvents such as xylene or heptane were added to the diverted coolant and the result was a precipitation of the heaviest high boilers. The remaining coolant was subsequently distilled to remove the solvent before returning to the main system. This method is not entirely effective and lighter high boilers remain in the coolant. When extracted volatiles were used as the solvent, the extraction was even less effective. The key advantage of this method was its simplicity as the volatile solvent was suitable for return to the main system[45]. Most likely, solvent extraction would be paired with one of the previously mentioned distillation techniques to constitute a viable reprocessing system.

2.2.7 Physical Properties of HB-40

Despite their complex compositions, the physical properties of organic coolants proved to be influenced by relatively few variables. Intuitively, temperature is often the most sensitive parameter affecting most physical properties while high boiler concentration is the only composition-related parameter that has significant influence. The concentrations of gases, volatiles, and intermediates tend to retain their proportions to each other and therefore have little influence on the coolant's physical properties[46].

The WR-1 project established correlations for numerous properties of HB-40. These relationships were characterized over a range of temperatures and high boiler concentrations. Throughout, the volatile concentration was maintained between 3 and 5%[47]. Of the many correlations presented, a couple are highly relevant to the neutronic modeling of the OCR in this research. Acting as a moderator, HB-40's density and carbon to hydrogen ratio significantly influence the reactor's neutron economy. Other thermodynamic and heat transfer properties become relevant when simulating the thermal hydraulics of the reactor.

The density of HB-40 was measured for temperatures between 25 and 400 ^{O}C with high boiler concentrations up to 43%. For HB-40 within this domain, the density can be expressed by[47]:

$$\rho = A + B * T + C * HB + D * T * HB \quad (1)$$

where:

ρ = density in kg m^{-3}

T = temperature in ^{O}C

HB = high boiler concentration in wt%

A = 1.0181 x 10^{3} kg m^{-3}

B = -7.3891×10^{-1} kg m^{-3} $^{O}C^{-1}$

C = 2.2343 kg m^{-3} per %

D = 1.6670×10^{-3} kg m^{-3} $^{O}C^{-1}$ per %

Figure 7 presents the correlation between HB-40's carbon to hydrogen ratio and its high boiler concentration at 350 ^{O}C and 400 ^{O}C.

2.2.8 Coking Control in WR-1

Two processes, coking and fouling, were known to deposit solids onto the cladding surfaces of OCRs. Of the two, understanding and control of coking were straightforward. Coking occurs as a result of the decomposition of an organic compound in solution. In the case of an OCR, the decomposition of the coolant can produce high concentrations of high boilers that then precipitate from solution as carbonaceous deposits on the fuel cladding. Coking is controlled by ensuring sufficient coolant flow in the reactor and minimizing stagnant regions so that high boilers remain in solution[48].

2.2.9 Research of Fouling in WR-1

Compared to coking, control of fouling was less understood at the time of the WR-1 project. To address the feasibility of OCR designs, AECL sought to characterize the fouling of fuel cladding surfaces and establish a means of controlling its progression over long-term reactor operation. Fouling was known to decrease the heat transfer at the cladding-coolant interface by depositing material with a low thermal conductivity on the cladding surface. Increased cladding temperatures due to this effect were known to decrease the lifespan of cladding in the reactor[50].

Two different forms of fouling were known to occur in organic coolants. First, mass transfer fouling produced an iron-based inorganic film on cladding surfaces[51]. Second, particulate fouling produced films mainly composed of organic compounds that adhered to cladding surfaces[52].

Research of fouling in WR-1 identified several components of the coolant that influenced fouling rates. Thus, the coolant composition could be controlled to maintain optimum fouling performance. Empirically, particulate concentrations were known to influence fouling rates. In WR-1, particulate concentrations were maintained below 1000 µg kg^{-1} to ensure optimum performance[53]. Additionally, several chemical impurities in the coolant were controlled in WR-1 including iron, chlorine, oxygen and water.

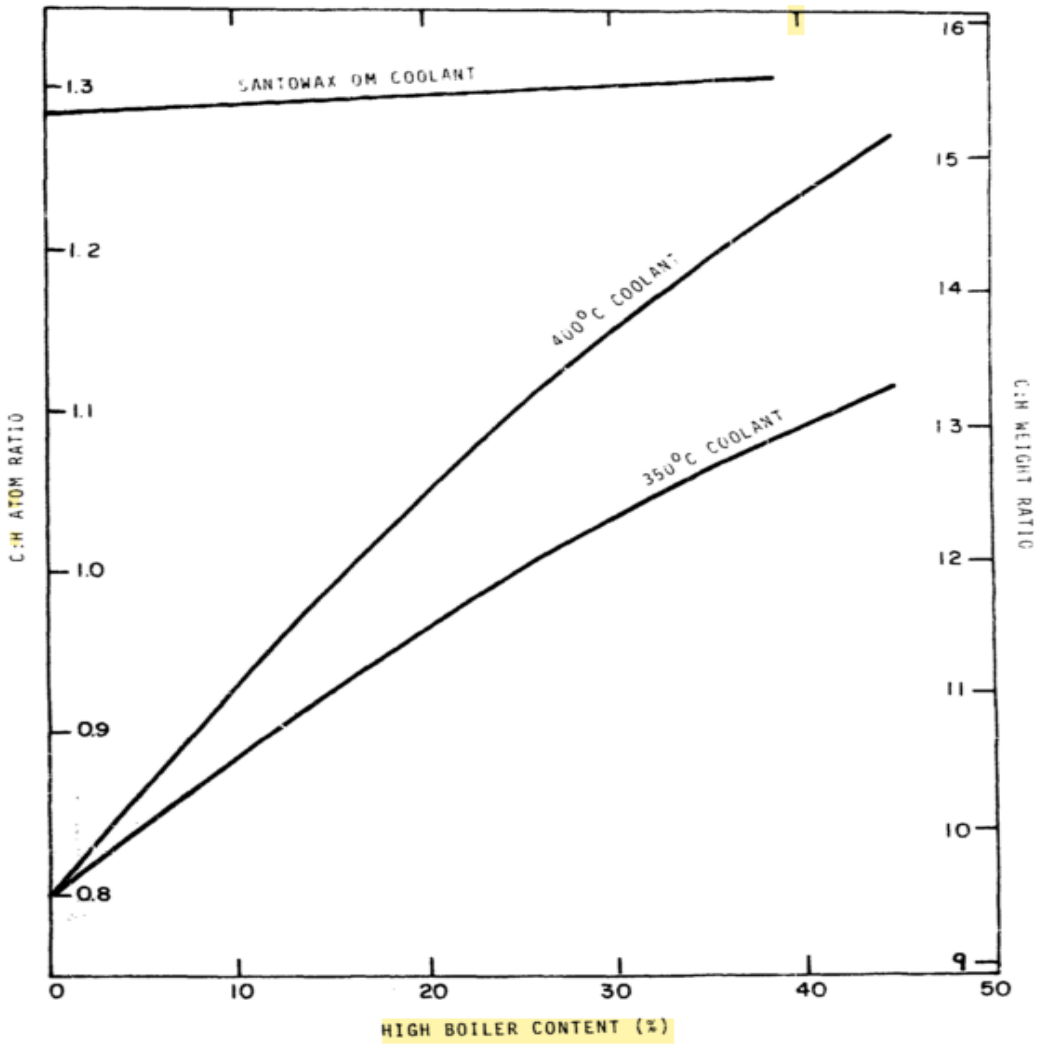

Figure 7: Carbon to Hydrogen Ratio of HB-40 Coolants[49]

The dissolved iron content in the coolant was closely related to mass transfer fouling rates. Reaction with dissolved chlorine in the coolant produced films of iron oxide and iron carbide on cladding surfaces. Therefore, a concentration limit of 500 µg kg^{-1} was established to limit the mass transfer fouling over long-term operation[54].

Regarding chlorine, fouling studies established that elevated concentrations in WR-1's coolant greatly increased fouling and therefore, a limit of 50 µg kg^{-1} was maintained during operation. Much of the coolant's chlorine content remained dissolved in the rejected water from the degassing system. Under normal operation, this removal pathway maintained an acceptable chlorine concentration[55].

Fouling research demonstrated that dissolved oxygen in the organic coolant only influenced fouling at temperatures between 150 °C and 340 °C. In this range, the reaction of the coolant with oxygen produces polar compounds that can contribute to particulate fouling. In WR-1, the oxygen content in the coolant was minimized by purging feed coolant, operating above atmospheric pressure, and employing clay columns to remove the oxygen from the coolant returning from the degassing system[56]. Optimum fouling performance was achieved with oxygen concentrations below 200 µg kg^{-1} [57].

Finally, the water content in the coolant was found to negatively influence the fouling potential in WR-1. Thus, an optimum water concentration would contribute to ideal fouling performance while not detrimentally increasing the corrosion potential or vapour pressure of the coolant. Over the operation of WR-1, the water concentration ranged from 150 µg kg^{-1} to 800 µg kg^{-1} [58]. The optimum range for water content was 200 µg kg^{-1} to 600 µg kg^{-1} [59].

2.3 Small Reactor Licensing in Canada

Before entering in to service in Canada, small reactor facilities such as that of the OCR proposed in this research must receive licensing from the Canadian Nuclear Safety Commission (CNSC). The regulatory document *RD-308: Deterministic Safety Analysis for Small Reactor Facilities* establishes the requirement of deterministic safety analysis for small reactor licensing[60]. As defined by the CNSC, "small reactor" denotes a reactor with less than 200 MW(th) output power. Accordingly, a small reactor may be employed in many roles including research, isotope production, district heating and power generation[60].

2.3.1 Graded Approach

The CNSC applies a graded approach to licensing of small reactor facilities meaning that the degree of regulation imposed on the design is determined by the risk associated with a particular facility. Risk factors such as intended use, reactor power, fuel enrichment and design, safety design, and proximity to populated areas influence the graded approach as it is applied to a reactor design[60].

2.3.2 Safety Analysis

There are three components comprising the overall assessment of a reactor design. These components are the hazards analysis, the deterministic safety analysis and the probabilistic safety analysis. Through these analyses, the assessment of the design ensures safety requirements concerning radiation doses and environmental impacts are addressed[60].

The objectives of the safety analyses are[60]:

a. to demonstrate that control systems can provide thorough mitigation of anticipated operational occurrences;
b. to demonstrate that safety systems are capable of mitigating design basis accidents while complying with dose regulations;
c. to establish operational limits and conditions that remain within safe operation of the design; and
d. to ensure resiliency such that modifications to the design or operation are not detrimental to safety.

2.3.3 Analyzed Events

The analyses must evaluate safety in all operations of the small reactor including start-up, shutdown, maintenance, and refuelling. In all operational configurations, the safety analyses must address the risk associated with equipment or component failure, operator error, and events internal or external to the reactor. From these analyses, identified events are categorized based on their estimated frequency as anticipated operational occurrences, design basis accidents and beyond design basis accidents[60].

CHAPTER 3: Design Approach

3.1 General Methodology

The design of the Organic-Cooled SLOWPOKE (OCSL) is approached by beginning with the present SLOWPOKE-2 as a baseline. To achieve the uprated power, parameters are altered including the number of fuel rods, the dimensions of the fuel rods and the lattice pitch of the core. Beyond the reactor's core, a radial reflector is designed to enhance the lifespan of the fuel in the reactor. Additionally, a preliminary control strategy is designed by replacing certain fuel channels with clusters of control rods capable of driving the core to subcritical and maintaining sub-critical under all circumstances.

The probabilistic code, MCNP 6 (MCNP) is employed as the primary design tool for detailed three-dimensional simulation of the reactor's neutronics. The deterministic code, WIMS-AECL (WIMS[†]) is utilized to reproduce MCNP models in a simplified two-dimensional geometry firstly to verify results from the MCNP model. Furthermore, the deterministic nature of WIMS coupled with simplified geometry enables faster computation of burnup and reactivity coefficients. Thus, results produced by WIMS are essential to vetting various design choices for the reactor. Ultimately, the employment of two fundamentally different codes provides continuous verification of results at each stage of the design.

3.2 Preliminary Modelling

The preliminary phase develops working knowledge of the design tool MCNP and establishes confidence that appropriate neutronic behaviour with an organic coolant can be simulated. First, a validated SLOWPOKE-2 MCNP 4A model is reproduced using MCNP and thus verifies the accuracy of the current iteration of MCNP. Working in this model, the light water coolant of the SLOWPOKE-2 is replaced with the organic coolant, HB-40 and the neutronics are simulated. Assuming poorer neutron moderation with HB-40 and a subcritical reactor in this step, addition of fuel into the vacant ports of the SLOWPOKE fuel cage will produce a critical reactor again. Confirmation of these hypotheses will instil confidence in the MCNP code as the reactor is designed in subsequent phases.

3.3 Core Design

The design of the OCSL reactor core begins with an estimation of its minimum critical dimensions using the modified one-group critical equation. From the reactor's length and the number of fuel pins, Newton's law of cooling estimates the thermal hydraulics required to achieve the greater power output. Slight variation of the core dimensions produces a series of potential cores displaying different excesses of reactivity when simulated using MCNP. When simulated, cores are modelled as reactors provided an infinite reflector of the HB-40 coolant. This method simplifies the vetting of each configuration by ensuring neutronic results are influenced by variation of the core only. Each possible core is reproduced using WIMS and the most suitable core is discerned by comparing the burnup and reactivity coefficients of the potential cores.

3.4 Reflector Design

Within the scope of this research, the reflector will only be an annulus around the core. Further design may consider axial reflection above or below the core. The design of the OCSL reflector is

[†] The British code, WIMS, and WIMS-AECL are not the same. Throughout this research, *WIMS* is used as short form for WIMS-AECL.

primarily an exercise in material selection. First, several potential materials are identified for the reflector. For each potential material, MCNP simulates increasing radial thicknesses of the reflector to ascertain its effective thickness. The ideal reflector material will offer the greatest increase in excess reactivity with a reasonable increase in reactor dimensions. The selected reflector is then added to a WIMS model for verification and for burnup calculations to determine the enhanced service life of the fuel.

During the initial phases of operation, the excess reactivity of the OSCP will be very large due to the fresh fuel in the core. This is essential to achieving the lowest possible fuelling frequency for the reactor. However, it also necessitates that the reflector be capable of disengaging from the core while fuel is fresh. As the fuel depletes, the reflector is positioned closer to the core counteracting the continued loss in excess reactivity. In this research, this mechanism is envisioned by symmetrical subdivision of the reflector and displacing each portion an equal distance radially from the core.

3.5 Control Strategy Design

With the reactor core and reflector selected, a control system is required to limit the excess reactivity and ensure safe operation of the reactor. At this stage, absorber rods are incorporated into the reactor's design as a means of controlling criticality. The size and dimensions of the absorber rods must be idealized to preserve as many fuel channels as possible in the reactor core. As mentioned, the reflector will be comprised of moveable reflector plates to aid in long-term regulating control of excess reactivity. Once designed, the various control system components must be configured to demonstrate safe start-up conditions for the reactor as well as continued safe operation.

CHAPTER 4: Theory

4.1 Introductory Comments

The purpose of this section is to provide theoretical background for several concepts that appear throughout this research. This is not intended as an all-encompassing review of nuclear reactor engineering but rather an explanation of these concepts as they apply to the heterogenous, thermal reactors discussed in this research.

4.2 Neutron Diffusion Theory

The essential task in nuclear reactor design is characterizing the average neutron behaviour in the system. Predicting the distribution of neutrons throughout the reactor is a complex task. As an approximation, neutron transport is often treated as a mass transfer phenomenon that may be predicted by diffusion theory[61].

For neutrons in an arbitrary volume of some material, continuity exists between neutron production, neutron absorption and leakage of neutrons from the volume. Furthermore, when the system is at steady-state, these three terms are considered in balance with one another. In other words, the production of neutrons in the system is equal to the loss of neutrons from the system[62].

The neutron diffusion equation may be regarded as a unification of neutron continuity with governing law of diffusion known as Fick's law. The neutron diffusion equation is given by[62]:

$$D\nabla^2\phi - \Sigma_a\phi + s = \frac{dn}{dt} \tag{2}$$

where:

D	= the diffusion constant of Fick's law with units of cm
ϕ	= the neutron flux with units of n cm^{-2} s^{-1}
Σ_a	= the macroscopic absorption cross section of the medium with units of cm^{-1}
s	= the rate of neutron production in the medium with units of n cm^{-3} s^{-1}
$\frac{dn}{dt}$	= the time differential of the neutron density in the medium with units of n cm^{-3} s^{-1}

In this research, the reactor will always be at steady-state. Therefore, the neutron diffusion equation becomes[62]:

$$D\nabla^2\phi - \Sigma_a\phi + s = 0 \tag{3}$$

4.3 Group Diffusion Method

In reality, neutrons in a nuclear reactor exist along an energy spectrum. Beginning with their emission in fission, neutrons disperse through the medium and are continuously scattered by collisions with nuclei. All the while, neutrons are losing energy in the collisions until they reach thermal energies. In thermal reactors, most neutrons will be thermalized before inducing fission; barring the occurrence of absorption or leakage during moderation. When a spectrum of neutron energies exists, group diffusion

method predicts the average particle behaviour for the system[63]. Deterministic reactor physics codes such as WIMS-AECL employ this method to simulate reactor neutronics.

In the group diffusion method, the spectrum of neutron energies is separated into numerous intervals. Furthermore, all neutron energies within an interval receive diffusion coefficients and cross sections averaged over the energy span defining the energy group. By this method, each interval or group may be treated similarly to the system in Section 3.2 except the continuity now includes moderation of neutrons into the group from more energetic groups and moderation out of the group. This addition leads to the steady state group neutron diffusion equation given by[64]:

$$D_g \nabla^2 \phi_g - \Sigma_{ag} \phi_g - \sum_{h=g+1}^{N} \Sigma_{g \to h} \phi_g + \sum_{h=1}^{g-1} \Sigma_{h \to g} \phi_h + s_g = 0 \tag{4}$$

where terms from Equation 3 with the subscript "g" indicate that term for the g^{th} energy group and:

$\Sigma_{g \to h}$ = the group transfer cross section with units of cm^{-1} for neutrons scattered from the g^{th} energy group to a less energetic group

$\Sigma_{h \to g}$ = the group transfer cross section with units of cm^{-1} for neutrons scattered into the g^{th} energy group from a more energetic group

ϕ_h = the neutron flux of a more energetic group scattering into the g^{th} group with units of n cm^{-2} s^{-1}

4.4 Effective Multiplication Factor

A nuclear reactor is considered a multiplying system with regards to neutron population. Thus, a multiplication factor relates the population of neutrons in one generation to that of the previous generation. This basic property of nuclear reactors is used to define criticality[61]. For a theoretical infinite reactor, the infinite multiplication factor is given by[65]:

$$k_\infty = \frac{rate\ of\ neutron\ production}{rate\ of\ neutron\ absorption} \tag{5}$$

However, this is an oversimplification when considering a finite reactor. For finite reactors, some neutrons in each generation are lost from the system through leakage. Therefore, an effective multiplication factor describes the state of criticality in finite reactors such as those in this research[62]. The effective multiplication factor is given by[65]:

$$k_{eff} = \frac{rate\ of\ neutron\ production}{rate\ of\ neutron\ absorption + rate\ of\ leakage} \tag{6}$$

Following this definition, a system is considered critical when $k_{eff} = 1$. Accordingly, when $k_{eff} < 1$, the system is subcritical and when $k_{eff} > 1$, the system is supercritical[65].

4.5 The Four Factor Formula

When designing a thermal reactor, the criticality may be estimated using a method known as the four factor formula. The multiplication factor of an infinite reactor given by the four factor formula is written as[66]:

$$k_\infty = \eta \varepsilon p f \tag{7}$$

where:

η = the ratio of neutrons liberated by fission to neutrons absorbed in the fuel
ε = the fast fission factor
p = the resonance escape probability
f = the thermal utilization

For thermal reactors, the fast fission factor may often be assumed to be 1. The resonance escape probability is the fraction of neutrons that escape resonance capture during moderation. The thermal utilization is defined as the ratio of neutrons absorbed in the fuel to neutrons absorbed in the reactor system. The effective multiplication factor of the reactor may be calculated with an additional term known as non-leakage probability. This is the fraction of neutrons that do not leak from the reactor system[66].

4.6 Estimation of Reactor Critical Dimensions

A reactor's minimum critical dimensions may be estimated if the reactor's shape and the ratio of fuel to moderator are known. Knowing the heterogenous lattice pitch, this ratio may be estimated from the ratio of fuel to moderator for a single fuel channel. This estimation is accomplished by employing the modified one-group critical equation given by[67]:

$$\frac{k_\infty}{1+B^2{M_T}^2} = 1 \tag{8}$$

where:

B^2 = the buckling of the reactor
${M_T}^2$ = the thermal migration area

For a heterogenous reactor, this estimation method requires homogenization of fuel and moderator. The multiplication factor of the infinite reactor may be computed by the four factor formula using the material composition of the reactor. Likewise, the migration area of the system may also be evaluated based upon the composition of the reactor. Rearranging Equation 8, the buckling may be calculated using the aforementioned terms. Equating the buckling to the geometric buckling of the reactor's shape will give the minimum critical dimensions of the reactor. For example, geometric buckling for a finite cylinder is given by[68]:

$$B^2 = \left(\frac{2.405}{R}\right)^2 + \left(\frac{\pi}{H}\right)^2 \tag{9}$$

where the minimum volume of a cylinder occurs when its height (H) is approximately 1.85 times its radius (R). The computed critical radius of the homogenous reactor may be superimposed over a lattice of fuel rods to determine the number and arrangement of rods in the heterogenous reactor. Due to the homogenous approximation in this method, the heterogenous reactor will be super-critical with the computed dimensions. However, the method is likely to produce a useful starting point for reactor design.

4.7 Reactivity

In a related fashion, the criticality in nuclear reactors may be described by the reactivity. The term reactivity is applied to quantify a system's fractional displacement relative to criticality. Reactivity is represented by ρ and is computed by[69]:

$$\rho = \frac{k_{eff}-1}{k_{eff}} \quad (10)$$

Accordingly, a positive value of reactivity indicates a super-critical reactor and the reactor is said to possess excess reactivity. Similarly, a zero value of reactivity corresponds to a critical reactor and a negative value of reactivity refers to a sub-critical reactor.

4.8 Reactivity Coefficients

Within the scope of this research, the potential for inherent safety in the reactor design is demonstrated by investigation of the reactor's reactivity coefficients. These coefficients demonstrate the reactor's response to changes in fuel temperature, moderator temperature and moderator density. Therefore, they may predict the reactor's behaviour as perturbations occur during operation. In general, a negative coefficient is a safe coefficient as it indicates the reactor will be prone to return to it initial conditions when encountering a perturbation. This section includes descriptions of the fuel temperature coefficient of reactivity, the moderator temperature coefficient of reactivity, and the void fraction coefficient of reactivity.

4.8.1 Temperature Coefficient of Reactivity

The temperature coefficient of reactivity (α_T) is defined as the differential of reactivity with temperature written as[70]:

$$\alpha_T = \frac{d\rho}{dT} \quad (11)$$

When the temperature refers to the fuel temperature, the coefficient is often referred to as the prompt temperature coefficient. An increase in reactor power initially manifests as a rise in fuel temperature. Therefore, the fuel temperature coefficient of reactivity relates to the reactor's immediate reactivity response to changes in power and fuel temperature[71].

When the temperature refers to the moderator temperature, the coefficient may be referred to as the delayed temperature coefficient. Accordingly, this coefficient determines the reactor's overall reactivity response to a change in fuel temperature. When the moderator's temperature changes, so too does its density and its nuclides' microscopic cross-sections. As a result, the effectiveness of the moderator is altered either increasing or decreasing reactivity in the reactor[72].

4.8.2 Void Fraction Coefficient of Reactivity

Voids are a term used to describe the occurrence of gas bubbles in the coolant/moderator when it reaches or is near to its boiling point. Because the gas is much less dense than the liquid, the action is regarded as a loss of coolant/moderator density. The void fraction describes the portion of the coolant/moderator volume that has transitioned to gas. When the liquid is much denser than the gas, the density of the mixture may be written as[73]:

$$\rho_d = (1 - x)\rho_l \quad (12)$$

where $\rho_d$is the coolant mixture density, ρ_l is the liquid density and x is the void fraction.

The void fraction relates to the reactivity in a similar way as the moderator temperature. In both cases, the moderator density strongly influences the neutron moderation and consequently the reactivity. The void fraction coefficient of reactivity is written as[73]:

$$\alpha_V = \frac{d\rho}{dx} \tag{13}$$

4.9 The Prompt Critical State

In nuclear fission, most liberated neutrons are emitted almost immediately after fission (usually at a time less than 10^{-13} s after the fission) and are referred to as prompt neutrons. However, a small portion of neutrons are emitted by certain fission products called precursors. These neutrons are referred to as delayed neutrons because they originate after the fission according to the half-life of the precursor[74]. The fraction of neutrons that are delayed for a given fuel is denoted by β.

The multiplication factor (k) of a reactor accounts for both types of fission neutron. However, at a given instant the multiplication factor sees prompt neutrons only and becomes $(1-\beta)k$. Should this term equal one, then the reactor is considered prompt critical meaning that it is critical on prompt neutrons alone. This state results from a reactivity insertion exceeding the value of β. For a uranium-235 fuelled reactor, β is equal to 0.0065 and therefore the reactor becomes prompt critical with step reactivity insertions greater than 6.5 mk. At and above prompt critical, the reactor is difficult to control. Many reactor control systems will limit potential step reactivity insertions below prompt critical levels[75].

4.10 Fuel Burnup

In this research, the service life of the reactor between refuelling is pertinent to the design's viability for employment in remote locations. Fuel burnup is defined as the energy released by fission in a reactor's fuel commonly expressed in megawatt days. Specific burnup is a similar expression, with the fuel burnup normalized by the mass of the fuel measured in megawatt days per metric ton or kilogram[76].

Burnup calculations or lifetime calculations predict the reactor's properties as they change over time. The results of these calculations will determine how long the reactor can operate before becoming subcritical. Furthermore, this information determines the fuelling frequency of the reactor[77]. For a heterogenous reactor, the burnup calculations are complex and must be computed numerically.

4.11 Heat Transfer to Coolants

In a reactor, Newton's law of cooling can be used to describe the heat transfer from the fuel elements to the coolant. This relationship is given per unit area by[78]:

$$q'' = h(T_c - T_b) \tag{14}$$

where q'' is the heat flux in W cm^{-2} , h is the convective heat transfer coefficient in W cm^{-2} K^{-1}, T_c is the temperature of the fuel element surface and T_b is the bulk temperature of the coolant. Furthermore, the rate of heat transfer (q) between the fuel elements and the coolant for a specific surface area (A) is given by[78]:

$$q = q''A = hA(T_c - T_b) \tag{15}$$

In this research, application of Newton's law of cooling provides a means of estimating the heat transfer and corresponding temperature distributions for a potential reactor core defined by the method in Section 3.6. The approximation given by the Newton's law of cooling indicates the feasibility of a possible reactor core by estimating maximum material temperatures and the required coolant mass flow rate.

4.11.1 Thermal Resistance in Cylindrical Fuel Rods

For cladded fuel rods, the overall heat transfer between the fuel and the coolant may be regarded as three continuous intervals: conduction through the fuel, conduction through the cladding and convection in the coolant. Accordingly, each interval is characterized by its thermal resistance. For a cylindrical fuel rod, the thermal resistance in the fuel (R_f) is given by[79]:

$$R_f = \frac{1}{4\pi H k_f} \tag{16}$$

where:

H = the length of the fuel rod in cm
k_f = the thermal conductivity of the fuel in W cm^{-1} K^{-1}

Likewise, the thermal resistance of the cladding is given by[79]:

$$R_c = \frac{\ln(1-\frac{a}{b})}{2\pi H k_c} \tag{17}$$

where:

H = the length of the fuel rod .in cm
k_c = the thermal conductivity of the cladding W cm^{-1} K^{-1}
a = the radius of the fuel in cm
b = the thickness of the cladding in cm

Finally, the thermal resistance of convection in the coolant is given by[78]:

$$R_h = \frac{1}{hA} \tag{18}$$

where:

h = the convective heat transfer coefficient of the coolant in W cm^{-2} K^{-1}
A = the outer surface area of the fuel rod in cm^2

The total thermal resistance of the cylindrical fuel is given by the sum of these three resistances. Consequently, the heat flow to the coolant (q) from the fuel rod is given by[78]:

$$q = \frac{(T_m - T_b)}{\mathrm{R}} \tag{19}$$

where:

T_m = the centreline temperature of the fuel
R = the total thermal resistance K W^{-1}

4.11.2 Temperature Distributions Along Fuel Channel

For the reactor design in this research, heat is removed from the fuel by coolant flowing parallel to the length of the fuel rod. Due to axial buckling, the heat generation is not constant along the rod's length. Therefore, the temperature of the coolant does not increase linearly as it travels the length of the core. Rather, the heat generation of the fuel as a function of axial position (z) resembles a cosine function centred at the reactor's midplane. Throughout this research, all heat transfer approximations assume a perfectly flat neutron flux in the radial direction such that the heat generation in each fuel rod is equal to that of the central fuel rod. For the central fuel rod, the relationship may be written as[80]:

$$q''' = q'''_{max}\cos(\frac{\pi z}{H}) \tag{20}$$

where:

q''' = the volume specific heat production of the fuel in W cm^{-3}
q'''_{max} = the volume specific fuel production of the fuel at the midplane of the core in W cm^{-3}
H = the length of the fuel rod in cm
$-\frac{H}{2} \leq z \leq \frac{H}{2}$

Reflecting this relationship, the temperature of the coolant [T_b(z)] along the fuel channel may be written as[80]:

$$T_b(\mathrm{z}) = T_{b0} + \frac{q'''_{max} V_f}{\pi \omega c_p}\left[1 + \sin(\frac{\pi z}{H})\right] \tag{21}$$

where:

T_{b0} = the temperature of coolant entering the reactor core in ^{O}C
V_f = the volume of fuel in the fuel rod in cm^3
ω = mass flow rate of the coolant in the fuel channel in kg s^{-1}
c_p = the heat capacity of the coolant at the bulk coolant temperature in W kg^{-1} K^{-1}

Consequently, the maximum coolant temperature occurs at the outlet of the core. This temperature may be computed by[80]:

$$T_{b,max} = T_{b0} + \frac{2q'''_{max} V_f}{\pi \omega c_p} \tag{22}$$

Conversely, Equation 22 may be employed to calculate the required coolant mass flow rate when heat generation, coolant inlet temperature and coolant outlet temperature are specified.

In a similar fashion, the cladding temperature along the core's length may be written as[80]:

$$T_c = T_{b0} + \frac{q'''_{max} V_f}{\pi \omega c_p}\left[1 + \sin(\frac{\pi z}{H})\right] + q'''_{max} V_f R_h \cos(\frac{\pi z}{H}) \quad (23)$$

and the maximum cladding temperature may be computed by[80]:

$$T_{c,max} = T_{b0} + q'''_{max} V_f R_h \left[\frac{1+\sqrt{1+\alpha^2}}{\alpha}\right] \quad (24)$$

where:

$$\alpha = \pi \omega c_p R_h \quad (25)$$

Unlike the coolant temperature, the maximum cladding temperature does not occur at the outlet of the reactor. Rather, the axial position of the maximum temperature ($z_{c,max}$) may be computed by[80]:

$$z_{c,max} = \frac{H}{\pi} cot^{-1}(\alpha) \quad (26)$$

Finally, the fuel temperature along the coolant channel behaves much alike the cladding temperature although it is augmented by the total thermal resistance. The fuel temperature at an axial position (z) may be written as[80]:

$$T_m(\mathrm{z}) = T_{b0} + \frac{q'''_{max} V_f}{\pi \omega c_p}\left[1 + \sin(\frac{\pi z}{H})\right] + q'''_{max} V_f R \cos(\frac{\pi z}{H}) \quad (27)$$

The maximum fuel temperature may be computed by[80]:

$$T_{m,max} = T_{b0} + q'''_{max} V_f R \left[\frac{1+\sqrt{1+\beta^2}}{\beta}\right] \quad (28)$$

where:

$$\beta = \pi \omega c_p R \quad (29)$$

and the location ($z_{m,max}$) may be computed by[80]:

$$z_{m,max} = \frac{H}{\pi} cot^{-1}(\beta) \quad (30)$$

4.12 Estimation of Organic Coolant Degradation

A study by the Massachusetts Institute of Technology (M.I.T.) investigated the degradation of terphenyl mixtures under reactor conditions. Drawing from this research, the coolant degradation rate may be estimated for the reactor at steady-state using the following relationship:[81]

$$W_T = w_i(C^F - C) = \frac{G}{11.65} r M_L \quad (31)$$

where W_T is the total terphenyl degradation rate in grams per hour. The feed rate of new coolant in grams per hour is denoted by w_i, the terphenyl concentration as a weight percentage is C^F and the steady-state concentration of terphenyl as a weight fraction is C. The terphenyl molecules degraded per 100 eV absorbed by the coolant is denoted by G and the energy absorbed by the coolant in watts is comprises the term rM_L.

CHAPTER 5: DESIGN TOOLS

5.1 Introductory Comments

As previously mentioned in Section 3.1, the OCR in this research will be designed by using two fundamentally different computer codes to simulate the reactor's neutronics. A deterministic code can compute the average neutron behaviour by numerically solving the mathematical equations governing the neutron transport. Contrastingly, a probabilistic code statistically analyzes the histories of many neutrons in a simulation to infer the average neutron behaviour of the system[82]. A dual code approach using both types of code provides verification of results when a particular result from one method is reproducible using the other method. In this research, the probabilistic code MCNP 6 and the deterministic code WIMS-AECL are employed to simulate the reactor's neutronics.

5.2 MCNP 6

Created by Los Alamos National Laboratory (LANL), MCNP 6 is a versatile Monte Carlo radiation transport code applicable to various simulations and particle types. MCNP 6 tracks particles over continuous energy ranges by interpolating values from nuclear data libraries. MCNP 6 is an amalgamation of two previously released versions of the code by LANL; MCNP 5 and MCNP X[83]. The primary purpose of MCNP 6 in this research is the computation of k_{eff} eigenvalues for the reactor.

5.2.1 The Monte Carlo Method

Reflecting the use of random numbers, the Monte Carlo method derives its name from the analogous concept of rolling dice or spinning a roulette in a casino. The method is employed in reactor neutronics to replicate the random process of particle interactions whereby individual particle interactions are simulated sequentially. These interactions are probabilistically governed by the various cross sections of the material. By sampling the histories of many particles in a simulation, the method can infer the average particle behaviour[84]. Figure 8 illustrates the Monte Carlo method as applied to an incident neutron travelling in a fissile medium.

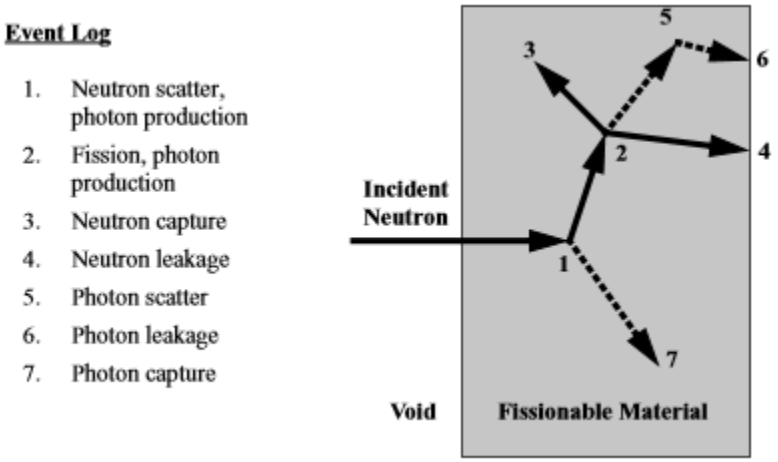

Figure 8: Monte Carlo Method Applied to an Incident Neutron[84]

In Figure 8, each of the seven numbered events represent a particle interaction where random numbers determine the location and type of the event. In the diagram, solid arrows denote the paths of neutrons while dotted arrows indicate photon paths. In the first event, the incident neutron is scattered producing a photon. Additional particles produced by an interaction are stored for later analysis. The incident neutron is then consumed by fission in the second interaction. This event produces two neutrons and a photon. The method selects one neutron to follow first and it is subsequently captured by the medium at the third event. The last neutron stored is the first to be tracked and it is terminated when it leaks from the medium in the fourth event. Returning to the photons, the method selects the last photon stored to analyze first. This photon is scattered in the fifth event and then leaks from the medium in the sixth event. Finally, the method follows the photon from the first event to the seventh event where it is captured by the medium. By accumulating many more particle histories in this manner, a statistical basis is formed and the average particle behaviour may be inferred[84].

5.2.2 Error in the Monte Carlo Method

As the Monte Carlo method is a statistical process, the results obtained by this method are mean values with associated standard deviations. Concerning precision and relative error, confidence intervals for a result can be estimated by the Central Limit Theorem. This means that with sufficiently large numbers of particle histories, the true result has a 68% chance of being within one standard deviation of the mean result and a 95% chance of being within two standard deviations of the mean result. However, this is only an estimation of the precision of the Monte Carlo method. The accuracy of a result can only be validated through comparison with experimental results[85].

5.2.3 MCNP Nuclear Data Libraries

As mentioned in Section 5.2, MCNP employs various nuclear data libraries to provide continuous energy input for use in simulations. Nuclear data libraries contain data representing various neutron and photon interactions that occur in simulations. Neutron interaction tables for around one hundred isotopes are contained in these libraries. MCNP's libraries are compiled from various sources such as the Evaluated Nuclear Data File (ENDF) and the Evaluated Nuclear Data Library (ENDL). The data in these libraries are continuously updated, revised, and expanded[86].

5.2.4 MCNP Input

In general, a MCNP 6 input file can be considered in three sections; the "cell cards", the "surface cards", and the "data cards".

In an MCNP model, the volume of interest, in this case the reactor, is subdivided into many small volumes known as cells. Each cell is composed of a single homogenized material. A cell card specifies the intersections, unions, and complements of surfaces that bound a particular cell[87]. The sense of a bounding surface is integral to specifying the space contained in a cell. Considering the points immediately located on a surface to have a sense of zero, points located on one side of the surface are said to have a positive sense while those on the opposite side are said to have a negative sense[87]. For instance, the interior of a cylindrical surface has a negative sense and positive sense would refer to the region outside of the surface. Additionally, the cell card further describes a cell by assigning it a material and material density. A density of zero would denote a void cell[87].

Surface cards define the surfaces that bound cells. The most common surfaces in MCNP are planes, cylinders, and spheres. MCNP operates in Cartesian coordinates. The three methods of defining a surface are by equations, points, or macrobodies[88]. Definition by equations requires the user specify a

mnemonic for the particular surface and appropriate coefficients for the corresponding surface equation. For example, a plane normal to the x-axis is represented by the mnemonic PX and requires card entry to specify its distance from the x-axis[88]. An alternate method of defining a surface is using points. A surface card of this type requires a user input of X, Y, or Z to prescribe an axis of rotational symmetry. This entry is followed by the coordinates of either one, two, or three points to define planes, linear surfaces or quadratic surfaces respectively[89]. The final method of surface specification is by using macrobodies. Essentially, a macrobody is a predetermined combination of surfaces that MCNP recognizes as a singular surface. The simplest example is a box designated by the card entry "BOX" and further specified by coordinates of one corner and three vectors to define the faces of the box. MCNP recognizes many other macrobodies including rectangular parallelepipeds, spheres, cylinders and various prisms[90].

Data cards serve a wide range of purposes that generally prescribe information vital to the type of simulation and the user's desired output. The various data cards are too numerous to be explained individually in this section, but there are several that are integral to the simulations in this research. First, material specification cards are used to define the composition of materials that have been assigned previously in cell cards. The card consists of nuclide identifiers for each component of the material and its respective mass or atomic fraction. A nuclide identifier has the form "ZZZAAA.abx" where "ZZZ" is the atomic number of the nuclide. "AAA" is either the mass number of the specific isotope or "000" for naturally occurring elements. The remaining portion of the identifier is optional with "ab" specifying a particular nuclear data library and "x" denoting a class of data. Atomic fractions are represented as positive numbers while mass fractions are input as negative numbers[91]. In criticality computations, the data card KCODE is required to prescribe a criticality source for the software to use in determining k_{eff}. This data card specifies the following necessary information for the simulation[92]:

a. number of particle histories per cycle;
b. initial guess for k_{eff};
c. number of cycles excluded from tallies; and
d. total cycles in simulation.

In conjunction with the KCODE card, the KSRC card in also necessary in criticality simulations. This card contains coordinates that designate source points for the first cycle. One of the initial source points must be located within a fissile material. The software will evenly distribute the total particles per cycle between the source points specified. While running, MCNP maintains a SRCTP file that stores fission sites from previous cycles. These locations replace the initial source points in subsequent cycles[92].

5.2.5 MCNP Physics

In MCNP, each individual particle simulated produces a particle track from a specified source[93]. Each particle track is assigned a weight to compensate for deviation from natural distributions. While the default is unit weight for each particle, the weight can be biased to enhance results in an area of interest[93]. In this research, the default particle weight is maintained while calculating k_{eff} for the entire reactor system. As well, neutrons and photons are the specific particles analyzed in these simulations.

To compute criticality and multiplication within a system, MCNP samples the collisions along a particle track. If a particle interaction results in additional particles, tracks are produced for the new particles with the weight of the initial track divided amongst the resultant number of tracks[93]. The distance a particle travels within a medium before a collision is given by[93]:

$$\ell = -\frac{1}{\Sigma_t} ln(\xi) \tag{32}$$

where Σ_t is the total macroscopic cross section of the medium and ξ is a random number greater than zero but less than or equal to one.

Upon collision of a particle with a nucleus, MCNP follows a routine to simulate the event. First, a random number determines the collision nuclide should the medium be composed of multiple nuclides[93]. Second, MCNP utilizes a free gas thermal treatment to account for the thermal motion of the collision nuclide. This process corrects the elastic cross section to capture the effect of the collision nuclide's velocity on the collision kinematics[93]. Next, photons resulting from the collision are generated when applicable and when enabled by the simulation[94].

Absorption and subsequent termination of the particle are simulated next according to the probability given by the ratio of the absorption cross section to the total cross section of the collision nuclide[95]. Assuming absorption does not occur, scattering is simulated next using a similar process. In this case, the elastic or inelastic nature of the interaction is probabilistically simulated using the ratio of the respective scattering cross section to the total cross section of the collision nuclide for events other than absorption. Should the scattering be inelastic, another random number is applied to determine the excitation of the collision nucleus[95].

5.3 WIMS-AECL

WIMS-AECL is the deterministic code to be employed in this research. WIMS-AECL functions in two dimensions and can provide numerical solutions for multigroup neutron transport in many reactor physics scenarios. Geometries that can be represented by cluster cells are preferable for WIMS-AECL simulations. Although a two-dimensional code, the user can specify geometric bucklings to permit WIMS-AECL to account for finite reactor effects[96]. Its two-dimensional nature allows WIMS-AECL to efficiently perform time-consuming computations such as fuel depletion and burnup routines.

The initial versions of WIMS were created by United Kingdom Atomic Energy Authority Establishment, Winfrith, U.K., and WIMS-AECL is an independent version developed in Canada by Atomic Energy of Canada Ltd. at its Chalk River Laboratories[96].

The input data of a WIMS-AECL input file may be categorized into two groups. First, the "Main" data establish the foundation for the simulation being performed by WIMS-AECL. It contains the geometry and material composition of the lattice cell, and defines the solution method and burnup control. Second, the "Edit" data specify the treatment of results from the main transport calculation. Geometric bucklings are part of the Edit data. Edit data largely depend of the user's desired results from the simulation[97].

As mentioned, WIMS-AECL solves the neutron transport equation in two dimensions for the prescribed geometry and materials. However, assumptions of rotational symmetry where possible may reduce the computational cost of the simulation. WIMS automatically assumes axial symmetry across the xy-plane thereby requiring user defined bucklings to constitute finite reactor effects. The output of a WIMS-AECL simulation is normalized to 1 cm of core length. Therefore, the results must be applied to the finite core length to obtain reactor-specific results[98].

CHAPTER 6: PRELIMINARY MODELLING OF SLOWPOKE-2

6.1 Introductory Comments

Due to the sheer number of parameters and variables, the notion of freely conceptualizing a new reactor design is arduous and impractical. However, the task may be simplified by approaching the design in a manner that reduces or restricts the number of design choices. In this research, this is accomplished in two ways. First, the design of the OCSL reactor is based on simulation of the reactor's neutronics at steady-state only. Assessment of the reactor's neutronics in transient states as well as detailed thermal hydraulic analyses are to be added after the initial design to enhance the overall model of the reactor. Secondly, the design of the OCSL reactor is an extension of an existing reactor design, the SLOWPOKE-2 research reactor.

Prior to introducing the organic coolant and extending the reactor's power, a suitable model of the SLOWPOKE-2 is established to serve as a baseline for further design. For this research, a MCNP 4A model of RMCC's SLOWPOKE-2 by Pierre[99] is reproduced using MCNP 6. Completed in 1996, the model by Pierre was validated with experimental results from the SLOWPOKE-2 reactor at RMCC. Reproduction of this model first verifies the accuracy of the current MCNP version employed in this research. Furthermore, the light water coolant in this preliminary model is replaced by the organic coolant, HB-40, to subsequently confirm adequate simulation of neutronic behaviour in the organic.

6.2 MCNP 4A Model of the SLOWPOKE-2

The MCNP 4A model of the SLOWPOKE-2 reactor by Pierre encapsulated all components of the reactor within the reactor pool. This included the fuel, the reflector, the control rod, irradiation sites, the thermal column, the reactor container, and the surrounding pool. When created, the model adapted dimensions from original technical drawings while reconciling discrepancies to best replicate the RMCC SLOWPOKE-2 from which experimental results were obtained. Throughout this section, images created using the VISED software of MCNP X are presented to aid in the description of the MCNP 4A model. It is important to note that these images visualize the recreated input and not the original input from the work of Pierre. A cross-section of the SLOWPOKE-2 as represented in this model is displayed in Figure 9.

The specifications of the fuel in the model are summarized in Table 3. Each fuel pin is represented by an internal cylinder of the uranium dioxide fuel encased by an air gap and zirconium cladding. The material card for the fuel represents uranium dioxide as a homogenized mixture of oxygen-16, uranium-238 and uranium-235 where the uranium-235 is enriched to 19.89 weight percent. Similarly, a mixture of nitrogen and oxygen represented the air and pure zirconium was assigned to represent the cladding. Although other metals are present in the zirconium alloy, their low concentrations, and the overall small thicknesses of cladding in the model led to a simplified representation of the material.

The SLOWPOKE-2 core contains 198 fuel pins arranged across a triangular lattice. The elements are uniquely distributed in a star-like pattern to maximize the thermal neutron flux at the irradiation sites. The fuel pin layout is visualized in Figure 10.

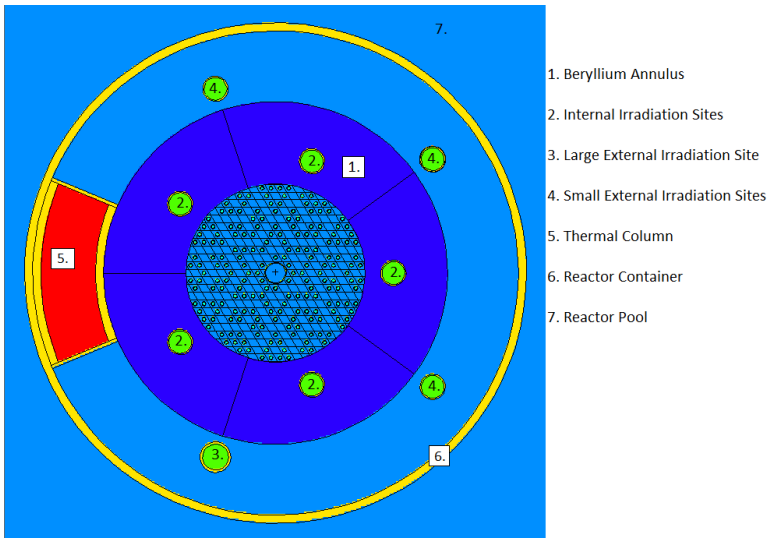

Figure 9: Cross-section of SLOWPOKE-2[99]

Table 3: Specifications of Fuel in MCNP 4A Model[99]

Fuel (enrichment)	Uranium Dioxide (19.89% by weight)
Fuel Pin Lattice Pitch	1.10363 cm
Fuel Pin Diameter	0.4128 cm
Fuel Pin Air Gap Thickness	0.0056 cm
Fuel Pin Cladding (thickness)	Zirconium (0.05 cm)
Fuel Pin Length	22.6975 cm

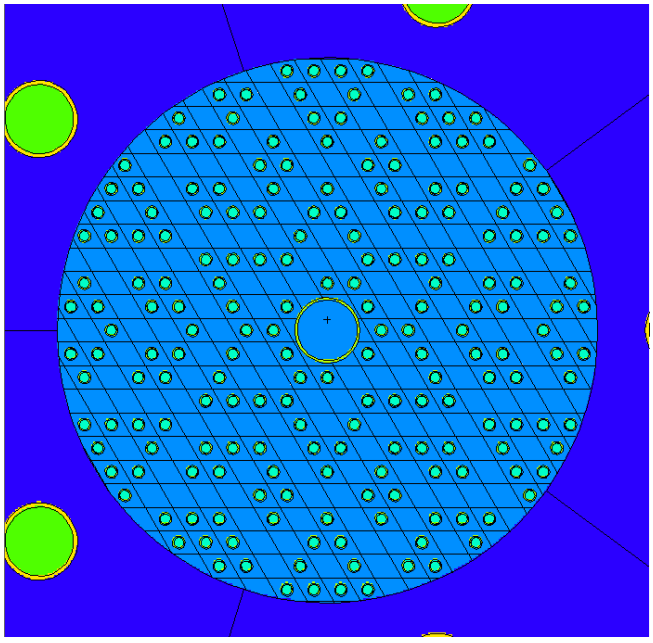

Figure 10: SLOWPOKE-2 Fuel Layout

The reflector of the SLOWPOKE-2 is comprised of three pieces; a bottom disc, a top shim and an annulus surrounding the core. The bottom disc measures 32.22625 cm in diameter and is 10.16 cm thick. The top reflector shim is a half disc with a cutaway for the central control rod. The outer radius is 12.065 cm and the inner radius is 1.3890625 cm. The shim was 0.15875 cm thick when the MCNP 4A model was created. In the years since, additional shim plates have been added to counteract excess reactivity lost due to depletion of the fuel and extend the life of the fuel in the core. Presently, the available space for shim plates in the RMCC SLOWPOKE-2 has essentially been exhausted and the next step will be refuelling reactor. The annulus of the reflector extends the length of the fuel bundle at 22.748cm long. Its inner and outer radii are 11.049 cm and 21.2344 cm respectively for an overall thickness of 10.1854 cm. The reflector annulus houses five internal irradiation sites. All portions of the reflector are assigned the same beryllium material. Unlike the zirconium cladding previously, the impurities within the beryllium were deemed significant to the outcome of the neutronics simulation. Therefore, all nuclides available with MCNP 4A were included in the material card.

The SLOWPOKE-2 control rod is comprised of a hollow cadmium tube encased in an aluminum alloy sheath. In the model, it is represented as three cells; the air filling the interior of the cadmium tube, the cadmium itself, and the surrounding aluminum. The cadmium tube has inner and outer radii of 0.09652 cm and 0.14732 cm respectively and is 24.76 cm long. The aluminum sheath has a diameter of 1.24732 cm and is 40.64 cm long. The tube is filled with the same air material as in the fuel. The cadmium material card is defined as elemental cadmium whereas the aluminum alloy material card is defined according to the AL 6061 T6 alloy specified. A side-profile section-cut of the control rod displaying the three materials is presented in Figure 11.

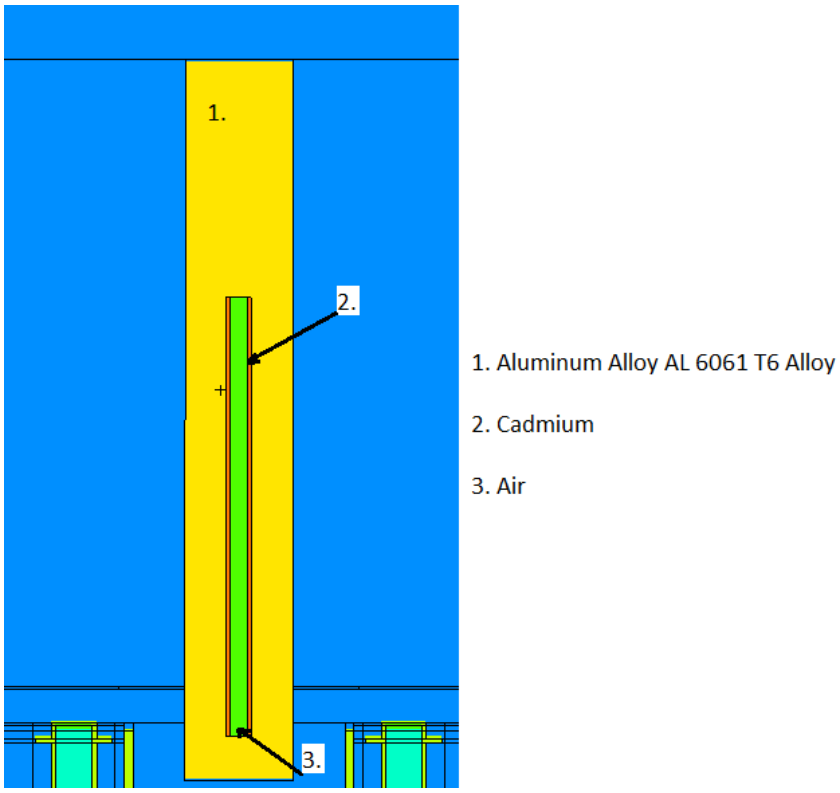

Figure 11: Control Rod Side-profile Section-cut

The RMCC SLOWPOKE-2 is equipped with five internal irradiation sites in the beryllium annulus and four external irradiation sites. For ease of input, the geometry of the internal sites was simplified in the MCNP 4A model so that they were aluminum tubes filled with air extending from the pool-top to their terminus in the annulus. The inner and outer radii of the aluminum tubes are 1.40208 cm and 1.56718 cm respectively the tube is 5.15332 m long. Of the four external irradiation sites, there is one large-diameter site and three smaller sites where one of the smaller sites is also lined with cadmium. Like the internal sites, these were simplified to be straight tubes of aluminum from the pool-top to a terminus at the reactor. The smaller sites are identical to the internal sites. In the case of the cadmium-lined site however, a 0.0508 cm thick layer of cadmium on its interior. The large site has inner and outer radii of 1.600 cm and 1.905 cm respectively. The cells that compose the irradiation sites are assigned the same material cards for air, AL 6061 T6 and cadmium that were mentioned previously. A side-profile section-cut of the reactor displaying an internal and external irradiation site is presented in Figure 12.

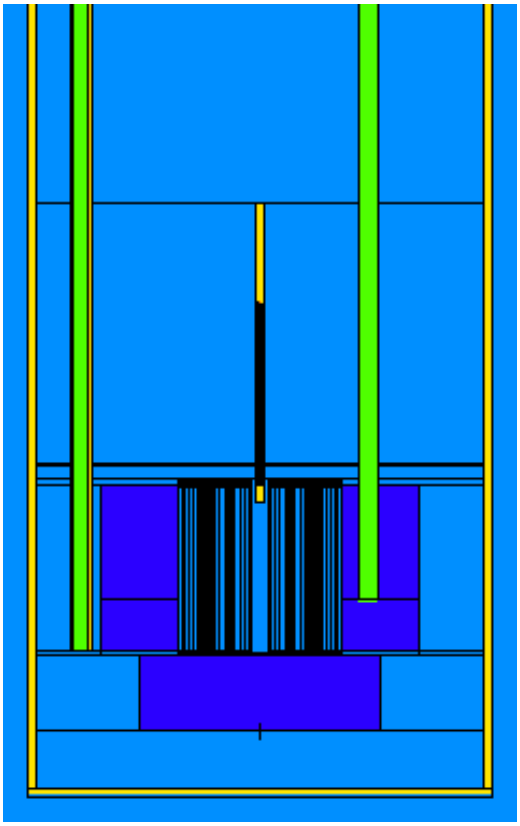

Figure 12: Side-profile Section-cut with Irradiation Sites

The thermal column of the SLOWPOKE-2 is an aluminum chamber filled with heavy water. It is situated between the reflector annulus and the reactor container. When the MCNP 4A model was written, an exact measurement of the inner and outer wall thickness was not available. These walls were estimated to be 1 cm thick. To support this estimate, a study confirmed that an error of 1 mm or less would not significantly impact the results of the KCODE simulation. The side walls of the thermal column are 1.082 cm thick. The column is 20.6975 cm long. The chamber walls are assigned the same AL 6061 T6 alloy previously mentioned while the heavy water material card is represented as a stoichiometric mixture of deuterium and oxygen.

The reactor container is a vessel made of aluminum and closed at the pool-top that surrounds the SLOWPOKE-2 core. It separates the light water coolant within the vessel from the surrounding pool water. The container is 1 cm thick and has an inner radius of 30 cm. It extends 5.42 m into the pool. The container is assigned the same AL 6061 T6 alloy material card described from previous components.

The pool that surrounds the SLOWPOKE-2reactor provides a large excess of cooling capacity while also serving as shielding from neutron radiation. In the model, the pool is represented by a large cylinder of light water in which the reactor and all components are contained. The pool is 5.64 m deep and 2.66 m in diameter. For perspective, the top of the fuel bundle is at a depth of about 5 m from the pool-top. Light water coolant fills all space within the pool that is not occupied by reactor components. The material card for light water is written as a stoichiometric mixture of hydrogen-1 and oxygen.

6.3 Comparison of SLOWPOKE-2 Models in Excess Reactivity Calculation

With the input of the MCNP 4A model by Pierre recreated, the KCODE simulation is recreated using MCNP 6. To best replicate the simulation, the definitions of cells, surfaces, and materials from MCNP 4A are retained as much as possible if not entirely. Additionally, the following conditions are maintained from the original simulation:

- the SLOWPOKE-2 core is freshly fueled;
- the entire reactor is at room temperature (the default when no temperature is specified with a TMP card);
- the control rod is withdrawn above the core;
- each cycle of the simulation contains one hundred thousand neutron histories; and
- the simulation consists of two hundred cycles with the first twenty cycles omitted from calculation of the reactor's effective multiplication factor (180 active cycles).

The results of the MCNP 6 KCODE simulation with the MCNP 4A results and experimental commissioning data used by Pierre are presented in Table 4.

Table 4: Comparison of SLOWPOKE-2 Models with Commissioning Data

	Effective Multiplication Factor (k_{eff})	Standard Deviation (σ)	Excess Reactivity (ρ) [mk]
Commissioning Data[100]	1.00316	N/A	3.15
MCNP 4A Model[100]	1.00318	0.0002	3.17
MCNP 6	1.00330	0.00018	3.29

Some discrepancy exists between the two versions of MCNP evidenced by the greater excess reactivity obtained from MCNP 6. However, it was unlikely that the newer code would exactly reproduce the results by Pierre. As nuclear data libraries are constantly revised, the various cross sections of the nuclides in the simulation are likely to have been updated in the decades since the MCNP 4A model was created. Therefore, a small discrepancy of 0.12 mk between the models is encouraging. This result sufficiently demonstrates that the version of MCNP used in this research is functioning properly. Within the scope of this research, this is satisfactory accuracy for designing the new reactor. Regarding the standard deviations in the two models, the precision of MCNP 6 is as good if not better than MCNP 4A.

6.4 Introducing Organic Coolant to SLOWPOKE-2 Model

The functioning SLOWPOKE-2 model presents an opportunity to further evaluate the suitability of MCNP 6 for designing the reactor in this research. With general knowledge of the elemental makeup and density of HB-40 at room temperature, hand calculations can predict how its moderation of neutrons will compare to light water under similar conditions. Table 5 presents calculation of macroscopic absorption and scattering cross sections for both light water and HB-40. Regarding absorption, HB-40 presents about a twenty percent decrease in macroscopic cross section from light water. This indicates an improvement over light water as fewer neutrons will be lost to absorption in the coolant/moderator. While a low absorption cross section is necessary, the scattering cross section of a moderator is a much stronger indicator of effectiveness. In this case, HB-40 sees a reduction in macroscopic scattering cross section of about thirty six percent from light water. The moderating power unifies absorption and scattering to provide a complete measure of moderator effectiveness. The moderating power of HB-40 is about half of that of light water. This means that neutrons must travel further before being moderated to a thermal energy level. Based on these calculations, a reasonable prediction would say that HB-40 will perform below light water as a moderator given similar circumstances. It is possible to test this prediction using the SLOWPOKE-2 model from the previous section and replacing the light water coolant with HB-40. Conversely, this simulation will further demonstrate MCNP 6's capability to represent the organic coolant in further simulations in this research.

Table 5: Calculation of Absorption and Scattering Cross Sections for Light Water and HB-40[101 102]

Material	Light Water (at 20^{O}C)	HB-40	
Element		Hydrogen	Carbon
Atomic Weight	18	1.008	12.011
Atomic Fraction	n/a	0.5370	0.4630
Mass Fraction	n/a	0.0887	0.9113
Density (g cm^{-3})	1.00	0.0884	0.9076
Atomic Density / 10^{23} (cm^{-3})	0.334	0.5279	0.4551
σ_a (barns)	0.66	0.332	0.0034
Σ_a (cm$^{-1)}$)	0.022	0.0175	0.00015
Total Σ_a (cm^{-1})	0.022	0.0177	
σ_s(barns)	103	38	4.75
Σ_s (cm$^{-1)}$)	3.45	2.0	0.216
Total Σ_s (cm$^{-1)}$)	3.45	2.2	
ξ	0.96	0.91	
Slowing Down Power ($\xi \Sigma_s$) [cm^{-1}]	3.3	2	
Moderating Power ($\xi \Sigma_s / \Sigma_a$)	151	113	

Replacing the light water in the SLOWPOKE-2 simulation is a relatively simple task. The material card for light water in the previous model is overwritten with a material definition for HB-40. This step requires an approximate ratio of carbon to hydrogen to define the material in MCNP. For modelling simplicity, the composition of HB-40 is drawn from its feed composition because the steady-

state composition is specific to the operating parameters and the coolant reprocessing. The mixture of biphenyl, o-terphenyl and hydro-terphenyl in the feed composition results in a ratio of 17.94:20.81 carbon to hydrogen respectively[102]. The simulation is run identically to the conditions stated in the previous section.

Upon initial simulation, the effective multiplication factor for the reactor drops to 0.97108 from 1.00330 with the swap of coolants. This result agrees with the prediction made previously and seemingly confirms that HB-40 will underperform when compared to light water under similar conditions.

To extend this design exercise, subsequent simulations add fuel pins to the core to determine the amount of fuel required for criticality. The fuel cage of the SLOWPOKE-2 reactor can hold up to 342 fuel elements. Therefore, adding fuel elements in the vacancies improves the fuel to moderator ratio and should reachieve criticallity. New elements are added systematically and incrementally from the inner positions outward and always symmetrically about the core. The series of simulations performed in this exercise are presented in Table 6 with their resulting effective multiplication factors. Criticality was achieved with a fuel layout consisting of 324 pins. The cross section of this core is shown in Figure 13.

Table 6: Addition of Fuel to SLOWPOKE-2 Core with HB-40

Number of Fuel Pins	Effective Multiplication Factor (k_{eff})	Standard Deviation
198	0.97108	0.00021
218	0.97852	0.00020
260	0.98629	0.00022
286	0.99132	0.00021
296	0.99380	0.00022
324	1.00066	0.00021

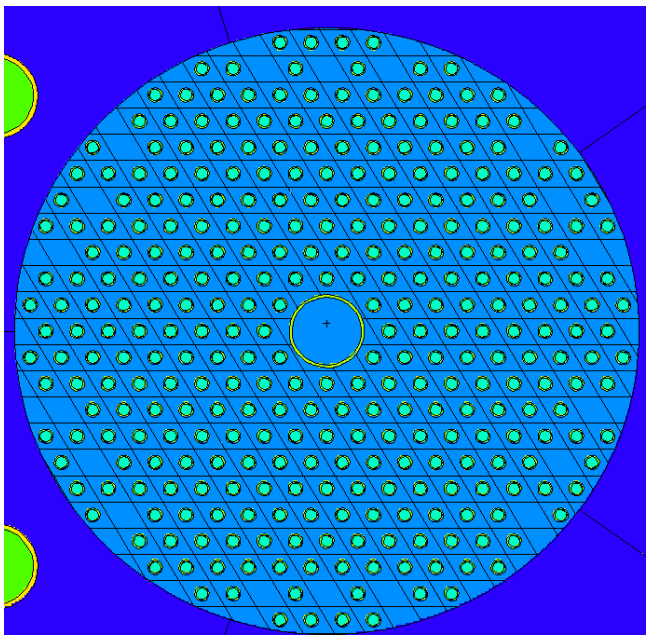

Figure 13: Critical SLOWPOKE-2 Core with HB-40

6.5 Temperature and Void Fraction Coefficients of Reactivity for HB-40 Moderator

A design criterium of this research is to address and demonstrate the potential for inherent safety of the organic-cooled SLOWPOKE design. To accomplish this in the most basic sense, the design tools must be capable of demonstrating negative temperature and void fraction coefficients of reactivity. From the previous section, the functioning model of SLOWPOKE-2 with HB-40 coolant provides an opportunity to assess this capability in MCNP 6. For this purpose, the model with 324 fuel pins that is supercritical at room temperature is employed in establishing these coefficients.

Regarding the temperature coefficient of reactivity, the specific component where temperature is being considered is the HB-40 moderator. In the MCNP model, a Free-Gas Thermal Temperature, or TMP, card is added to every cell containing HB-40. These cards allow for cell temperatures in MeV to be assigned throughout the model. As the initial simulation used the default of room temperature, temperatures within the range of 20 ^{O}C to 55 ^{O}C are employed to establish the coefficient. For each new temperature, the density of HB-40 must be updated correspondingly. Each temperature constitutes a new model that is then simulated as in the previous sections. The variation of the excess reactivity in the reactor with moderator temperature is presented in Figure 14.

The process for the void coefficient of reactivity is similar. However, only the densities of cells containing the moderator, HB-40, are changed. The coefficient is established over a range of void fractions from zero to thirty percent. The variation of the excess reactivity in the reactor with void fraction is presented in Figure 15. In the simulation, a decreased coolant/moderator density represents the void fraction according to Equation 12.

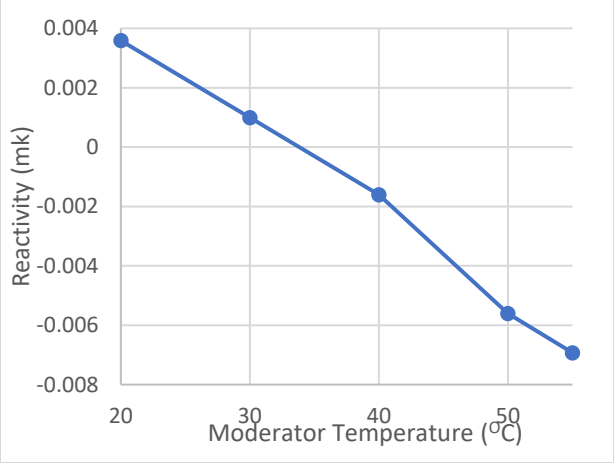

Figure 14: Variation of Reactivity with Moderator Temperature

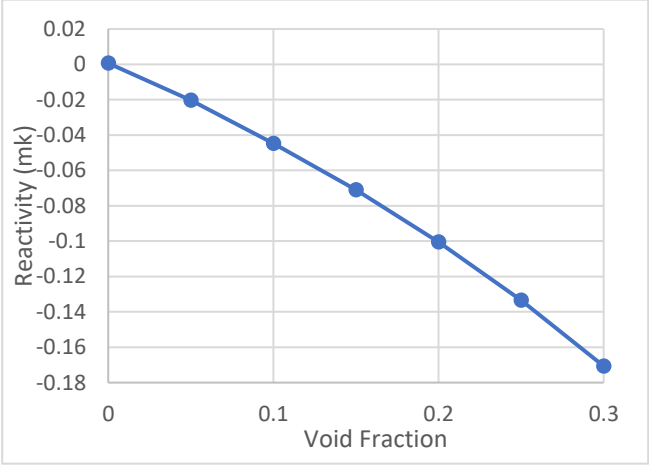

Figure 15: Variation of Reactivity with Void Fraction

The plots presented in Figure 14 and Figure 15 demonstrate negative temperature and void fraction coefficients of reactivity, respectively, for the reactor in this case. These coefficients are defined as the gradients of these curves. These results are encouraging because they first confirm that MCNP 6 can be used to demonstrate these coefficients in future design work. Secondly, these results are a good initial indication of inherent safety for this reactor concept, since they are essential conditions to inherent safety, although not sufficient. The actual organic-cooled SLOWPOKE will operate at a significantly higher temperature, so these predictions are limited in that respect. However, this approach to the

simulation of the reactor will be capable of determining the reactivity coefficients at higher temperatures as well.

6.6 Lattice Pitch Trial for SLOWPOKE-2 with HB-40 Moderator

As a final exercise in this preliminary modelling, the lattice pitch of fuel pins in the core is considered to further confirm appropriate representation of HB-40 neutronic behaviour in MCNP. In a heterogenous lattice of fuel and moderator, there is an ideal spacing or lattice pitch between fuel elements for which the effective multiplication factor is maximized. This lattice pitch is directly related to the scattering cross section of the moderator and thus the number of collisions required to thermalize neutrons. Referring to the calculations in Table 5, the lower scattering cross section of HB-40 should require a larger pitch between fuel pins than water with similar fuel arrangement. As the SLOWPOKE-2 core was designed for light water, it is reasonable to predict that the pitch is too small for HB-40 moderation and that the effective multiplication factor will improve if the pitch is increased.

To test this prediction, the outermost sixty-six fuel pins are deleted to allow for the lattice to be expanded. Starting with simulation at the design lattice pitch of the SLOWPOKE-2, the lattice pitch is increased in successive simulations and the resulting effective multiplication factors are tracked. Again, these simulations maintain the conditions stated in Section 3.2. The results of the lattice pitch trial are presented in Table 7 with a plot displayed in Figure 16. The cross section of the core with the final 1.25 cm lattice is pictured in Figure 17.

Table 7: Lattice Pitch Trial Results – 258 Pin SLOWPOKE-2 Core

Lattice Pitch (cm)	Effective Multiplication Factor (k_{eff})	Standard Deviation
1.10363 [Design Pitch]	0.92171	0.00021
1.15	0.94526	0.00021
1.20	0.96786	0.00022
1.25	0.98750	0.00023

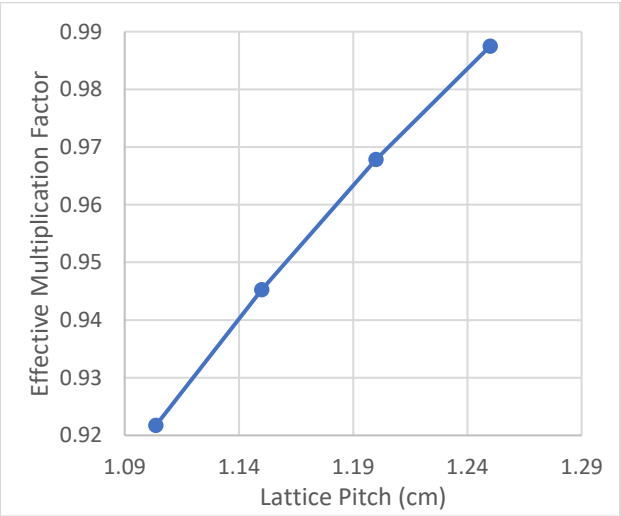

Figure 16: Plot of Lattice Pitch Trial

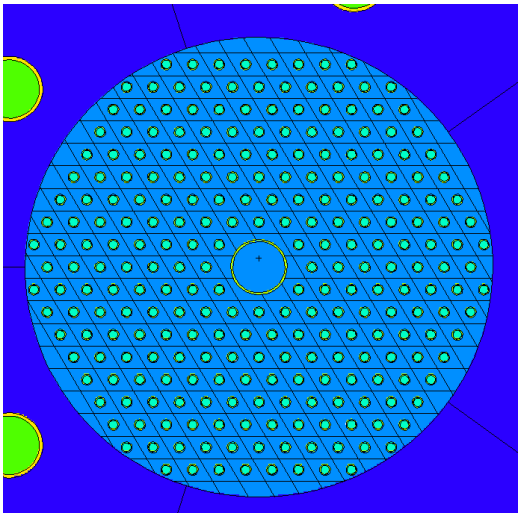

Figure 17: 258 Pin SLOWPOKE-2 Core with 1.25cm Lattice

The results clearly demonstrate that the optimum lattice pitch for the HB-40 moderator is much larger than the design pitch of the SLOWPOKE-2. Regarding Figure 16, no apparent plateau of the effective multiplication factor is shown in this range of lattice pitch sizes. Therefore, the optimum pitch must be significantly larger than those applied in these simulations. In future work, it will be necessary to identify this optimum pitch to properly design the Organic-Cooled SLOWPOKE Reactor. Overall, the results of this trial have further demonstrated the MCNP 6's capability to reproduce neutronic behaviour for HB-40. The simulation results have strongly agreed with theory-based predictions.

CHAPTER 7: OCSL REACTOR CORE DESIGN

7.1 Introductory Comments

The preliminary modelling from the previous chapter has demonstrated that an organic coolant, HB-40, can replace the water in the SLOWPOKE-2 and if provided with additional fuel, a critical reactor can be obtained. However, this modelling largely neglected the critical design constraint of extending the power of the reactor from 20 kW to 1 MW thermal power. Understandably, a core providing 1 MW will have to be larger than the SLOWPOKE-2 core and given the low vapour pressure of the coolant, will operate well above room temperature as assumed for the SLOWPOKE-2 models. The following chapter explains the design process employed to extend the power of the SLOWPOKE-2 core to arrive at an initial design of the OCSL reactor core. Furthermore, this chapter also presents the assumptions and simplifications necessary to achieve this design objective.

7.2 Simplifications to the SLOWPOKE-2 Model and General Assumptions

The SLOWPOKE-2 model adapted in the previous chapter was created to replicate certain experimental measurements from the RMCC SLOWPOKE-2. Therefore, it features a high level of detail as well as unnecessary components that would be either complicated or superfluous to include in the initial OCSL reactor design. To achieve a feasible core design, the reactor layout must be simplified to only essential components. Throughout this chapter and the remainder of this research, the OCSL reactor will be comprised of:

- the fuel pins in the core;
- the control rods in the core;
- an annular reflector radially surrounding the core; and
- the HB-40 coolant/moderator that surrounds all components.

To limit the possible permutations of the OCSL reactor core, the present diameter of the SLOWPOKE-2 fuel pin will be maintained although the length will be increased. Within the scope of this research, this choice is deemed reasonable to reduce the large number of variables at play in extending the reactor's power. Furthermore, the choice is appealing because using existing machining technology would likely reduce front-end costs for constructing prototypes.

This research is predominantly focusing on the reactor's neutronics and detailed thermal hydraulic analysis is relegated to future design work. To assume this course of action appropriately, several assumptions must be made regarding the reactor's thermal hydraulic design. First, the modelling in this research assumes that the coolant circulation pump supplies flow from below the core where an appropriate baffling arrangement directs the flow upwards in a perfectly vertical direction through the lattice of fuel pins. The coolant flow exits from the top of the core and travels through a theoretical heat removal loop before returning to the core via the aforementioned pump. Depending on the application of the reactor, the heat removal loop would likely be a steam generator or heat exchanger that would either support district heating or electrical power generation.

A second major thermal hydraulic assumption in this research is the temperature differential across the reactor core and the corresponding inlet and outlet temperatures. The choice is influenced by the operation of WR-1 where outlet temperatures often fell in the range of 320 ^{O}C to 425 ^{O}C and inlet temperatures ranged from 280 ^{O}C to 400 ^{O}C[103]. As the OSCL coolant is not to be pressurized, the outlet temperature is chosen to be 340 ^{O}C; slightly below HB-40's atmospheric boiling point of 342 ^{O}C. A fifty-

degree temperature increase across the core is chosen so that the inlet temperature of the coolant is 290 ^{O}C.

Finally, the design tools used to compute the reactor's neutronics do not permit temperature distributions within components. In MCNP, a temperature distribution across the fuel pins would require numerous subdivisions of the cells and individual temperature inputs for each cell. As this is impractical, average temperatures must be assigned to components in the reactor. Aside from the fuel and its cladding, all components and the HB-40 in the model are assigned an average temperature of 315 ^{O}C because it is exactly halfway between the inlet and outlet temperatures of the coolant. Given operation at steady-state, this assumption is reasonable for components that do not generate heat. The average temperatures of the fuel and its cladding are established iteratively during the lattice pitch optimization. The key detail of this assumption is that one temperature is assigned to the cells despite the temperature distributions present within them.

7.3 Computation of OCSL Core Dimensions

The first step in designing the core of the OCSL reactor is to estimate its critical dimensions. The simplest way to achieve this is from the geometric buckling of a cylinder using the modified one-group critical equation. In this case, the reactor is envisioned as a homogenous mixture of fuel and moderator. For simplicity, only the uranium-235 is considered as fuel in these calculations. The ratio of fuel to moderator is obtained from the cross-sectional areas of fuel and moderator in the lattice cell and their respective densities. These calculations result in a radius and length for the core. To simplify repetitions of these calculations, a calculator named mincrit.m was created using MATLAB® so that the user could obtain dimensions when altering parameters such as the pitch of the lattice cell. The default operation of mincrit.m outputs minimum critical dimensions for a cylinder. However, the user may fix either the radius or the length of the reactor and the other dimension will be computed according to the prescribed length or radius. Understandably, the default operation is preferable to reduce the fuel required for the core, but the provision was made in the case of thermal hydraulic constraints on the length of coolant channels.

The next step in the core design is to rationalize the results from mincrit.m for a heterogenous lattice of fuel pins. Fuel pins must be arranged to discretely approximate a cylindrical core. Another MATLAB® calculator called hexcircle.m was created to superimpose the radii computed by mincrit.m over a prescribed lattice and thus calculate the number of fuel pins in the core. Additionally, hexcircle.min writes the matrix that defines the reactor core for the MCNP input file.

At this stage, the core is defined by its length as well as the number of fuel pins distributed across the lattice. Although mincrit.m calculated minimum critical dimensions, the core will certainly be supercritical when simulated. This is due to simplifications in the mincrit.m calculation. First, a heterogenous arrangement of fuel and moderator will be more critical than a homogenous mixture of identical elemental composition. In a heterogenous mixture, the regions of pure moderator between fuel pins are much larger than the spaces between atoms of fuel in a homogenous mixture. As a result, neutrons in the heterogenous mixture are moderated more effectively resulting in greater number of fissions. Secondly, mincrit.m only considered uranium-235 as fuel and neglected uranium-238 and subsequent plutonium-239 production. This simplification leads to another underestimate of the core's reactivity. These limitations in the core size estimation, work in favour of the design, because excess reactivity is required for the core to have the desired lifespan for use in remote installations. To further consider this notion, a step was added to the mincrit.m calculation where the user may apply a factor, named *adjust* in the script, to the geometric buckling to help size the reactor to meet the desired excess reactivity. For example, when *adjust* is slightly less than one the size of the geometric buckling is

reduced, the reactor becomes larger, the excess reactivity increases, and the core will have a longer service life. The inverse becomes true if *adjust* is slightly greater than one. This function of mincrit.m aids in later sections of this chapter where a range of core sizes are required to vet the best core for the OCSL reactor.

7.4 Initial Thermal Hydraulic Estimation

As previously stated, the scope of thermal hydraulic analysis employed at this stage of the OCSL reactor design is limited. However, certain consideration is still required to ensure the reactor remains feasible given the assumed coolant inlet/outlet temperatures and the calculated dimensions of the core. For instance, the temperature distributions along the coolant channels must be well behaved and within bounds of safety. Additionally, the required flow rate of coolant must not necessitate an unrealistically large circulation pump.

The simplest way to estimate the thermal hydraulics of the OCSL core is to employ Newton's Law of Cooling along a single fuel channel. Consequently, this method requires two major assumptions for the results to apply to the whole core. First, the method assumes that the neutron flux across the core is perfectly flat so that the energy released by fission is the same in every fuel channel. Secondly, the method assumes that the neutron flux required to produce 1 MW of thermal output is achievable throughout the entire core.

To simplify repetitions of thermal hydraulic calculations, a MATLAB® calculator was created using the name htfuelchannel.m. In operation, the number and length of fuel pins are specified by the user and htfuelchannel.m performs the calculations according to Newton's Law of Cooling. The calculator delivers output consisting of the coolant mass flow rate, maximum temperatures for fuel and cladding, and complete temperature distributions for fuel, cladding and coolant. The properties of the coolant, such as cooling and heat capacity, are evaluated at the bulk coolant temperature of 315 ^{O}C using correlations developed specifically for HB-40 during the WR-1 research. The heat transfer coefficient of an organic coolant is generally about five times less than that of water under similar operation[104]. A modest estimate of the heat transfer coefficient of water in a power reactor is 25 kW m^{-2} K^{-1} [78]. Therefore, the heat transfer coefficient of HB-40 is estimated to be 5 kW m^{-2} K^{-1} in these calculations. Accordingly, attention must be paid to the turbulence of the coolant flow to ensure that this estimate remains reasonable.

7.5 Lattice Pitch Optimization

As concluded in Chapter 6, the ideal lattice pitch for the fuel pins with HB-40 moderator was much larger than the design pitch in the SLOWPOKE-2 core. Therefore, this ideal pitch must be determined to ensure the desired excess of reactivity is achieved with the most efficient amount of fuel.

To determine the optimum lattice pitch, a simulation is carried out using MCNP where the reactor core is provided with an infinite reflector of the moderator. In other words, the model consists of only the fuel pins in the core surrounded by a very large volume of the moderator. From here, the lattice pitch is slightly increased while maintaining the same number of fuel pins, and the model is simulated again. The result will be an increase in the core's effective multiplication factor. As this step is repeated, the effective multiplication factor will continue to increase until it plateaus and eventually decreases. The pitch corresponding to the centre of the plateau is considered the optimum lattice pitch for that core and moderator combination. An example of this process is presented in Figure 26.

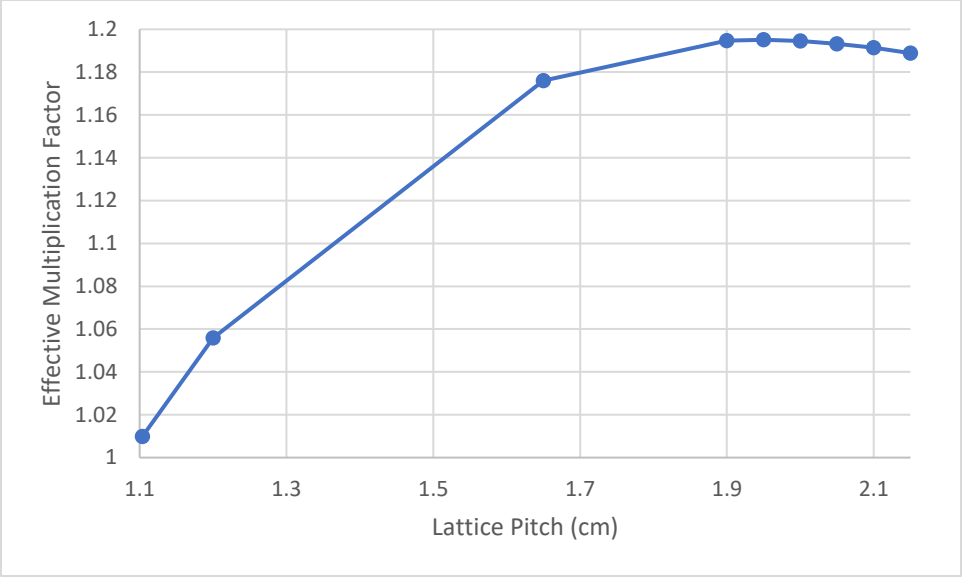

Figure 18: Response of Effective Multiplication Factor to Increased Lattice Pitch

In the case of the OCSL core design, the process is complicated by the need to identify appropriate average fuel and cladding temperatures to include in the MCNP model. Changes in fuel temperature will change the optimum lattice pitch while changes to the lattice pitch will change the average fuel and cladding temperatures. As a result, the process must be performed iteratively. The iterative method is expanded upon in Figure 19. The final outcome of the method was an optimum lattice pitch of 1.95 cm and average fuel and cladding temperatures of 399 ^{O}C and 337^{O}C respectively.

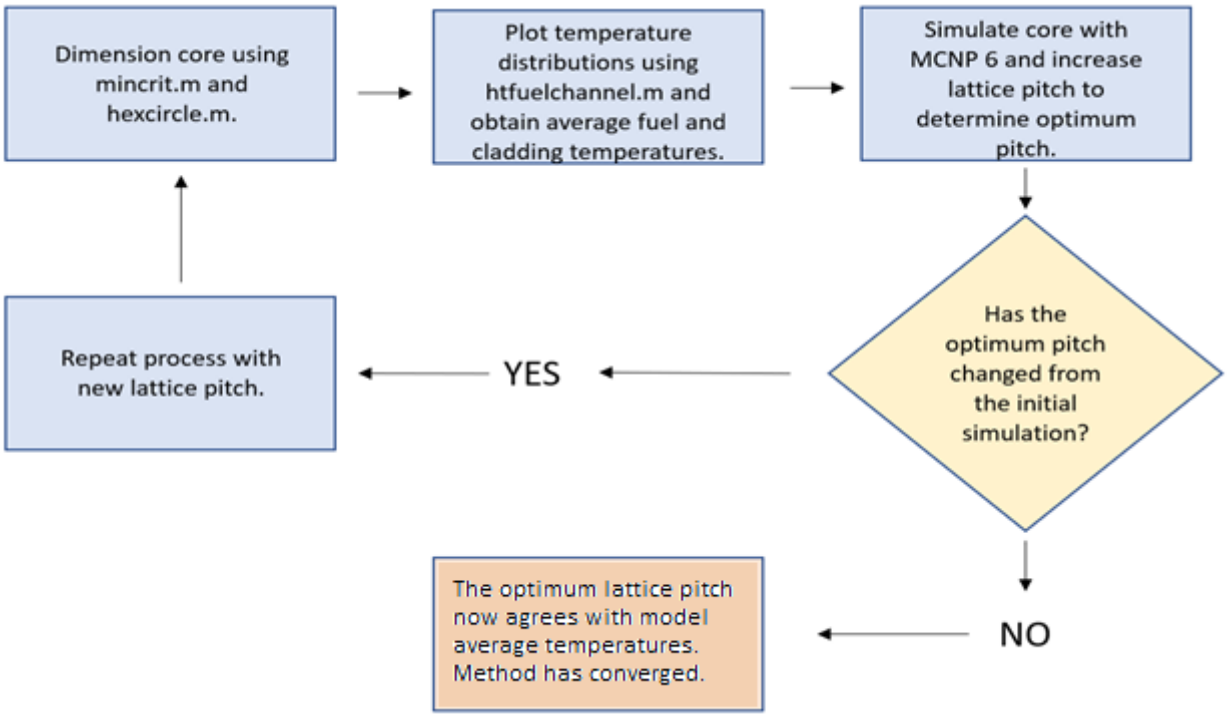

Figure 19: Iterative Process for Lattice Pitch Optimization

7.6 OCSL Reactor Core Vetting Process

With many parameters and conditions now defined, several potential core designs for the OCSL reactor can be produced using the methods previously described in this chapter. The series of potential cores must be vetted based upon three major design constraints; safety, power, and the core's service life. In practice, the procedure by which an ideal core is selected includes the following steps;

1. Using the MATLAB® calculators mincrit.m and hexcircle.m, estimate the minimum critical dimensions of the core. Using MCNP, simulate the core within an infinite volume of HB-40. Simulating cores within infinite reflectors of the moderator aids the vetting process because it ensures the criticality of each core is considered without bias towards any factors external to the core. Based on the criticality of the first estimate, vary the *adjust* parameter in mincrit.m to increase the size of the core. By simulating subsequently larger iterations of the core, develop a series of cores that vary in effective multiplication factor from approximately 1.1 to 1.2.

2. For each core in the series, estimate the thermal hydraulics using the MATLAB® calculator htfuelchannel.m. This stage ensures that each core can transfer 1 MW of thermal power to the coolant while remaining within the bounds of safety and feasibility. If any core experiences excessively high temperatures in fuel or cladding, it should be eliminated at this stage. The required mass flow rate is also considered at this stage. If the pump required is unrealistically large, the length of the core should be increased or the inlet temperature should be lowered to decrease the pump size. Understandably, this outcome will necessitate repeating the iterative process presented in the previous section.

3. For all remaining cores, recreate each MCNP simulation as model in WIMS and determine the geometric bucklings for the reactor. This stage will provide an estimate of the average thermal neutron flux in each potential core.

4. Still working with WIMS, perform detailed burnup calculation for each potential core. By estimating of the full-power service life for each core, the series of cores will be narrowed to those with the greatest service lives.

5. With the remaining cores, use WIMS to assess the moderator temperature and void fraction coefficients of reactivity for each core. This will ensure that cores still display the possibility for inherent safety. Using these results, select the best core configuration.

7.7 OCSL Reactor Cores Simulated Using MCNP

A total of twenty-two potential core configurations were produced using mincrit.m and hexcircle.m. These cores were simulated using MCNP as reactors provided with an infinite reflector of the moderator, HB-40. The dimensions of each potential core are presented in Table 8 in addition to the resultant effective multiplication factors from each MCNP simulation. The following conditions were common throughout all simulations:

- the fuel was assigned a temperature of 399 ^{O}C;
- the cladding of fuel elements was assigned a temperature of 337 ^{O}C;
- all other cells in the model were assigned a temperature of 315 ^{O}C;
- the lattice pitch between fuel pins in the cores was 1.95 cm;
- KCODE simulations consisted of 120 cycles:
- the first 20 cycles are inactive and are not used in final calculation of k_{eff}; and
- each cycle in the simulation consisted of one hundred thousand neutron histories.

Table 8: Potential OCSL Reactor Cores Simulated with MCNP 6

Reactor Core Design #	Outer Radius (m)	Length (m)	Number of Fuel Pins	Effective Multiplication Factor	Standard Deviation
1	0.232	0.43	511	1.12119	0.00026
2	0.236	0.436	517	1.12587	0.00028
3	0.240	0.443	559	1.14498	0.00027
4	0.244	0.451	571	1.15197	0.00025
5	0.248	0.459	583	1.15940	0.00025
6	0.253	0.468	595	1.16675	0.00025
7	0.258	0.477	649	1.18749	0.00024
8	0.263	0.486	661	1.19397	0.00025
9	0.268	0.496	673	1.20108	0.00026
10	0.217	0.500	439	1.11496	0.00027
11	0.221	0.500	463	1.12730	0.00024
12	0.226	0.500	499	1.14238	0.00025
13	0.232	0.500	511	1.14797	0.00024
14	0.237	0.500	535	1.15734	0.00027
15	0.243	0.500	559	1.16631	0.00025
16	0.257	0.500	637	1.19176	0.00027
17	0.235	0.550	517	1.16532	0.00027
18	0.241	0.550	559	1.18141	0.00025
19	0.248	0.550	583	1.19036	0.00026
20	0.255	0.550	625	1.20433	0.00025
21	0.270	0.500	685	1.20584	0.00026
22	0.263	0.500	661	1.19892	0.00024

Designs 1 to 9 are dimensioned according for minimum cylindrical volume. This is the default operation of mincrit.m. The remaining cores are dimensioned according to a prescribed core length. Designs 10 to 16 in addition to designs 21 and 22 have a prescribed length of 0.500 m while cores 17 to 20 have a prescribed length of 0.550 m. Despite having a prescribed length, design 21 also has a minimized volume due to the ratio between its radius and length.

7.8 Thermal Hydraulic Estimation of OCSL Reactor Cores

For each of the twenty-two core configurations, heat transfer along a single fuel channel was estimated using Newton's Law of Cooling as applied in the MATLAB® calculator htfuelchannel.m. These results are presented in Table 9. In Section 7.5, the average temperatures were determined for the zirconium cladding and the uranium dioxide fuel. To reflect this development, the thermal conductivities of these materials are updated in htfuelchannel.m. At 337 ^{O}C, the thermal conductivity of zirconium is interpolated to be 18.6 W m^{-1} K^{-1}. At 399 ^{O}C, the thermal conductivity of uranium dioxide is interpolated to be 4.67 W m^{-1} K^{-1} [105].

As stated in Section 7.2 the inlet and outlet coolant temperatures for all cores are set at 290 ^{O}C and 340 ^{O}C respectively. Based on this coolant temperature change and the heat capacity of HB-40 at the bulk temperature, the coolant mass flow rate required to produce 1 MW of thermal power was calculated to be 7.63 kg s^{-1}. This result indicates that the OCSL reactor could operate with one reasonably sized pump. In the interest of redundancy, the OCSL would likely operate with multiple pumps. A moderate coolant flow rate bodes well for the feasibility of the concept. If the pressure head to move the coolant through the reactor is assumed to be about 0.5 m, the power required to drive the pump is estimated to be about 40 W. This power rating is a very small fraction of the reactor's output power of 1 MW(th). If the reactor is employed in electrical power generation, the pump may be supplied power mechanically by an auxiliary drive from the turbine. Otherwise, the pump may be driven electrically by an AC motor receiving power from the Rankine cycle. Should the reactor be providing district heating, the pump must be powered by the electrical power supply in the installation. With the exception of Core Design 10, the Reynolds numbers computed for individual fuel channel coolant flow fall into the transitional region between laminar flow and fully developed turbulent flow. Overall, these results are satisfactory and indicate that the proposed thermal hydraulics of the reactor are appropriate.

From a safety standpoint, none of the results from these thermal hydraulic estimations warrant removal of a core design from further vetting. Maximum temperatures of fuel and cladding were found to be well under the design parameters of fuel for WR-1[106]. Additionally, the temperature distributions for each core demonstrated appropriate behaviour. An example of a temperature distribution from Core Design 1 is displayed in Figure 20.

Table 9: Thermal Hydraulic Estimation for OCSL Reactor Cores

Reactor Core Design #	Outer Radius (m)	Length (m)	Number of Fuel Pins	Fuel Channel Mass Flow rate (kg s^{-1})	Reynold's Number	Maximum Fuel Cladding Temperature (^{O}C)	Maximum Fuel Temperature (^{O}C)
1	0.232	0.430	511	0.01493	9030	405	514
2	0.236	0.436	517	0.01475	8970	403	509
3	0.240	0.443	559	0.01365	8250	396	492
4	0.244	0.451	571	0.01336	8120	393	485
5	0.248	0.459	583	0.01308	7940	390	479
6	0.253	0.468	595	0.01282	7760	388	472
7	0.258	0.477	649	0.01175	7150	381	457
8	0.263	0.486	661	0.01154	7000	379	452
9	0.268	0.496	673	0.01133	6870	377	447
10	0.217	0.500	439	0.01738	10500	405	514
11	0.221	0.500	463	0.01648	9990	401	504
12	0.226	0.500	499	0.01529	9270	395	490
13	0.232	0.500	511	0.01493	9050	394	486
14	0.237	0.500	535	0.01426	8640	390	479
15	0.243	0.500	559	0.01365	8270	388	472
16	0.257	0.500	637	0.01197	7260	380	453
17	0.235	0.550	517	0.01475	8950	386	469
18	0.241	0.550	559	0.01365	8270	382	458
19	0.248	0.550	583	0.01308	7930	379	452
20	0.255	0.550	625	0.01220	7400	376	443
21	0.270	0.500	685	0.01114	6750	376	444
22	0.263	0.500	661	0.01154	7000	378	448

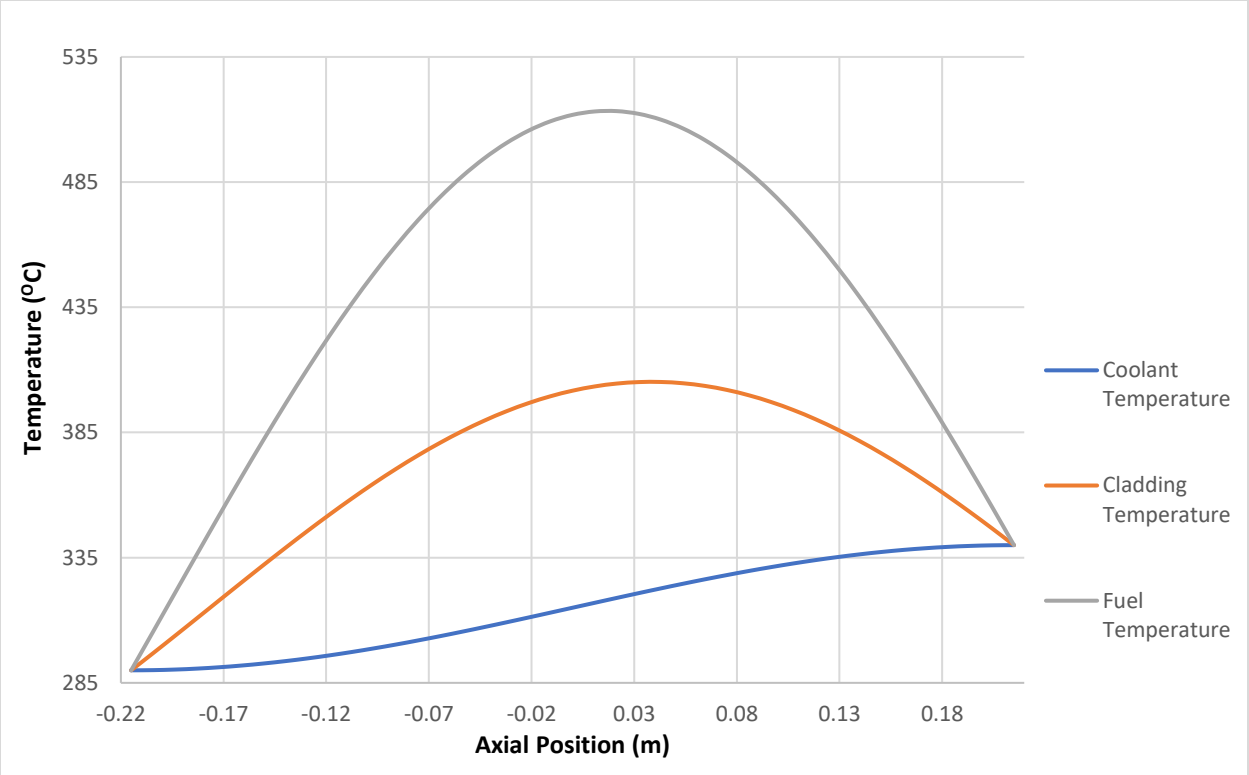

Figure 20: Temperature Distribution for Core Design 1

7.9 OCSL Reactor Cores Simulated Using WIMS

The remainder of the vetting process requires burnup calculations for each of the twenty-two core configurations to compare the length of their service lives. Additionally, the final selection will compare reactivity coefficients for the best cores to arrive at an ideal core configuration. Due to sheer number of simulations, the continued employment of MCNP will prove computationally expensive to complete these analyses. The deterministic code WIMS presents a much faster avenue although some geometric accuracy will be lost to adapt the models to the WIMS framework. For perspective, the average KCODE simulation from Section 5.7 ran for about twenty minutes using all available parallel processing power from the computer. In comparison, WIMS can return an effective multiplication factor in less than a minute without parallel processing. The slight deviations in geometric accuracy are acceptable because the objective of reliably comparing core configurations is still accomplished by this method.

The first step in performing burnup calculations with WIMS is to properly define the reactor geometry so that a correct effective multiplication factor is returned. The original MCNP models of the OCSL reactor cores arranged fuel pins in a triangular lattice with a pitch of 1.95 cm. In WIMS, the pins must be arranged in concentric arrays about a central origin. The most natural way to adapt the triangular lattice into the circular geometry is to treat hexagonal rings as arrays. Starting from the first pin at the centre of the core, the first array contains six pins, the second array contains twelve pins, the third array contains eighteen pins and so on until the outer radius of the core. The sequencing of fuel pins into arrays is further demonstrated up to the seventh array in Table 10. Figure 21 illustrates the application of concentric arrays to the MCNP lattice for the first two arrays.

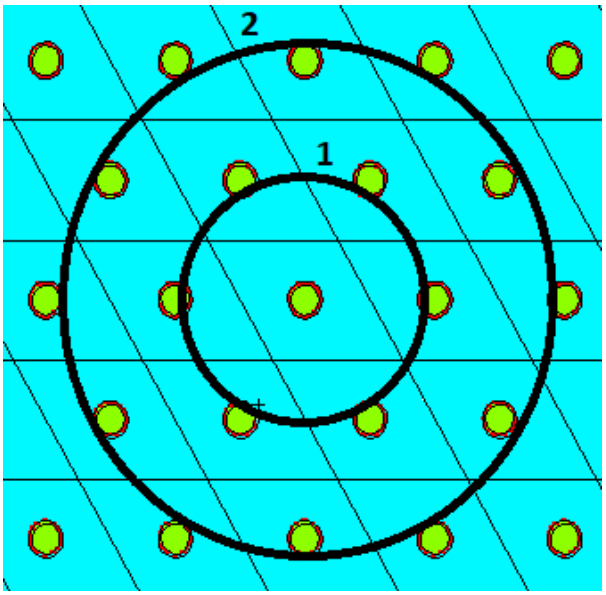

Figure 21: WIMS Concentric Arrays Applied to Original MCNP Lattice

Table 10: Comparison of MCNP and WIMS Geometries

Array No.	No. of Fuel Pins	Average Distance from Centre in MCNP Model (cm)	Array Radius in WIMS Model (cm)
0	1	0	0
1	6	1.95	1.773
2	12	3.639	3.547
3	18	5.159	5.320
4	24	7.154	7.093
5	30	8.924	8.867
6	36	10.697	10.640
7	42	12.472	12.413

However, not all pins along the hexagonal rings are equidistant from the centre in the MCNP geometry. Therefore, the arrays in WIMS must be spaced by an adapted measure different from the lattice pitch in MCNP to ensure fuel pins are placed as accurately as possible. This measure was defined as the radius corresponding to the circle of equal area to the hexagon formed by the lattice pitch. This radius, r, is given by:

$$r = \sqrt{\frac{3\sqrt{3}}{2\pi}\ell^2} \tag{33}$$

where ℓ is the lattice pitch from the MCNP model. For a pitch of 1.95 cm, the corresponding array spacing is 1.773 cm. Table 10 presents a comparison of the adapted WIMS spacing and the average distance of fuel pins from the core centre in MCNP. This demonstrates how the adapted spacing adequately recreates the core layout despite the change in geometrical framework. For the purposes of this research, this method is deemed sufficiently accurate because exact replication of geometry for each individual model is impractical.

With each core configuration detailed in the WIMS geometry, the code can return the effective multiplication factor for the reactor in addition to the average thermal neutron flux. However, WIMS only operates in two dimensions so the length of the core must be represented in the geometric buckling values input by the user. In practice, the geometric buckling values are varied by the user until the effective multiplication factor of the reactor matches that of the corresponding MCNP simulation. WIMS uses a normalization value to calculate the average thermal neutron flux of the reactor. In this analysis, the linear power rating in W cm^{-1} is specified for this value because the power and lengths of these reactors are known. The results produced in initial WIMS simulations of the potential reactor cores are presented in Table 11.

Table 11: Potential OCSL Reactor Cores Simulated with WIMS

Reactor Core Design #	Outer Radius (m)	Length (m)	Number of Fuel Pins	Effective Multiplication Factor (MCNP)	Effective Multiplication Factor (WIMS)	Linear Power Rating (W m^{-1})	Average Thermal Neutron Flux / 10^{12} (n cm^{-2} s^{-1})
1	0.232	0.430	511	1.12119	1.12113	23255.8	9.67
2	0.236	0.436	517	1.12587	1.12588	22935.8	9.40
3	0.240	0.443	559	1.14498	1.14499	22573.4	8.88
4	0.244	0.451	571	1.15197	1.15199	22172.9	8.41
5	0.248	0.459	583	1.15940	1.15940	21786.5	8.05
6	0.253	0.468	595	1.16675	1.16673	21367.5	7.67
7	0.258	0.477	649	1.18749	1.18748	20964.4	7.00
8	0.263	0.486	661	1.19397	1.19396	20576.1	6.57
9	0.268	0.496	673	1.20108	1.20108	20161.3	6.30
10	0.217	0.500	439	1.11496	1.11496	20000.0	9.62
11	0.221	0.500	463	1.12730	1.12731	20000.0	9.70
12	0.226	0.500	499	1.14238	1.14237	20000.0	8.61
13	0.232	0.500	511	1.14797	1.14799	20000.0	8.32
14	0.237	0.500	535	1.15734	1.15736	20000.0	8.55
15	0.243	0.500	559	1.16631	1.16632	20000.0	7.87
16	0.257	0.500	637	1.19176	1.19173	20000.0	6.72
17	0.235	0.550	517	1.16532	1.16532	18181.8	7.45
18	0.241	0.550	559	1.18141	1.18139	18181.8	7.16
19	0.248	0.550	583	1.19036	1.19036	18181.8	6.72
20	0.255	0.550	625	1.20433	1.20432	18181.8	6.28
21	0.270	0.500	685	1.20584	1.20585	20000.0	6.12
22	0.263	0.500	661	1.19892	1.19890	20000.0	6.38

7.10 Burnup Analysis for OCSL Reactor Cores

Burnup calculations performed using WIMS offer some perspective of how long each potential reactor core will remain super-critical. Understandably, the output of a reactor varies during operation, but it is unrealistic to estimate the detailed operational life of a reactor. Therefore, the burnup calculations using WIMS assume full power operation at 1 MW and thus, the result of the calculation will represent the core's lifespan in full power days (FPD). The results of these calculations are presented in Table 12. Two additional metrics are included to aid in vetting the best core design. First, the lifespan of the core normalized by the initial mass of uranium-235 gives a measure of the fuel efficiency of the core and aids is vetting between two cores of similar lifespan. Second, the average rate of reactivity loss gives a perspective of how quickly the core's excess reactivity diminishes. To obtain the average rate, the slope of the excess reactivity over time was calculated between day 210 and the point where the core becomes sub-critical. Starting with day 210 was somewhat arbitrary, but the starting point of the linear region had to be removed from the initial non-linear phase of the cores' lives. For a visual representation, plots of the burnup for each OCSL core design are presented in Figure 22, Figure 23 and Figure 24. The cores are

sorted with those of minimized volume in Figure 22, those with 0.500 m lengths in Figure 23, and those with 0.550m lengths in Figure 24.

These figures demonstrate the expected behaviour of the effective multiplication factor over the life span of each OCSL reactor core. Similar amongst all cores, the effective multiplication factor drops rapidly in the early days of operation before settling into a generally linear trend until the core becomes sub-critical. Displayed in Table 12, the average rate of reactivity loss in the linear region is different for each core. In general, the rate is less steep with larger cores and those that are dimensioned for minimum cylindrical volume. The core designs that see the best ratio of full power days to uranium-235 mass are designs 8, 9, and 21. Design 21 is the longest serving core with a lifespan of 3561 days or about nine and three-quarter years. Designs 8 and 9 are the fourth and second longest serving reactors respectively. Design 8 lasts 3264 days or nearly nine years while design 9 lasts 3425 days or nearly nine and a half years. In addition to their superior fuel efficiencies and lifespans, these three cores also demonstrate the shallowest rates of reactivity loss in the linear region of burnup. For these reasons, designs 8, 9, and 21 are carried forward for further vetting.

Table 12: Burnup Analysis for Potential OCSL Reactor Cores Using WIMS

Reactor Core Design #	Outer Radius (m)	Length (m)	Number of Fuel Pins	Total Volume of Fuel (m^3)	Initial Mass U-235 (kg)	Number of Full Power Days (FPD)	FPD per kg U-235	Average Rate of Reactivity Loss (mk d^{-1})
1	0.232	0.430	511	0.00312	5.73	1643	287	-0.0542
2	0.236	0.436	517	0.00320	5.88	1731	294	-0.0538
3	0.240	0.443	559	0.00351	6.46	2111	327	-0.0511
4	0.244	0.451	571	0.00365	6.72	2259	336	-0.0506
5	0.248	0.459	583	0.00380	6.98	2417	346	-0.0501
6	0.253	0.468	595	0.00395	7.27	2578	355	-0.0487
7	0.258	0.477	649	0.00439	8.08	3045	377	-0.0468
8	0.263	0.486	661	0.00456	8.38	3264	389	-0.0449
9	0.268	0.496	673	0.00474	8.71	3425	393	-0.0446
10	0.217	0.500	439	0.00311	5.73	1323	231	-0.0627
11	0.221	0.500	463	0.00328	6.04	1516	251	-0.0620
12	0.226	0.500	499	0.00354	6.51	1857	285	-0.0570
13	0.232	0.500	511	0.00362	6.67	1984	298	-0.0554
14	0.237	0.500	535	0.00379	6.98	2150	308	-0.0581
15	0.243	0.500	559	0.00397	7.29	2371	325	-0.0527
16	0.257	0.500	637	0.00452	8.31	3088	372	-0.0467
17	0.235	0.550	517	0.00403	7.42	2217	299	-0.0553
18	0.241	0.550	559	0.00436	8.02	2546	317	-0.0538
19	0.248	0.550	583	0.00455	8.37	2789	333	-0.0511
20	0.255	0.550	625	0.00488	8.97	3155	352	-0.0488
21	0.270	0.500	685	0.00486	8.94	3561	399	-0.0436
22	0.263	0.500	661	0.00469	8.62	3325	386	-0.0455

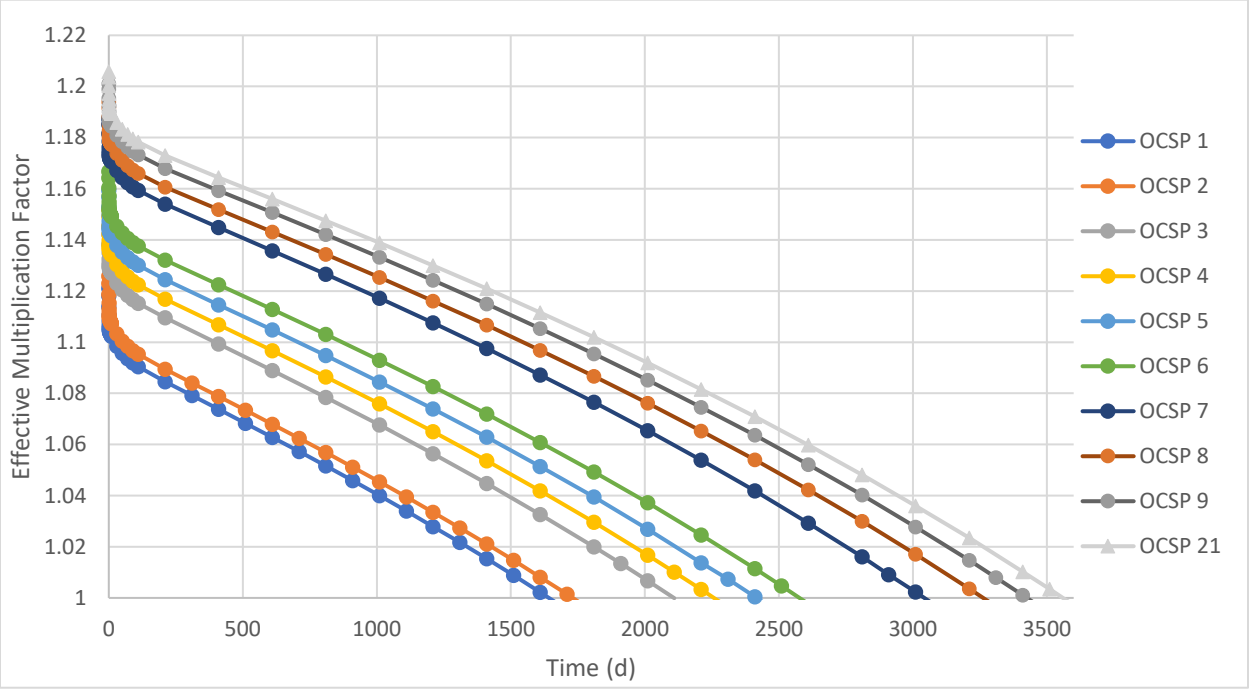

Figure 22: Plotted Burnup for Cores of Minimum Cylindrical Volume

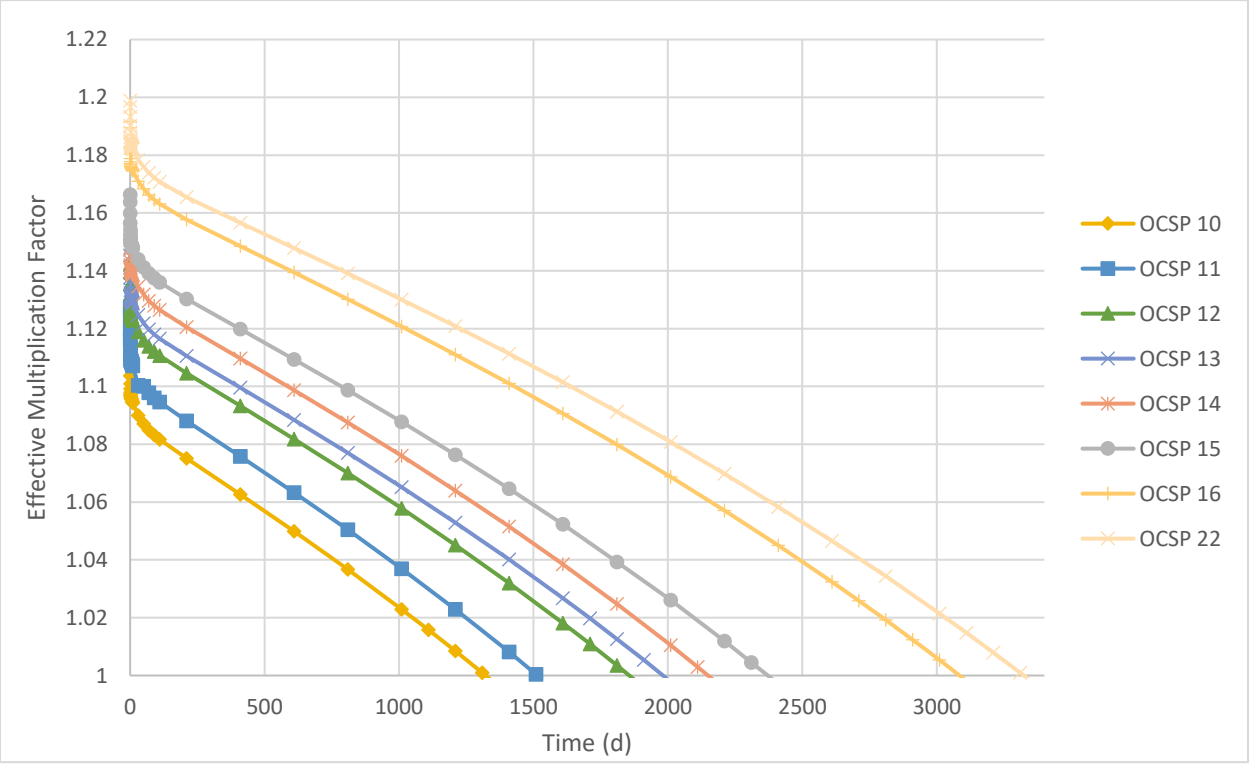

Figure 23: Plotted Burnup for Cores with 0.500m Length

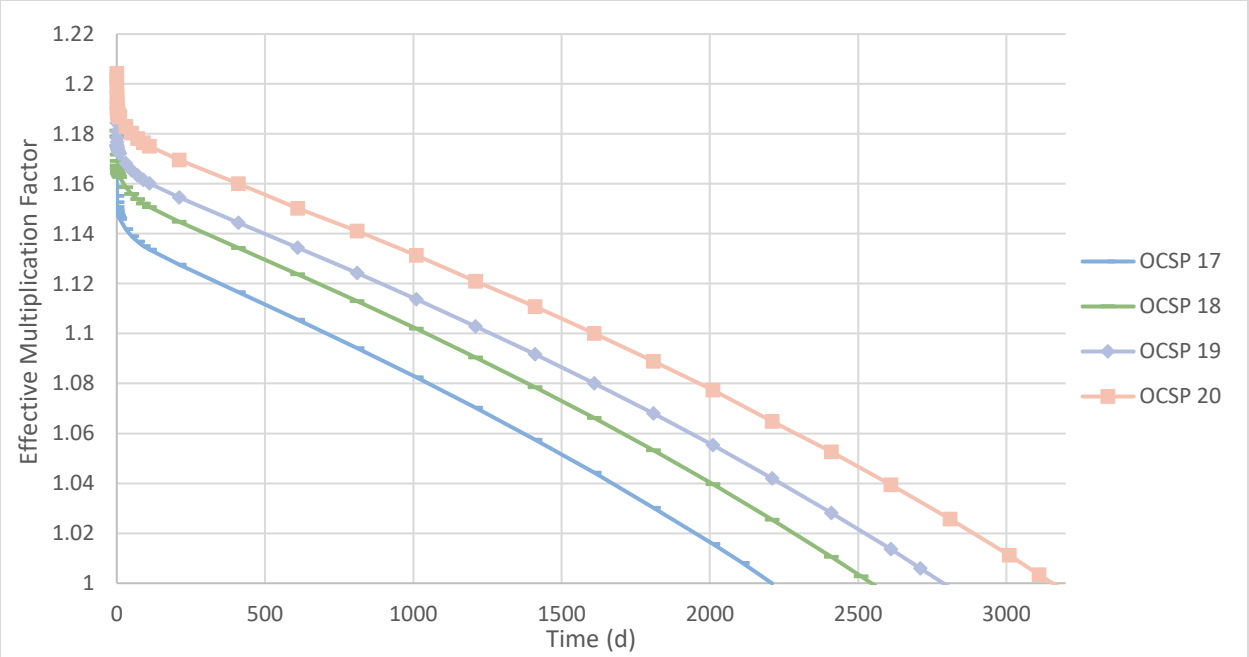

Figure 24: Plotted Burnup for Cores with 0.550m Length

7.11 Reactivity Coefficients for OCSL Reactor Cores

For a reactor operating in remote northern installations, it is understandably desirable to design a core with as long a service life as possible. Therefore, the cores retained from the previous section have large reserves of excess reactivity corresponding to long service lives. However, these designs can be deemed ideal only if they still demonstrate the potential for inherent safety. Again, the moderator temperature and void fraction coefficients of reactivity are the most practical indications of potential inherent safety. These two reactivity relationships provide a strong indication of the reactor's ultimate response in accident scenarios.

Using WIMS, the moderator temperature coefficient of reactivity is demonstrated by repeatedly simulating each core with varying temperatures of HB-40 coolant and tracking the resultant excess reactivity for the core. The temperature range varies from the coolant inlet temperature of 290 ^{O}C to the outlet temperature of 340 ^{O}C. At each new temperature, the atomic densities for hydrogen and carbon in HB-40 are recalculated and updated. All other parameters of the simulation are held constant from the initial simulation where the average temperature was 315 ^{O}C. This includes all other material temperatures and densities, the geometric buckling values, linear power rating, and the fresh composition of the fuel. The series of results for core designs 8, 9 and 21 are plotted in Figure 25.

For the void fraction coefficient of reactivity, the process is similar to the moderator temperature coefficient where excess reactivity is tracked in repeated WIMS simulations with varying densities of HB-40. The varied densities of HB-40 correspond to increasing void fractions. In these simulations, the HB-40 coolant is assigned a temperature of 342 ^{O}C; its atmospheric boiling point. The density of HB-40 at this temperature corresponds to void fraction of 0% and subsequent simulations assign a range of void fractions up to 28%. Again, all other parameters of the simulation are held constant in these simulations. The series of results for core designs 8, 9 and 21 are plotted in Figure 26.

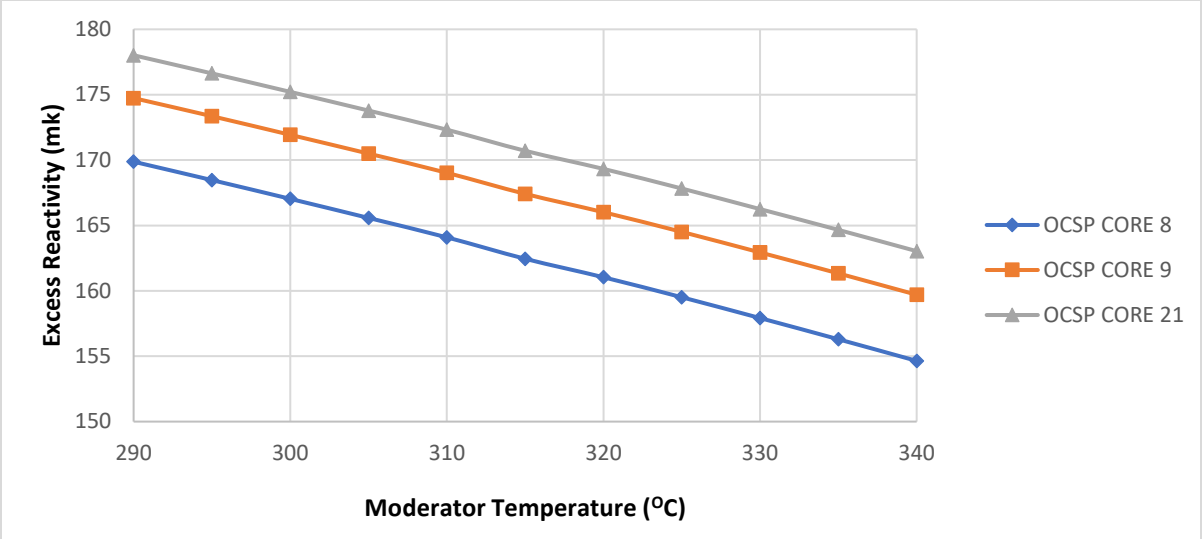

Figure 25: Variation of Excess Reactivity with Moderator Temperature for Potential OCSL Reactor Cores

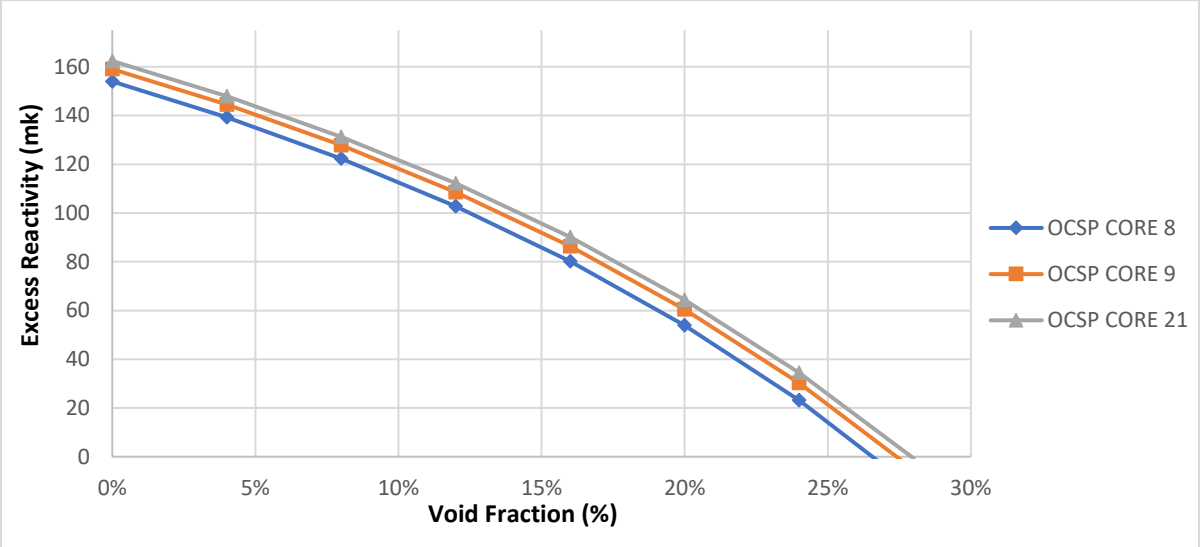

Figure 26: Variation of Excess Reactivity with Void Fraction for Potential OCSL Reactor Cores

For all three cores, the plots demonstrate strong negative relationships between excess reactivity and both moderator temperature and void fraction. The average reactivity coefficients within the examined ranges of moderator temperature and void fraction are presented in Table 13. The three potential cores that were examined demonstrate similar coefficients representative of the strong negative relationships confirmed by this analysis.

Since the three cores indicate the potential for inherent safety, the final selection of a core design should ultimately be determined by the burnup analysis results of the cores. Referring to Table 12, the designs 8, 9, and 21 are very similar in size, but design 21 exceeds the lifespans of all other cores by over a quarter of a year. Design 21 also demonstrates a superior rate of full power days relative to its initial mass of uranium-235 fuel. Finally, design 21 also see the shallowest decline in excess reactivity over time

when compared to the other cores. For these reasons, design 21 will be the core design employed in the OCSL Reactor. Henceforth, the title of OCSL Reactor refers to the reactor with this core design.

Table 13: Average Reactivity Coefficients for Potential OCSL Reactor Cores

Core Design #	Average Moderator Temperature Coefficient of Reactivity (mk $^{O}C^{-1}$)	Average Void Fraction Coefficient of Reactivity (mk per % Void)
8	-0.305	-5.45
9	-0.301	-5.37
21	-0.300	-5.33

7.12 Summary of OCSL Reactor Core Parameters

With a core design now selected, a significant milestone has been reached in the design of the OCSL Reactor. At this stage, the OCSL Reactor is a core surrounded by an infinitely large volume of the coolant/moderator, HB-40. A cross-sectional view of the core is displayed in Figure 27. A general description including the estimated thermal hydraulic parameters of the core is presented in Table 14.

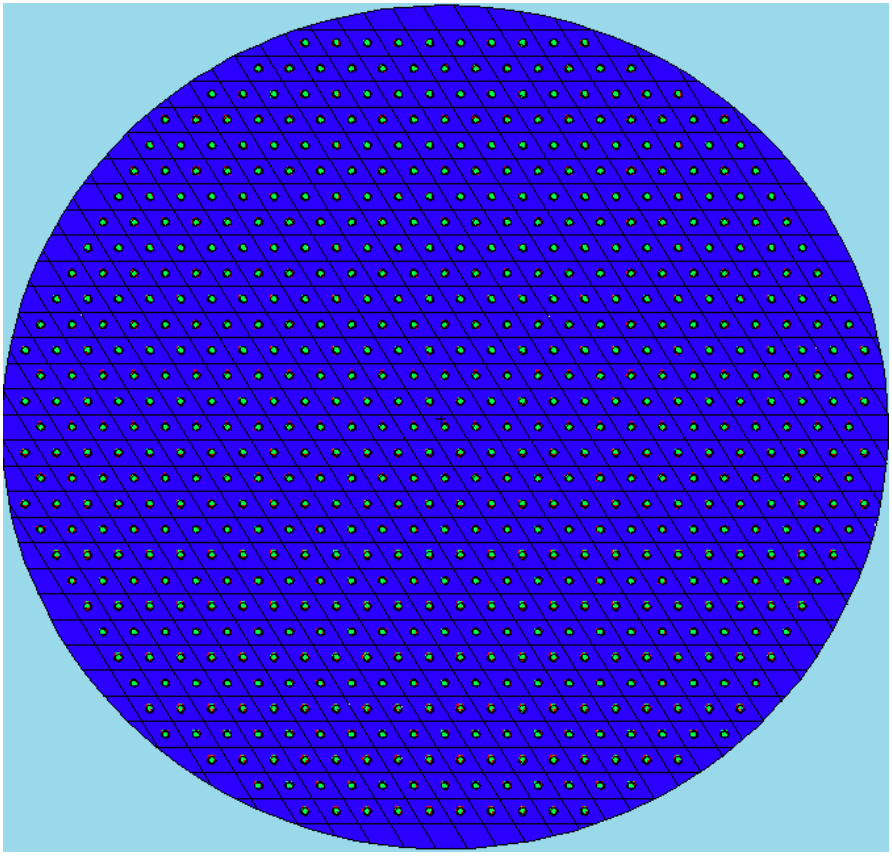

Figure 27: Cross Section View of OCSL Reactor Core

Table 14: General Description of OCSL Reactor Core

Core Arrangement	Cylindrical, Outer Radius of 27.8cm
Core Height	50 cm
Fuel	LEU UO_2
Number of Fuel Rods	685
Fuel Rod Pitch	1.95 cm
Fuel Rod Diameter	0.425 cm
Cladding Thickness	0.05 cm, Zirconium
Coolant / Moderator	HB-40
Thermal Power	1 MW
Average Thermal Flux	6.12×10^{12} n cm^{-2} s^{-1}
Coolant Inlet / Outlet Temperature	290 °C / 340 °C
Coolant Mass Flow rate	7.63 kg s^{-1}
Reynold's Number	6752
Maximum Fuel Temperature	444 °C
Maximum Cladding Temperature	376 °C

The predicted temperature distributions in the fuel, cladding, and coolant along the axis of coolant flow are displayed in Figure 28. From this point, the next phase of the OCSL Reactor design will add a radial reflector to extend the service life of the core and to provide a means of burnup control.

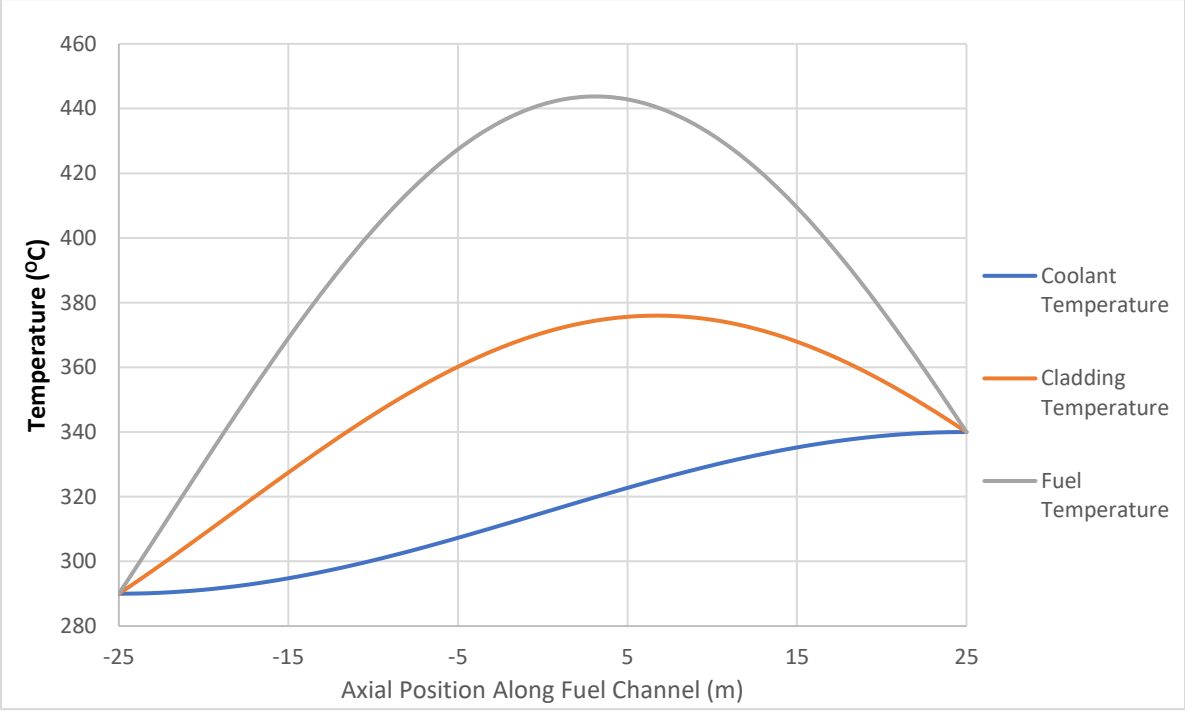

Figure 28: Estimated Temperature Distribution Along Fuel Channel in OCSL Reactor Core

CHAPTER 8: OCSL REACTOR REFLECTOR DESIGN

8.1 Introductory Comments

The addition of a reflector to the OCSL Reactor design will improve the neutron economy in the core by redirecting neutrons back into the core. In effect, this will extend the service life of the fuel in the OCSL Reactor core. This chapter will explain the material selection for the reflector and also the optimization of the reflector's dimensions.

Within the scope of this research, only an annular reflector around the core will be designed. Reduction of radial neutron leakage is considered more critical at this stage because the radial surface of the core comprises more than sixty percent of its surface area. This work assumes that a hypothetical baffling arrangement directs the coolant flow upward from the pump. For an actual pumping arrangement to be designed, a grid-plate reflector at the bottom of the core may impede or obstruct flow into the coolant channels. Therefore, this component is relegated to future design work.

The core design selected for the OCSL Reactor already has a large reserve of excess reactivity. In the interest of criticality safety, the OCSL reflector will be designed for variable position operation. This will allow the reflector to be disengaged in the early stages of operation when the fuel is fresh. As the fuel is depleted and excess reactivity diminishes, the reflector will be moved inward to compensate for burnup. A reflector that may be instantaneously retracted from the core also adds a safety mechanism in the event of a criticality excursion to supplement the reactor's control system.

8.2 Reflector Material Selection

As a thermal reactor, the ideal reflector materials for the OCSL reactor have much in common with ideal neutron moderators. Atoms with low mass numbers, low absorption cross sections and high scattering cross sections compose the best materials for reflecting neutrons[107]. Unlike the moderator, the reflector does not necessarily flow, so solid materials enhance the reflection of neutrons with their greater densities. Common materials employed in reflectors include light and heavy water, graphite, and beryllium. Due to the relatively high operating temperature of the OCSL Reactor, light and heavy water are not the best choices for the reflector, but the reactor's moderator, HB-40 will be considered to establish a baseline for comparison with other materials. Since HB-40 is a liquid, simulations will assume some structural component holds the HB-40 in the annular shape. Furthermore, it is assumed that the structure is made of some thin material that does not significantly influence the neutronics of the reactor such that it is required in these models. A comparison of the considered reflector materials in this research is presented in Table 15.

In this research, the reflector material will be selected primarily on the merits of its neutronic properties. Aspects such as cost and safety are considered, but on a secondary basis to the neutronic performance of the materials.

Carbon in the form of graphite is not as effective a reflector material as those composed of smaller atoms such as hydrogen and beryllium. However, it is an appealing choice due to its relatively cheap cost, versatility, and availability. It features good mechanical properties and is capable of functioning at the operating temperature of the OCSL Reactor. Unfortunately, graphite is reactive with water, carbon dioxide and oxygen at elevated temperatures and poses certain safety concerns[108].

Contrastingly, beryllium is a more effective reflector material than graphite but is much more difficult to acquire and costlier to machine. Compared to graphite, beryllium is also more chemically stable under reactor operating conditions. From a safety perspective, the high toxicity of beryllium poses certain safety concerns relating to the fabrication of reactor components.

Table 15: Comparison of Reflector Material[101]

	Graphite	Beryllium	HB-40	
Chemical Formula	C	Be	C_XH_Y	
Atomic Fraction	1	1	0.5370 (Hydrogen)	0.4630 (Carbon)
Atomic Mass (amu)	12.011	9.0122	1.008 (Hydrogen)	12.011 (Carbon)
Density (g cm^{-3})	1.60	1.85	0.785 (at 315 ^{O}C)	
σ_a (barns)	0.0034	0.0092	0.332 (Hydrogen)	0.0034 (Carbon)
Σ_a ($cm^{-1)}$)	0.0002728	0.001137	0.0177	
σ_s(barns)	4.75	6.14	38 (Hydrogen)	4.75 (Carbon)
Σ_s ($cm^{-1)}$)	0.3811	0.7589	2.2	
ξ	0.158	0.207	0.61	

8.3 Effective Thickness of Reflector Materials

To compare the neutronic performance, the effective thickness of each material must be established. As the reflector thickness increases, fewer neutrons diffuse through the reflector to reach the outer surface. This effect eventually produces a plateau where no significant increase in reactivity is produced by further addition of reflector material. The reflector thickness where the plateau begins is referred to as the effective thickness of the material. MCNP provides a practical method of ascertaining these values by successively simulating the OCSL Reactor with increasing thicknesses of each material. When the effective multiplication factor ceases to increase significantly between simulations, the effective thickness is interpolated from the plot of resulting effective multiplication factors up to the current thickness.

However, special attention must be paid to the boundary conditions of the simulations to ensure only reflection in the radial direction is considered. In Chapter 5, the OCSL core was surrounded by a large sphere of HB-40 that could be considered an infinite thickness of reflector material. Although unlikely, any neutron that reached the surface of the sphere would be terminated upon passing to the void cell on the other side. When designing the annular reflector, such a boundary condition provides extra reflection that will distort the effect of the actual reflector.

In this design phase, the simulation must be isolated so that only the effect of the added thickness of reflector material is captured. This is accomplished by bounding the simulation in two ways. First, the outer surface of the reflector is the boundary of the simulation in the radial direction. Any neutrons escaping the reflector in this direction are terminated. Secondly, the planes that define the top and bottom of the core and reflector are treated as boundaries in the axial direction. All neutrons that escape through these surfaces are terminated.

By bounding the simulation in this fashion, the resulting effective multiplication factor is reduced when compared to the same core and reflector immersed in the HB-40 moderator. Under realistic

operation, the core and reflector would have a volume of HB-40 surrounding them. The additional reflection provided by the HB-40 reflects a portion of leaked neutrons and thus will increase the effective multiplication factor. Once the effective thicknesses of the reflector materials are established, the cores and reflectors are simulated in a volume of HB-40 to demonstrate the increased reactivity provided by the reflector.

The conditions of the MCNP simulations are maintained from Section 5.7 including model temperatures and the KCODE parameters. The reflector is assigned a temperature of 315 ^{O}C because under steady-state operation, it is assumed the reflector would approach the average temperature of the coolant. The results of the simulation are illustrated in Figure 29. Table 16 presents the effective thicknesses of the reflector materials along with the effective multiplication factor when the reflector and core are simulated in a large volume of HB-40.

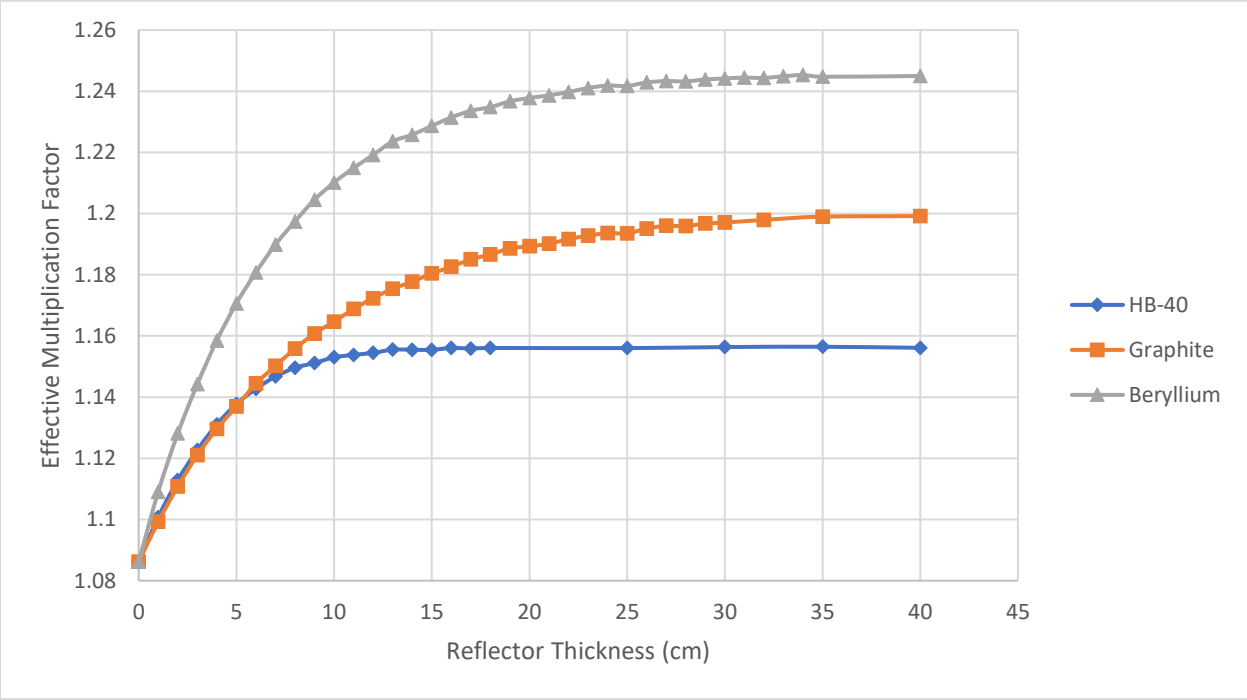

Figure 29: Variation of Effective Multiplication Factor with Reflector Thickness for Potential Materials

Table 16: Comparison of Potential OCSL Reactor Reflectors

Reflector Material	Effective Thickness (cm)	Maximum Effective Multiplication Factor	Standard Deviation
HB-40	15	1.20584	0.00026
Graphite	35	1.27047	0.00023
Beryllium	30	1.30617	0.00023

The results clearly show that beryllium is a much more effective reflector than graphite or HB-40. However, the high cost and potential hazards associated with beryllium necessitate further analysis. First, burnup calculations using each reflector will further establish the effectiveness of beryllium over the other materials. Second, analysis of the reactivity coefficients of the reactor with the beryllium reflector will confirm that the reactor still demonstrates basic inherent safety potential.

8.4 Burnup Calculations of OCSL Reactor with Various Reflectors

Burnup calculations are performed for two potential versions of the OCSL Reactor. The first is fitted with a graphite reflector with a thickness of 35 cm. The second is fitted with a beryllium reflector 30 cm thick. The calculations are performed using WIMS in the same manner as in Section 7.10. The results of the calculations are plotted in Figure 30. The original burnup for the core surrounded by HB-40 is included in the plot for relative comparison.

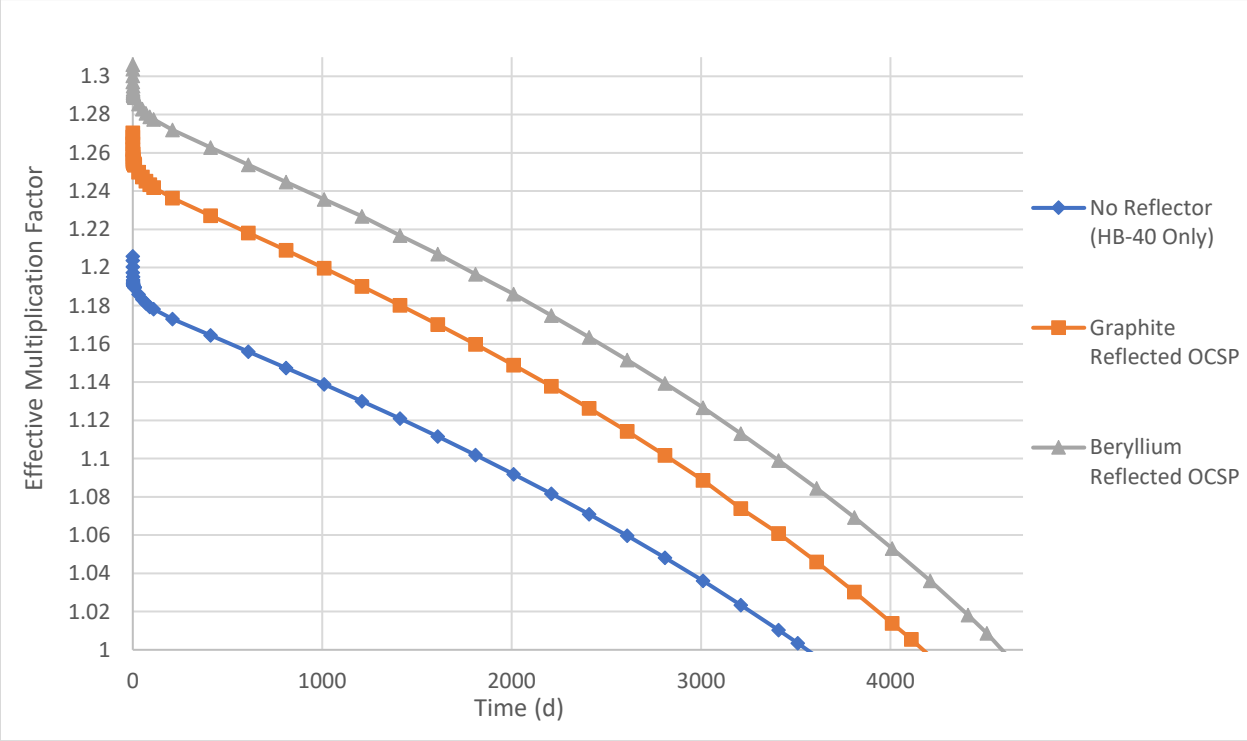

Figure 30: Variation of Effective Multiplication Factor with Time for Various Reflector Options

When the reflectors are added, the service life of the fuel in the OCSL Reactor increases significantly. In terms of full power days, the service life increases from 3561 FPD to 4174 FPD and 4603 FPD with the graphite and beryllium reflectors respectively. The ratio of full power days to initial uranium-235 mass increase from 399 FPD kg^{-1} to 467 FPD kg^{-1} and 515 FPD kg^{-1} for graphite and beryllium. Again, the effectiveness of beryllium is demonstrated in these results. The burnup calculations suggest a service life for the OCSL core that could exceed twelve and a half years. This aspect of the OCSL design is highly desirable for operation in remote locations. Time between refuelling will drastically influence the financial and logistical feasibility of this reactor. However, the reactivity coefficients must be analysed with the beryllium reflector before it can be selected. The calculations must demonstrate that the design of the reactor has not diverged from inherent safety.

8.5 Reactivity Coefficients for Beryllium Reflected OCSL Reactor

As in Section 7.11, the variations of the OCSL Reactor's excess reactivity with moderator temperature and void fraction are calculated using WIMS. For the variation with moderator temperature, the method is identical to the previous section. The moderator temperature is varied between 290 ^{O}C and

340 ^{O}C and the resulting excess reactivity is plotted. The results of this analysis are displayed in Figure 31. When analysing the reactivity variation with void fraction, WIMS began reporting a fatal error after a void fraction of twelve percent. The error proved difficult to resolve, so the analysis was performed using MCNP. Although MCNP simulations are a slower method, the process is very similar. Each moderator-containing cell must be assigned a temperature of 342 ^{O}C and then the density of each cell must be varied for each simulation. The initial excess reactivity of the reflected reactor is much higher than in the previous analyses. Therefore, the void fraction domain was extended to fifty-two percent to better capture the variation in excess reactivity. MCNP functioned without error and the results are plotted in Figure 32. Because MCNP did not encounter any issues, the error in WIMS was likely an input-related matter and not a reflection of the simulation itself.

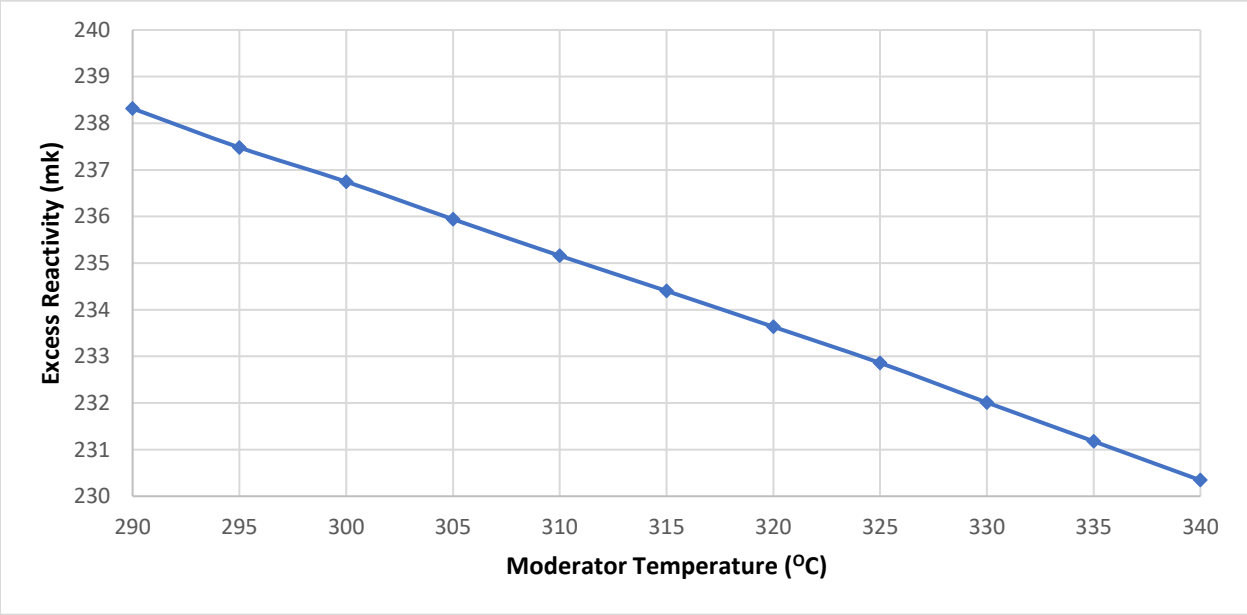

Figure 31: Variation of Excess Reactivity with Moderator Temperature for Beryllium Reflected OCSL Reactor

A negative correlation is clearly demonstrated between the excess reactivity and both moderator temperature and void fraction. However, the relationships are shallower when compared to the analysis of the core in HB-40 only. With the added reflector, the average moderator temperature coefficient of reactivity is -0.159 mk ^{O}C^{-1} where it had been -0.300 mk ^{O}C^{-1} previously for the non-reflected core. Regarding the void fraction coefficient of reactivity, the reflected core sees a coefficient of -2.66 mk per percent void where it was previously -5.33 mk per percent void. Despite these changes, the relationships remain strongly negative. These analyses imply that the OCSL Reactor fitted with the beryllium reflector is capable of inherent safety.

Beyond the moderator temperature and void fraction reactivity coefficients, the fuel temperature coefficient of reactivity is another important measure of safety in a reactor's design. Also known as the prompt coefficient of reactivity, the relationship between fuel temperature and reactivity serves as an indication of the reactor's instantaneous response to changes in load and thereby fuel temperature[71]. Regulatory bodies such as the United States' Nuclear Regulatory Commission mandate negative prompt reactivity coefficients for reactor licensing[71].

The method of assessing this relationship is like the process for assessing the moderator temperature coefficient of reactivity using WIMS. In successive WIMS simulations, the fuel temperature is varied, and the resulting excess reactivity of the reactor is recorded. The fuel temperature in this analysis varies from the minimum fuel temperature, 290 ^{O}C, to the maximum fuel temperature, 444 ^{O}C. The results of this analysis are plotted in Figure 33. A negative correlation between excess reactivity and fuel temperature is clearly demonstrated in these results. The average fuel temperature coefficient of reactivity is -9.8 x 10^{-3} mk $^{O}C^{-1}$. This is another encouraging and important outcome for the reactor's safety case.

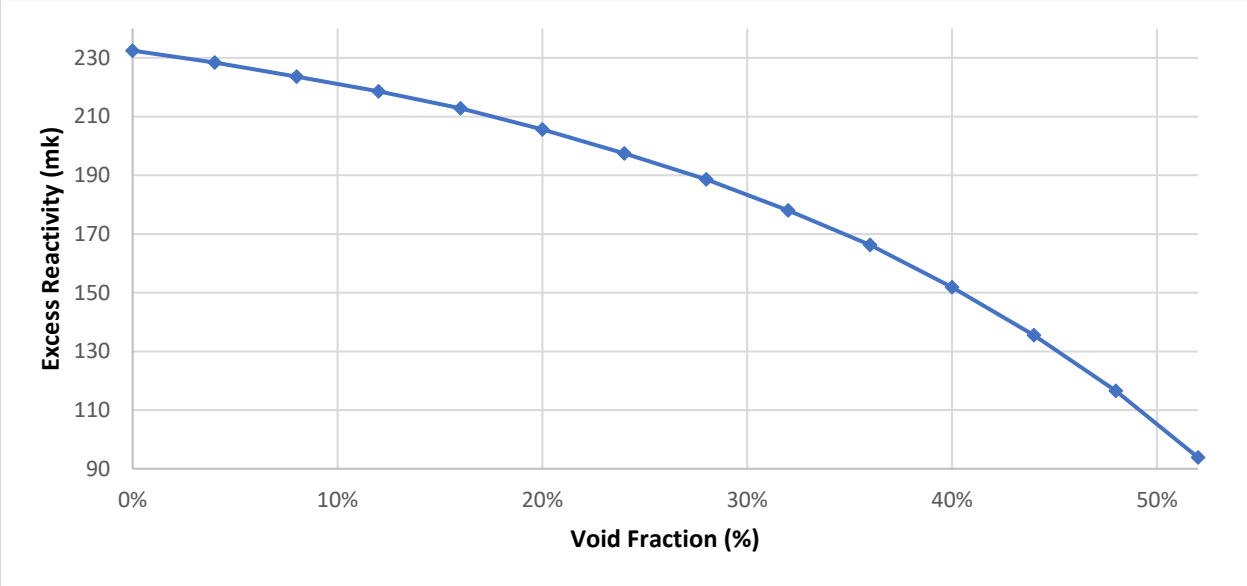

Figure 32: Variation of Excess Reactivity with Void Fraction for Beryllium Reflected OCSL Reactor

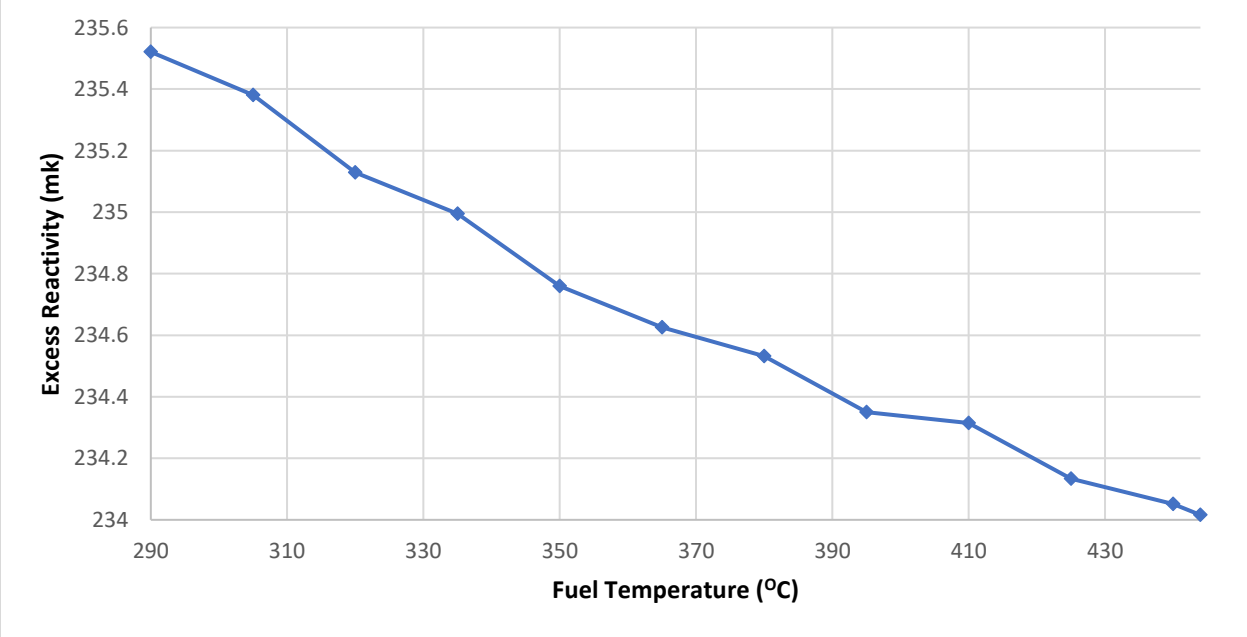

Figure 33: Variation of Excess Reactivity with Fuel Temperature for Beryllium Reflected OCSL Reactor

It is important to recognize that these analyses were conducted with fresh fuel and the reflector fully engaged at the core's edge. As previously mentioned in 8.1, the moveable reflector would be positioned away from the core while the fuel was fresh; only being fully engaged when sufficient burnup had occurred. Therefore, the situation represented in these analyses can be regarded as a worst-case scenario outside of normal operation. The reactivity correlations would only become more strongly negative with the reflector positioned farther from the core.

The results in Sections 8.3 and 8.4 have demonstrated that a beryllium reflector is highly effective in improving the neutron economy of the OCSL Reactor. The benefit of the beryllium reflector could potentially extend the service life of the OCSL fuel by almost three years. Furthermore, the basic neutronic safety analysis in this section has proven encouraging. For these reasons, the OCSL Reactor will be fitted with a 30 cm thick beryllium reflector.

Beryllium's associated toxicity does raise certain personnel and environmental safety concerns. However, it will be assumed that the OCSL containment system as well as safe handling practices can sufficiently mitigate this risk. Likewise, the costliness of beryllium could impede the financial feasibility of the reactor design. At this stage, this decision will be deferred until a cohesive financial analysis of the reactor design can be completed.

8.6 Flux Distributions for the Reflected and Non-Reflected OCSL Reactor

With a reflector now selected for the OCSL Reactor, an investigation of the reactor's neutron flux distribution can further consolidate the reflector design process. The previous sections have demonstrated the added excess reactivity contributed by the reflector results in a correspondingly longer service life of the fuel. However, these results are limited in their demonstration of the effect the reflector has on the neutronics of the reactor. Comparison of the neutron flux in the reactor with and without the reflector will verify that the desired effect has been achieved by the addition of the reflector.

In this research, neutron flux distributions are produced by MCNP simulations. The input for these simulations is the same as in KCODE calculations but an added command superimposes a counting mesh over a region of the reactor to tally the neutron flux at individual mesh points. The desired result of these simulations is the radial flux distribution at the midplane of the reactor. Consequentially, a cylindrical mesh is assigned that captures neutron flux at the midplane, at various radial distances from the centre of the core to the outer edge of the reflector, and along various azimuthal directions from the centre of the core. The OCSL Reactor is not rotationally uniform about the axis. Therefore, the flux distribution will vary slightly depending on the azimuthal direction and the materials present along that particular path. Throughout this research, neutron flux distributions will be presented for one azimuthal direction to maintain brevity. For clarity, the azimuthal direction of the radial neutron flux distributions (30^{O}) is shown in Figure 34. Additionally, the MCNP mesh also tallies neutrons by prescribed energy bins. To generate a two-group flux distribution, one bin is assigned for the thermal group and another bin is assigned for the fast group. The thermal bin tallies neutrons with energies of 0.025 eV or less while the fast bin tallies neutrons with energies greater than 0.025 eV up to 20 MeV.

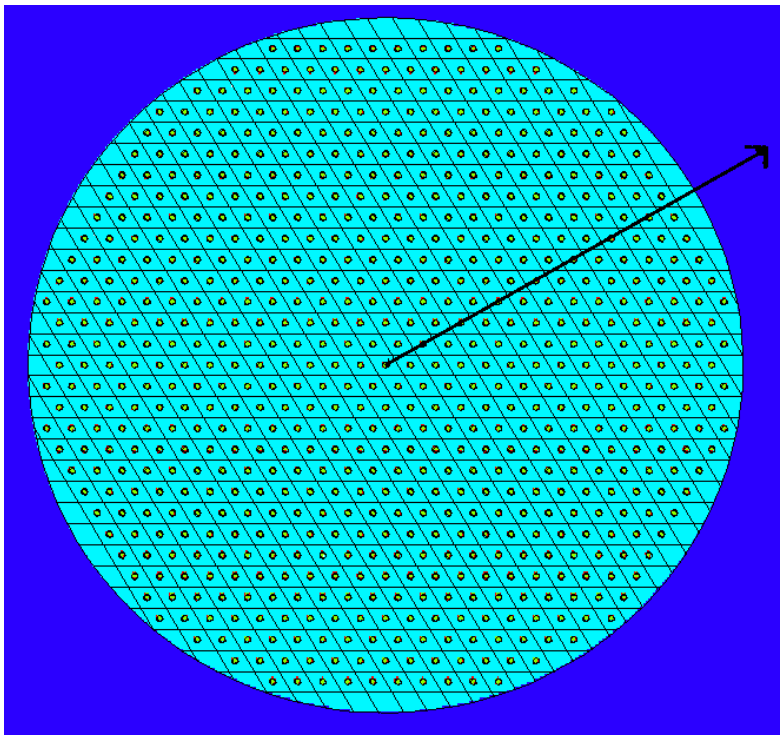

Figure 34: Azimuthal Direction of Radial Neutron Flux Distribution

To provide neutron flux distributions with adequate precision, MCNP requires far more neutron histories than when performing KCODE calculations. To sufficiently minimize the relative error, the simulations are run with the following conditions:

- simulations consisted of 1000 cycles;
- the first 50 cycles are inactive and not included in final calculations; and
- each cycle in the simulation consisted of one hundred thousand neutron histories.

To demonstrate how the added reflector affects the neutron flux in the reactor, a normalized flux distribution must first be produced without the reflector. For this purpose, one simulation generates the flux distribution for the OCSL reactor core surrounded by a large volume of HB-40. The two-group normalized neutron flux distribution for this case is presented in Figure 35. In the second simulation, the reactor is simulated with the beryllium reflector added. The two-group normalized neutron flux distribution for the case with the reflector is shown in Figure 36. All neutron fluxes in this research are normalized by the flux at the centre of the reactor.

From these figures, the neutron flux distributions are well-defined and continuous. The effect of the reflector is immediately recognizable in the distributions. With the added reflector, the flux distributions are relatively flatter across the core. At the reflector's edge, a pronounced thermal flux peak is present in the distribution with the added reflector. Correspondingly, the fast neutron flux diminishes much more gradually through the reflector than it does in HB-40. This is indicative of the beryllium reflecting neutrons back into the reactor core and thermalizing fast neutrons. The OCSL Reactor derives power primarily from thermal neutrons. Therefore, Figure 37 show the thermal neutron flux distributions compared with greater definition.

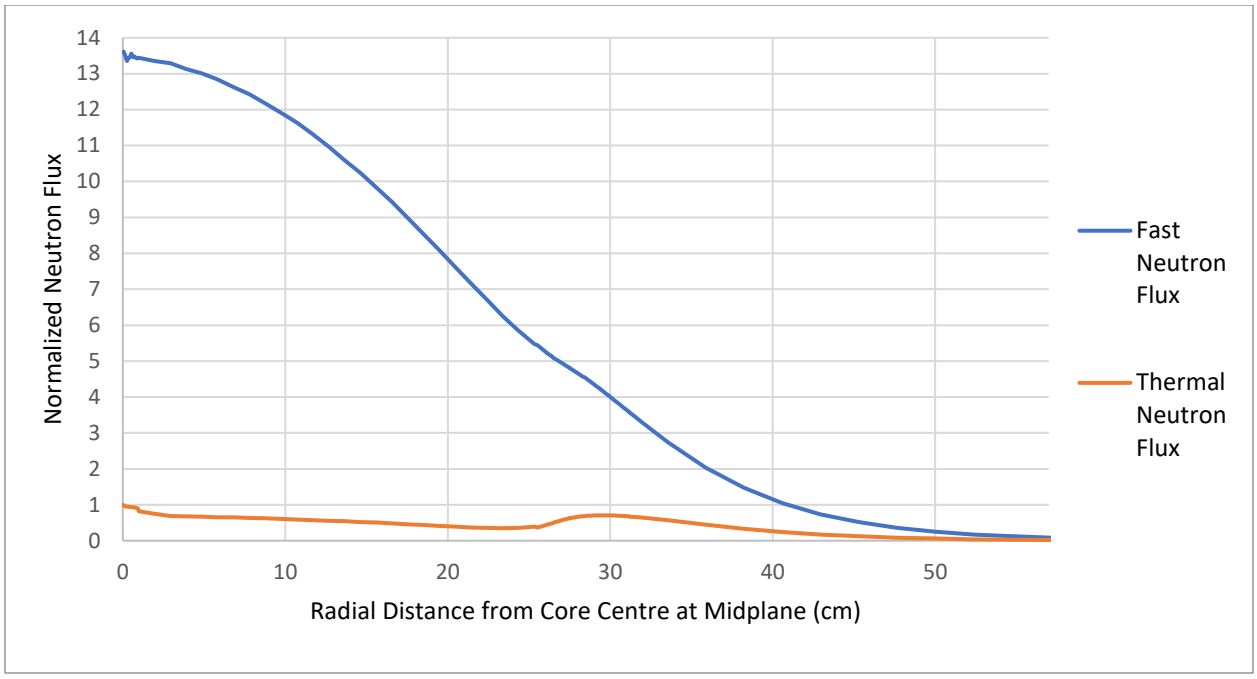

Figure 35: Two-Group Flux Distribution for OCSL Reactor Core Surrounded by HB-40

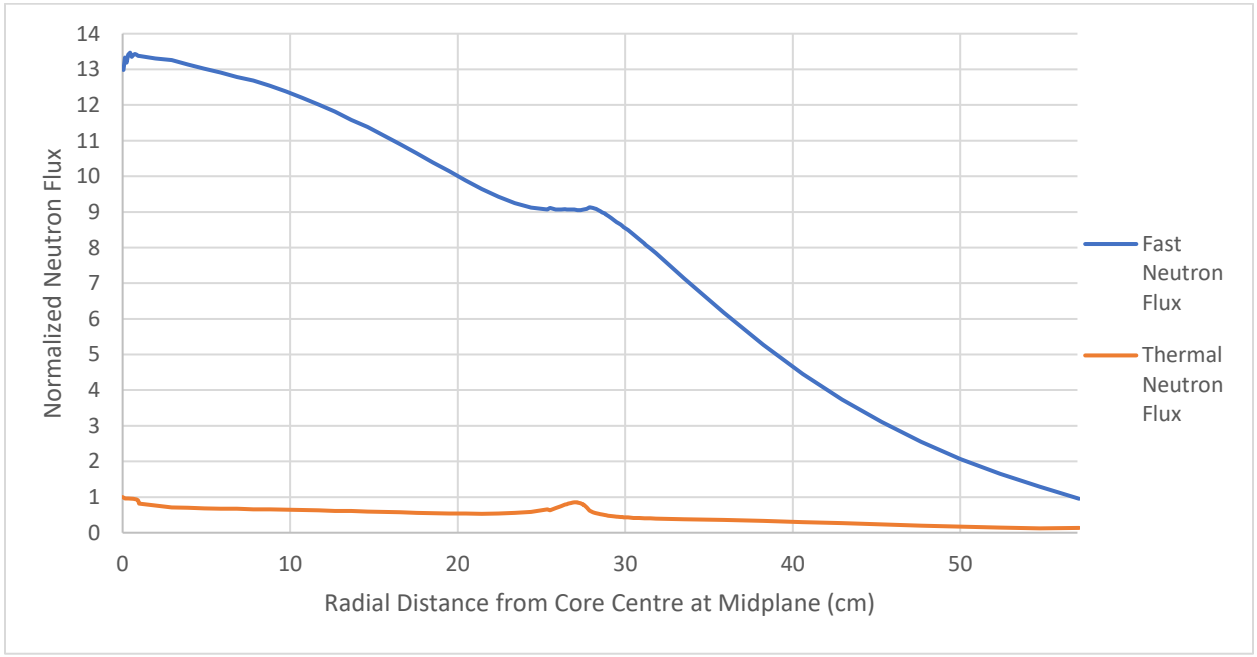

Figure 36: Two-Group Flux Distribution for OCSL Reactor with Beryllium Reflector

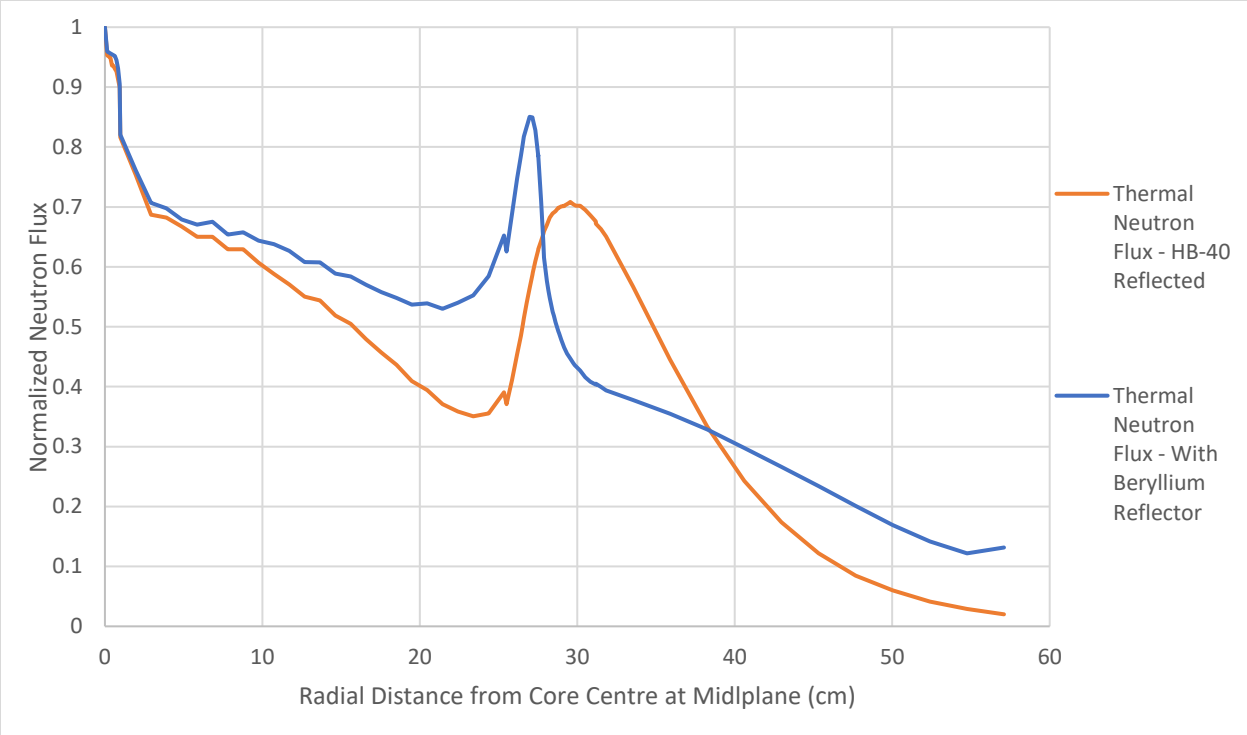

Figure 37: Comparison of Thermal Neutron Flux Distributions in OCSL Reactor with and without Beryllium Reflector

With enhanced resolution, the improvements to the thermal flux distribution yielded from the added reflector become more apparent. With the reflector, the thermal flux across the core is much flatter and the outer fuel pins experience a greater neutron flux than before. This effect will help ensure even heat generation and power distribution across the reactor core. The decision to add the beryllium reflector is strongly reinforced by comparing these two flux distributions.

8.7 OCSL Reflector with Variable Positions

In previous sections of this chapter, the notion of moveable reflector plates was discussed as a method of long-term burnup control. While the fuel in the core is fresh, the reflector plates are positioned away from the core. As the fuel is depleted under reactor operation, the reflector is moved towards the core in increments to compensate for the reduced excess reactivity in the core. The functionality of this feature will be better defined when the reactor control strategy is designed. To prepare the MCNP model for this, the current reflector is separated into plates that displace evenly in their respective radial directions.

To begin, the OCSL reflector is currently in the form of a solid annulus around the core. Numerous possibilities exist for how the reflector can be split. To illustrate this concept, several options are presented in Figure 38. Splitting the reflector into many small segments is appealing because the gaps created by the reflector withdrawing from the core are well dispersed around the core. This would prevent large irregularities in the flux distribution. However, many individual plates would necessitate many moving parts that would complicate the operating mechanism. Contrastingly, fewer divisions of the reflector is appealing for its operational simplicity but the localized and large gaps in the reflector could create flux irregularities. As a compromise, the OCSL reflector will be split into six plates.

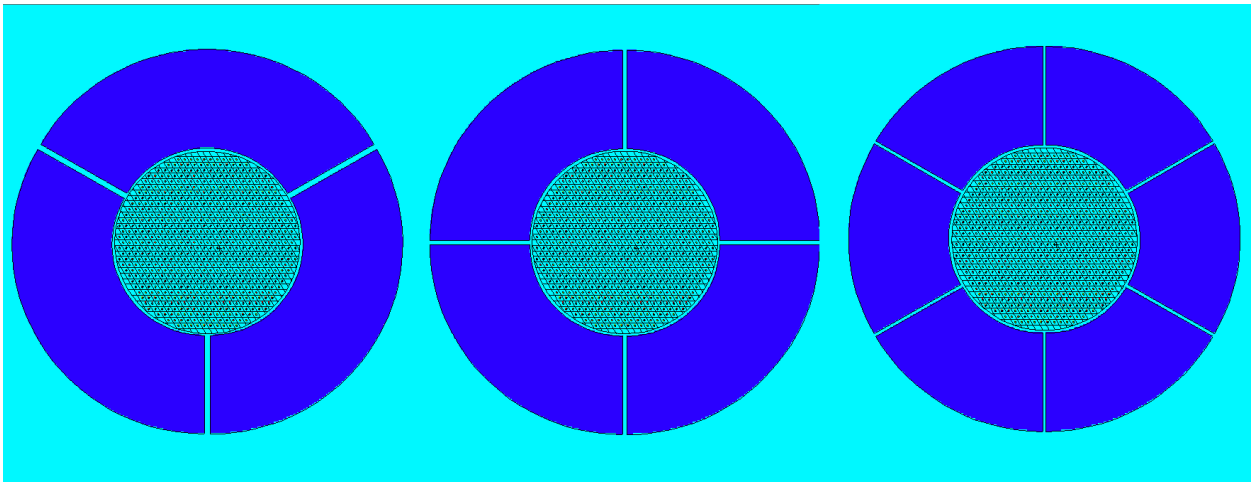

Figure 38: Various Subdivisions of the OCSL Reflector

To verify that the intended operation is feasible, a preliminary trial must confirm that the excess reactivity due to the reflector diminishes within a practical range of reflector plate displacement. If the range is too small, the mechanism could be overly sensitive and potentially dangerous. If the range is larger, it could complicate the design of the reactor's containment structures. To create the individual plates in MCNP, a cell is written for each plate. Each cell is comprised of its own series of surfaces. When the position of the reflector is to be changed, the surfaces making up each cell are recalculated and updated in the model. This is repeated for successive simulations ranging from the zero displacement position up to a displacement 16 cm from the core's edge. The results of this trial are plotted in Figure 39. These results demonstrate that the majority of excess reactivity due to the reflector diminishes as the reflector displaces 10 cm from the core's edge. This a desirable operating range for the moveable reflector because the reactor will not be excessively sensitive to reflector displacements. Displacements on the scale of centimetres and millimetres will translate to reasonable reactivity insertions. This will be favourable when designing the control strategy for the reactor in subsequent chapters.

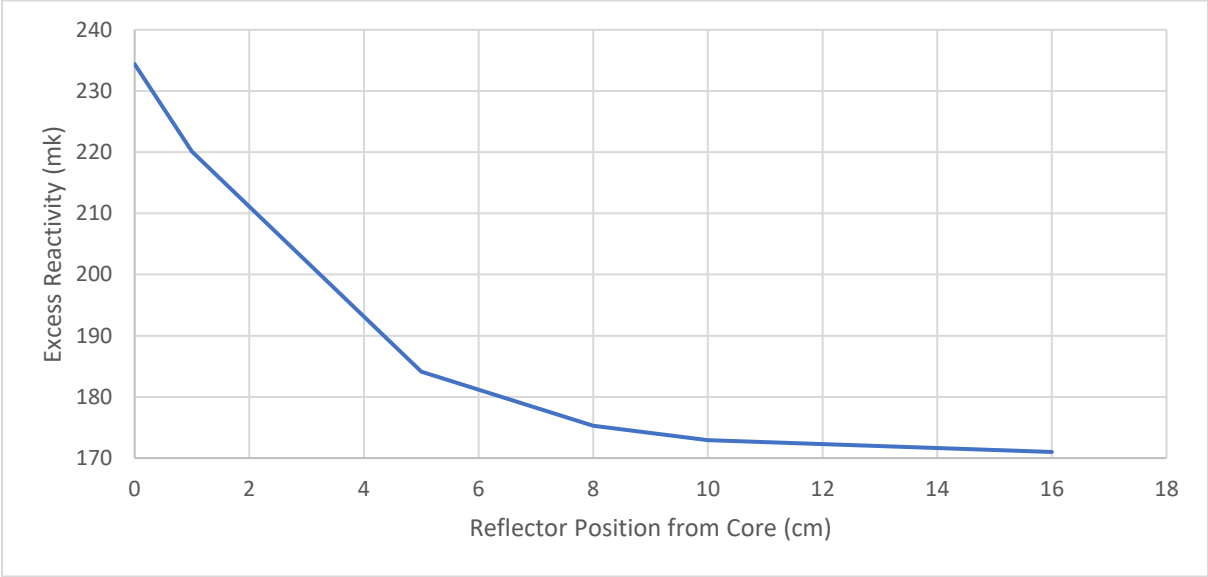

Figure 39: Variation of Excess Reactivity with Displacement of Reflector Plates

CHAPTER 9: OCSL REACTOR CONTROL STRATEGY

9.1 Introductory Comments

In the previous two chapters, the OCSL Reactor design has been developed to a stage where the excess reactivity enables the reactor to operate for well over twelve years before refuelling. While it is certainly a desirably long service life, the reactor requires a control system to manage the large reserve of reactivity to maintain safe operation of the reactor. During normal operation, the reactor control system must be capable of fine adjustments to power and criticality. In accident scenarios, the control system must possess a suitably large reserve of negative reactivity to bring and maintain the reactor sub-critical under all circumstances.

This chapter will explain the development of the control strategy for the OCSL Reactor. First, the components of OCSL Reactor control system must be identified. As mentioned in Section 8.7, the moveable reflector plates will factor into the reactor's control system. Reflecting the choice of control mechanism, a material selection must identify the most appropriate materials for the OCSL Reactor environment. The control system will then be implemented in the OCSL reactor to finally arrive at a start-up configuration for the OCSL Reactor. This stage will complete the design of the OCSL Reactor within the scope of this research.

Regarding nomenclature, *OCSL Reactor* will refer to the reactor with its fitted control system henceforth. The present design with 685 fuel pins and 30 cm beryllium reflector will be referred to as the *Baseline OCSL Reactor*.

9.2 The OCSL Reactor Control System

The two primary functions of any reactor control system are regulation of the reactor during normal operation and shutdown of the reactor during normal and emergency operation. Regulation control is further divided into two distinct domains of control; long-term and short-term. First, long-term control, or shim control, is the process of managing the excess reactivity of the reactor to compensate for depletion of fuel and buildup of poisons in the core. Secondly, short-term control refers to finely adjusting criticality in the core to increase, decrease or maintain reactor power in response to operational perturbations internal or external to the reactor. The shutdown function of the reactor control system must be capable of gradually rendering the reactor subcritical under normal operation. Furthermore, the control system must be able to quickly bring about shutdown in the event of an emergency[109]. The components of a reactor control system may serve one or both primary control functions. For example, the previously discussed moveable reflector plates mainly serve as a means of long-term control to compensate for declining excess reactivity over the core's service life. However, incorporation of a mechanism to quickly draw the plates away from the core would also serve the emergency shutdown function by removing a significant amount of excess reactivity.

In general, the control system operates by inserting into the reactor a material whose absorption cross section is large enough to compete with the fission cross section of the fuel. The presence of the absorbing material influences the neutron flux thereby adjusting the criticality of the reactor[110]. The simplest method of inserting absorptive materials into the reactor core is through employment of absorber rods. In this case, one or more rods containing absorptive material perform the two primary control functions. The extent of the controlling action is adjusted through the number of rods inserted and the depth of insertion of individual rods. Alternatively, absorptive materials can be dissolved into liquid

coolants and moderators to produce similar effects. For practicability, the absorption reaction must see the absorber nuclide transition to a nuclide with a lower absorption cross-section. These nuclides are known as burnable poisons[109]. Control action in this case is managed by the concentration of the absorber in the coolant or moderator. Within the scope of this research, burnable poisons will not be considered because supporting research for the employment of burnable poisons in organic coolants is presently non-existent.

The OCSL Reactor control system will consist of absorber rods distributed throughout the core and the moveable reflector plates previously described. The absorber rods are considered in two categories; control rods and shutdown rods. In this research, a control rod will refer to an absorber rod that replaces a fuel pin in the core. When referring to shutdown rods, these are absorber rods that are located in vacant space between the core and the reflector. Twenty-four locations are identified around the periphery of the core where a reasonably sized absorber rod could be placed. These rods exist primarily to counteract the excess reactivity contributed by the reflector when it is at the core's edge with fresh fuel. They ensure the reactor remains in a shutdown state even in this worst-case scenario. By incorporating shutdown rods, fewer control rods are required in the core. This reduces the number of fuel channels replaced by absorber rods and improves the lifespan of the core. Shutdown rods also enhance the redundancy of OCSL Reactor's emergency shutdown control thereby improving overall safety. Figure 40 illustrates the two types of absorber rods in the OCSL Reactor core with control rods shown in red and shutdown rods shown in green. This figure also illustrates the twenty-four shutdown rod locations. Table 17 presents a summary of the components of the OCSL Reactor's control system by the control functions they serve.

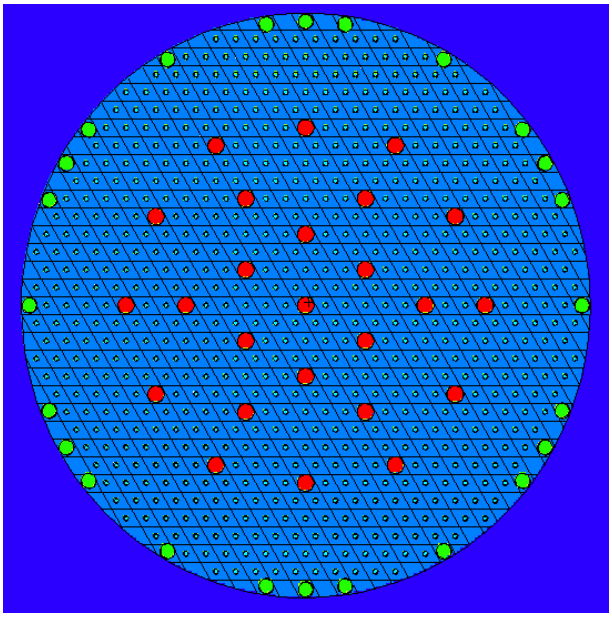

Figure 40: Control Rods and Shutdown Rods in OCSL Reactor

Table 17: Summary of OCSL Reactor Control System

Control Function	Control System Component(s)
Regulation (Short-term)	Control Rods
Regulation (Long-term)	Control Rods Moveable Reflector Plates
Shutdown	Control Rods Shutdown Rods
Emergency Shutdown	Moveable Reflector Plates

9.3 Absorber Rod Material Selection

The OCSL Reactor is meant to extend the power of the SLOWPOKE-2 reactor to meet demands of district heating or electrical power generation. Therefore, the logical starting point in the material selection is with the original control material of the SLOWPOKE-2. The SLOWPOKE-2 employs a single cadmium rod in the centre of the core as a means of controlling the reactor's power. Considering

only neutronics, cadmium is an appealing material choice because of its large thermal neutron absorption cross-section. However, the material is severely limited by its melting point of 321 ^{O}C[111]. For the SLOWPOKE-2, this is not a concern because the unpressurized water that cools the reactor would likely never reach a temperature above 100 ^{O}C. Operating with organic coolant, the OCSL Reactor's average coolant temperature is 315 ^{O}C with a maximum temperature of 340 ^{O}C. Due to these conditions, cadmium is an unsuitable control material for the OCSL Reactor.

From an operating temperature standpoint, the OCSL Reactor is more like a pressurized water reactor (PWR) than it is the SLOWPOKE-2. Therefore, the next logical step in material selection is to consider PWR control materials for employment in the OCSL Reactor. PWR control materials include alloys that contain absorptive nuclides of boron, cadmium, indium, silver, or hafnium as well as metallic hafnium. Of these materials, metallic hafnium is often preferred for its superior balance of neutronic, mechanical and physical properties. Table 18 presents hafnium's neutronic properties with the previously discussed cadmium material for relative comparison. As the table shows, hafnium has a moderate absorption cross-section compared to cadmium. However, its neutronic suitability as a control material is enhanced by containing four isotopes that contribute to absorption. These four isotopes comprise nearly ninety-five percent of hafnium's natural abundance and each isotope has a large resonance cross-section. Natural hafnium demonstrates a long service life because lighter isotopes transition to heavier isotopes with subsequent neutron captures and remain effective until becoming hafnium-181. Hafnium metal is stable at the OCSL's operating temperature. From a mechanical standpoint, the metal has sufficient strength but can also be machined with relative ease[111]. Because of its superior performance, the absorber rods in the OCSL Reactor will be fabricated with natural hafnium metal.

Table 18: Control Material [111]

Material	Nuclide	Abundance (%)	Microscopic 0.0253 eV Absorption Cross-Section (barns)	Macroscopic 0.0253 eV Absorption Cross-Section / 10^2 (m^{-1})	Major Resonances	
					Energy (eV)	Microscopic Cross-Section (barns)
Cadmium			2450	113		
	Cadmium-113	12.3	19800		0.18	7200
Hafnium			113	5.06		
	Hafnium-177	18.5	390		2.36	6000
	Hafnium-178	27.2	90		7.8	10000
	Hafnium-179	13.8	84		5.69	1100
	Hafnium-180	35.1	14		74	130

9.4 Absorber Rod Dimensions

Absorber rods must be appropriately dimensioned for a particular reactor to ensure efficiency and effectiveness in the reactor's control system. In all OCSL models, the absorber rods will have the same length as the core; 50cm. However, the ideal diameter for the rods requires certain consideration. Should the rod diameter be too small, more rods will be required to control the reactor leading to fewer fuel channels and shorter service life for the core. This will also over-complicate the control system due to the sheer number of rods to incorporate and actuate for regulation of the reactor. On the other hand, the absorber rods can be designed with larger diameters so that they replace more than one fuel channel. However, this approach could cause the same issues as rods that are too small.

To ease the process, it is best to determine whether an optimum absorber rod dimension exists at the scale of the reactor. As the absorber rod's diameter is increased, its negative reactivity, or worth, also increases. For some large diameter, neutrons will cease to penetrate deeper into the rod and the worth of subsequently larger rods will only benefit from the additional moderator they displace. A diminished slope between rod worth and diameter would likely signal this effect. If such a transition occurred at a rod diameter that was feasible for the scale of the reactor, this diameter could be regarded as an optimum diameter.

This procedure is tested using MCNP simulations. Working from a central absorber rod position, the diameter of the rod is increased in consecutive simulations. To estimate rod worth, the resulting effective multiplication factor is compared with the effective multiplication factor of the reactor with a vacant channel in place of the rod. As the rod diameter increases and begins to invade adjacent fuel channels, those fuel elements are removed. At this point, results are compared to the reactor with these added vacancies. Figure 41 displays a plot of the results of the trial starting from an equivalent diameter to the fuel pin up to 92 mm. Table 19 presents the results in full.

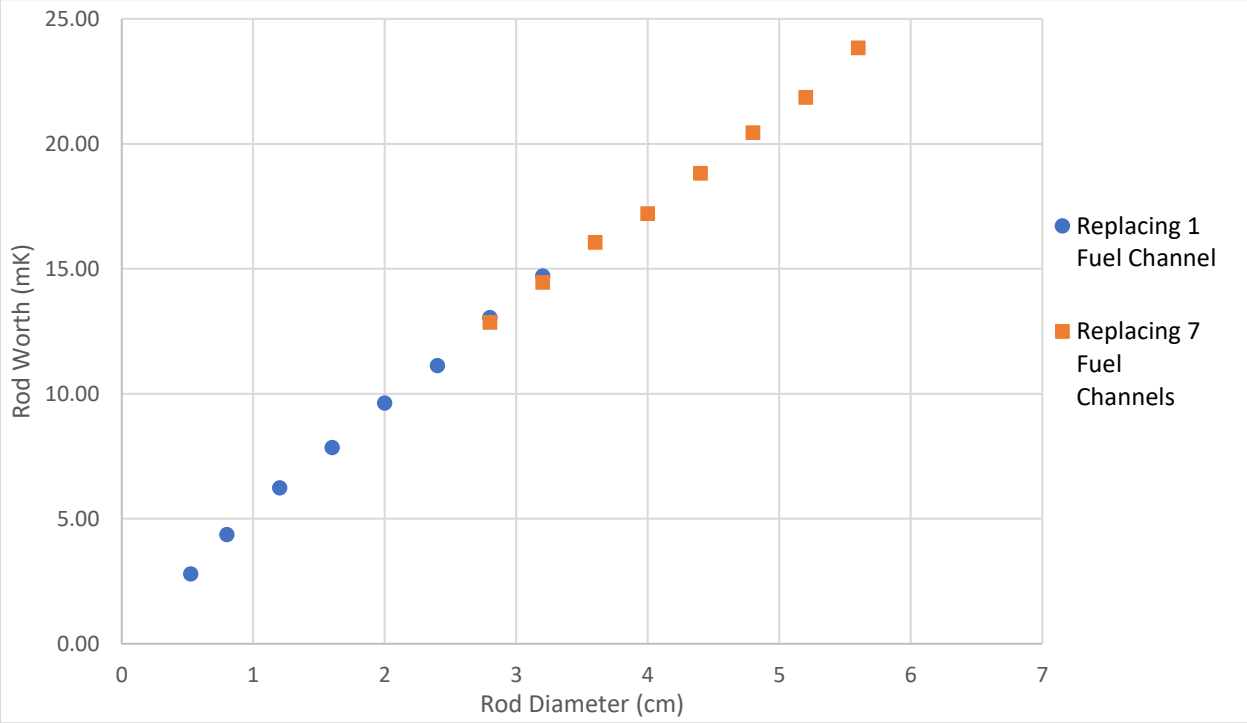

Figure 41: Plot of Absorber Rod Dimensioning Trial

Table 19: Absorber Rod Dimensioning Trial

Absorber Rod Diameter (cm)	Fuel Rods Replaced	Absorber Rod In		Absorber Rod Out		Approximate Rod Worth (mk)
		Effective Multiplication Factor	Standard Deviation	Effective Multiplication Factor	Standard Deviation	
0.525	1	1.30112	0.00024	1.30586	0.00028	2.79
0.8	1	1.29846	0.00022	1.30586	0.00028	4.36
1.2	1	1.29532	0.00023	1.30586	0.00028	6.23
1.6	1	1.29261	0.00022	1.30586	0.00028	7.85
2.0	1	1.28965	0.00023	1.30586	0.00028	9.63
2.4	1	1.28716	0.00023	1.30586	0.00028	11.13
2.8	1	1.28398	0.00024	1.30586	0.00028	13.05
3.2	1	1.28124	0.00025	1.30586	0.00028	14.72
2.8	7	1.27971	0.00026	1.3011	0.00023	12.85
3.2	7	1.27709	0.00022	1.3011	0.00023	14.45
3.6	7	1.27448	0.00022	1.3011	0.00023	16.05
4.0	7	1.27262	0.00025	1.3011	0.00023	17.20
4.4	7	1.27001	0.00026	1.3011	0.00023	18.81
4.8	7	1.26738	0.00025	1.3011	0.00023	20.45
5.2	7	1.26513	0.00022	1.3011	0.00023	21.85
5.6	7	1.26196	0.00023	1.3011	0.00023	23.84

The results clearly show a consistent slope between the worth and diameter of the absorber rods. Accordingly, this result implies that such an optimal diameter is not possible at the scale of the OCSL Reactor. Moving forward, the most ideal diameter for the control rods must be the largest diameter that replaces a single fuel channel. By this method, the greatest amount of negative reactivity is gained for each fuel channel sacrificed. For the OCSL Reactor lattice, this ideal diameter is 1.688 cm. When similar logic is applied to a rod replacing seven fuel channels, the ideal diameter is 3.377 cm. The final control rod layout with 1.688 cm rods will be compared to a layout with 3.377 cm rods. This step will verify which rod size results in the greatest number of fuel channels retained in the design.

The inner edge of the reflector limits the diameter of the shutdown rods. As a starting point, all shutdown rods will be assigned a diameter corresponding to the smallest location available. This initial shutdown rod diameter is 0.9 cm. However, some locations can house a larger shutdown rod, so design of the absorber rod layout must consider the benefits of increasing the size of some shutdown rods.

9.5 Numbering of Multiple Control Rods

The OCSL Reactor requires multiple control rods distributed across its core to safely regulate the excess reactivity. The process of arranging multiple control rods to achieve an ideal layout quickly becomes haphazard due to the sheer number of possible configurations. In this research, the process is maintained as logical and methodical as possible by developing a clear numbering system for rods.

When numbering the control rods, the obvious starting point is the centre of the core where one central control rod will always be placed. As rod worth depends highly on the neutron flux at a particular

location before insertion, control rods are always placed at the centre of the core where neutron flux generally reaches a maximum[112]. In the OCSL Reactor, this central control rod will be assigned the number “1”. Moving outward from the core axis, preserving rotational symmetry in the core becomes an important facet of designing the control rod layout. By maximizing symmetry in the layout, fewer flux distortions are created and the uniformity of heat generation and fuel depletion throughout the core is improved. Core symmetry is accomplished by grouping multiple control rods into clusters. In operation, a common plate connects the cluster of rods so that actuation of the cluster moves the rods in unison with each other. In the OCSL Reactor, symmetrical clusters are governed by the symmetry of the lattice that arranges the fuel pins in the core. The OCSL lattice can be regarded as triangular or hexagonal. Either way, clusters contain either six or twelve rods based on this type of lattice.

Figure 42 presents a general illustration of the numbering scheme for control rods in the OCSL Reactor. For reasons explained later in this section, two control rods are never placed adjacent one another. At least one fuel channel will always be kept between control rods. Starting from central control rod “1”, the first available position for control rods moving outward is denoted in the figure with cluster “3”. This position only has space for six rods while respecting the mentioned rod spacing. Following Figure 42, the next available positions are denoted by “5”. In this case, two different clusters are possible and are therefore identified by letters as “5a” and “5b”. Both clusters contain six control rods. Moving again to the next available positions in this example, two more clusters are denoted by “7”. However, cluster “7a” is a unique case compared to previous examples. Displayed in the figure, cluster “7a” is composed of twelve control rods to maintain symmetry about the core axis. Alternatively, cluster “7a” could contain only six control rods if they replaced the fuel channel between the rods shown in the figure. This example not only illustrates the general rules for control rod numbering but also demonstrates the presence of complexity and contradiction despite the rules. This numbering system will not always be perfect or exact, therefore figures will be included when pertinent.

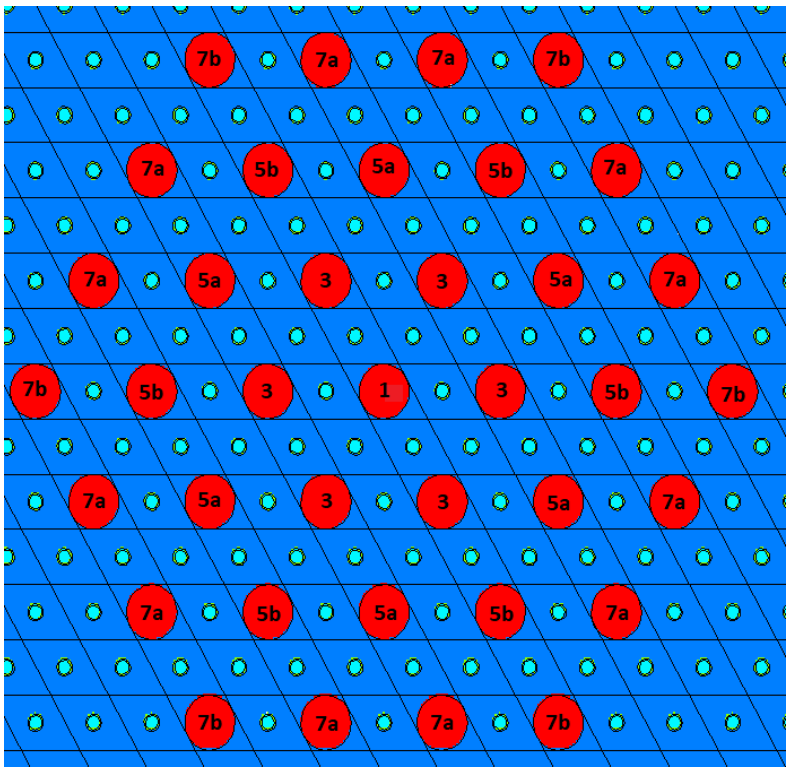

Figure 42: Control Rod Numbering

9.6 Position and Orientation of Control Rod Clusters

As the previous section stated, arranging control rods to achieve the most effective layout can be a daunting task. An understanding of the rod-to-rod interaction that occurs between multiple control rods makes the process more methodical. When multiple absorber rods are employed in a reactor, the spacing between rods has a significant effect on each rods' worth. The process of idealizing a reactor's control rod layout is often a matter of idealizing the spacing between individual rods so that the total worth of all rods is maximized. In turn, fewer rods are required to control the reactor and the total number of fuel channels is maximized. This process is not being described as optimization in this research because flux shaping is not within the scope of this work. Future design work may optimize the core layout for a greater number of parameters besides total fuel channels.

Figure 43 illustrates the effect of one absorber rod on the surrounding radial flux distribution. From the picture, the neutron flux increases to a maximum at some distance from the first rod and then decreases for larger distances. Understanding that the rod worth is proportional to the neutron flux at a location, the worth of a second rod will initially increase as it is placed further from the first rod. Eventually, the worth will reach a maximum and then begin to diminish for larger distances. When designing the control rod layout, this effect must be idealized in two dimensions. This effect can be demonstrated with two preliminary trials.

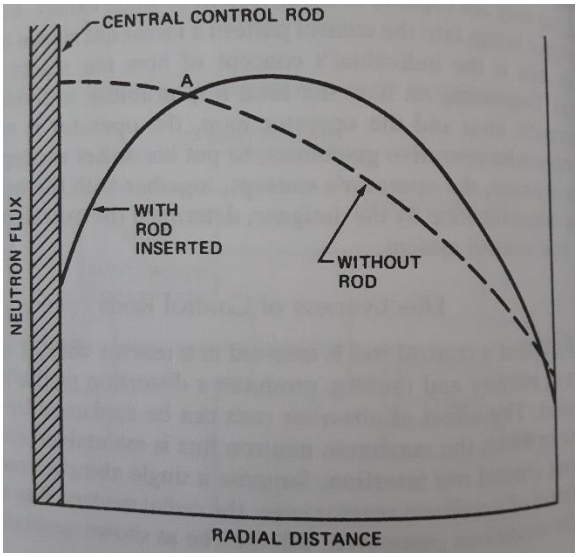

Figure 43: Effect of Central Control Rod on Radial Neutron Flux Distribution[112]

The first trial employs MCNP simulations to demonstrate the rod-to-rod interaction in the radial direction. Working with a central control rod and a single six rod cluster, the cluster is moved farther from the centre in consecutive simulations and the resultant effective multiplication factors are tracked. The results are presented in Table 20 and Figure 44. The maximum rod worth for the cluster occurs around the "6c" and "7c" positions. This trial shows that the maximum worth of the cluster occurs relatively far from the central rod. If this method were continued for subsequent clusters, the core would never be sub-critical because available space in the core would run out before sufficient negative reactivity was added. Therefore, a sub-critical control rod arrangement will be prioritized when designing the layout. Starting from a subcritical arrangement of clusters, cluster positions can be varied to achieve a greater total rod worth and a lower effective multiplication factor.

In the second trial, MCNP simulations are again employed to demonstrate the rod-to-rod interactions when the orientation of a cluster about the axis is varied. The OCSL core in these simulations is fitted with thirteen control rods; one central rod, a six-rod cluster in the "4" position, and a six-rod cluster in the "7" position. In the first simulation, the outermost cluster is oriented in the "7b" position. In the next simulation, this cluster is rotated thirty degrees so that the control rods now sit in the "7a" position. The two cases are illustrated in Figure 45 and Figure 46. The effective multiplication factor for the first simulation was 1.17526 with a standard deviation of 0.00025. The effective multiplication factor of the second simulation was 1.17950 with a standard deviation of 0.00024.

Table 20: Trial of Various Control Rod Spacings

Control Rod Positions Fully Inserted	Control Rod Spacing (cm)	Effective Multiplication Factor	Standard Deviation
1, 3	3.9	1.24295	0.0003
1, 4	5.85	1.23057	0.00025
1, 5b	7.8	1.22522	0.00027
1, 6c	9.75	1.22328	0.00027
1, 7c	11.7	1.22327	0.00025
1, 8d	13.65	1.22534	0.00024
1, 9e	15.6	1.22961	0.00026

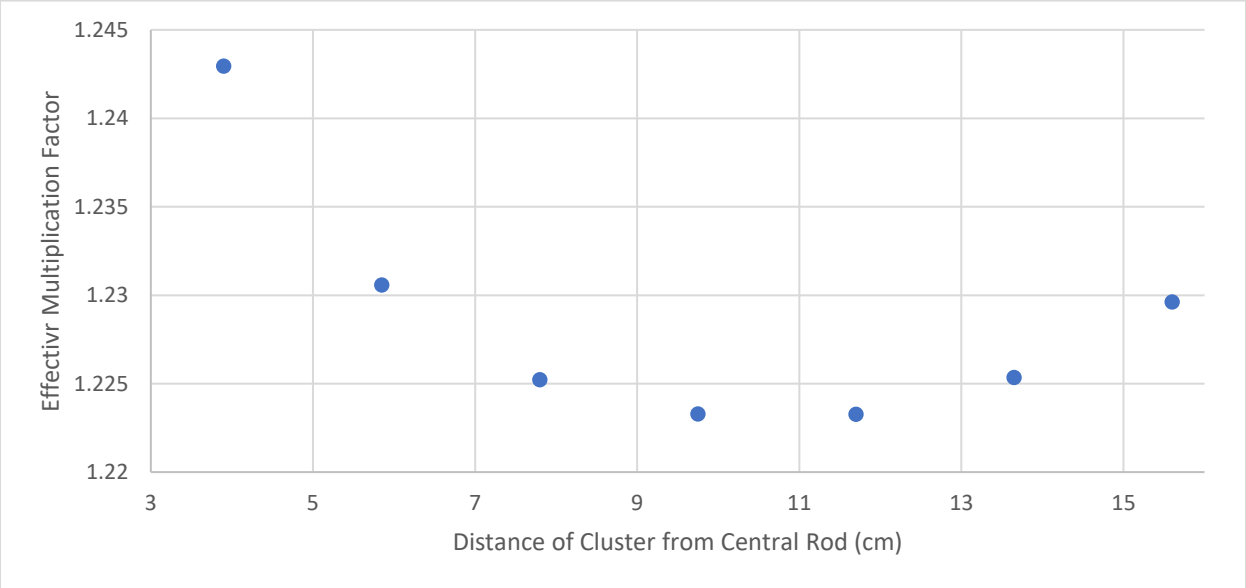

Figure 44: Variation of Effective Multiplication Factor with Control Rod Spacing

An investigation of these results requires a representation of the average spacing between rods that are directly interacting with each other. For this purpose, the average spacing was defined as the average distance between a control rod and its five nearest neighbouring rods. Effectively, these are the rods whose worth are most influenced by that particular rod. By this definition, the average spacing was 8.1 cm for the first case while the second case saw a lesser average spacing of 7.0 cm. If the average spacing is accepted as a measure of the overall dispersal of the control rods, the results between the two simulations make sense. By changing the orientation of the number "7" cluster, the control rods became

less dispersed and the net effect was a reduction in rod worth and a greater effective multiplication factor. Moving forward, the orientation of control rod clusters must be considered when idealizing the rod layout in the OCSL Reactor. Like cluster positioning, alternate cluster orientations will be investigated once an overall sub-critical layout is achieved. With this practice, the overall rod worth in the control rod layout will be maximized.

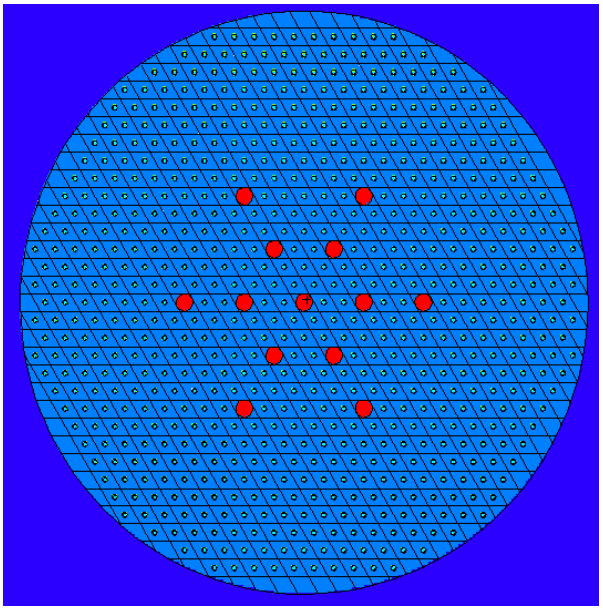

Figure 45 Control Rod Arrangement with 7b Outer Cluster

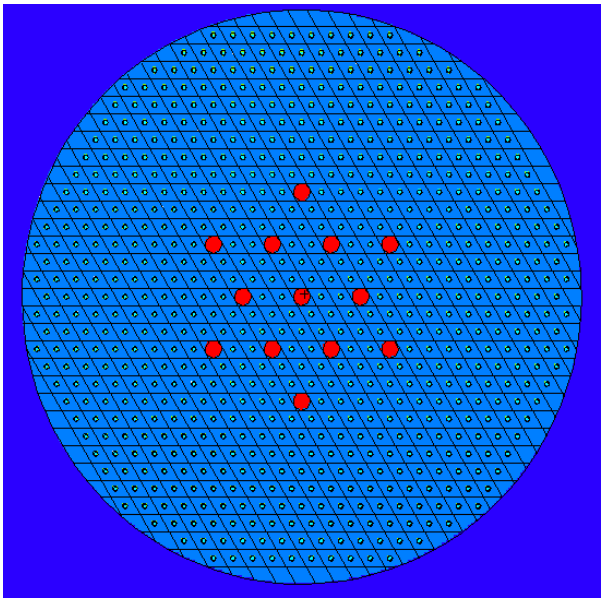

Figure 46: Control Rod Arrangement with 7a Outer Cluster

9.7 Absorber Rod Arrangement for the OCSL Reactor

The absorber rod arrangement for the OCSL Reactor is first designed using MCNP simulations. The control system must be capable of maintaining the reactor sub-critical under all conditions. Therefore, the simulations are conducted with fresh fuel and the reflector plates fully inward at the core's edge. These conditions represent the worst-case scenario where excess reactivity is at a maximum. This situation may arise during installation and start-up of the reactor.

The conclusions drawn from the previous section inform the general method to be applied in developing an idealized absorber rod layout. The sequence of steps used to arrive at a final arrangement are as follows;

1. Starting with a central control rod, rod clusters are added moving in an outward fashion. With each addition to the arrangement, the reactor is simulated, and the resulting effective multiplication factors are tracked. In this stage, a pattern is followed as control rod positions are filled. This ensures the process remains well-ordered. For instance, if the first cluster added is in the "3" position, the next cluster will be at "5a", the next at "5b", the next at "7a", and so on.

2. When the reactor becomes subcritical with all control rods inserted, the addition of new control rod clusters is ceased. At this stage, the twenty-four 0.9 cm shutdown rods are added to the model and the reactor is simulated again. The effective multiplication factor will become very sub-critical upon the addition of shutdown rods.

3. With shutdown rods added, the total fuel channels are increased by an iterative process of removing and adding clusters. With each iteration, clusters are reverted to fuel elements and the reactor is simulated. In some cases, a twelve-rod cluster is reverted while a six-rod cluster is added for a net decrease in the effective multiplication factor. The conclusions regarding control rod spacing from the previous section guide the selection of clusters for reversion. The objective of this stage is to increase the fuel channels while maintaining the effective multiplication factor sub-critical and as low as possible.

4. If the total number of fuel channels or the effective multiplication factor is unsatisfactory, the diameters of certain shutdown rods may be increased. Step 3 is then repeated attempting to increase the total fuel channels.

5. When the total number of fuel channels is satisfactory, the remaining clusters are adjusted to ensure maximum rod worth. Employing the conclusions drawn from preliminary trials, the position or orientation of clusters are individually adjusted, and the reactor is simulated. This is repeated for more clusters until the effective multiplication factor is minimized.

The results of the first step of designing the absorber rod arrangement are presented in . A sub-critical arrangement is achieved in both highlighted cases with 37 control rods. These arrangements reduce the total number of fuel channels to 648. Understandably, the addition of shutdown rods can improve this number.

Table 21: First Round of Absorber Rod Arrangements

Control Rod Positions Fully Inserted	Control Rod Diameter (cm)	Total Control Rods	Shutdown Rod Diameter (cm)	Total Shutdown Rods Rods	Fuel Channels	Effective Multiplication Factor	Standard Deviation
Baseline		0		0	685	1.30617	0.00023
1, 3	1.688	7	0.9	0	678	1.24295	0.00030
1, 4	1.688	7	0.9	0	678	1.23057	0.00025
1, 4, 7a	1.688	13	0.9	0	672	1.1795	0.00024
1, 4, 7a, 7b	1.688	19	0.9	0	666	1.1344	0.00028
1, 4, 7a, 7b, 10a	1.688	31	0.9	0	654	1.03971	0.00028
1, 4, 7a, 7b, 10a, 10b	1.688	37	0.9	0	648	0.99212	0.00028
1, 5b	1.688	7	0.9	0	678	1.22522	0.00027
1, 5b, 9a, 9c	1.688	19	0.9	0	666	1.11062	0.00024
1, 5b, 9a, 9c, 13b, 13d	1.688	37	0.9	0	648	0.95424	0.00024

Once the shutdown rods are added, the third step is followed for the two sub-critical arrangements from the first round. presents the results of adding the shutdown rods and subsequently reducing the total control rods in the arrangements. As expected, the effective multiplication factor decreases drastically with added negative reactivity from the shutdown rods. The reduction permits the reversion of 12 control rods back to fuel channels increasing the total number of fuel channels to 660. All attempts to further increase the total number of fuel channels are unsuccessful. As a result, the arrangement with 660 fuel channels and the lowest effective multiplication factor are retained for further refinement.

Table 22: Second Round of Absorber Rod Arrangements with Shutdown Rods Added

Control Rod Positions Fully Inserted	Control Rod Diameter (cm)	Total Control Rods	Shutdown Rod Diameter (cm)	Total Shutdown Rods Rods	Fuel Channels	Effective Multiplication Factor	Standard Deviation
1, 4, 7a, 7b, 10a, 10b	1.688	37	0.9	24	648	0.8965	0.00028
1, 4, 7a, 7b, 10b	1.688	25	0.9	24	660	0.99384	0.00027
1, 4, 7b, 9a, 10b	1.688	25	0.9	24	660	0.98346	0.00024
1, 5a, 7b, 9a, 10b	1.688	25	0.9	24	660	0.98151	0.00025
1, 5b, 9a, 9c, 13b, 13d	1.688	37	0.9	24	648	0.89421	0.00028
1, 5b, 9a, 9c, 13d	1.688	25	0.9	24	660	0.9881	0.00028
1, 5b, 9a, 10c	1.688	19	0.9	24	666	1.03192	0.00024
1, 5b, 10b	1.688	19	0.9	24	666	1.03206	0.00024
1, 5a, 10b	1.688	19	0.9	24	666	1.03316	0.00025
1, 5b, 9a, 9c	1.688	19	0.9	24	666	1.03118	0.00029
1, 5b, 8c, 9a	1.688	19	0.9	24	666	1.03402	0.00028

In subsequent simulations, the diameters of six of the shutdown rods are enlarged from 0.9 cm to 1.5 cm in an effort to improve the arrangement. At this stage, only six shutdown rods are enlarged because the others are limited in diameter by the reflector edge. presents an illustration of this alteration. The larger shutdown rods reduce the effective multiplication factor but attempts to increase the total number of fuel channels are unsuccessful. Therefore, the fifth step is followed to further reduce the effective multiplication factor and idealize the arrangement. The results of this stage are presented in Table 23. As the positions and orientations of clusters are adjusted, a new minimum effective multiplication is achieved in the highlighted case. This result implies that the worth of the absorber rods has been maximized as much as possible. Therefore, this arrangement is retained for finalization. The selected arrangement is the one seen in .

Originally, a configuration was to be attempted using control rods of 3.377 cm diameter that would replace seven fuel channels each. However, such a trial becomes impractical given the previously developed arrangement. As the current absorber rod arrangement only contains twenty-five control rods, any new and improved arrangement would need to further increase the total fuel channels. By simple math, the arrangement of larger control rods would be limited to three rods. Any such arrangement is unlikely to comprise enough negative reactivity to control the reactor. Furthermore, large distortions in the neutron flux distribution are likely to result from the lack of symmetry in a three-rod arrangement.

Table 23: Third Round of Absorber Rod Arrangements with Some Shutdown Rods Enlarged

Control Rod Positions Fully Inserted	Control Rod Diameter (cm)	Total Control Rods	Shutdown Rod Diameter (cm)	Total Shutdown Rods Rods	Fuel Channels	Effective Multiplication Factor	Standard Deviation
1, 5a, 7b, 9a, 10b	1.688	25	6x 1.5cm + 18 x 0.9cm		660	0.97294	0.00026
1, 5b, 9a, 9c	1.688	19	6x 1.5cm + 18 x 0.9cm		666	1.02279	0.00023
1, 3, 7b, 9a, 10b	1.688	25	6x 1.5cm + 18 x 0.9cm		660	0.98668	0.00027
1, 7a, 7b, 9a, 10b	1.688	25	6x 1.5cm + 18 x 0.9cm		660	0.981	0.00023
1, 5a, 6b, 9a, 10b	1.688	25	6x 1.5cm + 18 x 0.9cm		660	0.97641	0.00026
1, 5a, 8b, 9a, 10b	1.688	25	6x 1.5cm + 18 x 0.9cm		660	0.97509	0.00023
1, 5a, 7a, 7b, 10b	1.688	25	6x 1.5cm + 18 x 0.9cm		660	0.98645	0.00028
1, 5a, 7b, 10b, 11a	1.688	25	6x 1.5cm + 18 x 0.9cm		660	0.96992	0.00023
1, 5a, 7b, 11a, 9b	1.688	25	6x 1.5cm + 18 x 0.9cm		660	0.97425	0.00028
1, 5a, 7b, 11a, 11b	1.688	25	6x 1.5cm + 18 x 0.9cm		660	0.97074	0.00027

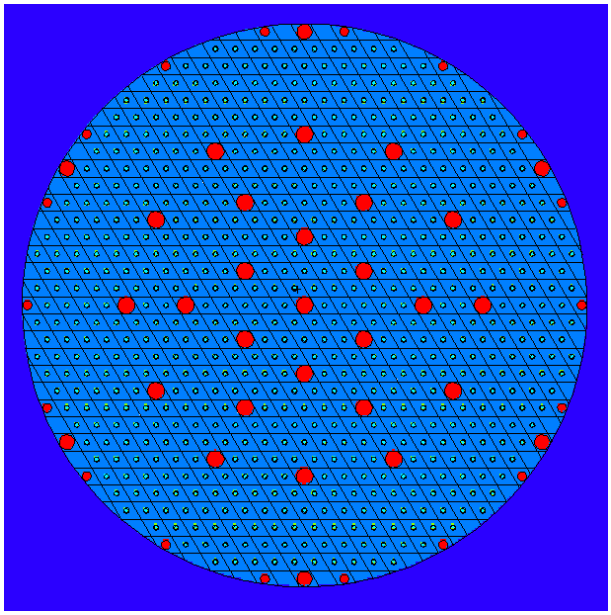

Figure 47: Absorber Rod Arrangement with Six Enlarged Shutdown Rods

9.8 The Water-Gap Effect in the OCSL Reactor

An ideal control rod layout has been selected for the OCSL Reactor, but certain design considerations must be made before the arrangement is deemed final. Until this stage of development, the absorber rod arrangement has only dealt with rods that are fully inserted into the reactor core. Understandably, the rods must withdraw from the core during reactor operation. Consequently, a material must replace the volume of the withdrawn rods within the core. In some cases, no boundary exists between the absorber rods and the coolant so when the rod is withdrawn, the coolant material fills the void of the withdrawn rod. In water-moderated reactors, this is known as the water-gap effect, but a similar effect would occur with the organic coolant/moderator. In other cases, the absorber rods move within tubes so that upon withdrawal, the void is filled with air inside the tube. This design choice has a significant impact on reactor operation and flux distribution because the moderating properties of air and the coolant are very different.

As mentioned, the water-gap effect occurs in water-moderated reactors when absorber rods are withdrawn and water, a comparably poor neutron absorber, fills the gap. As a result, peaks in the flux distribution occur where depressions originally existed due to the absorber rods. In general, the effect creates hot regions in the core that complicate the reactor's thermal hydraulics. In extreme cases, the effect can cause fuel located around the gap to overheat. The effect can be mitigated when absorber rods are closely surrounded by fuel rods that are relatively larger in diameter[113].

Regarding the OCSL Reactor, Table 24 shows that the water-gap effect would be present given the similar moderating properties of HB-40 and water. Furthermore, the effect is likely to be exacerbated by two factors. First, the OCSL absorber rods are much larger than the fuel pins so a large volume is filled by moderator when rods are withdrawn. Second, the lattice pitch in the OCSL Reactor is relatively large compared to a light water reactor so the flux peak in the gap cannot be strongly mitigated by surrounding rods. Consequently, the best mitigation for this effect is to enclose the absorber rods in tubes so that air replaces the gap of the withdrawn rod. Although air is a weak absorber, it is also a weak moderator. Therefore, the thermal neutron flux will not increase as significantly in the air gap as when it is filled with HB-40. Since the OCSL Reactor is primarily generating power from thermal fission, the air should keep power and fuel temperatures around the gap from peaking drastically.

Table 24: Water-Gap Effect Comparison for OCSL Reactor Materials [101] [111]

	Hafnium	Light Water	HB-40 (at 315°C)		Air	
σ_a (barns)	113	0.664	0.332 (Hydrogen)	0.0034 (Carbon)	1.85 (Nitrogen)	0.00027 (Oxygen)
Σ_a (cm^{-1})	5.06	0.02220	0.0177		0.000074	
σ_s(barns)	8	103	38 (Hydrogen)	4.75 (Carbon)	10.6 (Nitrogen)	3.76 (Oxygen)
Σ_s (cm^{-1})	0.3606	3.443	2.2		0.00046	

To further reinforce this theory, MCNP simulations are employed to compare the two possible cases. One model is created with all absorber rods withdrawn above the core and HB-40 fills the absorber rod gaps. The second model is similar, but 0.5 mm thick aluminum tubes are created around the absorber rods so that air replaces the gap left by the withdrawn absorber rods. Due to limited space, the tubes replace the outer annulus of the original absorber rods and reduce their diameter by 1 mm. This alteration will affect the effective multiplication factor with all rods inserted. Neutron flux distributions are obtained from MCNP as they were in Section 8.6. The thermal flux distributions for each model are normalized by

the value the centre peak in each respective model. The distributions are presented in Figure 48. For comparison, the effective multiplication factor for the model without absorber rod tubes was 1.29058 with a standard deviation of 0.00008 and in the model with absorber rod tubes it was 1.28573 with a standard deviation of 0.00008.

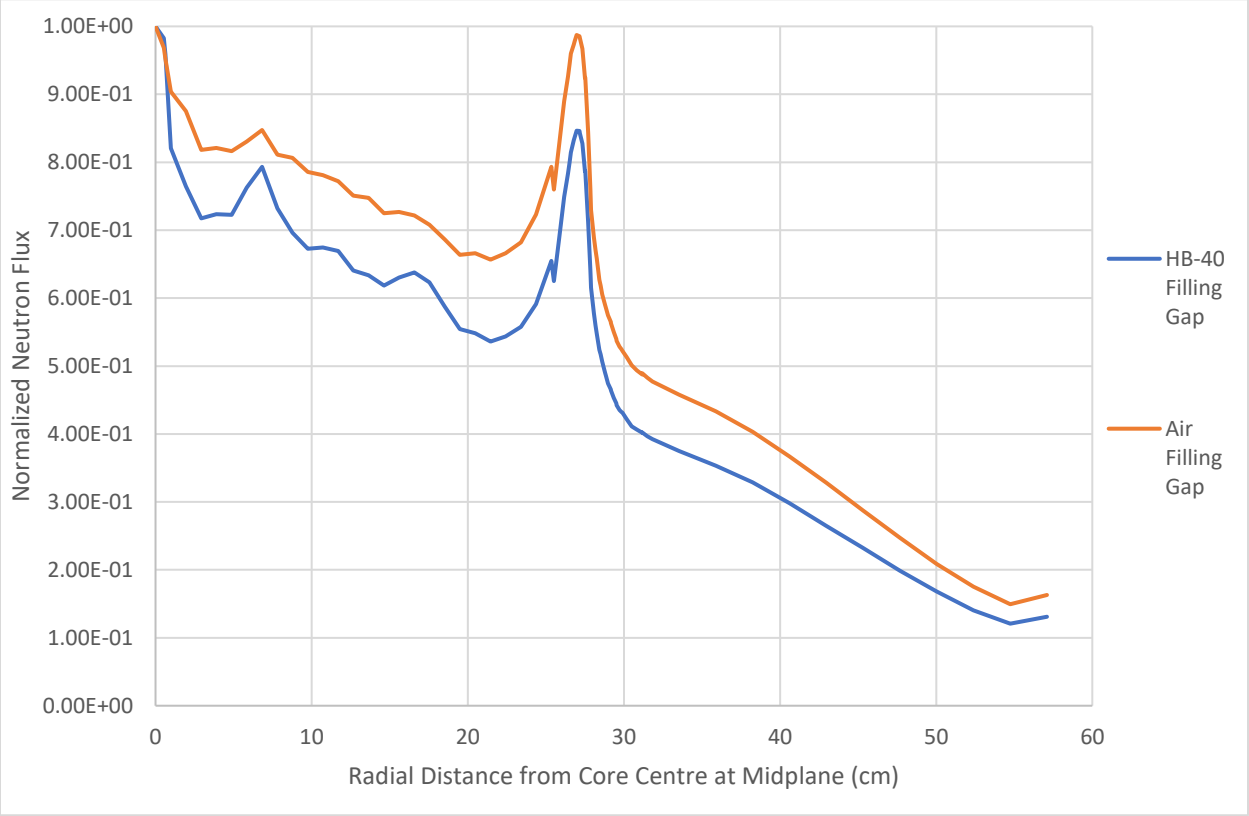

Figure 48: Thermal Neutron Flux Comparison for OCSL Reactor with and without Absorber Rod Tubes

Between the two distributions, the water-gap effect is very apparent when HB-40 fills the gaps of the withdrawn absorber rods. First, the flux peak at the centre of the core is noticeably greater when HB-40 replaces the control rod volume. Secondly, there is an obvious flux peak at 6.825 cm where the mesh point fell directly on an absorber rod gap. The peak is relatively minor in the case with tubes. Additionally, a less severe peak occurs around 16.575 cm in the distribution without tubes. This peak is again corresponding to a gap. With tubes, the gap only manifests as a slight distortion. In general, the flux distribution is better behaved and much less distorted with the aluminum tubes added around the absorber rods.

The MCNP simulations produced results that supported the addition of tube around the absorber rods. The distributions demonstrate the water-gap effect is mitigated by the tubes. Although corrosion is not a primary concern with an organic coolant, the tubes also separate the hafnium rods from the coolant. In effect, this change would likely reduce contamination and wear on the rods. Considering these benefits, the aluminum tubes will be added to the OCSL Reactor design.

9.9 Finalization of OCSL Reactor Absorber Rod Arrangement

Now that tubes surround the absorber rods, a significant volume of hafnium has been lost from the OCSL Reactor design. As a result, the reactor must be simulated again with all rods inserted to obtain the new effective multiplication factor. The result of this simulation is contained in Table 25. While the reactor remains sub-critical, the addition of tubes has certainly reduced the reserve of negative reactivity. In Section 9.7, all possible control rod arrangements were exhausted when attempting to maximize the overall rod worth. Enlarging the shutdown rods is the only remaining option to increase the reserve of negative reactivity.

In the current arrangement, eighteen shutdown rods have a diameter of 0.8 cm while only six have a diameter of 1.4 cm. The diameters were reduced by 1 mm due to the addition of tubes. Originally, only six shutdown rods were enlarged because the reflector edge limited the diameters of the other shutdown rods. However, the necessary space can be achieved by shifting the smaller shutdown rods 3 mm inward from their lattice positions. This alteration permits all shutdown rods to have the same diameter of 1.5 cm. In addition to increasing the reserve of negative reactivity, altering the size of these rods simplifies the fabrication of reactor components by making all shutdown rods the same size. Simulations are run with absorber rods fully inserted and fully withdrawn to reflect this alteration.

Table 25 presents a summary of the design progression of the absorber rod arrangement. The worth of the absorber rods is estimated by comparing the excess reactivity when the rods are fully withdrawn and when they are fully inserted. The worth of the absorber rods has been satisfactorily maximized through the design process. An image of the final absorber rod layout is presented in Figure 49

Table 25: Progression of OCSL Reactor Absorber Rod Arrangements

Version Absorber Rod Arrangement	Volume of Hafnium (cm^3)	Absorber Rods Inserted		Absorber Rods Withdrawn		Estimated Worth of Absorber Rods (mk)
		Effective Multiplication Factor	Standard Deviation	Effective Multiplication Factor	Standard Deviation	
No Tubes	1241	0.96992	0.00023	1.29058	0.00008	256
Tubes Added	1079	0.98638	0.00026	1.28573	0.00008	236
Tubes Added and Shutdown Rods Enlarged	1376	0.95364	.00026	1.28591	0.00020	271

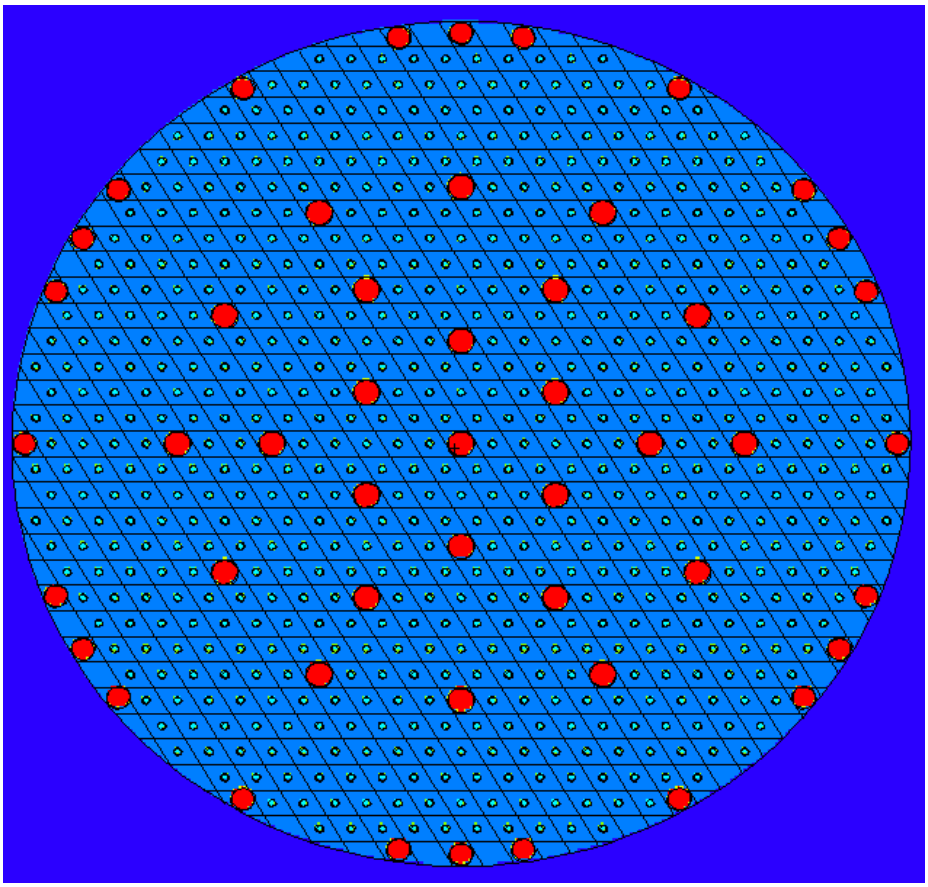

Figure 49: Final Absorber Rod Arrangement

9.10 Flux Distributions

The implementation of the absorber rod arrangement has significantly altered the geometry and materials of the OCSL Reactor core. The effect of the absorber rods on the reactor is best demonstrated by analysing the resulting neutron flux distributions. Normalized neutron flux distributions are produced using MCNP as they were in Section 8.6. In these simulations, the reactor is freshly fuelled and the reflector plates are at the core's edge. For this analysis, a distribution is produced for the reactor with all absorber rods withdrawn and a second distribution is created with all absorber rods fully inserted.

Compared to the Baseline OCSL Reactor, the OCSL Reactor has seen 25 fuel channels converted into absorber rod channels and 24 shutdown rods added around the periphery of the core. In Figure 50, the distribution with absorber rods withdrawn is compared to the Baseline OCSL distribution from Section 8.6. The design of the absorber rod arrangement aimed at minimizing the total fuel channels replaced by control rods. As a result, the neutron flux distributions remain similarly shaped to the distributions in the Baseline OCSL Reactor. The thermal neutron flux distribution appears slightly flatter in the OCSL Reactor. Recalling Section 9.8, mitigation of the water-gap effect with aluminum absorber rod tubes slightly flattened the thermal neutron flux. Meanwhile, the fast flux distribution appears greater relative to the thermal distribution in the OCSL Reactor than in the Baseline OCSL Reactor. When the absorber rod tubes were introduced, nearly 4.6 litres of the moderator were replaced by weaker neutron moderators such as aluminum and air. This alteration likely accounts for the relative increase in fast flux distribution.

From WIMS, the average thermal neutron flux in the Baseline OCSL Reactor was 8.39 x 10^{12} n cm^{-2} s^{-1}. In the OCSL Reactor, the average thermal flux is slightly less at 8.31 x 10^{12} n cm^{-2} s^{-1}.

When fully inserted, the absorber rods drastically alter the neutron flux in the reactor. To demonstrate this effect, the normalized flux distributions for the OCSL Reactor with all absorber rods inserted are presented in Figure 51. The influence of the absorber rods is very apparent in the fast flux distribution. Large recesses in the fast neutron flux are visible at distances corresponding to control rod locations. These recesses are also indicative of the large resonance cross-sections of hafnium isotopes identified in Table 18 in Section 9.3.

Upon inspection, the thermal neutron flux is diminished significantly with the insertion of the absorber rods. As the OCSL Reactor generates power primarily from thermal fission, thermal flux distributions with absorber rods fully withdrawn and fully inserted are presented in Figure 52 with improved resolution. With the more detailed plot, recesses in the thermal flux are apparent around the control rod locations. Comparing the two distributions, the control rods can feasibly be employed to flatten the thermal flux across the core and ensure optimal power distribution.

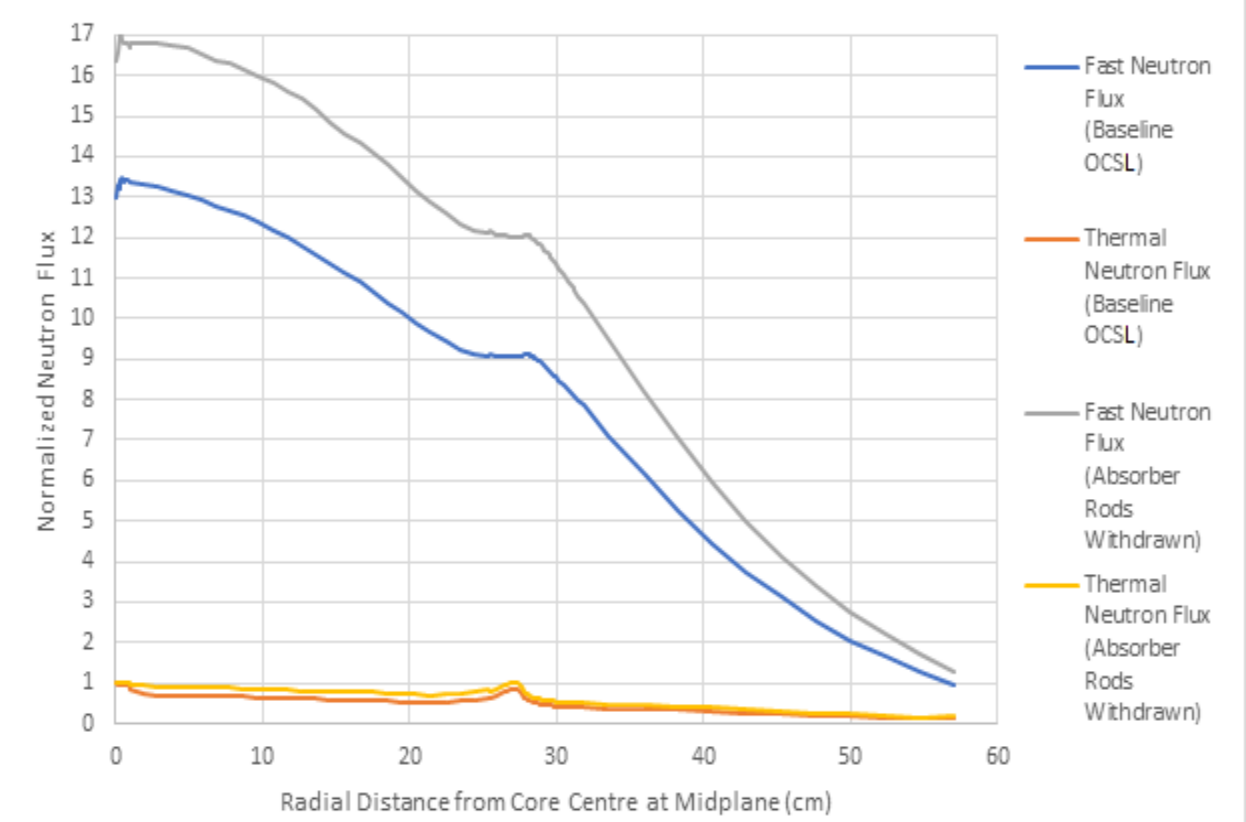

Figure 50: Comparison of OCSL Normalized Flux Distributions with Baseline

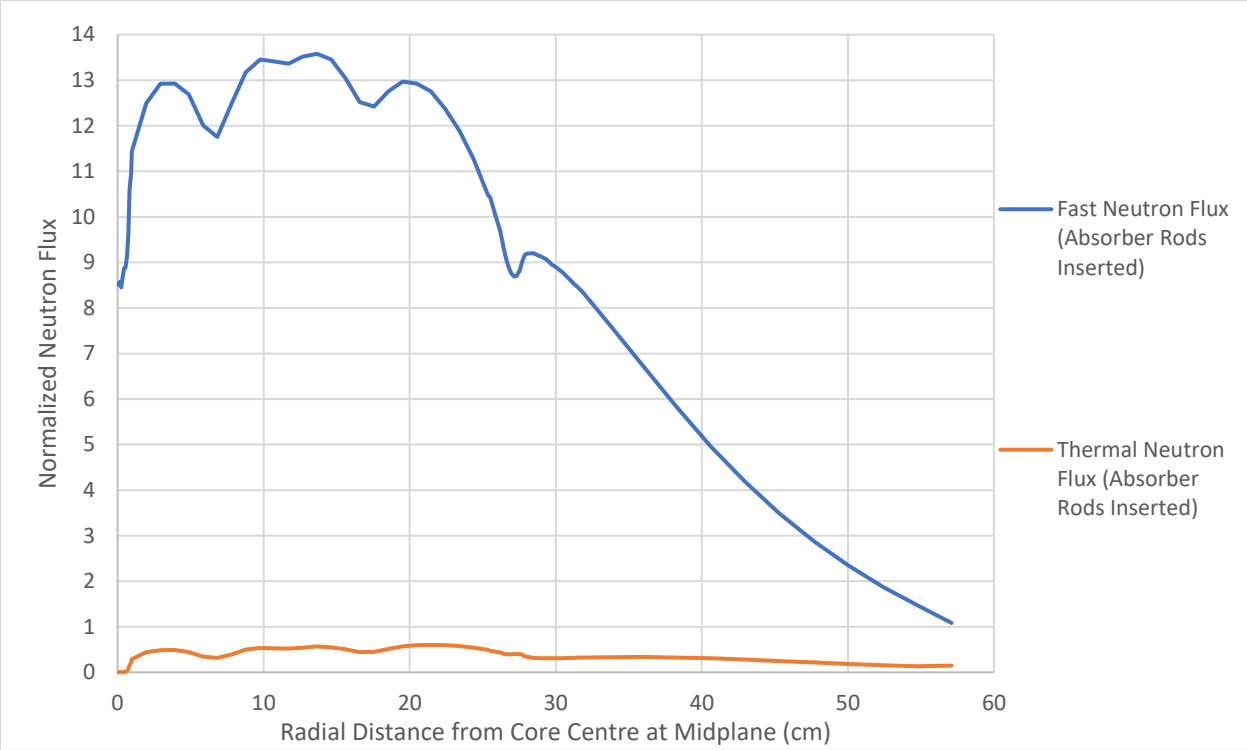

Figure 51: Normalized Neutron Flux Distributions for OCSL Reactor with all Absorber Rods Inserted

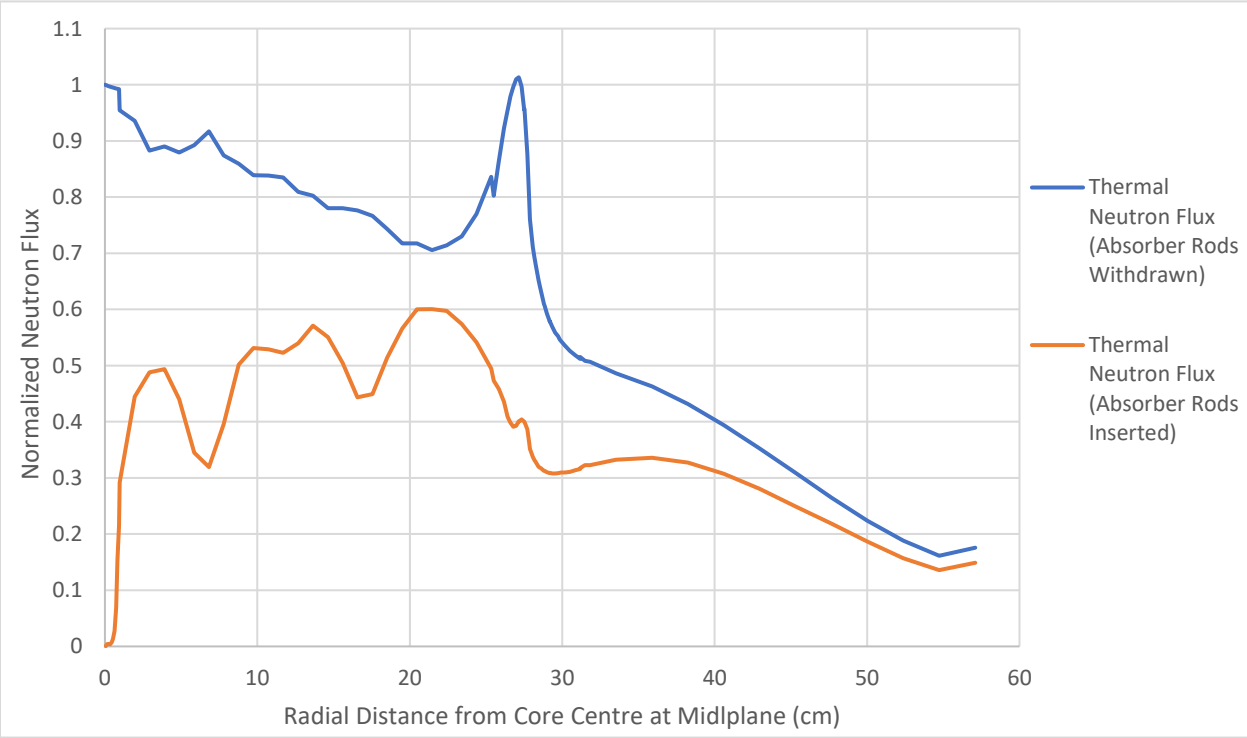

Figure 52: Normalized Thermal Flux Distributions for OCSL Reactor with Absorber Rods Withdrawn and Inserted

9.11 Re-evaluation of OCSL Reactor Thermal Hydraulic Parameters

The selected absorber rod arrangement has reduced the total fuel channels in the Baseline OCSL Reactor core by 25. In order to retain a thermal output of 1 MW, the remaining 660 fuel channels must compensate for the heat generation lost by converting those 25 channels to control rod channels. In effect, this alteration increases the average heat production in the fuel pins resulting in differing coolant mass flow rates and temperature distributions along the fuel channels. Consequentially, the thermal hydraulic estimation must be re-evaluated for the OCSL Reactor.

Estimation of the reactor's thermal hydraulic parameters is performed as in Chapter 7 with the MATLAB® script htfuelchannel.m. A comparative summary of the OCSL Reactor's parameters with the parameters of the Baseline OCSL Reactor is presented in Table 26. The updated temperature distributions along the fuel channel are illustrated in Figure 53. By reducing the total fuel channels, the channel mass flow rate of the coolant must increase resulting in a greater Reynolds number. Greater turbulence in the channel coolant flow improves heat transfer between the fuel pins and the coolant. Regarding the temperature distributions, the effect of reducing the total number of fuel channels manifests as slight increases in the fuel and cladding maximum temperatures. However, the temperatures do not become unsafe and the distributions remain well behaved.

Table 26: Comparative Summary of OCSL Reactor's Thermal Hydraulic Parameters

Parameter	Baseline OCSL Reactor	OCSL Reactor
Number of Fuel Channels	685	660
Number of Control Rods	0	25
Average Specific Heat Production (W cm^{-3})	205.8	210.5
Channel Coolant Mass Flow Rate (kg s^{-1})	0.0111	0.0116
Reynolds Number	6752	7007
Inlet Coolant Temperature (^{O}C)	290	290
Outlet Coolant Temperature (^{O}C)	340	340
Average Coolant Temperature (^{O}C)	315	315
Maximum Fuel Temperature (^{O}C)	440	449
Maximum Cladding Temperature (^{O}C)	376	378

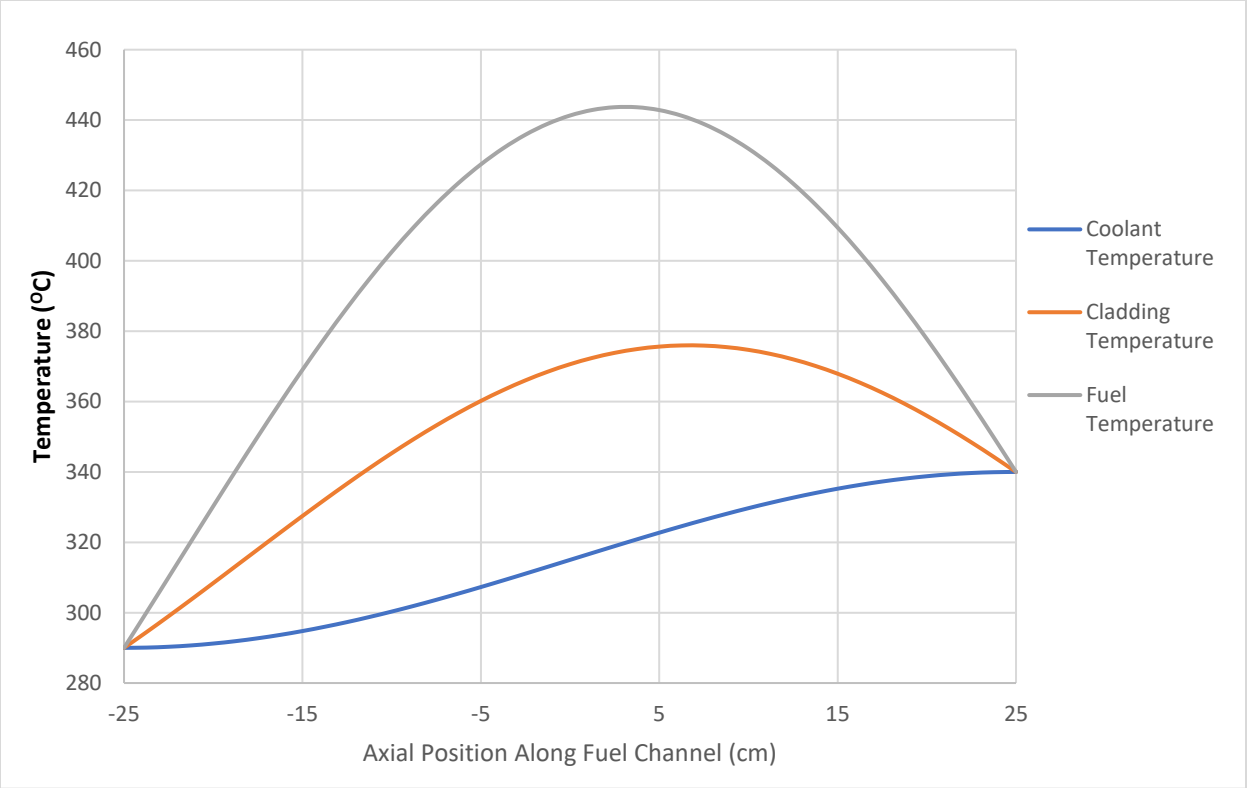

Figure 53: Estimated Temperature Distributions Along OCSL Reactor Fuel Channel

9.12 Re-evaluation of OCSL Reactor Burnup and Reactivity Coefficients

Similar to the reactor's thermal hydraulic estimation, calculations of the reactor's burnup and reactivity coefficients are affected by reducing the number of fuel channels to fit the absorber rod arrangement. As a result, these calculations are performed using WIMS and MCNP for the OCSL Reactor with the absorber rod arrangement in place.

The burnup calculations are performed using WIMS as in previous sections. To maintain consistency, the burnup is computed for the OCSL Reactor with fresh fuel, all absorber rods withdrawn, and the reflector plates at the core's edge. The results of the burnup calculations are plotted with comparison to the Baseline OCSL Reactor in Figure 54. Upon inspection, the reduced fuel in the OCSL Reactor translates to a shorter service life for the core. The service life of the fuel in the OCSL Reactor is 4233 full power days where the Baseline OCSL Reactor originally had a service life of 4603 full power days. Adding the absorber rod arrangement reduces the OCSL Reactor's service life by about a year.

The reactivity coefficients for the OCSL Reactor are determined as they were in Section 8.5. The moderator temperature coefficient of reactivity is demonstrated using WIMS. The moderator/coolant temperature is varied between the inlet and outlet temperatures of the coolant. The results of this analysis are plotted in Figure 55 alongside the corresponding plot for the Baseline OCSL Reactor. The average moderator temperature coefficient of reactivity for the OCSL Reactor is -0.197 mk $^{O}C^{-1}$ where it had been -0.159 mk $^{O}C^{-1}$ for the Baseline OCSL Reactor.

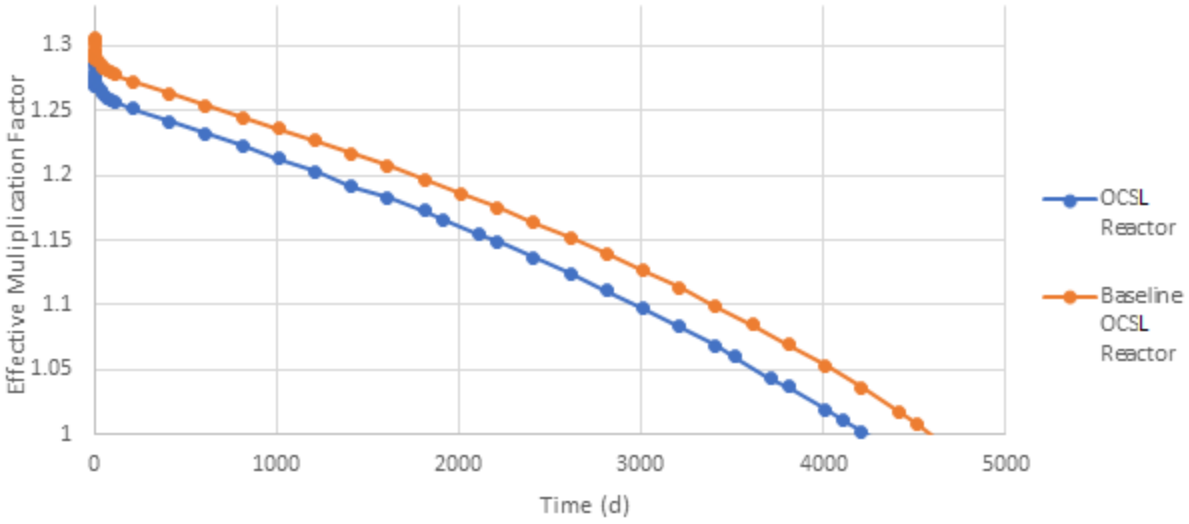

Figure 54: Variation of Effective Multiplication Factor with Time for Baseline OCSL and OCSL Reactors

The void fraction coefficient of reactivity is demonstrated using MCNP to maintain consistency with the method in Section 8.5. Similarly, the void fraction is varied between 0% and 52% in a series of simulations. The results of this analysis are presented in Figure 56 with the plot for the Baseline OCSL Reactor for comparison. For the OCSL Reactor, the average void fraction coefficient of reactivity is -3.03 mk per percent void while it was -2.66 mk per percent void in the Baseline OCSL Reactor.

The fuel temperature coefficient of reactivity is computed using WIMS by varying the fuel temperature between its minimum and maximum temperatures in successive simulations. The results of this analysis are compared with the plot from the Baseline OCSL Reactor in Figure 57. The average fuel temperature coefficient of reactivity for the OCSL Reactor is -7.6×10^{-3} mk $^{O}C^{-1}$ while in the Baseline OCSL Reactor, the coefficient was -9.8×10^{-3} mk $^{O}C^{-1}$.

The plots presented in Figure 55, Figure 56, and Figure 57 all indicate clearly negative correlations. Compared to the Baseline OCSL Reactor, the OCSL Reactor demonstrates slightly stronger negative correlations for all relationships except fuel temperature. This result is anticipated due to the reduced fuel in the OCSL Reactor. The continued presence of clearly negative reactivity coefficients is a strong indication of inherent safety in the OCSL Reactor design.

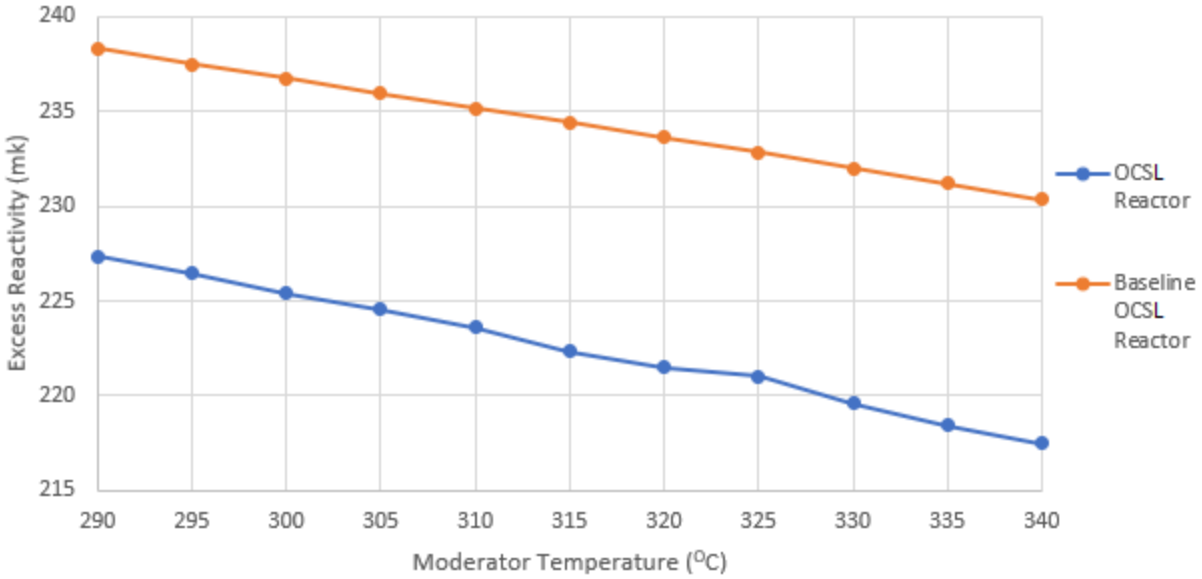

Figure 55: Variation of Excess Reactivity with Moderator Temperature for Baseline OCSL and OCSL Reactors

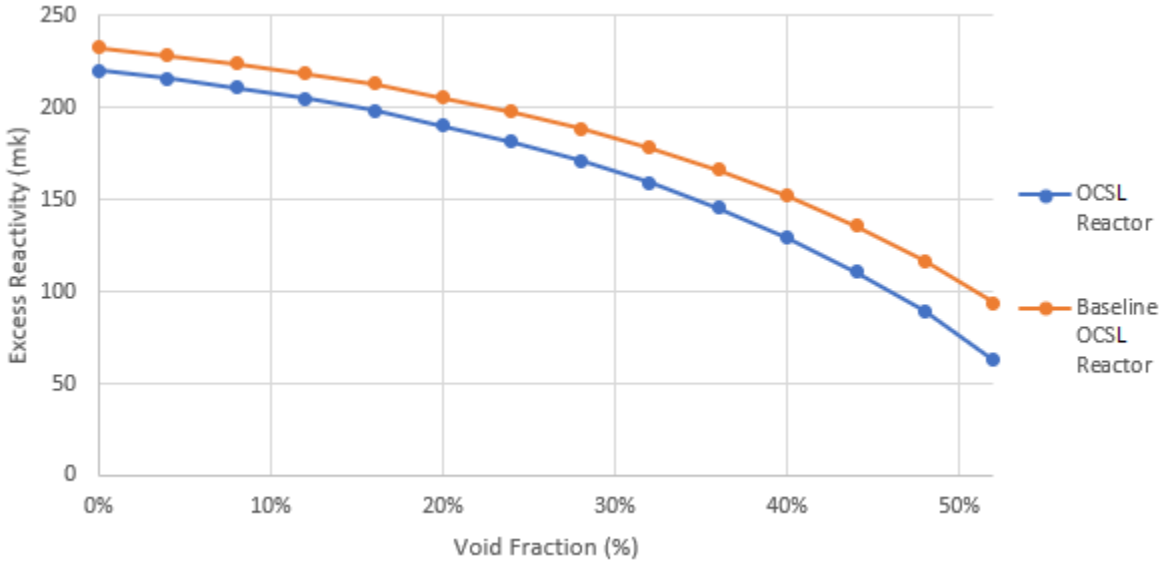

Figure 56: Variation of Excess Reactivity with Void Fraction for Baseline OCSL and OCSL Reactors

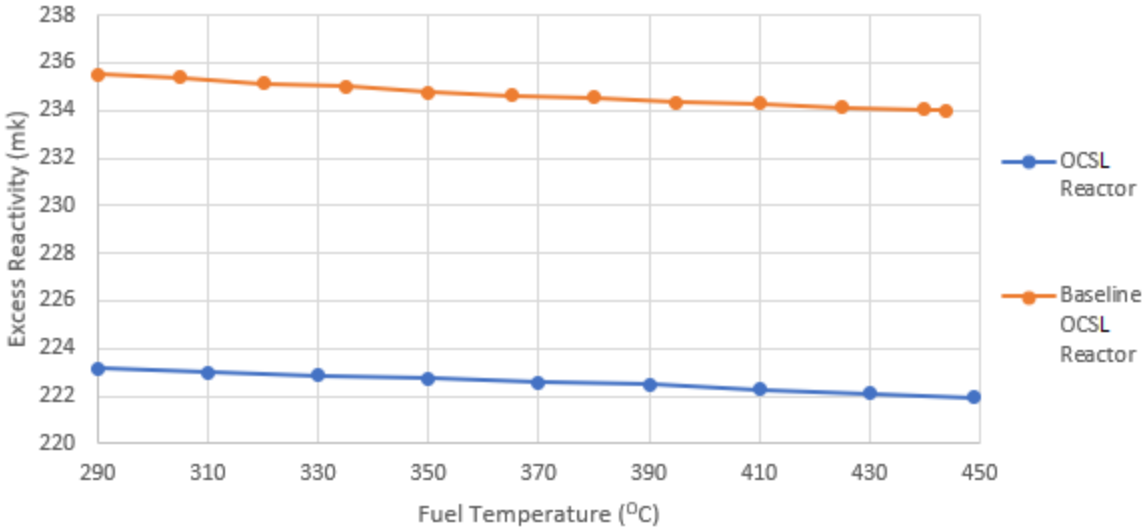

Figure 57: Variation of Excess Reactivity with Fuel Temperature for Baseline OCSL and OCSL Reactors

9.13 OCSL Reactor Start-Up Configuration

So far in this chapter, a control system has been implemented in the OCSL Reactor consisting of control rods, shutdown rods, and moveable reflector plates. The design process has demonstrated how the worth of the absorber rods is maximized to provide the OCSL Reactor with a large reserve of negative reactivity. In turn, this reserve will enable the system to maintain control of the reactor under all circumstances and to bring the reactor to sub-critical under normal and emergency operation. With the system now in place, a start-up configuration will demonstrate how the individual components of the system are utilized to safely bring the reactor from shutdown to a state of generating power.

To establish the starting point of this exercise, a shutdown state will be defined as the freshly-fuelled OCSL Reactor with all control and shutdown rods fully inserted and reflector plates fully engaged at the core's edge. The reactor is well-below criticality with an effective multiplication factor of 0.95364. To generally explain the start-up process, the reflector plates first move outwards to a certain distance from the core. Next, the shutdown rods are withdrawn from the core. The effective multiplication factor increases, but the reactor remains sub-critical. From this state, a group of control rods are withdrawn from the core to achieve criticality and the reactor begins generating power. All the other control rods remain fully inserted providing long-term regulating control. To maintain safe operation, the moving group of control rods must be selected such that when fully withdrawn, the reactor remains below a prompt critical state. As the OCSL Reactor is primarily fuelled by uranium-235, a prompt critical state is obtained when a step increase in reactivity yields an excess of reactivity greater than 6.5 mk.[75]

The OCSL start-up configuration must quantify each portion of the start-up process. This is accomplished by a series of simulations where the reflector plates are progressively withdrawn from the core. In each iteration, different absorber rods are withdrawn from the core and the reflector withdrawal is repeated. This step will identify the start-up position of the reflector plates and the initial moving group of control rods. MCNP simulations are employed in this analysis because of the greater spatial detail available in three dimensions. The results of this analysis are presented in Figure 58.

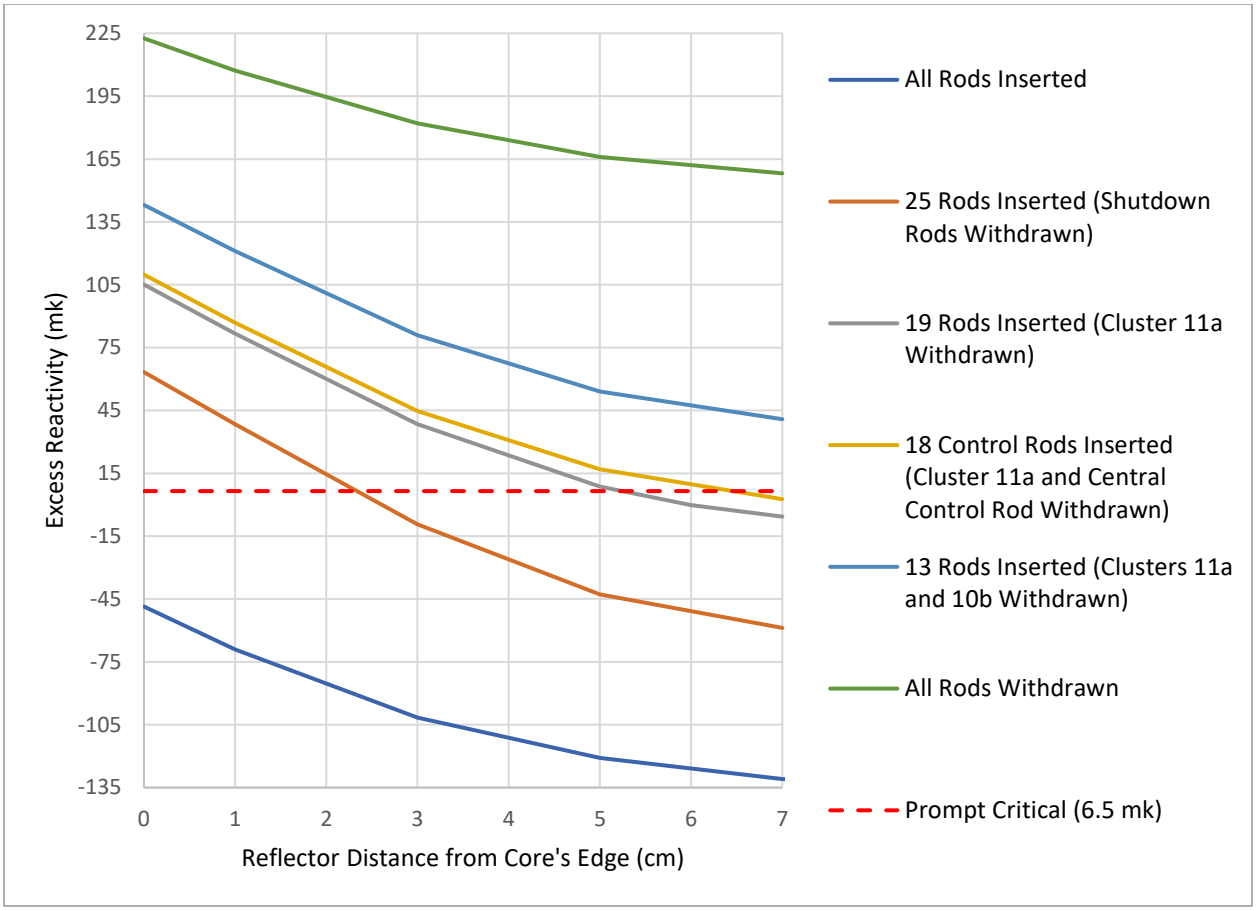

Figure 58: Withdrawing Reflector Plates from OCSL Core for Various Absorber Rod Combinations

Regarding Figure 58, the first iteration of the analysis saw the reflector withdrawn with all absorber rods inserted. This plot in navy represents a lower limit for the analysis as well as the initial step in start-up where the reflector plates are withdrawn to the start-up distance. The second iteration of the analysis fully withdrew the reflector with all absorber rods withdrawn. The plot is shown in green and it demonstrates the reactor is prompt supercritical with all control rods moving, regardless of reflector position. A single miscalculated movement of the rods could put the reactor into a prompt critical state. Therefore, a portion of the control rods must remain inserted to limit the excess reactivity below 6.5 mk.

In the third iteration, the shutdown rods are withdrawn, and the reflector is moved away from the core. Plotted in orange, this trial demonstrates the distance the reflector must be displaced before the shutdown rods can be safely withdrawn. Interpolating from this plot, the shutdown rods may be fully withdrawn when the reflector is more than 2.7 cm from the core's edge. Beyond this distance, the reactor will remain sub-critical with the removal of the shutdown rods. Referring again to the plot, it is theoretically possible to start the reactor by removing the shutdown rods. However, these absorber rods are designated solely for shutdown control. Furthermore, the peripheral position of the shutdown rods would limit their ability to flatten the neutron flux in the reactor. This makes them an undesirable choice for short-term regulating control.

With the first three iterations establishing certain limits and thresholds, subsequent iterations determine the combination of control rods that will make up the moving group during start-up. First, the reflector is displaced with control rod cluster "11a" withdrawn. In this case (grey curve), the excess

reactivity in the reactor falls under the prompt critical limit with the reflector somewhere between 5 cm and 6 cm from the core. As a result, cluster "11a" could become the moving group during start-up. Continuing the analysis, clusters "11a" and "10b" are withdrawn in the next iteration but the excess reactivity never falls below the prompt critical limit. Plotted in blue in Figure 58, this trial demonstrates that inherent safety cannot be maintained with these two clusters employed simultaneously in regulating control.

At this stage, cluster "11a" appears to be the logical choice for regulating control during start-up. However, the position of "11a" in the core likely limits its ability to shape the neutron flux similar to the shutdown rods mentioned previously. Therefore, a final iteration withdraws cluster "11a" and the central control rod (yellow curve). Fortunately, the reactor falls below the prompt critical limit with this combination when the reflector is moved approximately 6.5 cm from the core. This combination is more ideal than cluster "11a" alone because the central control rod will enable better flux shaping.

For closer inspection, more reflector positions are simulated to better define the curve for this control rod combination. The curve with better definition is presented in Figure 59. From these simulations the ideal reflector position for start-up is 6.4 cm from the core's edge. At this distance, the excess reactivity is limited well-below the prompt critical limit at 5.7 mk. With the reflector's start-up position identified, the start up configuration of the OCSL Reactor is fully defined.

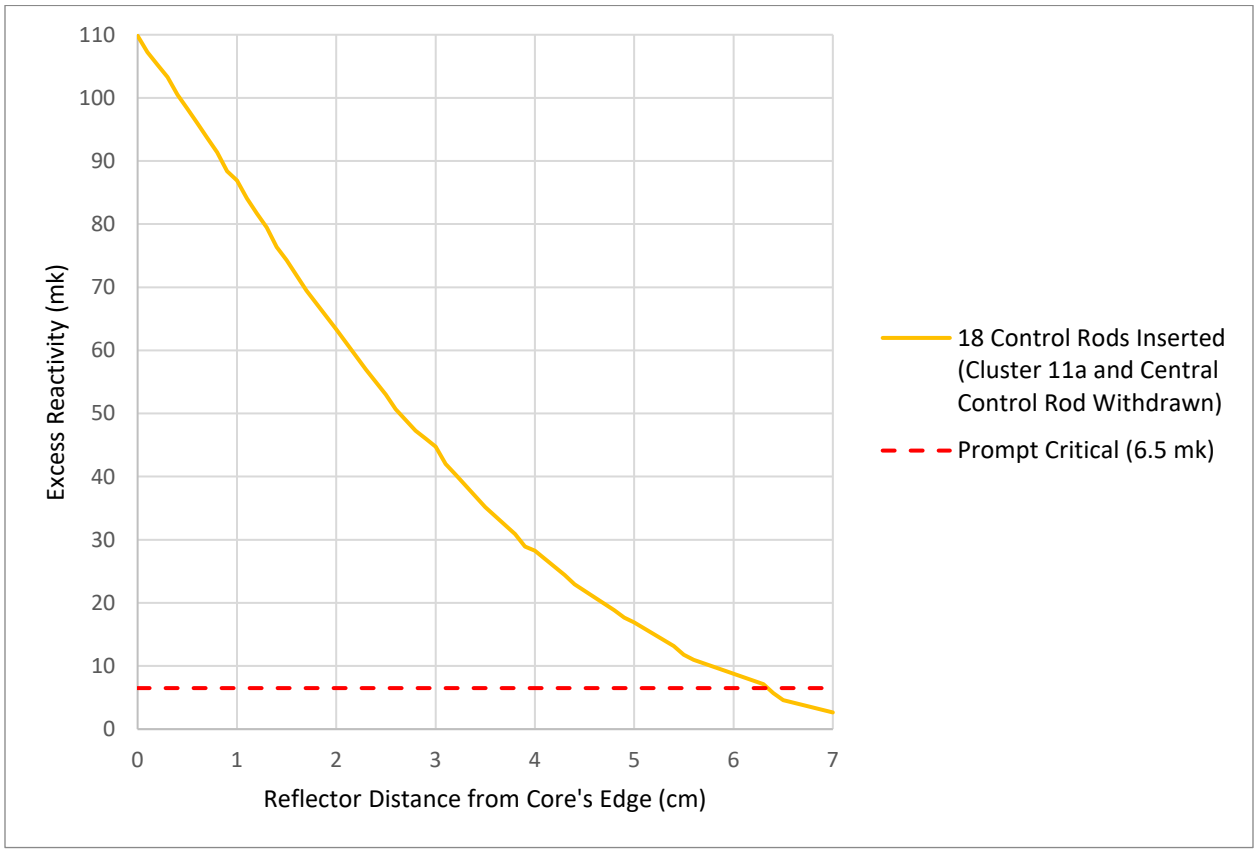

Figure 59: Variation of Excess Reactivity with Reflector Position for OCSL Reactor with Central Control Rod and Cluster 11a Withdrawn

9.14 OCSL Reactor Start-up

To summarize, start-up begins with moving the reflector plates 6.4 cm away from the core. In this configuration the reactor's effective multiplication factor is calculated as 0.89688 with a standard deviation of 0.00028. From here, the shutdown rods are fully withdrawn, and the effective multiplication factor increases to 0.94760 with a standard deviation of 0.00026. Now at the start-up configuration, cluster "11a" and the central control rod are partially withdrawn to achieve criticality in the reactor. Successive MCNP simulations vary the insertion of these control rods to assess the response in the reactor's effective multiplication factor. For simplicity, cluster "11a" and the central control rod are envisioned to move in unison for these simulations. In reality, they move independently allowing for the neutron flux to be shaped. Figure 60 presents the results of these simulations. The control rods must be withdrawn more than 80% from the core before the reactor becomes critical.

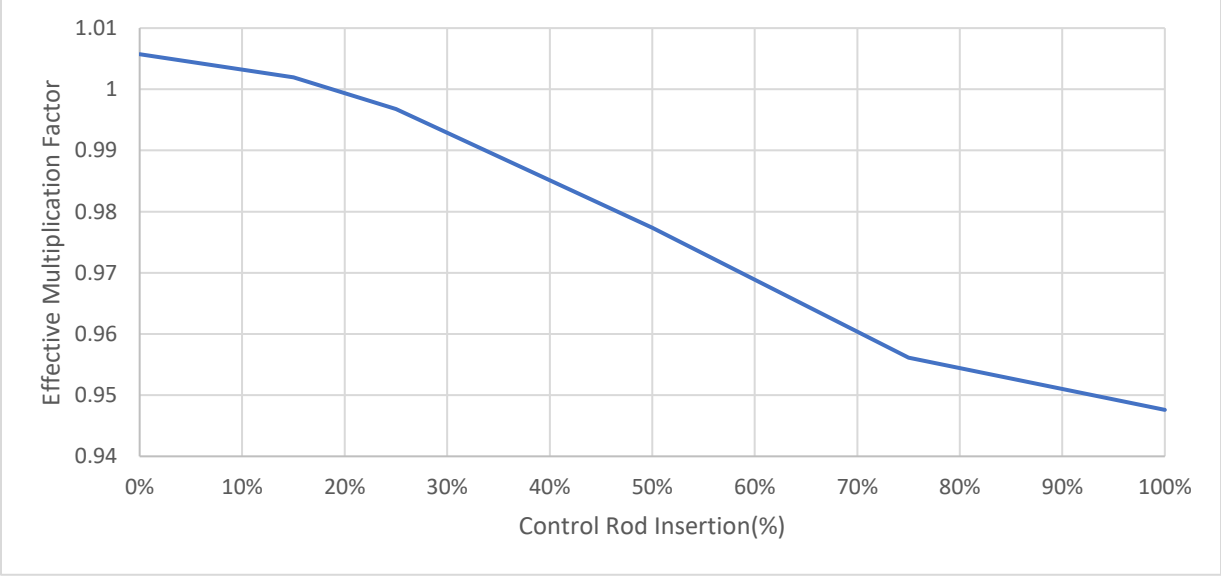

Figure 60: Variation of Effective Multiplication Factor with Control Rod Insertion at Start-up

The simulation that fell nearest to criticality was with a control rod insertion of 15%. The effective multiplication factor of the OCSL Reactor in this configuration was 1.00170 with standard deviation of 0.00009. To estimate the OCSL's thermal neutron flux distribution at start-up, another simulation is run with this model to capture the distribution. In Figure 61, the thermal neutron flux distribution at reactor start-up is compared against the flux distributions with absorber rods fully withdrawn and fully inserted. Due to the azimuthal path followed in this distribution, the large flux depression around 6 cm is very apparent because the mesh point falls directly on the control rod. Elsewhere, the thermal neutron flux is relatively flat between this depression and the edge of the core. The large flux peak around 30 cm corresponds to the region of moderator between the core and the withdrawn reflector. The core's edge is at 27.8 cm and the reflector's inner edge is 6.4 cm from the core. Understanding that the reflector would still reflect some neutrons at this distance, it makes sense that thermal neutrons would accumulate in this region.

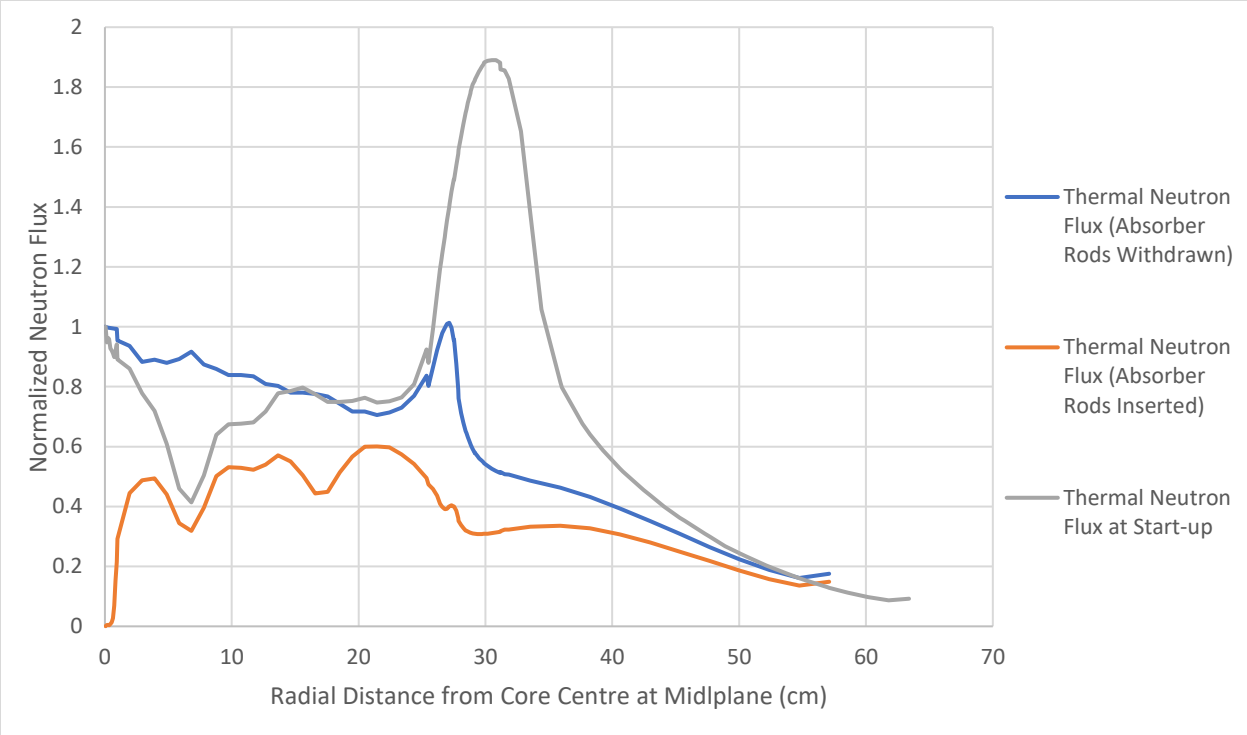

Figure 61: OCSL Reactor Thermal Flux Distribution at Start-up

9.15 Control Rod Sensitivity

As Figure 60 in the previous section demonstrates, the profile of the effective multiplication factor naturally conforms to a shape as one or more control rods are inserted into the core. This shape is indicative of the flux distribution in the core. Like the radial flux distribution, the neutron flux distribution in the axial direction reaches a maximum at the centre (mid-plane) of the core. Thus, the rate of reactivity change as the control rod is inserted or withdrawn is greatest when the rod is moving through the centre of the core. This effect results in an S-shaped curve where the rate of reactivity change is initially low as the rod is first inserted. The rate increases significantly as the control rod reaches the centre of the core and diminishes once the control rod is fully occupying the middle region of the core[114]. From a control perspective, the rate of reactivity change with control rod movement is analogous to its sensitivity.

To demonstrate the appropriate sensitivity of the OCSL's control rods, trials similar to the one plotted in Figure 60 are conducted for each control rod cluster. With all absorber rods withdrawn and reflector plates engaged, each control rod cluster is gradually inserted into the core in successive MCNP simulations. Plotted results for the central control rod and the four control rod clusters are presented in Figure 62, Figure 63, Figure 64, Figure 65, and Figure 66. To quantify the sensitivity in each case, the average change in excess reactivity per unit of the rod's length is calculated. These results are tabulated in Table 27. All rods show the anticipated sensitivity behaviour as they are inserted into the core. These results demonstrate that the control rods are capable of short-term regulating control of the reactor and of flux shaping.

The central control rod appears to be the least sensitive in all the cases. However, the central control rod is the most sensitive individual control rod in the reactor. This is due to the neutron flux reaching a maximum at the centre of the core. As a result, the central control rod is vital in flux shaping.

This result reinforces the previous decision in Section 9.13 to include the central control rod in the moving group during start-up.

The sensitivities of clusters “5a” and “7b” are similar while clusters “10b” and “11a” are similar in sensitivity and slightly less sensitive than the first two clusters. The control rods’ sensitivities generally follow the neutron flux distribution and decrease at greater distances from the centre of the reactor. This effect largely explains the disparity in the sensitivities of the first and second pairs of clusters. However, cluster “7b” is slightly more sensitive than cluster “5a” despite a significantly greater distance from the centre. Previously, Section 7.6 explained the interactions of neighbouring controls rods. Regarding the absorber rod arrangement in Figure 49, the control rods in cluster “5a” are closer together than those in cluster “7b”. Recalling Section 9.6, each control rod in the cluster depresses its surrounding neutron flux thereby reducing the sensitivity of nearby rods in the cluster. Comparatively, the control rods in cluster “7b” have greater space between them and the self-diminishing effect is less than in cluster “5a”. As a result, the two clusters have similar sensitivities despite their differing radial positions.

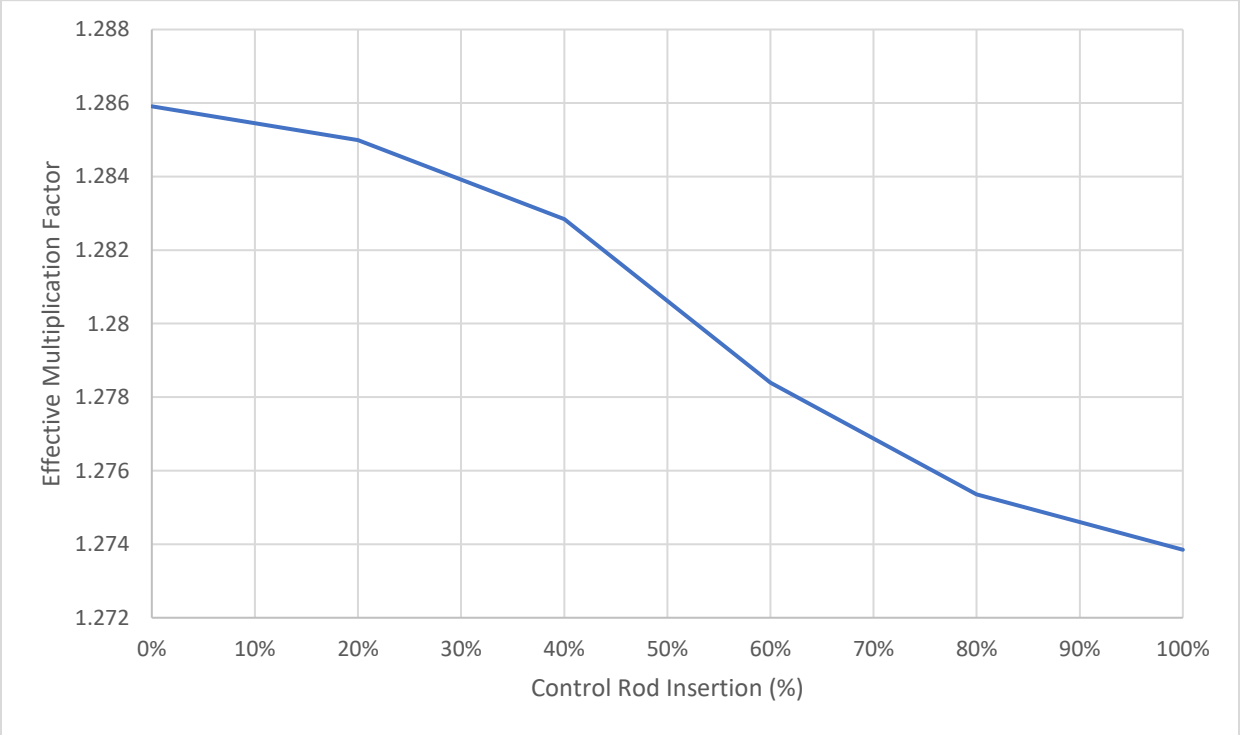

Figure 62: Variation of Effective Multiplication Factor with Insertion of Central Control Rod

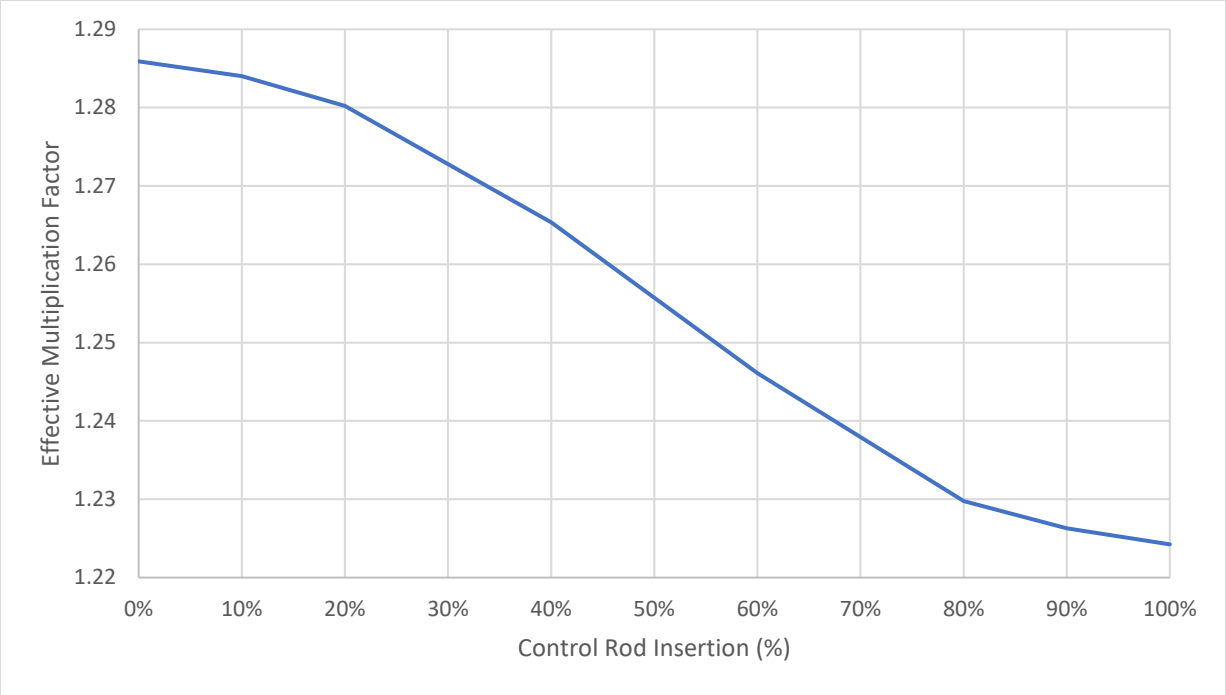

Figure 63: Variation of Effective Multiplication Factor with Insertion of Cluster "5a"

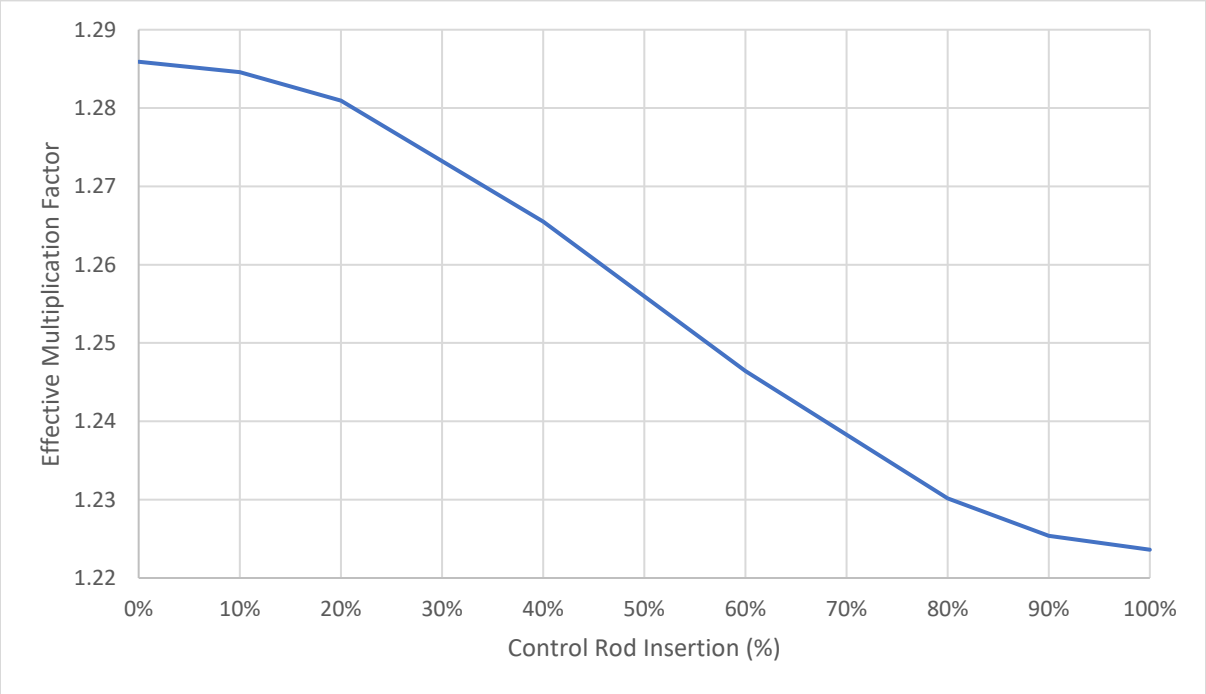

Figure 64: Variation of Effective Multiplication Factor with Insertion of Cluster "7b"

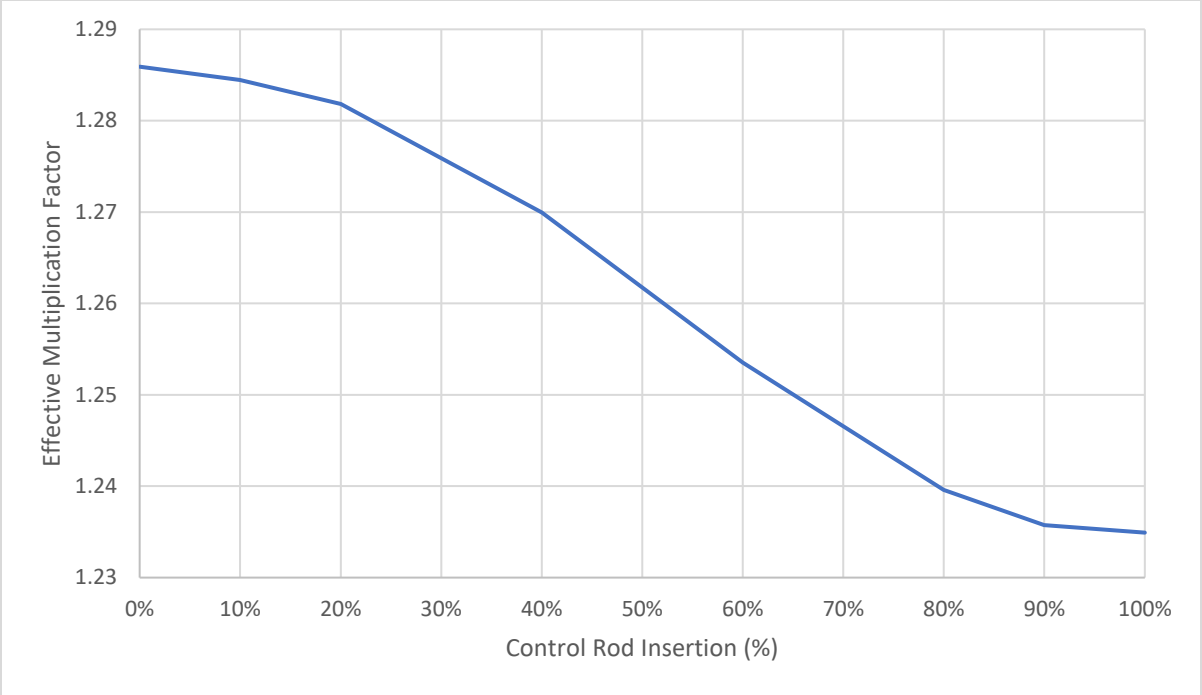

Figure 65: Variation of Effective Multiplication Factor with Insertion of Cluster "10b"

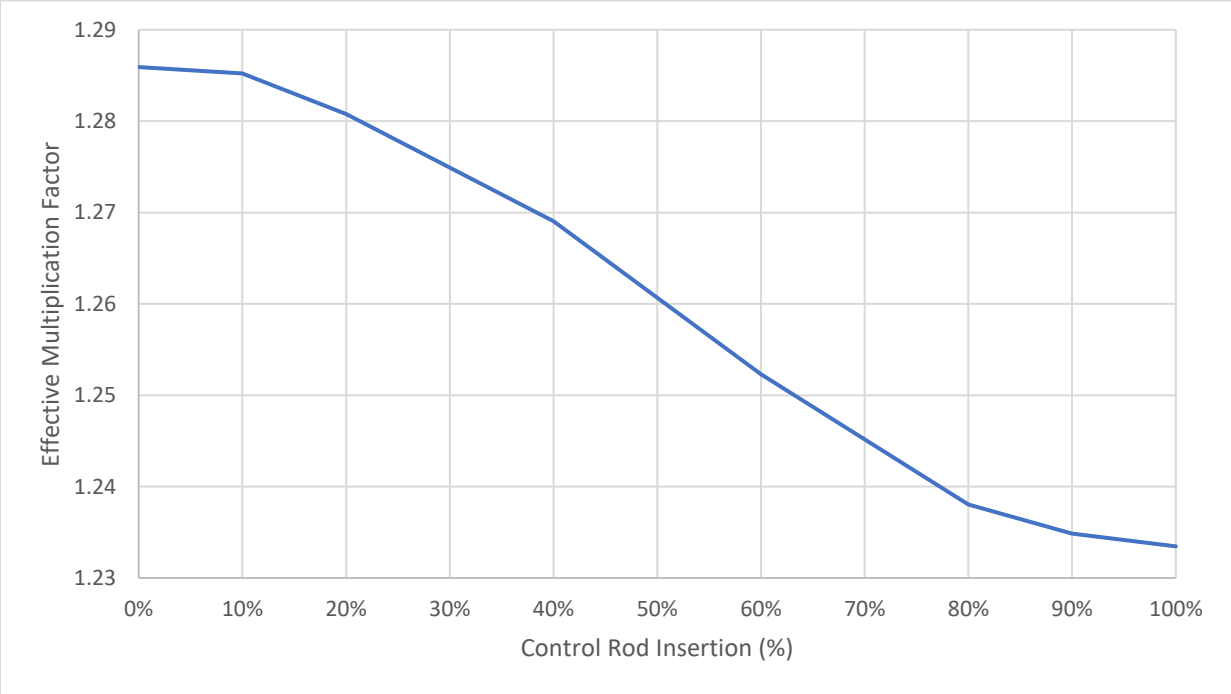

Figure 66: Variation of Effective Multiplication Factor with Insertion of Cluster "11a"

Table 27: Sensitivities of OCSL Reactor Control Rods

Control Rod / Cluster	Number of Control Rods	Distance from Centre of Reactor (cm)	Average Sensitivity (mk cm^{-1})
1	1	0	0.15
5a	6	6.75	0.78
7b	6	11.70	0.79
10b	6	17.55	0.64
11a	6	16.89	0.66

9.16 Burnup Control Strategy

The start-up configuration of the OCSL Reactor has established the moving group of control rods that provide short-term regulating control to the reactor. Furthermore, the remaining control rods and the reflector plates are positioned to maintain long-term regulating control by limiting excess reactivity below prompt critical (6.5 mk). To achieve this, all remaining control rods are fully inserted into the core and the reflector plates are 6.4 cm from the core's edge.

Over time, the reactor's excess reactivity will diminish as the fuel is depleted by generating power. To counteract the lost reactivity, the average position of the control rods of the moving group will become increasingly withdrawn from the core. Eventually, the moving group will encounter difficulty making fine adjustments to the reactor's power due to diminished sensitivity when the control rods are nearing complete withdrawal. When the fuel is slightly more depleted, even complete withdrawal of the moving group will not yield criticality in the reactor. To maintain reactor operation, the control system must be reconfigured once the moving group's sensitivity has diminished but before criticality has been lost. Reconfiguring the control system ensures the moving group of control rods remains capable of fine adjustments to reactor power.

While the reflector plates are withdrawn from the core's edge, reconfiguring the control system constitutes a displacement of the plates toward the core to increase the reactor's excess reactivity. In practice, the moving control rod group is inserted into the core for criticality safety during the reconfiguration. Next, the reflector plates are shifted inward to a pre-calibrated distance from the core. The displacement of the reflector plates is calibrated to augment the excess reactivity and control system effectiveness. However, the position of the reflector plates also limits excess reactivity below prompt critical in case the moving group of control rods are fully withdrawn.

This cycle will repeat over long-term operation with the reflector plates gradually moving closer to the core. The calibrated displacements of the reflector plates are estimated using successive MCNP simulations. Repeated simulations vary the reflector plate positions for the reactor with the moving control rod group fully withdrawn. By analysing the changes in excess reactivity, the reflector displacements that yield a reactivity insertion as close as possible to 6.5 mk are estimated. This trial is presented in Table 28. Understandably, these estimates are limited by not accounting for depletion of fuel, but they do present some indication of the reactivity worth of the reflector plates as they are displaced closer to the core. Additionally, the trial demonstrates the numerous reconfigurations required before the reflector plates reach the core.

When the reflector plates are fully inward, the next reconfiguration of the control system is slightly more involved. While cluster "11a" in the moving group remains withdrawn, the central control rod is fully inserted into the core. Similar to reactor start-up, the reflector plates are then moved away

from the core to a predetermined position. At this stage, the moving control rod group consists of cluster "10b" and the central control rod. As in start-up, the predetermined reflector position limits the excess reactivity below prompt critical if the moving group is fully withdrawn. In this configuration, the OCSL Reactor will continue to generate power with the control system functioning safely and effectively.

The previously outlined procedures repeat for each control rod cluster until the OCSL's excess reactivity is ultimately reduced to zero. In turn, each cluster joins the central rod in the moving group and the reflector plates are gradually displaced until they reach the core's edge. At this stage, the cluster remains withdrawn when the system reconfigures, and the next cluster begins the process anew with the reflector plates displaced. The fuel in the reactor is considered spent when the reactor is subcritical with all control rods fully withdrawn and reflector plates located at the core's edge. By this method, the reactor can never reach prompt critical under normal operation. Furthermore, the moving control rod group always has ample sensitivity to produce fine changes in the reactor's power and neutron flux shape.

Table 28: Estimation of Calibrated Reflector Plate Positions

Reflector Distance from Core(cm)	Effective Multiplication Factor	Standard Deviation	Excess Reactivity (mk)	Reactivity Added (mk)
6.4	1.00573	0.00025	5.7	Start-up Position
5.5	1.01192	0.00026	11.8	6.1
4.9	1.018	0.00022	17.7	5.9
4.4	1.02348	0.00024	22.9	5.3
3.9	1.02979	0.00025	28.9	6.0
3.5	1.03646	0.00028	35.2	6.2
3.2	1.04204	0.00025	40.3	5.2
2.9	1.0482	0.00025	46.0	5.6
2.6	1.0534	0.00026	50.7	4.7
2.3	1.06037	0.00022	56.9	6.2
2	1.06765	0.00025	63.4	6.4
1.7	1.07467	0.00028	69.5	6.1
1.5	1.08025	0.00024	74.3	4.8
1.3	1.08631	0.00027	79.5	5.2
1.1	1.09181	0.00024	84.1	4.6
0.9	1.09695	0.00023	88.4	4.3
0.7	1.10333	0.00025	93.7	5.3
0.5	1.10895	0.00028	98.2	4.6
0.3	1.11517	0.00022	103.3	5.0
0.1	1.12011	0.00026	107.2	4.0
0	1.12339	0.00028	109.8	2.6

CHAPTER 10: SUMMARY AND DISCUSSION

10.1 General

The Organic-Cooled SLOWPOKE (OCSL) Reactor is a small modular nuclear reactor designed for district heating and electrical power generation applications in remote installations in Northern Canada. Envisioned as an enhancement of the SLOWPOKE-2 Reactor design, the OCSL Reactor capitalizes on the low vapour pressure of an organic coolant to increase operating temperatures and extend thermal power up to 1 MW. With such a thermal output, the OCSL Reactor may provide heat and hot water to an installation of small, well-insulated buildings. Alternatively, a modular group of OCSL Reactors may be employed to supply larger heat demands or to generate electrical power with added redundancy. The OCSL Reactor core has been designed to remain in service for more than a decade before refuelling is required. The overall design of the OCSL has emphasized safety with the intention of fulfilling the characteristics of inherent safety.

Previous chapters have established designs for the core, reflector, and control system of the OCSL Reactor. In this chapter, the overall design of the OCSL Reactor and its operating parameters will be described. Furthermore, the intentions and implications of certain design decisions will be discussed with respect to the design constraints of this research. Finally, this discussion will address the validity of the results in this research.

10.2 Final OCSL Reactor Model (MCNP)

In this early stage of development, the model of the OCSL Reactor is a simple design consisting of the core, a control system of absorber rods and a series of moveable reflector plates. Two perspectives of the final MCNP model of the OCSL Reactor are presented in Figure 67 and Figure 68. A summary of the OCSL Reactor's physical specifications is presented in Table 29.

The OCSL Reactor core contains 660 fuel channels, 25 control rods, and 24 shutdown rods. In the model, the fuel material is represented as 19.89% enriched uranium dioxide and is surrounded by zirconium cladding. Drawing from the SLOWPOKE-2, the fuel pins of the OCSL bear a similar design albeit with a greater length to facilitate the increased thermal power. The fuel pins are arranged with a triangular lattice. The lattice pitch has been optimized to maximize the reactor's excess reactivity and thus the fuel's lifespan.

All absorber rods are composed of hafnium and are contained within AL 6061 T6 aluminum alloy tubes. The absorber rods are inserted from above the reactor core and travel within aluminum tubes. When withdrawn, air replaces the volume of the absorber rod within the tube. The arrangement of absorber rods and their dimensions are idealized to maximize the number of fuel channels in the OCSL Reactor's core. In the OCSL Reactor, the absorber rods belong to one of two categories. Control rods are found within the core in place of select fuel channels. Besides the central control rod, the remaining twenty-four control rods are regarded as four six-rod clusters that move in unison as a single rod. Located around the periphery of the core, shutdown rods are situated between the fuel and the reflector, and do not replace fuel channels.

An annular reflector of beryllium surrounds the core. The thickness of the reflector is optimized to ensure maximized reflection of neutrons into the core. The reflector is comprised of six equivalent plates that may withdraw from the core. They are shown in a withdrawn state in Figure 68.

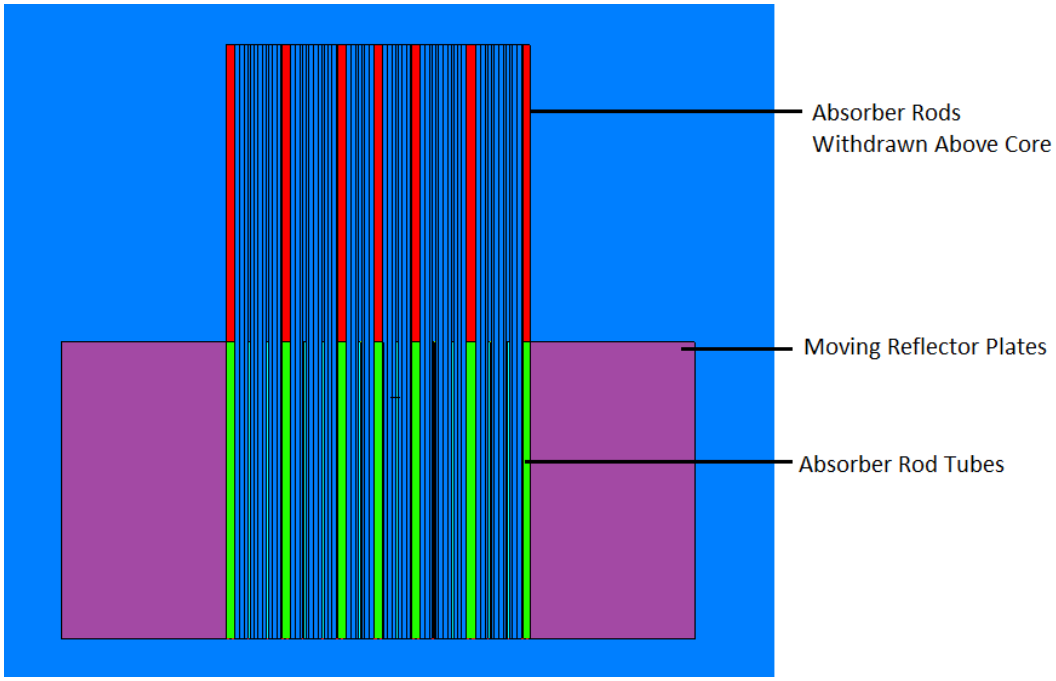

Figure 67: Side Profile Section-Cut of OCSL Reactor

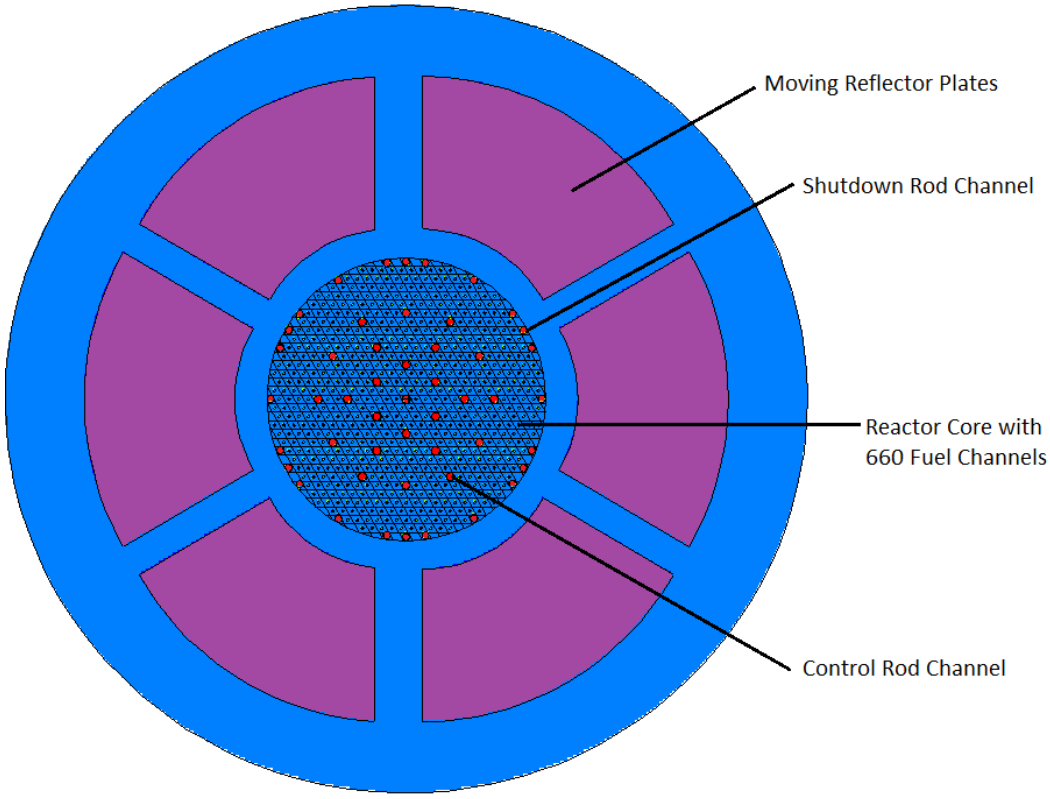

Figure 68: Cross-Sectional View of OCSL Reactor

In the present model, the OCSL Reactor is immersed in a large volume of the organic coolant / moderator. The organic liquid, a hydrogenated terphenyl mixture known as HB-40, fills all voids within the core and the space surrounding the reactor. The surrounding HB-40 represents the interior of the reactor vessel.

Table 29: Summary of OCSL Reactor Specifications

Specification	Description
Core Arrangement	Cylindrical
Core Radius	27.8 cm
Core Height	50 cm
Coolant / Moderator	HB-40 (Hydrogenated Terphenyl Mixture)
Fuel (Cladding)	19.89% Enriched Uranium Dioxide (Zirconium)
Total Fuel Pins	660
Fuel Pin Diameter (Cladding Thickness)	0.425 cm (0.05 cm)
Fuel Lattice	Triangular (1.95 cm Lattice Pitch)
Absorber Rod Material	Metallic Hafnium
Total Absorber Rods (Control Rods / Shutdown Rods)	49 (25 / 24)
Absorber Rod Diameter (Control Rod / Absorber Rod)	1.688 cm / 1.5 cm
Reflector Material	Beryllium
Reflector Thickness	30 cm

10.3 OCSL Reactor Operation

Echoing the SLOWPOKE-2 reactor, the OCSL Reactor is designed for maximum simplicity, reliability, and safety. Throughout this research, the operating parameters of the OCSL Reactor have been developed for a full power rating of 1 MW (th). A summary of the OCSL Reactor's full power operating parameters as well as other operational characteristics are found in Table 30.

Table 30: Full Power Operation of OCSL Reactor

Operating Parameter / Characteristic	Value
Coolant Mass Flow Rate	7.63 kg s^{-1}
Coolant Inlet Temperature	290 ^{O}C
Coolant Outlet Temperature	340 ^{O}C
Maximum Fuel Temperature	449 ^{O}C
Maximum Cladding Temperature	378 ^{O}C
Thermal Power	1 MW
Average Thermal Neutron Flux to Generate 1 MW (Initial)	8.31 x 10^{12} n cm^{-2} s^{-1}
Average Thermal Neutron Flux to Generate 1 MW (End of Service Life)	1.47 x 10^{13} n cm^{-2} s^{-1}
Service Life of Fuel	4233 days (11.6 years)

In operation, the coolant flow in the OCSL Reactor is supplied by a pumping arrangement situated at the base of the reactor vessel. At full power, the pump delivers a constant, unpressurized

coolant flow rate of 7.63 kg s^{-1} through a hypothetical baffling arrangement. Baffles direct the coolant flow perfectly upward and into the reactor's fuel channels. The coolant enters the fuel channels at 290 ^{O}C and absorbs heat from the fuel as it travels the length of the core. Reaching a maximum temperature of 340 ^{O}C, the coolant exits from the top of the fuel channels and is directed to a heat removal loop. In this loop, steam generators or heat exchangers extract heat from the coolant which is then returned to the reactor via the pumping arrangement. The heat extracted from the coolant may be directly employed in district heating or supplied to generate electrical power by means of a Rankine cycle.

At full power, the excess reactivity in the OCSL Reactor drops rapidly over the first days of operation. As saturating fission products reach equilibrium, the decline of the excess reactivity assumes a shallower slope over the remainder of the fuel's service life. Under constant full power conditions, the service life of fuel in the OCSL Reactor is 4233 days or about 11.6 years.

10.4 From SLOWPOKE-2 to OCSL

To achieve an uprated thermal power, the design of the OCSL Reactor alters numerous characteristics of the SLOWPOKE-2 reactor. Most notably, the OCSL Reactor sees an increased operating temperature by replacing the light water coolant/moderator of the SLOWPOKE-2 with the organic coolant, HB-40. However, the extension of power from 20 kW to 1 MW is similarly attributed to alterations in geometry, materials selection and reactor operation. A comparative summary of the two reactors is presented in Table 31. As the OCSL Reactor currently represents a simplified model, comparisons are drawn from the simplified SLOWPOKE-2 model in Chapter 6.

Table 31: Comparison of SLOWPOKE-2 and OCSL Reactors

Characteristic	RMCC SLOWPOKE-2 Reactor	OCSL Reactor
Core Radius	11.049 cm	27.8 cm
Core Length	22.6975 cm	50 cm
Fuel	19.89 % Enriched UO_2	19.89 % Enriched UO_2
Fuel Mass ^{235}U	1.173 kg	8.610 kg
Total Fuel Pins	198	660
Control Rod Material	Cadmium Embedded in Aluminum Alloy	Hafnium Contained within Aluminum Tubes
Total Control Rods	1	25
Total Shutdown Rods	0	24
Annular Reflector Thickness	10.1584 cm	30 cm
Reflector Material	Beryllium	Beryllium
Thermal Power	20 kW	1 MW
Average Thermal Neutron Flux	10^{12} n cm^{-2} s^{-1} (At Inner Irradiation Sites)[6]	8.31 x 10^{12} n cm^{-2} s^{-1}
Cooling Mechanism	Natural Convection	Pumping Arrangement Supplying Coolant at 7.63 kg s^{-1}
Heat Removal	Dissipation to Reactor Pool	Removal by Steam Generator or Heat Exchanger

Referring to Section 6.2, the SLOWPOKE-2's control rod is composed of cadmium encased in aluminum alloy. When designing its control system, the OCSL Reactor's elevated operating temperature necessitated a more suitable absorber material than cadmium. Therefore, the OCSL's absorber rods are composed of natural hafnium because hafnium remains solid at the OCSL Reactor's operating temperature. Where the SLOWPOKE-2 utilizes one central control rod, the OCSL Reactor has twenty-five control rods and twenty-four shutdown rods. In the OCSL Reactor, the absorber rods are separated from the coolant by aluminum tubes instead of being embedded in an alloy. This decision is due in part to the large gaps of moderator created when the absorber rods are withdrawn. These gaps were likely to create large flux distortions and heat concentrations in the core. The absorber rod tubes in the OCSL Reactor fill with air when the rods are withdrawn to diminish the gap effect.

Due to is superior neutronic properties, the beryllium reflector material of the SLOWPOKE-2 is retained in the OCSL Reactor's reflector design. Presently, the OCSL Reactor only features an annular reflector. The beryllium annulus of the OCSL Reactor is about three times as thick as the SLOWPOKE-2's. The OCSL Reactor's reflector is designed for moveable operation. This makes the reflector more versatile as it serves the long-term regulating control of the reactor while also extending the service life of the reactor's fuel.

Where the SLOWPOKE-2 is cooled by natural convection, the OCSL Reactor's increased thermal power demands a flow of coolant to transfer heat from its core. Therefore, a pumping arrangement is included in the OCSL Reactor design. The pump delivers coolant through a baffling arrangement from below the core. The coolant travels upward through the core and absorbs the heat along the length of the fuel channels. As the OCSL Reactor is designed for power generation, the hot coolant is drawn from above the reactor to a heat extraction loop. Heat in the SLOWPOKE-2 is not extracted but rather dissipates through the reactor pool.

10.5 Organic Coolant Performance in OCSL Reactor

The organic coolant in the OCSL Reactor is a hydrogenated terphenyl mixture. Models of the OCSL Reactor have defined the coolant according to the composition of HB-40; a well-characterized coolant originally distributed by the Monsanto Company and historically trialed in the Whiteshell Reactor (WR-1). Low cost and comparatively low liquidus temperatures among terphenyl mixtures make hydrogenated terphenyl mixtures an ideal coolant choice for remote northern installations.

Replacing the light water coolant of the SLOWPOKE-2, HB-40 is a comparatively inferior heat transfer fluid. A conservative estimate of its convective heat transfer coefficient places it about five times less than that of light water. However, the organic coolant presents significant benefits due to an atmospheric boiling point of 342 ^{O}C[123]. The low vapour pressure of HB-40 allows the reactor to operate between 290 ^{O}C and 340 ^{O}C without pressurization of the coolant. As a result of its elevated operating temperature, the OCSL Reactor's thermal efficiency is improved to overcome its lacking heat transfer properties and deliver 1 MW of thermal power while remaining a relatively small reactor. By avoiding pressurization, the design of the OCSL Reactor is generally made safer by removing a significant source of operating hazards. Concerning manufacturing, the reactor may utilize cheaper and lighter structural materials and components due to reduced stresses. Furthermore, the long-term operation of the OCSL reactor will be simplified by not requiring regular pressure vessel inspections for licensing.

Regarding neutronics, HB-40 performs well as a neutron moderator in the OCSL Reactor. The abundance of hydrogen in the organic coolant places it nearly on par with the moderating properties of light water. The most significant difference between the two moderators is their macroscopic scattering

cross-sections. Like oxygen in light water, the carbon nuclei in HB-40 reduce its macroscopic scattering cross-section. However, the ratio of hydrogen to carbon is nearly 1:1 whereas in light water, the hydrogen to oxygen ratio is 2:1. Additionally, the density of HB-40 at the reactor's operating temperature is significantly less than unpressurized light water at only 0.785 g cm^{-3}. As a result, the macroscopic cross-section of HB-40 is over thirty percent less than that of light water. In effect, this results in less moderating power in HB-40 and necessitates greater amounts of organic coolant for neutron moderation similar to light water. For the OCSL, this effect manifested in the increased lattice pitch between fuel pins required to maximize excess reactivity.

From a safety perspective, the OCSL Reactor has demonstrated negative moderator temperature and void fraction coefficients of reactivity throughout its development. As its temperature is increased, the macroscopic scattering cross section of HB-40 falls with its material density. Consequentially, the neutron moderation is hindered resulting in decreased thermal neutron flux and decreased power in the reactor. This negative correlation between moderator temperature and reactivity aids the reactor in accident scenarios such as loss of coolant flow due to pump failure. Should the coolant reach its boiling point, the negative void fraction coefficient of reactivity indicates that the power will continue to drop as bubbles or voids are formed. Again, the falling density of the HB-40 continues to slow the rate of fission in the fuel. A negative relationship between reactivity and void fraction will aid the reactor in progressive loss of coolant flow scenarios or loss of coolant accidents. Regarding personnel and environmental safety, any hazards related to toxicity or activity of the organic coolant may be mitigated through the OCSL Reactor's containment system and safe handling procedures.

Coolant degradation is an inherent complication in the operation of OCRs. High temperatures and large radiation dose rates within reactors tend to cause terphenyls to decompose and reform producing volatile gases and high boilers that impede the coolant flow and heat transfer. In the past, this problem contributed to dwindling interest in large organic-cooled reactors such as WR-1. For the OCSL Reactor, its design anticipates that degradation will be reduced or at least manageable in a smaller and less powerful reactor.

From the models produced in this research, ascertaining the potential coolant degradation in the OCSL Reactor is difficult. However, Equation 31 in Section 4.12 presents a method to estimate the degradation in a preliminary manner for this research.

In the OCSL Reactor, the HB-40 coolant feed is assumed to be composed entirely terphenyl by disregarding the trace concentrations of biphenyl[102]. From the operation of WR-1 using HB-40, the steady-state concentration of terphenyl in the reactor is estimated as 28%[35]. For perspective, the M.I.T. research conducted irradiation trials between temperatures of 300 ^{O}C and 427 ^{O}C using a small reactor operating at thermal powers between 2 MW and 5 MW[115]. Amongst several trials, the value of G ranged from 0.0998 to 0.532. Therefore, a relatively low value of 0.1 is assumed for G in the OCSL Reactor operating at 1 MW to maintain a conservative estimate. Historically, HB-40 was believed to absorb 0.58% of the fission power in WR-1[116]. If this is assumed for the OCSL Reactor, Equation 33 with the other mentioned assumptions indicates that the terphenyl degradation rate is about 50 grams per hour while the new coolant feed rate is 70 grams per hour.

Although this is far from a complete study of coolant degradation in the OCSL Reactor, these rates give some indication of the coolant consumption in the reactor. Some form of coolant reprocessing will undoubtedly be required as part of the OCSL Reactor plant design. Although new coolant can be added to replace the degraded terphenyl, high boiler compounds will accumulate in the coolant and affect both heat transfer and coolant flow through the reactor. A hydrocracking system will remove a portion of high boilers from the coolant and crack the molecules to reform mixtures of similar molecular weight to

the coolant. In turn, the reformed coolant may be returned to the reactor to supplement the new coolant feed rate. Besides improving reactor operation, a hydrocracking system will improve operating costs by reducing the new coolant feed rate.

10.6 Control and Monitoring of OCSL Reactor

The remote locations in Northern Canada where the OCSL Reactor could be employed vary from Canadian Armed Forces installations to mining operations to even small residential communities. In all cases, the probability of highly-skilled, highly-trained nuclear power plant operators being located on-site is extremely low. Furthermore, the prospect of relocating such personnel to these locations for long-term residency certainly undermines the feasibility of installing these reactors due to the costs and salaries involved. Likewise, attempting to develop such personnel by training those on-site is also impractical. Consequentially, the OCSL Reactor control system is designed for maximum simplicity, redundancy, and survivability. As a result, any on-site operation can be performed by moderately trained personnel, but primary control and monitoring can be performed remotely.

The OCSL Reactor is controlled entirely by physically moving the components of its control system. This is the simplest form of control system to monitor because the positions of various components may be verified by either rudimentary sensors or by line-of-sight through sight glasses and cameras. Consequentially, a remote operator may have confidence in the state of the control system by comparing visual and electronic indicators. Additionally, on-site personnel with moderate training will be able to conduct visual rounds of the equipment and verify correct configuration. The simplicity of a mechanical control system allows the functionality of the system to be conveyed with minimal training.

Furthering its simplicity, the OCSL Reactor control system is relatively static besides a small portion of the control rods. At any given time, seven control rods make up the moving group that provide short-term regulating control to the reactor. These moving rods are the central control rod and one of the reactor's four six-rod clusters. All remaining control rods are either fully withdrawn or full inserted for long-term reactivity control. Likewise, the moveable reflector plates are stationary in the periods between reconfigurations. The configuration of the control system at a given time limits the potential excess reactivity in the reactor to values below prompt critical (6.5 mk). This design mitigates the risk of a criticality excursion due to operator error or mechanical error in the actuation of the moving control rods. However, reconfiguring the control system will require a highly-skilled, highly-trained operator on-site to reposition the reflector plates and control rods. By inspecting Figure 54 in Section 9.12, reconfiguration would only be required about once every four months. This frequency provides a natural schedule for inspections of the reactor by highly-skilled, highly-trained personnel.

Redundancy is built into the design of the OCSL Reactor control system by providing a large reserve of negative reactivity to always maintain control of the reactor. Assuming a worst-case scenario, the system was designed to maintain the reactor sub-critical with fresh fuel and the reflector plates against the core. The arrangement of control rods was idealized to maximize their reactivity worth. In this worst-case scenario, the OCSL Reactor is almost 50 mk from criticality. However, the system's redundancy allows the reactor's effective multiplication factor to be reduced further by withdrawing the reflector plates away from the core. Due to the combined reactivity worth of the control rods, shutdown rods and reflector plates, the OCSL Reactor always has a large reserve of negative reactivity to achieve shutdown.

Survivability is built into design of the OCSL Reactor control system by providing operators with fallback options should normal operation of the reactor fail. For instance, the primary control and monitoring of the reactor may be conducted from a remote location. However, a local control console with independent sensors will be available at the reactor should the remote system fail. Furthermore, the

previously mentioned mechanical overrides will permit manual shutdown of the reactor in the event of complete electronic control failure. Survivability is also present in the multiple methods of powering down the reactor. In normal shutdown operation, all control rods and shutdown rods will be inserted into the core to render the core sub-critical. Should actuation of any rods fail, withdrawing the moveable reflector plates presents an alternative method of achieving shutdown.

10.7 Inherent Safety in OCSL Reactor Design

As explained in Chapter 1, an inherently safe reactor design must eliminate or severely mitigate all hazards and risks associated with the reactor's operation. For the OCSL Reactor in Northern Canada, its design must be inherently safe so that highly-skilled and highly-trained operators can remotely control and monitor the reactor while on-site personnel are only moderately trained in reactor operation. The models of the OCSL Reactor in this research represent the reactor operating under steady-state conditions only. As a result, confirmation of the design's inherent safety is limited in this research. Certain risks and hazards may be mitigated by the intended designs of the reactor's control and containment systems, but the inherent safety of the reactor in operation with perturbations can only be fully demonstrated by a kinetic model. Throughout this research, the reactivity coefficients of the OCSL Reactor at steady-state have provided an indication of the possibility of inherent safety in its design.

Mentioned in Section 10.4, the OCSL Reactor's negative moderator temperature and void fraction coefficients of reactivity are strong indicators of inherent safety. Evaluated in Section 9.12, the average moderator temperature coefficient of reactivity of the OCSL Reactor is -0.197 mk $^{O}C^{-1}$ within the normal operation temperature range of the moderator. For comparison, the coefficient in the inherently safe SLOWPOKE-2 reactor is -0.13 mk $^{O}C^{-1}$ [141]. This demonstrates that the relationship as evaluated in this analysis is more strongly negative in the OCSL Reactor. When the coolant is at its boiling point of 342 ^{O}C, the average void fraction coefficient of reactivity in the OCSL Reactor is -3.03 mk per percent void up to 52% void. These negative relationships demonstrate the reactor's response to increase coolant temperature and decreasing coolant density. In both cases, the reactor's excess reactivity and power diminishes indicating stability at the prescribed operating parameters. These safety characteristics aid the reactor in various accident scenarios.

Further to these relationships, the fuel temperature coefficient of reactivity was also assessed throughout the OCSL Reactor's design. From Section 9.12, the OCSL Reactor's average fuel temperature coefficient of reactivity is -7.6×10^{-3} mk $^{O}C^{-1}$ within the normal range of fuel temperatures in the reactor. In the SLOWPOKE-2, the fuel temperature coefficient of reactivity is comparable at -8.5×10^{-3} mk $^{O}C^{-1}$ [141]. Perturbation of the reactor's output power will initially manifest as a change in fuel temperature. Therefore, the negative relationship between fuel temperature and reactivity suggests the reactor will be prone to return to its original state following an increase or decrease in fuel temperature.

To reiterate, the assessment of reactivity coefficients in this research is limited because parameter variation in the static OCSL reactor model was relatively isolated. Understandably, this method oversimplifies the widespread effects of reactor kinetics on parameters throughout the model. However, these results are encouraging because they demonstrate strong negative correlations and the temperature coefficients are comparable to those in the inherently safe SLOWPOKE-2. Therefore, a comprehensive kinetic model of the OCSL Reactor may confirm inherent safety.

10.8 Validity of Results

The OCSL Reactor is presently a conceptual design represented by steady-state models of the reactor's neutronics. At this early stage, validation of results from the computer-based models is a

fundamental challenge of designing the reactor. Without a physical version of the reactor, quantification of the accuracy in the models is impossible. As a result, the results may only be indirectly verified rather than be validated by experimental results.

Relative comparison of similar reactor designs is one method of indirectly verifying the model results. As was stated in Section 2.1, contemporary designs of organic-cooled small nuclear reactors are relatively scarce. Therefore, relative comparison with similar existing reactors is not possible for the OCSL Reactor. The relative comparison between the OCSL Reactor and the SLOWPOKE-2 throughout this research is a relatively weak source of verification.

Lacking any physical reactors for comparison, the best source of model verification is the agreement between two fundamentally different computer codes. Throughout this research, OCSL Reactor models have been replicated between MCNP and WIMS. As explained in Chapter 5, MCNP infers the average neutron behaviour by statistically analyzing the results of numerous particle simulations in the three-dimensional reactor model. On the other hand, WIMS solves the neutron transport equations by numerical methods for the reactor represented as a two-dimensional cell. The notion that two independent methods calculate results that agree with one another provides some credibility for the OCSL Reactor design.

Despite this agreement, each computer code has associated limitations and error that may affect the validity of the OCSL Reactor models. Therefore, the following subsections will further discuss each computer code's results.

10.8.1 Limitations and Error of MCNP Results

The OCSL Reactor models created using MCNP are considered more accurate than those produced for WIMS. In MCNP, the reactor is defined in three dimensions and the model therefore represents the geometry exactly as intended. The Visual Editor software that is part of MCNPX provides a graphic interface for developing models. Using this tool, user errors in the MCNP input may be identified and rectified. As a result, there is confidence that the materials and geometry of the model are defined exactly as the user intends. However, the systematic error attributed to the virtual dimensions and boundaries in the model is unknown.

The Nuclear Data Libraries used by MCNP are also a potential source of error in the results. While these libraries are regularly updated, they may not contain cross-section data for the exact energies in the model. Therefore, an error is associated with interpolation of cross-section data in the MCNP model. However, the accuracy of the most current data libraries has been well-demonstrated and the uncertainty in cross-section data is not considered a significant source of error in this research.

Explained in Section 7.2, the temperatures assigned throughout the MCNP model represent a major simplification to the temperature distributions in the fuel, cladding, and coolant. By assigning average temperatures to each of these materials, cross-sections are treated as constant through cells where there would normally be some variation with a temperature distribution. This simplification contributes to the uncertainty of results from MCNP but is deemed acceptable for practicability.

As a probabilistic code, the results of MCNP represent mean values across all active cycles of the simulation. Accordingly, every result produced by MCNP has an associated standard deviation or relative error. Therefore, the application of central limit theorem dictates that for sufficiently large sample sizes, there is a 68% chance the true result falls within one standard deviation of the mean and a 95% chance the true result falls within two standard deviations of the mean. However, the standard deviation of a

particular result is only a measure of MCNP's precision in calculating said result. Again, the accuracy of a result is only quantifiable with experimental results.

In practice, reducing the standard deviation of a result is a compromise with computing time. Depending on the desired result, the conditions of the simulation must be tailored to deliver satisfactory precision in a practical computing time. For example, KCODE simulations in this research consisted of 100 active cycles with 100,000 neutron histories per cycle. These simulations delivered the effective multiplication factor for the reactor with an acceptable standard deviation and generally required about thirty minutes to compute. The sheer number of KCODE simulations in this research necessitated relatively quick simulations. However, a greater number of neutron histories were required when producing neutron flux distributions for the reactor. To sufficiently reduce the relative error in the flux distribution, the simulation required 950 active cycles with 100,000 neutron histories per cycle. This type of simulation generally required around four hours to complete. As a limited number of flux distributions were required, the longer computing time was tolerable.

10.8.2 Limitations and Error of WIMS Results

Throughout this research, WIMS was employed to create secondary models of the reactor as it was designed using MCNP. By adapting the MCNP models into two dimensions, WIMS could deliver burnup calculations and analysis of reactivity coefficients much faster than MCNP. However, the geometric deviations required by the adaptation process are a source of error in the WIMS results.

As explained in Section 7.9, the positions of the fuel pins in the two-dimensional model differ slightly from their positions in the three-dimensional MCNP model. This discrepancy is deemed acceptable and is necessary to practically adapt the MCNP geometry to the WIMS framework. To account for the third dimension in the WIMS model, the geometric buckling values are varied until the effective multiplication factor closely matches the value from MCNP. Previous small reactor designs by Paquette and Cole have established this method as a means of accounting for neutron leakage in the WIMS model[117 118]. Nonetheless, the method does present uncertainty in how accurately the WIMS model is replicating the geometry of the MCNP model.

In later models, the addition of absorber rods presented a complication for the WIMS models. The geometry of WIMS makes assigning different repeated structures to the same array difficult. Therefore, defining arrays that contained both fuel pins and control rods became complicated. Homogenizing the two structures was the most practical method for defining these arrays. As a result, there was only one repeated structure for each array. However, the repeated structures for arrays containing control rods actually represent the average material composition of the fuel and control rods in that array. This method signified a large departure from reality in the WIMS model but was deemed acceptable because there were relatively few control rods. Therefore, the overall deviation in material composition was small.

Similar to MCNP, the WIMS calculations rely on nuclear data libraries that may or may not contain exact cross-sections for a material at a particular energy. Therefore, uncertainty of WIMS results is partially attributed to interpolation of material cross-sections. Average temperatures were also assigned in WIMS models as they were in MCNP models. Again, the average temperature may not fully capture the influence of temperature distributions. However, these uncertainties are again considered appropriately small and necessary for the purposes of this research.

CHAPTER 11: CONCLUSION AND RECOMMENDATIONS

11.1 Conclusion: The OCSL Reactor

Northern Canada's numerous off-grid, remote locations present unique opportunities for emerging technology in the field of small modular reactor design. The 1 MW_{th} Organic-Cooled SLOWPOKE Reactor is a small nuclear reactor based upon the existing SLOWPOKE-2 nuclear reactor design. With an uprated thermal power from the SLOWPOKE-2, an OCSL Reactor is intended to supply district heating to small, remote installations in Northern Canada. Due to their relatively small size, multiple reactors may operate together to supply greater heating demands or even generate electrical power. Presently, the OCSL Reactor represents a conceptual design of reactor neutronics demonstrated using the computer codes MCNP 6 and WIMS-AECL. The initial design phases of the OCSL Reactor have demonstrated a simple reactor with strong potential for inherent safety like its namesake reactor. Furthermore, initial estimates of the lifespan of fuel in the OCSL Reactor indicate a service life of more than a decade.

The OCSL Reactor accomplishes extension of the SLOWPOKE-2's power by first replacing the light water coolant of the SLOWPOKE-2 with an organic coolant. The organic coolant, HB-40, is a well-researched hydrogenated terphenyl mixture with a boiling point of 342 ^{O}C. Due to the reduced vapour pressure of the coolant, the operating temperature range of the reactor is elevated without need for pressurization. Coolant enters the OCSL Reactor at 290 ^{O}C flowing at 7.63 kg s^{-1} and exits the reactor at 340 ^{O}C. The OCSL Reactor's increased operating temperature improves its thermal efficiency aiding the delivery of 1 MW_{th}.

The second component of the SLOWPOKE-2 power extension is the overall increased size of the OCSL Reactor. In order to transfer 1 MW_{th}, the SLOWPOKE-2 fuel pins are extended to 50 cm in length. Additionally, the OCSL Reactor core is comprised of 660 fuel pins arranged in a triangular lattice with a pitch of 1.95 cm. As a result, the approximate outer radius of the core is 27.8 cm. The annular reflector of the OCSL Reactor is composed of beryllium and is 30 cm thick. The annulus itself is formed by six identical plates that may withdraw from the core as part of the control system.

With its increased size, the OCSL Reactor requires a larger and more involved control system to ensure safe and reliable operation. Consequently, the control system is comprised by twenty-five hafnium control rods, twenty-four hafnium shutdown rods, and six moving beryllium reflector plates. The control system of the OCSL Reactor is designed to effectively serve three primary control functions: short-term regulating control, long-term regulating control, and shutdown control.

First, short-term regulating control ensures fine control of the reactor's power. At a given time, the central control rod and one six-rod cluster move to adjust power and excess reactivity in the core. Second, long-term regulating control in the OCSL Reactor prevents criticality excursions by limiting the reactor's excess reactivity below prompt critical level. Serving this function, the remaining control rods and the moveable reflector plates are configured such that excess reactivity with the moving control group withdrawn will be below prompt critical. Finally, shutdown control ensures the reactor may be rendered sub-critical under all circumstances. In normal operation, shutdown is accomplished by shutdown rods and control rods being inserted into the reactor core. In emergencies, negative reactivity may be supplemented by fully withdrawing the reflector plates.

In addition to the safety provided by the OCSL Reactor's control system, the reactor demonstrates negative reactivity coefficients for moderator temperature, fuel temperature and void fraction. These are considered a strong indicator of inherent safety in the design and constitute a

necessary requirement for inherent safety. However, only the simulation of the reactor in transient states and in accident scenarios will confirm the inherent safety of the OCSL Reactor. This investigation ensures that under non-steady-state conditions, the reactor will not incur material damage resulting in the release of radioactive and toxic substances.

11.2 Recommendations for Future Design Work

The present design iteration of the OCSL Reactor represents the steady-state neutronics of the reactor as demonstrated using the computer codes MCNP 6 and WIMS-AECL. This research has estimated the thermal hydraulics of the reactor by applying Newton's Law of Cooling. As a result, the current design depends upon numerous simplifications and assumptions to present a working model of the reactor. Therefore, future design work must improve upon the limitations of this research to develop a more comprehensive and cohesive model of the OCSL Reactor. The following recommendations are intended to aid in directing future research:

- The assumptions required to assign temperatures in the OCSL Reactor models are considered a source of uncertainty. A steady-state thermal hydraulic model of the reactor that reflects power and flux distributions will better define the temperature distributions along the core as well as across the core. Finite element software such as COMSOL Multiphysics® provide the best tools for such a model.[119]

- Inherent safety of the OCSL Reactor can only be confirmed by studying the reactor's transient response to perturbation. A kinetic model that couples reactor neutronics with thermal hydraulics may be used to demonstrate the reactor's behaviour in numerous transient scenarios including loss of coolant accidents (LOCA) and loss of coolant flow accidents (LOCFA).

- Beyond neutronics and thermal hydraulics, an inherently safe reactor design requires sufficient containment and shielding to mitigate hazards to personnel and the environment. Future work may design the containment system for this reactor and demonstrate its safety using commercial software such as MicroShield®.[120]

- This research assumed a functioning heat extraction loop for the transfer of thermal power from the reactor. In reality, the reactor may power a steam generator, or it may deliver heat to a hot water tank via secondary heat exchangers. An investigation of the heat transfer potential of the hot flowing HB-40 will better define the district heating applications of the OCSL Reactor.

- This research relied on historic research of the coolant, HB-40, to best define the material in models of the OCSL Reactor. However, modern coolants may exist now or in the near future that significantly improve upon HB-40's performance. Future designs may consider incorporating modern terphenyl coolants into the reactor model.

- A thorough investigation of the coolant's performance under reactor conditions was not in the scope of this research. Coolant degradation was only addressed by limited means. Future work may attempt to better characterize the degradation of coolant in the OCSL Reactor. To combat degradation, incorporation of solid moderators such as graphite may reduce the radiation dose absorbed by the coolant and decrease the coolant make-up rate. Furthermore, understanding of the coolant make-up rate in the OCSL Reactor will aid in designing or selecting an appropriate hydrocracking system to incorporate into the design.

- Neutron flux shaping is often a secondary function of the reactor's control system. The design of the OCSL Reactor control system emphasized criticality rather than flux shape. Future research may seek to incorporate more control rod movement or experiment with other methods of flattening the neutron flux.

References

[1] V. H. M. Visschers, C. Keller, and M. Siegrist, “Climate change benefits and energy supply benefits as determinants of acceptance of nuclear power stations: Investigating an explanatory model,” *Energy Policy*, vol. 39, no. 6, 2011, page 3621.

[2] A. Lajeunesse, “The Canadian Armed Forces in the Arctic: Purpose, Capabilities, and Requirements,” Canadian Defence and Foreign Affairs Institute, 2015, page 1.

[3] M. Arriaga, C. A. Cañizares, and M. Kazerani, “Renewable Energy Alternatives for Remote Communities in Northern Ontario , Canada,” *IEEE Trans. Sustain. Energy*, vol. 4, no. 3, 2013, page 1.

[4] Z. Liu and J. Fan, “Review: Technology readiness assessment of Small Modular Reactor (SMR) designs,” *Prog. Nucl. Energy*, vol. 70, 2014, page 20.

[5] K. Shirvan and E. Forrest, “Design of an Organic Simplified Nuclear Reactor,” *Nucl. Eng. Technol.*, vol. 48, no. 4, 2016, page 894.

[6] J. W. Townes, B.M; Hilborn, “THE SLOWPOKE-2 REACTOR WITH LOW ENRICHMENT URANIUM OXIDE FUEL,” 1988, page 1.

[7] “Terms for describing new, advanced nuclear power plants”, International Atomic Energy Agency, TECDOC-936, April, 1997, page 17.

[8] J.L. Smee, V.R. Puttagunta, R.F.S. Robertson, and S.R. Hatcher, “Organic Coolant Summary Report,” Atomic Energy of Canada Limited Report AECL-4922, August, 1975, pages 4-5.

[9] “Treaty on the non-proliferation of nuclear weapons’, International Atomic Energy Agency, INFCIRC/140, April, 1970, pages 2-3.

[10] Reference 5., page 893.

[11] Id., page 901.

[12] Id., page 903.

[13] Id., page 898.

[14] Id., page 899.

[15] Id., page 902.

[16] Id., page 900.

[17] G. F. Lynch, “DISTRICT HEATING WITH SLOWPOKE ENERGY SYSTEMS,” Atomic Energy of Canada Limited Report AECL-9720, March, 1988, page 4.

[18] Id., page 2.

[19] Id., page 5.

[20] Id., page 6.

[21] Id., page 3.

[22] G. F. Lynch, "SLOWPOKE - ITS APPLICATION TO DISTRICT HEATING SLOWPOKE - SON APPLICATION AU CHAUFFACE URBAIN," Atomic Energy of Canada Limited Report AECL-9720, July, 1987, page 5.

[23] Reference 6, pages 1-3.

[24] Reference 8, page 3.

[25] Id., page 2.

[26] D.R. Tegart, "Operation of the WR-1 Organic Cooled Research Reactor," Atomic Energy of Canada Limited Report AECL-3523, August, 1970, page 1.

[27] Id., page 2.

[28] "WR-1 Design Details," Canadian Nuclear Society, March, 1982. Website: www.cns-snc.ca/media/history/wr-1/wr-1_4.html.

[29] Reference 8, page 1.

[30] Id., page 6.

[31] Id., page 8.

[32] Id., pages 9-10.

[33] Id., page 11.

[34] Id., page 12.

[35] Id., page 13.

[36] Id., page 14.

[37] Id., pages 16-17.

[38] Id., page 20.

[39] Id., page 23.

[40] Id., page 27.

[41] Id., pages 24-25.

[42] Id., page 28.

[43] Id., page 30-31.

[44] Id., page 32.

[45] Id., page 33.

[46] Id., page 35.

[47] Id., pages 37-38.

[48] Id., page 54.

[49] Id., page 43.

[50] Id., page 50.

[51] Id., page 55.

[52] Id., page 56.

[53] Id., pages 63-65.

[54] Id., page 69.

[55] Id., pages 67-68.

[56] Id., pages 70-71.

[57] Id., page 77.

[58] Id., pages 71-72.

[59] Id., page 78.

[60] "RD-308 Deterministic Safety Analysis for Small Reactor Facilities," Canadian Nuclear Safety Commission, February, 2014. Website: nuclearsafety.gc.ca/eng/acts-and-regulations/regulatory-documents/published/html/rd308.

[61] J.R. Lamarsh, and A.J. Baratta, "Introduction to Nuclear Engineering Third Edition," Prentice Hall, Upper Saddle River, N.J., 2001, page 230.

[62] Id., pages 236-237.

[63] Id., page 248.

[64] Id., page 250.

[65] S. Glasstone, and A. Sesonske, "Nuclear Reactor Engineering, Fourth Edition", Springer Science+Business Media Dordrecht, 1994, page 150.

[66] Id., page 191.

[67] Reference 61, page 291.

[68] Id., page 280.

[69] Reference 65, page 241.

[70] Reference 61, page 365.

[71] Id., page 366-367.

[72] Id., page 372.

[73] Id., pages 374-375.

[74] Id., pages 85-87.

[75] Id., pages 340-341.

[76] Id., pages 127-128.

[77] Id., page 389.

[78] Id., pages 428-430.

[79] Id., pages 424-425.

[80] Id., pages 431-435.

[81] E.A. Mason, T.H. Timmins, D.T. Morgan, and W.N. Bley, "Effect of Reactor Irradiation on Santowax WR," Massachusetts Institute of Technology Department of Nuclear Engineering, MITNE-78, October, 1966, page 5.27.

[82] X-5 Monte Carlo Team, "MCNP – A General Monte Carlo N-Particle Transport Code, Version 5," Los Alamos National Laboratory, LA-UR-03-1987, 24 April 2003, page 1-2.

[83] D.B. Pelowitz, "MCNP6™ User's Manual Version 1.0," Los Alamos National Laboratory, LA-CP-13-00634, May 2013, page 1-1.

[84] Reference 82, pages 1-2 – 1-3.

[85] Id., page 1-6.

[86] Id., page 1-4.

[87] Id., pages 1-12 – 1-13.

[88] Reference 83, pages 3-7 – 3-8.

[89] Id., pages 3-12 – 3-13.

[90] Id., page 3-15.

[91] Id., pages 3-54 – 3-56.

[92] Id., pages 3-160 – 3-162.

[93] Reference 82, pages 2-27 – 2-28.

[94] Id., page 2-31.

[95] Id., pages 2-34 – 2-36.

[96] G. Jonkmans, "WIMS-AECL Version 3.1 User's Manual," CANDU Owners Group Inc., ISTP-05-5115, August 2006, page 1-1.

[97] Id., page 4-2.

[98] Id., page 6-1.

[99] J.R.M. Pierre, "Low Enrichment Urainum (LEU)-Fueled SLOWPOKE-2 Nuclear Reactor Simulation with the Monte-Carlo Based MCNP 4A Code", Master's Thesis, Royal Military College of Canada, May, 1996.

[100] Id., page 53.

[101] Reference 65, page 484.

[102] Reference 5, page 897.

[103] Id., page 896.

[104] P. Gierszewski, and B. Hollies, "Organic Coolants and Their Applications to Fusion Reactors," Atomic Energy of Canada Limited Report AECL-8405, August, 1986, page 7.

[105] Reference 61, page 756.

[106] R.F.S. Robertson, "Fuel, Materials and Coolants for WR-1," Atomic Energy of Canada Limited Report AECL-2553, page 7.

[107] Reference 65, pages 454-455.

[108] Reference 61, pages 455-456.

[109] Reference 65, page 308.

[110] Id., page 301.

[111] Id., page 306-307.

[112] Id., page 304-305.

[113] Id., pages 305 - 306.

[114] Id., page 316.

[115] Reference 81, page 1.13.

[116] Reference 8, page 26.

[117] S. Paquette, "Conceptual Design of a Small Nuclear Reactor to Supply District Heating and Electrical Energy to Canadian Forces Bases Located in the Arctic or the Northern Remote Communities," Master's Thesis, Royal Military College of Canada, April 2010.

[118] S. Paquette, and H.W. Bonin, "Neutronic Design and Analysis of a Small Nuclear Reactor to Supply District Heating and Electrical Energy to Canadian Forces Bases Located in the Arctic or the Northern Remote Communities," Nuclear Technology, 176, December 2011, pages 315-336.

[119] "COMSOL Multiphysics," COMSOL Inc., 2018. Website: https://www.comsol.com/comsol-multiphysics.

[120] "MicroShield® Version 11," Grove Software, April, 2017. Website: http://radiationsoftware.com/microshield.

APPENDIX A: SAMPLE MCNP 6 CODE INPUT AND OUTPUT

This appendix presents a sample MCNP 6 input file with a portion of its resulting output listing. The output presented here is limited to maintain a reasonable length in this appendix. Specifically, the model featured here is that of the completed reactor design with all absorber rods withdrawn. The result of this simulation was previously presented in Section 9.9 in Table 25.

Input File

```
OCSL W/ FINAL ABSORBER ROD LAYOUT (RODS WITHDRAWN)
c ==== Data ======================================
c 660 elements, 1.95cm hex pitch
c 5.25mm diameter, 50 cm length
c 30 cm Be Reflector, Moving plates at core edge
c 25 1.588cm OD Hf Control Rods, 24 1.4cm OD Hf Shutdown Rods,
c HB40 represented as 1% biphenyl, 0.99x18% o-terphenyl, 0.99x82% hydroterphenyl
c Fuel temp is 399 oC, Clad temp is 337 oC and Coolant temp is 315 oC.
c
c ====Cell Cards==============================================
c Cell#  Mat  Density  Surf                                                    Comments
999 0 999                                                                     $ outside space
1         3    -10.6   -100 -102 103 u=1  TMP=5.790e-8                       $ fuel
2         5    -6.49    (100 -101 -102 103):(-101 102 -104):(-101 -103 105) u=1 $ clad
               TMP=5.257e-8
3         2    -0.785   101 u=1  TMP=5.068e-8                                $ hb40 around clad
13        2    -0.785   -101 -106 104 u=1 TMP=5.068e-8                       $hb40 above fuel
c
101       9    -13.36  -106 104 -2101 u=3 TMP=5.068e-8                       $Hf Control Rod (withdrawn)
102       4    5.0807e-5   -106 104 2101 u=3                                 $ air around Control Rod
103       4    5.0807e-5   -104 105 -2101 u=3                                $ air below Control Rod
104       6    -2.70      -104 105 2101 -2102 u=3 TMP=5.068e-8               $ Ctrl Rod Hole
105       2    -0.785     -104 105 2102 u=3   TMP=5.068e-8                   $ HB40 outside hole
c
106       9    -13.36  -104 105 -2101 u=6 TMP=5.068e-8                       $Hf Control Rod (inserted)
107       4    5.0807e-5   -106 104 2101 u=6                                 $ air above Control Rod
108       4    5.0807e-5   -106 104 -2101 u=6                                $ air above Control Rod
109       6    -2.70      -104 105 2101 -2102 u=6 TMP=5.068e-8               $ Ctrl Rod Hole
110       2    -0.785     -104 105 2102 u=6   TMP=5.068e-8                   $ HB40 outside hole
c
2101       9    -13.36  -106 104 -4101 u=5 TMP=5.068e-8                    $ Hf Shutdown Rod (withdrawn)
2102       4    5.0807e-5   -106 104 4101 u=5                                $ air around Shutdown Rod
2103       4    5.0807e-5   -104 105 -4101 u=5                               $ air below Shutdown Rod
2104       6    -2.70      -104 105 4101 -4102 u=5 TMP=5.068e-8              $ Shutdown Rod Hole
2105       2    -0.785     -104 105 4102 u=5 TMP=5.068e-8                        $ HB40 outside hole
c
2106       9    -13.36  -104 105 -4101 u=8 TMP=5.068e-8                  $ Hf Shutdown Rod (inserted)
2107       4    5.0807e-5   -106 104 4101 u=8                                $ air above Shutdown Rod
2108       4    5.0807e-5   -106 104 -4101 u=8                               $ air above Shutdown Rod
2109       6    -2.70      -104 105 4101 -4102 u=8 TMP=5.068e-8              $ Shutdown Rod Hole
2110       2    -0.785     -104 105 4102 u=8 TMP=5.068e-8                        $ HB40 outside hole
c
4         2     -0.785   -106 105 -11 301 303 305 307 309 311 313 315 317 319 $ Core Volume
                         321 323 325 327 329 331 333 335 fill=2 TMP=5.068e-8
5         2    -0.785    -200 201 -202 203 u=2 lat=1 TMP=5.068e-8           $ Lattice Filling Core Volume
               fill=-16:16 -16:16 -0:0
```

```
           2 2 2 2 2 2 2 2 2 2 2 2 2 2 2 2 2 2 2 2 2 2 2 5 2 2 2 2 2 2 2 2
           2 2 2 2 2 2 2 2 2 2 2 2 2 2 2 2 2 2 2 2 1 1 1 1 1 1 1 1 1 1 2 2 2 2
           2 2 2 2 2 2 2 2 2 2 2 2 2 2 2 2 2 2 1 1 1 1 1 1 1 1 1 1 1 1 1 2 2 2
           2 2 2 2 2 2 2 2 2 2 2 2 2 2 2 2 1 1 1 1 1 1 1 1 1 1 1 1 1 1 1 2 2
           2 2 2 2 2 2 2 2 2 2 2 2 2 2 2 1 1 1 1 1 1 1 1 1 1 1 1 1 1 1 1 1 2
           2 2 2 2 2 2 2 2 2 2 2 2 2 2 1 1 1 1 1 1 1 1 1 1 1 1 1 1 1 1 1 1 2
           2 2 2 2 2 2 2 2 2 2 2 2 2 1 1 1 1 1 1 1 1 1 1 1 3 1 1 1 1 1 1 1 2
           2 2 2 2 2 2 2 2 2 2 2 1 1 1 1 1 1 1 1 1 1 1 3 1 1 1 1 1 1 1 3 1 2
           2 2 2 2 2 2 2 2 5 1 1 1 1 1 1 1 1 1 1 1 1 1 1 1 1 1 1 1 1 1 1 5
           2 2 2 2 2 2 2 2 1 1 1 1 1 1 1 1 1 1 1 1 1 1 1 1 1 1 1 1 1 1 1 2
           2 2 2 2 2 2 2 1 1 1 1 1 1 1 1 3 1 1 1 1 1 1 1 1 1 1 1 1 1 1 1 2
           2 2 2 2 2 2 1 1 1 1 1 1 3 1 1 1 1 1 1 1 1 1 1 1 1 1 1 3 1 1 1 2
           2 2 2 2 2 1 1 1 1 1 1 1 1 1 1 1 1 1 1 3 1 1 1 1 1 1 1 1 1 1 1 2
           2 2 2 2 1 1 1 1 1 1 1 1 1 1 1 1 1 1 1 1 1 1 1 1 1 1 1 1 1 1 1 2
           2 2 2 2 1 1 1 1 1 1 1 1 1 1 3 1 1 1 1 1 3 1 1 1 1 1 1 1 1 1 2 2
           2 2 2 1 1 1 1 1 1 1 1 1 1 1 1 1 1 1 1 1 1 1 1 1 1 1 1 1 1 1 2 2
           2 2 2 1 1 1 1 3 1 1 3 1 1 1 1 1 3 1 1 1 1 1 3 1 1 3 1 1 1 1 2 2 2
           2 2 1 1 1 1 1 1 1 1 1 1 1 1 1 1 1 1 1 1 1 1 1 1 1 1 1 1 1 1 2 2 2
           2 2 1 1 1 1 1 1 1 1 1 1 3 1 1 1 1 1 3 1 1 1 1 1 1 1 1 1 1 2 2 2 2
           2 1 1 1 1 1 1 1 1 1 1 1 1 1 1 1 1 1 1 1 1 1 1 1 1 1 1 1 1 2 2 2 2
           2 1 1 1 1 1 1 1 1 1 1 1 1 1 3 1 1 1 1 1 1 1 1 1 1 1 1 1 2 2 2 2 2
           2 1 1 1 1 1 3 1 1 1 1 1 1 1 1 1 1 1 1 1 1 3 1 1 1 1 1 2 2 2 2 2 2
           2 1 1 1 1 1 1 1 1 1 3 1 1 1 1 1 3 1 1 1 1 1 1 1 1 1 2 2 2 2 2 2 2
           2 1 1 1 1 1 1 1 1 1 1 1 1 1 1 1 1 1 1 1 1 1 1 1 1 1 2 2 2 2 2 2 2
           5 1 1 1 1 1 1 1 1 1 1 1 1 1 1 1 1 1 1 1 1 1 1 1 1 1 5 2 2 2 2 2 2 2
           2 1 1 1 1 1 1 3 1 1 1 1 1 1 1 1 3 1 1 1 1 1 1 2 2 2 2 2 2 2 2 2 2
           2 1 1 1 1 1 1 1 1 1 1 3 1 1 1 1 1 1 1 1 1 2 2 2 2 2 2 2 2 2 2 2 2
           2 1 1 1 1 1 1 1 1 1 1 1 1 1 1 1 1 1 1 1 1 1 2 2 2 2 2 2 2 2 2 2 2
           2 1 1 1 1 1 1 1 1 1 1 1 1 1 1 1 1 1 1 1 1 1 1 2 2 2 2 2 2 2 2 2 2
           2 2 1 1 1 1 1 1 1 1 1 1 1 1 1 1 1 1 1 1 1 1 2 2 2 2 2 2 2 2 2 2 2
           2 2 2 1 1 1 1 1 1 1 1 1 1 1 1 1 1 1 1 1 2 2 2 2 2 2 2 2 2 2 2 2 2
           2 2 2 2 1 1 1 1 1 1 1 1 1 1 1 1 1 1 1 2 2 2 2 2 2 2 2 2 2 2 2 2 2
           2 2 2 2 2 2 2 2 5 2 2 2 2 2 2 2 2 2 2 2 2 2 2 2 2 2 2 2 2 2 2 2 2
6 1    -1.85 11 -12 -104 105 TMP=5.068e-8             $ Be Reflector
7 2    -0.785  #(-11 -106 105) #6 -999 TMP=5.068e-8   $ HB-40 Surrounding Reactor
c
c $Cells 308 to 361 are individual shutdown rods that do not sit perfectly on lattice points. Each rod has
an inserted definition (preceded by “c” in this withdrawn model to disregard these cells) and a withdrawn
definition (active in this model).
c
c 308        9    -13.36 -300 -104 105 TMP=5.068e-8
c 309        6    -2.70 300 -301 -106 105 TMP=5.068e-8
c 310       4    5.0807e-5 -300 -106 104
308        9    -13.36 -300 -106 104 TMP=5.068e-8
309        6    -2.70 300 -301 -106 105 TMP=5.068e-8
310       4    5.0807e-5 -300 -104 105
c
c 311        9    -13.36 -302 -104 105 TMP=5.068e-8
c 312        6    -2.70 302 -303 -106 105 TMP=5.068e-8
c 313       4    5.0807e-5 -302 -106 104
311        9    -13.36 -302 -106 104 TMP=5.068e-8
312        6    -2.70 302 -303 -106 105 TMP=5.068e-8
313       4    5.0807e-5 -302 -104 105
c
c 314        9    -13.36 -304 -104 105 TMP=5.068e-8
c 315        6    -2.70 304 -305 -106 105 TMP=5.068e-8
c 316       4    5.0807e-5 -304 -106 104
314        9    -13.36 -304 -106 104 TMP=5.068e-8
315        6    -2.70 304 -305 -106 105 TMP=5.068e-8
316       4    5.0807e-5 -304 -104 105
c
c 317        9    -13.36 -306 -104 105 TMP=5.068e-8
c 318        6    -2.70 306 -307 -106 105 TMP=5.068e-8
c 319       4    5.0807e-5 -306 -106 104
317        9    -13.36 -306 -106 104 TMP=5.068e-8
318        6    -2.70 306 -307 -106 105 TMP=5.068e-8
319       4    5.0807e-5 -306 -104 105
c
c 320        9    -13.36 -308 -104 105 TMP=5.068e-8
```

```
c 321        6    -2.70 308 -309 -106 105 TMP=5.068e-8
c 322       4    5.0807e-5 -308 -106 104
320         9    -13.36 -308 -106 104 TMP=5.068e-8
321         6    -2.70 308 -309 -106 105 TMP=5.068e-8
322        4    5.0807e-5 -308 -104 105
c
c 323        9    -13.36 -310 -104 105 TMP=5.068e-8
c 324        6    -2.70 310 -311 -106 105 TMP=5.068e-8
c 325       4    5.0807e-5 -310 -106 104
323         9    -13.36 -310 -106 104 TMP=5.068e-8
324         6    -2.70 310 -311 -106 105 TMP=5.068e-8
325        4    5.0807e-5 -310 -104 105
c
c 326        9    -13.36 -312 -104 105 TMP=5.068e-8
c 327        6    -2.70 312 -313 -106 105 TMP=5.068e-8
c 328       4    5.0807e-5 -312 -106 104
326         9    -13.36 -312 -106 104 TMP=5.068e-8
327         6    -2.70 312 -313 -106 105 TMP=5.068e-8
328        4    5.0807e-5 -312 -104 105
c
c 329        9    -13.36 -314 -104 105 TMP=5.068e-8
c 330        6    -2.70 314 -315 -106 105 TMP=5.068e-8
c 331       4    5.0807e-5 -314 -106 104
329         9    -13.36 -314 -106 104 TMP=5.068e-8
330         6    -2.70 314 -315 -106 105 TMP=5.068e-8
331        4    5.0807e-5 -314 -104 105
c
c 332        9    -13.36 -316 -104 105 TMP=5.068e-8
c 333        6    -2.70 316 -317 -106 105 TMP=5.068e-8
c 334       4    5.0807e-5 -316 -106 104
332         9    -13.36 -316 -106 104 TMP=5.068e-8
333         6    -2.70 316 -317 -106 105 TMP=5.068e-8
334        4    5.0807e-5 -316 -104 105
c
c 335        9    -13.36 -318 -104 105 TMP=5.068e-8
c 336        6    -2.70 318 -319 -106 105 TMP=5.068e-8
c 337       4    5.0807e-5 -318 -106 104
335         9    -13.36 -318 -106 104 TMP=5.068e-8
336         6    -2.70 318 -319 -106 105 TMP=5.068e-8
337        4    5.0807e-5 -318 -104 105
c
c 338        9    -13.36 -320 -104 105 TMP=5.068e-8
c 339        6    -2.70 320 -321 -106 105 TMP=5.068e-8
c 340       4    5.0807e-5 -320 -106 104
338         9    -13.36 -320 -106 104 TMP=5.068e-8
339         6    -2.70 320 -321 -106 105 TMP=5.068e-8
340        4    5.0807e-5 -320 -104 105
c
c 341        9    -13.36 -322 -104 105 TMP=5.068e-8
c 342        6    -2.70 322 -323 -106 105 TMP=5.068e-8
c 343       4    5.0807e-5 -322 -106 104
341         9    -13.36 -322 -106 104 TMP=5.068e-8
342         6    -2.70 322 -323 -106 105 TMP=5.068e-8
343        4    5.0807e-5 -322 -104 105
c
c 344        9    -13.36 -324 -104 105 TMP=5.068e-8
c 345        6    -2.70 324 -325 -106 105 TMP=5.068e-8
c 346       4    5.0807e-5 -324 -106 104
344         9    -13.36 -324 -106 104 TMP=5.068e-8
345         6    -2.70 324 -325 -106 105 TMP=5.068e-8
346        4    5.0807e-5 -324 -104 105
c
c 347        9    -13.36 -326 -104 105 TMP=5.068e-8
c 348        6    -2.70 326 -327 -106 105 TMP=5.068e-8
c 349       4    5.0807e-5 -326 -106 104
347         9    -13.36 -326 -106 104 TMP=5.068e-8
348         6    -2.70 326 -327 -106 105 TMP=5.068e-8
349        4    5.0807e-5 -326 -104 105
c
```

```
c 350        9    -13.36 -328 -104 105 TMP=5.068e-8
c 351        6    -2.70 328 -329 -106 105 TMP=5.068e-8
c 352       4    5.0807e-5 -328 -106 104
350        9    -13.36 -328 -106 104 TMP=5.068e-8
351        6    -2.70 328 -329 -106 105 TMP=5.068e-8
352       4    5.0807e-5 -328 -104 105
c
c 353        9    -13.36 -330 -104 105 TMP=5.068e-8
c 354        6    -2.70 330 -331 -106 105 TMP=5.068e-8
c 355       4    5.0807e-5 -330 -106 104
353        9    -13.36 -330 -106 104 TMP=5.068e-8
354        6    -2.70 330 -331 -106 105 TMP=5.068e-8
355       4    5.0807e-5 -330 -104 105
c
c 356        9    -13.36 -332 -104 105 TMP=5.068e-8
c 357        6    -2.70 332 -333 -106 105 TMP=5.068e-8
c 358       4    5.0807e-5 -332 -106 104
356        9    -13.36 -332 -106 104 TMP=5.068e-8
357        6    -2.70 332 -333 -106 105 TMP=5.068e-8
358       4    5.0807e-5 -332 -104 105
c
c 359        9    -13.36 -334 -104 105 TMP=5.068e-8
c 360        6    -2.70 334 -335 -106 105 TMP=5.068e-8
c 361       4    5.0807e-5 -334 -106 104
359        9    -13.36 -334 -106 104 TMP=5.068e-8
360        6    -2.70 334 -335 -106 105 TMP=5.068e-8
361       4    5.0807e-5 -334 -104 105

c ====Surface Cards=========================================
c
c Surface#  Type  Parameters                                                    Comments
100         cx   0.2125                                                      $ fuel radius
101         cx   0.2625                                                       $ clad radius
2101        cx   0.794                                                     $control rod radius
2102        cx   0.844                                                     $control rod hole
4101        cx   0.70                                                      $shutdown rod radius
4102        cx   0.75                                                      $shutdown rod hole
102         px   24.95                                                       $ top plane of fuel
103         px   -24.95                                                    $ top plane of fuel
104         px   25                                                      $ top plane of clad
105         px   -25                                                        $ bottom plane of clad
106         px   75                                                  $top plane of absorber rods when withdrawn
11   cx   27.8                                                          $ Reflector inner radius
12   cx   57.8                                                          $ Reflector outer radius
13   px   -200
14   px   200
200  p 0.0 -1.6887495 -0.975 1.6465308                                        $ lattice
201  p 0.0 -1.6887495 -0.975 -1.6465308                                       $ lattice
202  pz 0.8443748                                                          $ lattice
203  pz -0.8443748                                                          $ lattice
999  sx   0 200                                                          $surrounding sphere of HB-40
c
c $Surfaces 300 to 335 define the individual Hf Shutdown rods
c
300 c/x 27 0 0.70
301 c/x 27 0 0.75
302 c/x -27 0 0.70
303 c/x -27 0 0.75
304 c/x 25.07 10.02 0.70
305 c/x 25.07 10.02 0.75
306 c/x 25.07 -10.02 0.70
307 c/x 25.07 -10.02 0.75
308 c/x -25.07 10.02 0.70
309 c/x -25.07 10.02 0.75
310 c/x -25.07 -10.02 0.70
311 c/x -25.07 -10.02 0.75
312 c/x 21.21 16.70 0.70
313 c/x 21.21 16.70 0.75
314 c/x 21.21 -16.70 0.70
```

```
315 c/x 21.21 -16.70 0.75
316 c/x -21.21 16.70 0.70
317 c/x -21.21 16.70 0.75
318 c/x -21.21 -16.70 0.70
319 c/x -21.21 -16.70 0.75
320 c/x 13.5 23.38 0.70
321 c/x 13.5 23.38 0.75
322 c/x 13.5 -23.38 0.70
323 c/x 13.5 -23.38 0.75
324 c/x -13.5 23.38 0.70
325 c/x -13.5 23.38 0.75
326 c/x -13.5 -23.38 0.70
327 c/x -13.5 -23.38 0.75
328 c/x 3.86 26.72 0.70
329 c/x 3.86 26.72 0.75
330 c/x 3.86 -26.72 0.70
331 c/x 3.86 -26.72 0.75
332 c/x -3.86 26.72 0.70
333 c/x -3.86 26.72 0.75
334 c/x -3.86 -26.72 0.70
335 c/x -3.86 -26.72 0.75

c ==== Data Cards=======================================================
c Material Data
c Beryllium with pre-irradiation impurities
IMP:N 0 1 1 1 1 1 1 1 1 1 1 1 1 1 1 1 1 1 1 1 1 1 1 1 1 1 1 1 1 1 1 1 1 1 1 1 1
        1 1 1 1 1 1 1 1 1 1 1 1 1 1 1 1 1 1 1 1 1 1 1 1 1 1 1 1 1 1 1 1 1 1 1 1
        1 1 1 1 1 1 1 1 1 1
m1    4009.50c -0.9953863
      8016.50c -9.701130e-6
      13027.50c -1.010534e-3
      6000.50c -1.515802e-3
      26000.50c -1.31695e-3
      14000.50c -6.063207e-4
      5011.50c -1.616855e-6
      25055.50c -1.515802e-4
      48000.50c -7.376901e-7
      3006.50c  -1.313695e-7
      3007.55c  -1.92001e-6
      62149.50c -6.497736e-7
      64155.50c -3.53687e-8
      64157.50c -3.132657e-8
      63151.50c -2.425283e-7
      63153.50c -2.627389e-7
      5010.50c  -4.345298e-7
c HB40
m2    6000 17.94 1001 20.81
c UO2
m3    92235.50c -.1735 92238.50c -.7059 8016.50c -.1188
c Air
m4    8016.50c 0.21174 7014.50c 0.78826
c Zr
m5    40000 1
c Al 6061 T6
m6 13027.50c -0.9792 14000.50c -0.006 29000.50c -0.0028 12000.50c
            -0.01 24000.50c -0.002
c Pure Cadmium
m7    48000.50c 1
c H2O
m8    1001.50c 2 8016.50c 1
c HAFNIUM
m9 72000.50c 1
c
c
c K Calculations : (Histories / Cycle, Keff Guess, Tally Start Cycle, Total Cycles = should be 120)
KCODE 100000 1.000000 20 120
ksrc -1.95 0 0
c
print
```

Output File Excerpt

```
the initial fission neutron source distribution used the   1 source points that were input on the ksrc card.
 the criticality problem was scheduled to skip  20 cycles and run a total of  120 cycles with nominally   100000 neutrons
per cycle.
 this problem has run  20 inactive cycles with  2036950 neutron histories and  100 active cycles with     9999267 neutron
histories.
 this calculation has completed the requested number of keff cycles using a total of    12036217 fission neutron source
histories.
 all cells with fissionable material were sampled and had fission neutron source points.
 comment.
 comment. Average fission-source entropy for the last half of cycles:
 comment.      H=  1.06E+01  with population std.dev.=  2.09E-03
 comment.
 comment.
 comment. Cycle    7 is the first cycle having fission-source
 comment.   entropy within 1 std.dev. of the average
 comment.   entropy for the last half of cycles.
 comment.   At least this many cycles should be discarded.
 comment.
 comment. Source entropy convergence check passed.
 comment.
 the results of the w test for normality applied to the individual collision, absorption, and track-length keff cycle
values are:
           the k( collision) cycle values appear normally distributed at the 95 percent confidence level
           the k(absorption) cycle values appear normally distributed at the 99 percent confidence level, but not at 95
percent
           the k(trk length) cycle values appear normally distributed at the 95 percent confidence level
 ------------------------------------------------------------------------------------------------------------------------
| the final estimated combined collision/absorption/track-length keff = 1.28591 with an estimated standard deviation of
0.00020   |
 | the estimated 68, 95, & 99 percent keff confidence intervals are 1.28570 to 1.28611, 1.28550 to 1.28631, and 1.28537
to 1.28644 |
| the final combined (col/abs/tl) prompt removal lifetime = 1.8765E-04 seconds with an estimated standard deviation of
8.0466E-07 |
| the average neutron energy causing fission = 3.6436E-02 mev
 | the energy corresponding to the average neutron lethargy causing fission = 8.9704E-08 mev
 | the percentages of fissions caused by neutrons in the thermal, intermediate, and fast neutron ranges are:
 |         (<0.625 ev):  91.47%         (0.625 ev - 100 kev):   6.98%          (>100 kev):   1.55%
 | the average fission neutrons produced per neutron absorbed (capture + fission) in all cells with fission = 1.9477E+00
 | the average fission neutrons produced per neutron absorbed (capture + fission) in all the geometry cells = 1.2604E+00
 | the average number of neutrons produced per fission = 2.441

 the estimated average keffs, one standard deviations, and 68, 95, and 99 percent confidence intervals are:

        keff estimator       keff     standard deviation      68% confidence        95% confidence        99% confidence
corr

             collision     1.28583         0.00024          1.28559 to 1.28607    1.28536 to 1.28630    1.28521 to
1.28645
            absorption     1.28596         0.00021          1.28574 to 1.28617    1.28553 to 1.28638    1.28540 to
1.28651
          track length     1.28576         0.00042          1.28534 to 1.28619    1.28492 to 1.28661    1.28464 to
1.28689
            col/absorp     1.28591         0.00021          1.28571 to 1.28612    1.28551 to 1.28632    1.28537 to
1.28646    0.6941
            abs/trk len     1.28593         0.00021          1.28572 to 1.28613    1.28552 to 1.28634    1.28539 to
1.28647    0.2238
            col/trk len     1.28582         0.00023          1.28559 to 1.28606    1.28536 to 1.28629    1.28521 to
1.28644    0.3827
       col/abs/trk len     1.28591         0.00020          1.28570 to 1.28611    1.28550 to 1.28631    1.28537 to
1.28644

 if the largest of each keff occurred on the next cycle, the keff results and 68, 95, and 99 percent confidence intervals
would be:

        keff estimator       keff     standard deviation      68% confidence        95% confidence        99% confidence

             collision     1.28590         0.00024          1.28565 to 1.28614    1.28541 to 1.28638    1.28525 to
1.28654
            absorption     1.28602         0.00022          1.28580 to 1.28624    1.28558 to 1.28646    1.28544 to
1.28661
          track length     1.28586         0.00043          1.28543 to 1.28629    1.28500 to 1.28672    1.28472 to
1.28700
       col/abs/trk len     1.28598         0.00021          1.28576 to 1.28619    1.28555 to 1.28640    1.28542 to
1.28654
```

the estimated average prompt removal lifetimes, one standard deviations, and 68, 95, and 99 percent confidence intervals are (sec):

estimator	lifetime	std. dev.	68% confidence	95% confidence	99% confidence	corr
collision	1.83899E-04	1.31192E-07	1.8377E-04 to 1.8403E-04	1.8364E-04 to 1.8416E-04	1.8355E-04 to 1.8425E-04	
absorption	1.83926E-04	1.25336E-07	1.8380E-04 to 1.8405E-04	1.8368E-04 to 1.8418E-04	1.8360E-04 to 1.8426E-04	
track length	1.88014E-04	1.12927E-07	1.8790E-04 to 1.8813E-04	1.8779E-04 to 1.8824E-04	1.8772E-04 to 1.8831E-04	
col/absorp	1.83943E-04	1.25639E-07	1.8382E-04 to 1.8407E-04	1.8369E-04 to 1.8419E-04	1.8361E-04 to 1.8427E-04	0.9805
abs/trk len	1.87715E-04	7.99706E-07	1.8691E-04 to 1.8852E-04	1.8612E-04 to 1.8931E-04	1.8560E-04 to 1.8983E-04	0.8831
col/trk len	1.88001E-04	7.09738E-07	1.8729E-04 to 1.8871E-04	1.8659E-04 to 1.8941E-04	1.8613E-04 to 1.8988E-04	0.8598
col/abs/trk len	1.87647E-04	8.04655E-07	1.8684E-04 to 1.8845E-04	1.8604E-04 to 1.8925E-04	1.8552E-04 to 1.8977E-04	

absorption estimates of prompt lifetimes (sec):

	escape	capture	fission	removal
fraction	2.13355E-03	4.82542E-01	5.15325E-01	1.00000E+00
lifetime(abs)	8.62066E-02	3.81162E-04	3.56914E-04	1.83926E-04
lifetime(c/a/t)	8.79507E-02	3.88873E-04	3.64134E-04	1.87647E-04

1average keff results summed over 2 cycles each to form 50 batch values of keff print table 178

batch number	start cycle	end cycle	keff estimators by batch k(coll)	k(abs)	k(track)	average keff estimators and deviations k(coll)	st dev	k(abs)	st dev	k(track)	st dev	col/abs/tl keff k(c/a/t)	st dev
1	21	22	1.28696	1.28651	1.29068								
2	23	24	1.28894	1.28763	1.28650	1.28795	0.00099	1.28707	0.00056	1.28859	0.00209		
3	25	26	1.28540	1.28663	1.28888	1.28710	0.00102	1.28692	0.00035	1.28869	0.00121		
4	27	28	1.28554	1.28621	1.28365	1.28671	0.00082	1.28674	0.00031	1.28743	0.00152	1.28677	0.00036
5	29	30	1.28644	1.28669	1.28380	1.28666	0.00064	1.28673	0.00024	1.28670	0.00138	1.28676	0.00022
6	31	32	1.28617	1.28499	1.28420	1.28658	0.00053	1.28644	0.00035	1.28628	0.00121	1.28645	0.00045
7	33	34	1.28681	1.28501	1.28341	1.28661	0.00045	1.28624	0.00036	1.28587	0.00110	1.28636	0.00044
8	35	36	1.28553	1.28578	1.28034	1.28647	0.00041	1.28618	0.00032	1.28518	0.00118	1.28632	0.00038
9	37	38	1.28349	1.28480	1.28303	1.28614	0.00049	1.28603	0.00032	1.28494	0.00106	1.28612	0.00039
10	39	40	1.28994	1.28989	1.29246	1.28652	0.00058	1.28641	0.00048	1.28569	0.00121	1.28659	0.00050
11	41	42	1.28469	1.28507	1.28679	1.28636	0.00055	1.28629	0.00045	1.28579	0.00110	1.28638	0.00048
12	43	44	1.28690	1.28699	1.28344	1.28640	0.00050	1.28635	0.00042	1.28560	0.00102	1.28646	0.00046
13	45	46	1.28645	1.28662	1.28840	1.28640	0.00046	1.28637	0.00038	1.28581	0.00097	1.28645	0.00041
14	47	48	1.28640	1.28731	1.28477	1.28640	0.00043	1.28644	0.00036	1.28574	0.00090	1.28652	0.00039
15	49	50	1.28424	1.28371	1.28721	1.28626	0.00043	1.28625	0.00038	1.28584	0.00084	1.28626	0.00041
16	51	52	1.28670	1.28727	1.28903	1.28629	0.00040	1.28632	0.00036	1.28604	0.00081	1.28632	0.00039
17	53	54	1.28463	1.28370	1.28285	1.28619	0.00039	1.28616	0.00037	1.28585	0.00079	1.28619	0.00039
18	55	56	1.28611	1.28465	1.29107	1.28619	0.00036	1.28608	0.00036	1.28614	0.00080	1.28613	0.00037
19	57	58	1.28466	1.28638	1.28608	1.28611	0.00035	1.28610	0.00034	1.28614	0.00075	1.28610	0.00035
20	59	60	1.28265	1.28292	1.28404	1.28593	0.00038	1.28594	0.00036	1.28603	0.00072	1.28594	0.00037
21	61	62	1.28540	1.28525	1.29056	1.28591	0.00036	1.28590	0.00035	1.28625	0.00072	1.28592	0.00036

```
     22     63     64     1.28403  1.28631  1.28107       1.28582 0.00035   1.28592 0.00033   1.28601 0.00073
1.28589 0.00034
     23     65     66     1.28956  1.28849  1.28923       1.28599 0.00038   1.28603 0.00034   1.28615 0.00071
1.28603 0.00035
     24     67     68     1.28368  1.28481  1.28964       1.28589 0.00037   1.28598 0.00032   1.28630 0.00069
1.28600 0.00034
     25     69     70     1.28456  1.28606  1.28578       1.28584 0.00036   1.28599 0.00031   1.28628 0.00066
1.28599 0.00033
     26     71     72     1.28757  1.28422  1.28751       1.28590 0.00035   1.28592 0.00031   1.28632 0.00064
1.28594 0.00031
     27     73     74     1.28504  1.28600  1.28213       1.28587 0.00034   1.28592 0.00030   1.28617 0.00064
1.28593 0.00030
     28     75     76     1.28614  1.28641  1.28537       1.28588 0.00033   1.28594 0.00029   1.28614 0.00061
1.28594 0.00029
     29     77     78     1.28614  1.28499  1.28220       1.28589 0.00032   1.28591 0.00028   1.28600 0.00061
1.28591 0.00028
     30     79     80     1.28776  1.28799  1.28679       1.28595 0.00031   1.28598 0.00028   1.28603 0.00059
1.28597 0.00028
 ------------------------------------------------------------------------------------------------------------------------
-----------
     31     81     82     1.28631  1.28570  1.28352       1.28596 0.00030   1.28597 0.00027   1.28595 0.00057
1.28597 0.00027
     32     83     84     1.28524  1.28508  1.28659       1.28594 0.00029   1.28594 0.00026   1.28597 0.00056
1.28594 0.00026
     33     85     86     1.28624  1.28691  1.28486       1.28595 0.00029   1.28597 0.00025   1.28594 0.00054
1.28596 0.00025
     34     87     88     1.28820  1.28727  1.28932       1.28602 0.00028   1.28601 0.00025   1.28604 0.00053
1.28601 0.00025
     35     89     90     1.28445  1.28646  1.28504       1.28597 0.00028   1.28602 0.00024   1.28601 0.00052
1.28601 0.00024
     36     91     92     1.28548  1.28676  1.28577       1.28596 0.00027   1.28604 0.00024   1.28600 0.00050
1.28602 0.00024
     37     93     94     1.28510  1.28521  1.28591       1.28593 0.00027   1.28602 0.00023   1.28600 0.00049
1.28600 0.00023
     38     95     96     1.28358  1.28414  1.28927       1.28587 0.00027   1.28597 0.00023   1.28608 0.00048
1.28596 0.00023
     39     97     98     1.28534  1.28776  1.28284       1.28586 0.00026   1.28601 0.00023   1.28600 0.00048
1.28598 0.00023
     40     99    100     1.28587  1.28657  1.28280       1.28586 0.00025   1.28603 0.00022   1.28592 0.00047
1.28598 0.00022
 ------------------------------------------------------------------------------------------------------------------------
-----------
     41    101    102     1.28414  1.28358  1.28140       1.28582 0.00025   1.28597 0.00023   1.28581 0.00047
1.28592 0.00022
     42    103    104     1.28813  1.28950  1.28641       1.28587 0.00025   1.28605 0.00024   1.28583 0.00046
1.28598 0.00023
     43    105    106     1.28297  1.28415  1.28279       1.28580 0.00025   1.28601 0.00024   1.28575 0.00046
1.28593 0.00023
     44    107    108     1.28260  1.28273  1.28427       1.28573 0.00026   1.28593 0.00024   1.28572 0.00045
1.28586 0.00024
     45    109    110     1.28812  1.28610  1.28013       1.28578 0.00026   1.28594 0.00024   1.28560 0.00046
1.28586 0.00023
     46    111    112     1.28813  1.28714  1.28605       1.28584 0.00026   1.28596 0.00023   1.28561 0.00045
1.28589 0.00023
     47    113    114     1.28659  1.28674  1.28874       1.28585 0.00025   1.28598 0.00023   1.28567 0.00044
1.28592 0.00022
     48    115    116     1.28573  1.28644  1.29011       1.28585 0.00025   1.28599 0.00022   1.28577 0.00044
1.28593 0.00022
     49    117    118     1.28557  1.28546  1.28585       1.28584 0.00024   1.28598 0.00022   1.28577 0.00043
1.28592 0.00022
     50    119    120     1.28514  1.28479  1.28557       1.28583 0.00024   1.28596 0.00022   1.28576 0.00042
1.28590 0.00021

 average keff results summed over   4 cycles each to form 25 batch values of keff

  batch  start    end     keff estimators by batch              average keff estimators and deviations
col/abs/tl keff
 number  cycle  cycle     k(coll)  k(abs)  k(track)       k(coll)  st dev    k(abs)  st dev   k(track) st dev
k(c/a/t) st dev

      1     21     24     1.28795  1.28707  1.28859
      2     25     28     1.28547  1.28642  1.28627       1.28671 0.00124   1.28674 0.00032   1.28743 0.00116
      3     29     32     1.28630  1.28584  1.28400       1.28658 0.00073   1.28644 0.00035   1.28628 0.00133
      4     33     36     1.28617  1.28539  1.28187       1.28647 0.00052   1.28618 0.00036   1.28518 0.00145
1.28650 0.00004
      5     37     40     1.28671  1.28734  1.28774       1.28652 0.00041   1.28641 0.00036   1.28569 0.00123
1.28669 0.00019
      6     41     44     1.28580  1.28603  1.28512       1.28640 0.00036   1.28635 0.00030   1.28560 0.00101
1.28664 0.00017
```

```
      7     45     48     1.28643  1.28696  1.28659       1.28640 0.00030   1.28644 0.00027   1.28574 0.00087
1.28669 0.00016
      8     49     52     1.28547  1.28549  1.28812       1.28629 0.00029   1.28632 0.00026   1.28604 0.00081
1.28634 0.00028
      9     53     56     1.28537  1.28418  1.28696       1.28619 0.00027   1.28608 0.00033   1.28614 0.00072
1.28617 0.00031
     10     57     60     1.28365  1.28465  1.28506       1.28593 0.00035   1.28594 0.00033   1.28603 0.00065
1.28594 0.00035
 ------------------------------------------------------------------------------------------------------------------------
-----------
     11     61     64     1.28472  1.28578  1.28581       1.28582 0.00034   1.28592 0.00030   1.28601 0.00059
1.28590 0.00032
     12     65     68     1.28662  1.28665  1.28943       1.28589 0.00031   1.28598 0.00028   1.28630 0.00061
1.28596 0.00031
     13     69     72     1.28606  1.28514  1.28664       1.28590 0.00029   1.28592 0.00027   1.28632 0.00056
1.28592 0.00028
     14     73     76     1.28559  1.28621  1.28375       1.28588 0.00027   1.28594 0.00025   1.28614 0.00055
1.28592 0.00026
     15     77     80     1.28695  1.28649  1.28450       1.28595 0.00026   1.28598 0.00023   1.28603 0.00052
1.28597 0.00024
     16     81     84     1.28577  1.28539  1.28505       1.28594 0.00024   1.28594 0.00022   1.28597 0.00049
1.28594 0.00022
     17     85     88     1.28722  1.28709  1.28709       1.28602 0.00024   1.28601 0.00022   1.28604 0.00047
1.28601 0.00022
     18     89     92     1.28497  1.28661  1.28540       1.28596 0.00023   1.28604 0.00021   1.28600 0.00044
1.28601 0.00021
     19     93     96     1.28434  1.28468  1.28759       1.28587 0.00024   1.28597 0.00021   1.28608 0.00043
1.28596 0.00021
     20     97    100     1.28560  1.28716  1.28282       1.28586 0.00023   1.28603 0.00021   1.28592 0.00044
1.28597 0.00020
 ------------------------------------------------------------------------------------------------------------------------
-----------
     21    101    104     1.28613  1.28654  1.28391       1.28587 0.00021   1.28605 0.00020   1.28583 0.00043
1.28597 0.00019
     22    105    108     1.28278  1.28344  1.28353       1.28573 0.00025   1.28593 0.00022   1.28572 0.00042
1.28587 0.00023
     23    109    112     1.28813  1.28662  1.28309       1.28584 0.00026   1.28596 0.00022   1.28561 0.00042
1.28589 0.00021
     24    113    116     1.28616  1.28659  1.28943       1.28585 0.00025   1.28599 0.00021   1.28577 0.00043
1.28594 0.00021
     25    117    120     1.28535  1.28512  1.28571       1.28583 0.00024   1.28596 0.00020   1.28576 0.00041
1.28591 0.00020

 average keff results summed over   5 cycles each to form 20 batch values of keff

  batch  start    end     keff estimators by batch              average keff estimators and deviations
col/abs/tl keff
 number  cycle  cycle     k(coll)  k(abs)  k(track)       k(coll)  st dev    k(abs)  st dev   k(track) st dev
k(c/a/t) st dev

      1     21     25     1.28817  1.28728  1.28989
      2     26     30     1.28514  1.28619  1.28352       1.28666 0.00152   1.28673 0.00054   1.28670 0.00318
      3     31     35     1.28619  1.28499  1.28303       1.28650 0.00089   1.28615 0.00066   1.28548 0.00221
      4     36     40     1.28658  1.28720  1.28635       1.28652 0.00063   1.28641 0.00054   1.28569 0.00158
1.28684 0.00020
      5     41     45     1.28559  1.28640  1.28479       1.28634 0.00052   1.28641 0.00041   1.28551 0.00124
1.28678 0.00016
      6     46     50     1.28589  1.28548  1.28746       1.28626 0.00043   1.28625 0.00037   1.28584 0.00106
1.28637 0.00038
      7     51     55     1.28588  1.28552  1.28733       1.28621 0.00037   1.28615 0.00033   1.28605 0.00092
1.28620 0.00034
      8     56     60     1.28402  1.28445  1.28590       1.28593 0.00042   1.28594 0.00036   1.28603 0.00080
1.28594 0.00042
      9     61     65     1.28566  1.28642  1.28649       1.28590 0.00037   1.28599 0.00032   1.28608 0.00071
1.28597 0.00036
     10     66     70     1.28523  1.28594  1.28802       1.28584 0.00034   1.28599 0.00029   1.28628 0.00066
1.28595 0.00033
 ------------------------------------------------------------------------------------------------------------------------
-----------
     11     71     75     1.28663  1.28584  1.28420       1.28591 0.00032   1.28597 0.00026   1.28609 0.00063
1.28596 0.00028
     12     76     80     1.28643  1.28601  1.28540       1.28595 0.00029   1.28598 0.00024   1.28603 0.00057
1.28597 0.00026
     13     81     85     1.28584  1.28565  1.28556       1.28594 0.00027   1.28595 0.00022   1.28599 0.00053
1.28595 0.00023
     14     86     90     1.28633  1.28691  1.28618       1.28597 0.00025   1.28602 0.00021   1.28601 0.00049
1.28601 0.00022
     15     91     95     1.28497  1.28587  1.28725       1.28590 0.00024   1.28601 0.00020   1.28609 0.00046
1.28599 0.00021
```

```
    16     96    100     1.28518  1.28630  1.28338       1.28586 0.00023   1.28603 0.00019   1.28592 0.00047
1.28599 0.00020
    17    101    105     1.28595  1.28605  1.28447       1.28586 0.00022   1.28603 0.00018   1.28584 0.00045
1.28599 0.00019
    18    106    110     1.28443  1.28437  1.28154       1.28578 0.00022   1.28594 0.00019   1.28560 0.00048
1.28591 0.00020
    19    111    115     1.28694  1.28705  1.28760       1.28585 0.00022   1.28600 0.00019   1.28570 0.00047
1.28597 0.00020
    20    116    120     1.28552  1.28518  1.28692       1.28583 0.00021   1.28596 0.00018   1.28576 0.00045
1.28592 0.00019


 average keff results summed over  10 cycles each to form 10 batch values of keff

  batch  start    end     keff estimators by batch              average keff estimators and deviations
col/abs/tl keff
 number  cycle  cycle     k(coll)  k(abs)  k(track)       k(coll)  st dev    k(abs)  st dev   k(track) st dev
k(c/a/t) st dev

     1     21     30     1.28666  1.28673  1.28670
     2     31     40     1.28639  1.28609  1.28469       1.28652 0.00013   1.28641 0.00032   1.28569 0.00101
     3     41     50     1.28574  1.28594  1.28612       1.28626 0.00027   1.28625 0.00024   1.28584 0.00060
     4     51     60     1.28495  1.28499  1.28662       1.28593 0.00038   1.28594 0.00036   1.28603 0.00047
1.28599 0.00034
     5     61     70     1.28545  1.28618  1.28726       1.28584 0.00031   1.28599 0.00028   1.28628 0.00044
1.28595 0.00026
     6     71     80     1.28653  1.28592  1.28480       1.28595 0.00028   1.28598 0.00023   1.28603 0.00043
1.28598 0.00018
     7     81     90     1.28609  1.28628  1.28587       1.28597 0.00024   1.28602 0.00020   1.28601 0.00037
1.28596 0.00015
     8     91    100     1.28507  1.28609  1.28532       1.28586 0.00023   1.28603 0.00017   1.28592 0.00033
1.28594 0.00018
     9    101    110     1.28519  1.28521  1.28300       1.28578 0.00022   1.28594 0.00018   1.28560 0.00044
1.28589 0.00023
    10    111    120     1.28623  1.28611  1.28726       1.28583 0.00020   1.28596 0.00016   1.28576 0.00042
1.28593 0.00019


 average keff results summed over  20 cycles each to form  5 batch values of keff

  batch  start    end     keff estimators by batch              average keff estimators and deviations
col/abs/tl keff
 number  cycle  cycle     k(coll)  k(abs)  k(track)       k(coll)  st dev    k(abs)  st dev   k(track) st dev
k(c/a/t) st dev

     1     21     40     1.28652  1.28641  1.28569
     2     41     60     1.28535  1.28546  1.28637       1.28593 0.00059   1.28594 0.00048   1.28603 0.00034
     3     61     80     1.28599  1.28605  1.28603       1.28595 0.00034   1.28598 0.00028   1.28603 0.00020
     4     81    100     1.28558  1.28619  1.28559       1.28586 0.00026   1.28603 0.00020   1.28592 0.00018
1.28601 0.00003
     5    101    120     1.28571  1.28566  1.28513       1.28583 0.00020   1.28596 0.00017   1.28576 0.00021
1.28586 0.00019


 average keff results summed over  25 cycles each to form  4 batch values of keff

  batch  start    end     keff estimators by batch              average keff estimators and deviations
col/abs/tl keff
 number  cycle  cycle     k(coll)  k(abs)  k(track)       k(coll)  st dev    k(abs)  st dev   k(track) st dev
k(c/a/t) st dev

     1     21     45     1.28634  1.28641  1.28551
     2     46     70     1.28534  1.28556  1.28704       1.28584 0.00050   1.28599 0.00042   1.28628 0.00076
     3     71     95     1.28604  1.28606  1.28572       1.28590 0.00030   1.28601 0.00025   1.28609 0.00048
     4     96    120     1.28560  1.28579  1.28478       1.28583 0.00022   1.28596 0.00018   1.28576 0.00047
1.28622 0.00035


 average keff results summed over  50 cycles each to form  2 batch values of keff

  batch  start    end     keff estimators by batch              average keff estimators and deviations
 number  cycle  cycle     k(coll)  k(abs)  k(track)       k(coll)  st dev    k(abs)  st dev   k(track) st dev

     1     21     70     1.28584  1.28599  1.28628
     2     71    120     1.28582  1.28592  1.28525       1.28583 0.00001   1.28596 0.00003   1.28576 0.00051
```

1average individual and combined collision/absorption/track-length keff results for 7 different batch sizes

cycles per keff batch	number of k batches	average keff estimators and deviations k(col) st dev	k(abs) st dev	k(trk) st dev	co/ab/trk	normality k(c/a/t) st dev	average k(c/a/t) 95% confidence	k(c/a/t) confidence intervals 99% confidence
1	100	1.2858 0.0002	1.2860 0.0002	1.2858 0.0004	95/99/95	1.28591 0.00020	1.28550-1.28631	1.28537-1.28644
2	50	1.2858 0.0002	1.2860 0.0002	1.2858 0.0004	95/95/95	1.28590 0.00021	1.28548-1.28633	1.28534-1.28647
4	25	1.2858 0.0002	1.2860 0.0002	1.2858 0.0004	95/95/95	1.28591 0.00020	1.28549-1.28633	1.28534-1.28648
5	20	1.2858 0.0002	1.2860 0.0002	1.2858 0.0004	95/95/95	1.28592 0.00019	1.28552-1.28632	1.28537-1.28647
10	10	1.2858 0.0002	1.2860 0.0002	1.2858 0.0004	95/95/95	1.28593 0.00019	1.28548-1.28638	1.28526-1.28660
20	5	1.2858 0.0002	1.2860 0.0002	1.2858 0.0002	95/95/95	1.28586 0.00019	1.28504-1.28668	1.28396-1.28776
25	4	1.2858 0.0002	1.2860 0.0002	1.2858 0.0005	95/95/95	1.28622 0.00035	1.28181-1.29062	1.26415-1.30828

1individual and average keff estimator results by cycle

keff cycle	neutron histories	keff estimators by cycle k(coll)	k(abs)	k(track)	average keff estimators and deviations k(coll) st dev	k(abs) st dev	k(track) st dev	average k(c/a/t) st dev	fom
1	100000	1.56036	1.56556	1.55451					
2	156074	1.44108	1.44083	1.44279					
3	92437	1.35735	1.35902	1.36433					
4	94340	1.32230	1.32183	1.32144					
5	97598	1.30202	1.30231	1.30672					
6	98472	1.29487	1.29446	1.29114					
7	99432	1.29239	1.29328	1.29164					
8	99640	1.28824	1.28775	1.28483					
9	99709	1.28834	1.29013	1.28332					
10	99731	1.28781	1.28824	1.28625					
11	99833	1.28149	1.28281	1.27678					
12	99492	1.28608	1.28759	1.28961					
13	100153	1.28834	1.28722	1.29102					
14	99828	1.28664	1.28485	1.29391					
15	99925	1.28179	1.28677	1.27852					
16	99765	1.28760	1.28856	1.28826					
17	100405	1.28512	1.28617	1.28729					
18	99767	1.27937	1.28244	1.27650					
19	99456	1.28983	1.28892	1.29967					
20	100893	1.28847	1.28989	1.28990					
		begin active keff cycles							
21	99944	1.28791	1.28623	1.28885					
22	100299	1.28602	1.28680	1.29250	1.28696	0.00095	1.28651 0.00029	1.29068 0.00183	
23	99922	1.28774	1.28521	1.28754	1.28722	0.00060	1.28608 0.00046	1.28963 0.00148	
24	100077	1.29013	1.29004	1.28545	1.28795	0.00084	1.28707 0.00104	1.28859 0.00148	1.28838 0.00020 5456510
25	100287	1.28906	1.28811	1.29507	1.28817	0.00069	1.28728 0.00083	1.28989 0.00173	1.28855 0.00108 145896
26	99692	1.28174	1.28515	1.28270	1.28710	0.00121	1.28692 0.00077	1.28869 0.00185	1.28709 0.00104 129502
27	99335	1.28244	1.28663	1.28394	1.28643	0.00122	1.28688 0.00065	1.28801 0.00171	1.28709 0.00085 167605
28	100220	1.28865	1.28579	1.28336	1.28671	0.00109	1.28674 0.00058	1.28743 0.00159	1.28677 0.00070 217621
29	100604	1.28633	1.28752	1.28483	1.28667	0.00097	1.28683 0.00052	1.28714 0.00143	1.28685 0.00060 260134
30	99813	1.28655	1.28586	1.28277	1.28666	0.00086	1.28673 0.00047	1.28670 0.00135	1.28673 0.00054 292160
31	99921	1.28820	1.28585	1.28440	1.28680	0.00079	1.28665 0.00044	1.28649 0.00124	1.28666 0.00049 322535
32	100380	1.28414	1.28413	1.28399	1.28658	0.00076	1.28644 0.00045	1.28628 0.00115	1.28645 0.00050 282599
33	99480	1.28528	1.28605	1.28280	1.28648	0.00070	1.28641 0.00042	1.28602 0.00109	1.28642 0.00046 309204
34	99931	1.28833	1.28396	1.28403	1.28661	0.00066	1.28624 0.00042	1.28587 0.00102	1.28631 0.00045 291474

```
    35      100169 | 1.28500  1.28494  1.27991  |  1.28650 0.00063   1.28615 0.00040   1.28548 0.00103  |  1.28625
0.00044    295125
    36      100049 | 1.28606  1.28661  1.28076  |  1.28647 0.00059   1.28618 0.00038   1.28518 0.00101  |  1.28627
0.00041    305391
    37      100100 | 1.28350  1.28336  1.27751  |  1.28630 0.00058   1.28601 0.00039   1.28473 0.00105  |  1.28619
0.00043    264119
    38       99770 | 1.28348  1.28623  1.28854  |  1.28614 0.00057   1.28603 0.00037   1.28494 0.00101  |  1.28613
0.00039    299768
    39      100118 | 1.28726  1.28697  1.29077  |  1.28620 0.00054   1.28608 0.00035   1.28525 0.00100  |  1.28617
0.00037    329371
    40      100227 | 1.29261  1.29280  1.29416  |  1.28652 0.00061   1.28641 0.00047   1.28569 0.00105  |  1.28654
0.00049    176380
 ------------------------------------------------------------------------------------------------------------------------
-----------
    41      100510 | 1.28444  1.28516  1.29122  |  1.28642 0.00058   1.28635 0.00046   1.28596 0.00103  |  1.28640
0.00047    181780
    42       99328 | 1.28495  1.28498  1.28236  |  1.28636 0.00056   1.28629 0.00044   1.28579 0.00100  |  1.28635
0.00045    187595
    43      100201 | 1.28915  1.28693  1.28829  |  1.28648 0.00055   1.28632 0.00042   1.28590 0.00096  |  1.28639
0.00043    195493
    44      100477 | 1.28465  1.28705  1.27860  |  1.28640 0.00053   1.28635 0.00040   1.28560 0.00097  |  1.28642
0.00042    199324
    45       99736 | 1.28476  1.28786  1.28345  |  1.28634 0.00051   1.28641 0.00039   1.28551 0.00093  |  1.28646
0.00041    203574
    46      100020 | 1.28815  1.28539  1.29335  |  1.28640 0.00050   1.28637 0.00038   1.28581 0.00095  |  1.28641
0.00039    216756
    47      100255 | 1.28928  1.28912  1.28620  |  1.28651 0.00049   1.28647 0.00038   1.28583 0.00091  |  1.28651
0.00039    205569
    48      100007 | 1.28353  1.28550  1.28334  |  1.28640 0.00049   1.28644 0.00037   1.28574 0.00088  |  1.28646
0.00038    210029
    49       99464 | 1.28796  1.28731  1.29154  |  1.28646 0.00047   1.28647 0.00035   1.28594 0.00087  |  1.28649
0.00036    219894
    50      100385 | 1.28053  1.28010  1.28289  |  1.28626 0.00050   1.28625 0.00040   1.28584 0.00085  |  1.28626
0.00041    163607
 ------------------------------------------------------------------------------------------------------------------------
-----------
    51       99251 | 1.28769  1.28865  1.28592  |  1.28631 0.00048   1.28633 0.00040   1.28584 0.00082  |  1.28633
0.00041    163455
    52      100548 | 1.28571  1.28589  1.29215  |  1.28629 0.00047   1.28632 0.00038   1.28604 0.00082  |  1.28631
0.00039    170884
    53       99964 | 1.28588  1.28359  1.28199  |  1.28628 0.00045   1.28624 0.00038   1.28591 0.00081  |  1.28625
0.00039    170412
    54      100229 | 1.28339  1.28382  1.28372  |  1.28619 0.00045   1.28616 0.00038   1.28585 0.00078  |  1.28617
0.00038    168975
    55       99639 | 1.28675  1.28564  1.29287  |  1.28621 0.00044   1.28615 0.00037   1.28605 0.00079  |  1.28616
0.00037    175244
    56      100139 | 1.28547  1.28365  1.28927  |  1.28619 0.00042   1.28608 0.00036   1.28614 0.00077  |  1.28611
0.00036    175866
    57       99826 | 1.28743  1.28955  1.28563  |  1.28622 0.00041   1.28617 0.00037   1.28613 0.00075  |  1.28619
0.00036    173266
    58      100146 | 1.28189  1.28320  1.28654  |  1.28611 0.00042   1.28610 0.00036   1.28614 0.00073  |  1.28610
0.00036    168227
    59       99474 | 1.28397  1.28701  1.28506  |  1.28605 0.00041   1.28612 0.00036   1.28611 0.00071  |  1.28610
0.00035    172828
    60       99869 | 1.28133  1.27883  1.28303  |  1.28593 0.00042   1.28594 0.00039   1.28603 0.00070  |  1.28594
0.00038    145418
 ------------------------------------------------------------------------------------------------------------------------
-----------
    61       99701 | 1.28586  1.28546  1.29192  |  1.28593 0.00041   1.28593 0.00038   1.28618 0.00069  |  1.28595
0.00037    148882
    62      100399 | 1.28495  1.28503  1.28919  |  1.28591 0.00040   1.28590 0.00037   1.28625 0.00068  |  1.28593
0.00036    151953
    63       99975 | 1.28548  1.28813  1.27732  |  1.28590 0.00039   1.28596 0.00037   1.28604 0.00070  |  1.28594
0.00035    156537
    64      100267 | 1.28258  1.28449  1.28482  |  1.28582 0.00039   1.28592 0.00036   1.28601 0.00068  |  1.28590
0.00035    157021
    65       99776 | 1.28945  1.28901  1.28919  |  1.28590 0.00039   1.28599 0.00036   1.28608 0.00067  |  1.28597
0.00035    153709
    66      100462 | 1.28967  1.28798  1.28926  |  1.28599 0.00039   1.28603 0.00035   1.28615 0.00066  |  1.28603
0.00035    153280
    67      100002 | 1.28149  1.28336  1.28380  |  1.28589 0.00039   1.28598 0.00035   1.28610 0.00065  |  1.28597
0.00034    150465
    68       99405 | 1.28588  1.28625  1.29549  |  1.28589 0.00038   1.28598 0.00034   1.28630 0.00066  |  1.28599
0.00034    152212
    69      100361 | 1.28319  1.28643  1.28704  |  1.28583 0.00038   1.28599 0.00034   1.28631 0.00065  |  1.28598
0.00033    154418
    70       99866 | 1.28592  1.28570  1.28453  |  1.28584 0.00037   1.28599 0.00033   1.28628 0.00064  |  1.28598
0.00033    158058
```

```
 ------------------------------------------------------------------------------------------------------------------------
-----------
    71      100140 | 1.28728  1.28293  1.28977  |  1.28586 0.00036   1.28593 0.00033   1.28635 0.00063  |  1.28595
0.00032    160493
    72      100064 | 1.28785  1.28551  1.28524  |  1.28590 0.00036   1.28592 0.00032   1.28632 0.00062  |  1.28595
0.00031    164441
    73      100124 | 1.28504  1.28641  1.28564  |  1.28589 0.00035   1.28593 0.00032   1.28631 0.00060  |  1.28595
0.00031    167705
    74       99692 | 1.28503  1.28560  1.27862  |  1.28587 0.00035   1.28592 0.00031   1.28617 0.00061  |  1.28593
0.00030    171175
    75       99876 | 1.28794  1.28874  1.28173  |  1.28591 0.00034   1.28597 0.00031   1.28609 0.00060  |  1.28597
0.00030    172390
    76      100170 | 1.28434  1.28408  1.28900  |  1.28588 0.00034   1.28594 0.00031   1.28614 0.00060  |  1.28594
0.00029    174153
    77       99633 | 1.28771  1.28632  1.28369  |  1.28591 0.00033   1.28595 0.00030   1.28610 0.00059  |  1.28595
0.00029    177768
    78      100184 | 1.28456  1.28366  1.28071  |  1.28589 0.00033   1.28591 0.00030   1.28600 0.00058  |  1.28591
0.00029    177501
    79       99819 | 1.28725  1.28690  1.28803  |  1.28591 0.00032   1.28592 0.00029   1.28604 0.00058  |  1.28593
0.00028    179771
    80      100186 | 1.28828  1.28908  1.28556  |  1.28595 0.00032   1.28598 0.00029   1.28603 0.00057  |  1.28597
0.00028    178577
 ------------------------------------------------------------------------------------------------------------------------
-----------
    81       99936 | 1.28710  1.28574  1.28286  |  1.28597 0.00032   1.28597 0.00029   1.28598 0.00056  |  1.28597
0.00028    181774
    82       99957 | 1.28552  1.28567  1.28418  |  1.28596 0.00031   1.28597 0.00028   1.28595 0.00055  |  1.28596
0.00027    184742
    83       99852 | 1.28552  1.28588  1.28992  |  1.28596 0.00031   1.28597 0.00028   1.28601 0.00055  |  1.28597
0.00027    187813
    84      100006 | 1.28496  1.28427  1.28325  |  1.28594 0.00030   1.28594 0.00028   1.28597 0.00054  |  1.28594
0.00026    189168
    85       99792 | 1.28612  1.28671  1.28757  |  1.28594 0.00030   1.28595 0.00027   1.28599 0.00053  |  1.28595
0.00026    191922
    86      100004 | 1.28635  1.28711  1.28216  |  1.28595 0.00029   1.28597 0.00027   1.28594 0.00053  |  1.28596
0.00026    194854
    87      100222 | 1.28965  1.28743  1.28976  |  1.28600 0.00029   1.28599 0.00027   1.28599 0.00052  |  1.28599
0.00025    194285
    88      100185 | 1.28675  1.28711  1.28889  |  1.28602 0.00029   1.28601 0.00026   1.28604 0.00052  |  1.28601
0.00025    196340
    89       99955 | 1.28505  1.28583  1.28452  |  1.28600 0.00029   1.28600 0.00026   1.28601 0.00051  |  1.28600
0.00025    199178
    90       99994 | 1.28385  1.28710  1.28556  |  1.28597 0.00028   1.28602 0.00025   1.28601 0.00050  |  1.28601
0.00024    202048
 ------------------------------------------------------------------------------------------------------------------------
-----------
    91       99858 | 1.28613  1.28640  1.28942  |  1.28597 0.00028   1.28603 0.00025   1.28606 0.00050  |  1.28601
0.00024    204735
    92      100223 | 1.28483  1.28713  1.28212  |  1.28596 0.00028   1.28604 0.00025   1.28600 0.00049  |  1.28601
0.00024    207522
    93       99773 | 1.28352  1.28363  1.28449  |  1.28592 0.00027   1.28601 0.00025   1.28598 0.00049  |  1.28598
0.00024    206476
    94       99847 | 1.28669  1.28679  1.28733  |  1.28593 0.00027   1.28602 0.00024   1.28600 0.00048  |  1.28599
0.00023    208919
    95      100308 | 1.28368  1.28542  1.29291  |  1.28590 0.00027   1.28601 0.00024   1.28609 0.00048  |  1.28599
0.00023    211154
    96       99338 | 1.28348  1.28287  1.28564  |  1.28587 0.00027   1.28597 0.00024   1.28608 0.00048  |  1.28596
0.00023    208801
    97      100016 | 1.28654  1.28897  1.28371  |  1.28588 0.00026   1.28601 0.00024   1.28605 0.00047  |  1.28598
0.00023    209093
    98      100290 | 1.28414  1.28654  1.28196  |  1.28586 0.00026   1.28601 0.00024   1.28600 0.00047  |  1.28597
0.00023    211239
    99       99789 | 1.28827  1.28892  1.28388  |  1.28589 0.00026   1.28605 0.00024   1.28597 0.00046  |  1.28600
0.00022    210585
   100      100147 | 1.28346  1.28421  1.28172  |  1.28586 0.00026   1.28603 0.00024   1.28592 0.00046  |  1.28597
0.00022    209645
 ------------------------------------------------------------------------------------------------------------------------
-----------
   101       99592 | 1.28476  1.28483  1.28103  |  1.28585 0.00025   1.28601 0.00023   1.28586 0.00046  |  1.28595
0.00022    210701
   102      100094 | 1.28351  1.28233  1.28178  |  1.28582 0.00025   1.28597 0.00024   1.28581 0.00045  |  1.28591
0.00022    206313
   103      100058 | 1.28662  1.28958  1.28535  |  1.28583 0.00025   1.28601 0.00024   1.28581 0.00045  |  1.28593
0.00022    204709
   104      100332 | 1.28963  1.28943  1.28747  |  1.28587 0.00025   1.28605 0.00024   1.28583 0.00044  |  1.28597
0.00022    200484
   105      100113 | 1.28521  1.28411  1.28671  |  1.28586 0.00025   1.28603 0.00024   1.28584 0.00044  |  1.28596
0.00022    202392
```

```
   106       99580 | 1.28072  1.28420  1.27888  |  1.28580 0.00025   1.28601 0.00023   1.28575 0.00044  |  1.28593
0.00022    197440
   107       99674 | 1.28480  1.28283  1.29113  |  1.28579 0.00025   1.28597 0.00023   1.28582 0.00044  |  1.28590
0.00022    198933
   108      100532 | 1.28041  1.28262  1.27741  |  1.28573 0.00025   1.28593 0.00023   1.28572 0.00045  |  1.28586
0.00022    190149
   109       99646 | 1.29133  1.28714  1.28337  |  1.28579 0.00026   1.28595 0.00023   1.28569 0.00044  |  1.28589
0.00022    191600
   110      100620 | 1.28491  1.28506  1.27688  |  1.28578 0.00026   1.28594 0.00023   1.28560 0.00045  |  1.28587
0.00022    191904
 ------------------------------------------------------------------------------------------------------------------------
-----------
   111       99405 | 1.28882  1.28836  1.28555  |  1.28582 0.00026   1.28596 0.00023   1.28560 0.00044  |  1.28589
0.00022    191414
   112      100328 | 1.28744  1.28592  1.28654  |  1.28584 0.00025   1.28596 0.00023   1.28561 0.00044  |  1.28590
0.00022    193753
   113      100258 | 1.28674  1.28743  1.29140  |  1.28585 0.00025   1.28598 0.00022   1.28567 0.00044  |  1.28592
0.00022    194489
   114      100010 | 1.28643  1.28605  1.28608  |  1.28585 0.00025   1.28598 0.00022   1.28567 0.00043  |  1.28592
0.00021    196696
   115       99862 | 1.28527  1.28749  1.28844  |  1.28585 0.00025   1.28600 0.00022   1.28570 0.00043  |  1.28593
0.00021    197933
   116       99959 | 1.28619  1.28539  1.29179  |  1.28585 0.00024   1.28599 0.00022   1.28577 0.00043  |  1.28593
0.00021    200450
   117       99971 | 1.28730  1.28744  1.28679  |  1.28586 0.00024   1.28600 0.00022   1.28578 0.00043  |  1.28595
0.00021    201570
   118      100219 | 1.28383  1.28349  1.28490  |  1.28584 0.00024   1.28598 0.00022   1.28577 0.00042  |  1.28593
0.00021    201234
   119       99676 | 1.28449  1.28517  1.27849  |  1.28583 0.00024   1.28597 0.00021   1.28569 0.00042  |  1.28591
0.00020    201798
   120       99938 | 1.28579  1.28440  1.29264  |  1.28583 0.00024   1.28596 0.00021   1.28576 0.00042  |  1.28591
0.00020    204325

  the largest active cycle keffs by estimator are:                                the smallest active cycle keffs by
estimator are:

                   collision 1.29261 on cycle  40                                                collision 1.28041 on
cycle 108
                  absorption 1.29280 on cycle  40                                               absorption 1.27883 on
cycle  60
                track length 1.29549 on cycle  68                                             track length 1.27688 on
cycle 110

1plot of estimated col/abs/track-length keff one-standard-deviation interval versus cycle number        print table 179
 | = final keff =  1.28591

    cycle   active 1.285                 1.286                   1.287                   1.288
1.289
   number   cycles  |---------------------|-----------------------|-----------------------|-----------------------|
       26        6  |                     |   (-----------------------k-----------------------)                    |
       27        7  |                     |        (--------------------k--------------------)                     |
       28        8  |                     |   (-----------------k----------------)                                 |
       29        9  |                     |        (--------------k--------------)                                 |
       30       10  |                     |      (-------------k------------)                                      |
       31       11  |                     |      (-----------k-----------)                                         |
       32       12  |                     |(------------k-----------)                                              |
       33       13  |                     | (----------k----------)                                                |
       34       14  |                   (|---------k-----------)                                                 |
       35       15  +                  (-|--------k----------)                                                  +
       36       16  |                   (|--------k----------)                                                   |
       37       17  |                 (--|------k----------)                                                    |
       38       18  |                (---|-----k---------)                                                      |
       39       19  |                  (-|------k--------)                                                      |
       40       20  |                     |   (-----------k-----------)                                         |
       41       21  |                     |(-----------k----------)                                             |
       42       22  |                     |----------k-----------)                                              |
       43       23  |                     |(----------k----------)                                              |
       44       24  |                     |  (---------k---------)                                              |
       45       25  +                     |   (---------k---------)                                             +
       46       26  |                     |  (---------k--------)                                               |
       47       27  |                     |    (---------k---------)                                            |
       48       28  |                     |    (--------k--------)                                              |
       49       29  |                     |     (--------k--------)                                             |
       50       30  |                   (|--------k---------)                                                   |
       51       31  |                    |(---------k---------)                                                |
       52       32  |                    |---------k---------)                                                 |
       53       33  |                  (|--------k--------)                                                    |
       54       34  |                 (--|------k--------)                                                     |
       55       35  +                 (--|------k--------)                                                     +
```

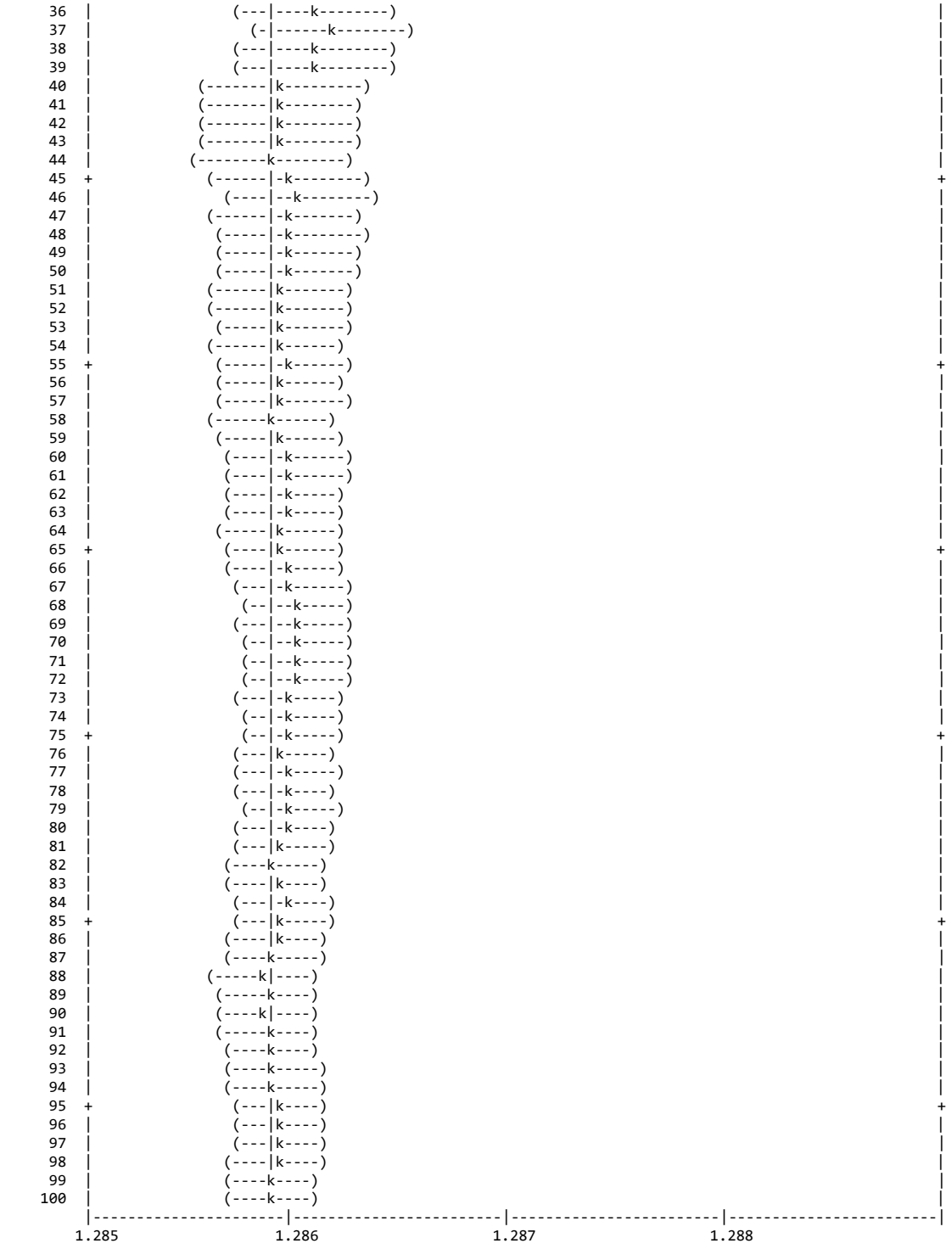

1individual and collision/absorption/track-length keffs for different numbers of inactive cycles skipped for fission source settling

skip cycles	active cycles	active neutrons	k(col) st dev	k(abs) st dev	k(trk) st dev	co/ab/tl	k(c/a/t) st dev	average k(c/a/t) 95% confidence	k(c/a/t) confidence intervals 99% confidence
0	120	12036217	1.2906 0.0027	1.2909 0.0027	1.2906 0.0027	no/no/no	1.28987 0.00271	1.28447-1.29526	1.28271-1.29702
1	119	11936217	1.2883 0.0015	1.2886 0.0015	1.2884 0.0016	no/no/no	1.28846 0.00150	1.28548-1.29145	1.28450-1.29242

```
     2    118     11780143| 1.2870 0.0007  1.2873 0.0007  1.2871 0.0009 |no/no/no| 1.28714 0.00073  1.28568-1.28860
1.28520-1.28908
     3    117     11687706| 1.2864 0.0004  1.2867 0.0004  1.2864 0.0005 |no/no/no| 1.28661 0.00040  1.28581-1.28741
1.28555-1.28767
     4    116     11593366| 1.2861 0.0003  1.2864 0.0003  1.2861 0.0005 |no/no/99| 1.28629 0.00026  1.28577-1.28681
1.28560-1.28698
     5    115     11495768| 1.2860 0.0002  1.2862 0.0002  1.2860 0.0004 |95/no/95| 1.28615 0.00022  1.28571-1.28658
1.28557-1.28673
     6    114     11397296| 1.2859 0.0002  1.2861 0.0002  1.2859 0.0004 |95/95/95| 1.28607 0.00021  1.28566-1.28649
1.28552-1.28662
     7    113     11297864| 1.2859 0.0002  1.2861 0.0002  1.2859 0.0004 |95/95/95| 1.28602 0.00020  1.28562-1.28642
1.28549-1.28655
     8    112     11198224| 1.2858 0.0002  1.2861 0.0002  1.2859 0.0004 |95/95/95| 1.28600 0.00020  1.28560-1.28640
1.28547-1.28653
     9    111     11098515| 1.2858 0.0002  1.2860 0.0002  1.2859 0.0004 |95/95/95| 1.28597 0.00020  1.28557-1.28637
1.28544-1.28650
    10    110     10998784| 1.2858 0.0002  1.2860 0.0002  1.2859 0.0004 |95/95/95| 1.28595 0.00020  1.28555-1.28636
1.28542-1.28649
 ------------------------------------------------------------------------------------------------------------------------
-----------
    11    109     10898951| 1.2858 0.0002  1.2860 0.0002  1.2860 0.0004 |95/95/95| 1.28599 0.00020  1.28559-1.28639
1.28546-1.28652
    12    108     10799459| 1.2858 0.0002  1.2860 0.0002  1.2859 0.0004 |95/95/95| 1.28598 0.00020  1.28557-1.28638
1.28544-1.28651
    13    107     10699306| 1.2858 0.0002  1.2860 0.0002  1.2859 0.0004 |95/95/95| 1.28596 0.00020  1.28555-1.28636
1.28542-1.28650
    14    106     10599478| 1.2858 0.0002  1.2860 0.0002  1.2858 0.0004 |95/95/95| 1.28596 0.00021  1.28555-1.28637
1.28542-1.28650
    15    105     10499553| 1.2858 0.0002  1.2860 0.0002  1.2859 0.0004 |95/95/95| 1.28597 0.00021  1.28555-1.28638
1.28542-1.28651
    16    104     10399788| 1.2858 0.0002  1.2860 0.0002  1.2859 0.0004 |95/95/95| 1.28594 0.00021  1.28553-1.28636
1.28540-1.28649
    17    103     10299383| 1.2858 0.0002  1.2860 0.0002  1.2858 0.0004 |95/95/95| 1.28594 0.00021  1.28553-1.28636
1.28539-1.28650
    18    102     10199616| 1.2859 0.0002  1.2860 0.0002  1.2859 0.0004 |95/95/95| 1.28598 0.00021  1.28557-1.28639
1.28544-1.28653
    19    101     10100160| 1.2859 0.0002  1.2860 0.0002  1.2858 0.0004 |95/95/95| 1.28594 0.00020  1.28553-1.28635
1.28540-1.28648
    20    100*     9999267| 1.2858 0.0002  1.2860 0.0002  1.2858 0.0004 |95/99/95| 1.28591 0.00020  1.28550-1.28631
1.28537-1.28644
 ------------------------------------------------------------------------------------------------------------------------
-----------
    22     98      9799024| 1.2858 0.0002  1.2859 0.0002  1.2857 0.0004 |95/95/95| 1.28588 0.00021  1.28547-1.28629
1.28534-1.28643
    24     96      9599025| 1.2857 0.0002  1.2859 0.0002  1.2856 0.0004 |95/95/95| 1.28584 0.00021  1.28543-1.28626
1.28530-1.28639
    26     94      9399046| 1.2857 0.0002  1.2859 0.0002  1.2856 0.0004 |95/99/95| 1.28582 0.00021  1.28541-1.28623
1.28527-1.28637
    28     92      9199491| 1.2858 0.0002  1.2859 0.0002  1.2856 0.0004 |95/95/95| 1.28582 0.00021  1.28540-1.28624
1.28526-1.28638
    30     90      8999074| 1.2857 0.0002  1.2859 0.0002  1.2857 0.0004 |95/95/95| 1.28581 0.00022  1.28538-1.28624
1.28524-1.28638
    32     88      8798773| 1.2857 0.0002  1.2859 0.0002  1.2857 0.0005 |95/95/95| 1.28582 0.00022  1.28538-1.28626
1.28524-1.28640
    34     86      8599362| 1.2857 0.0003  1.2859 0.0002  1.2857 0.0005 |95/95/95| 1.28583 0.00023  1.28538-1.28629
1.28524-1.28643
    36     84      8399144| 1.2857 0.0003  1.2859 0.0002  1.2859 0.0005 |95/95/95| 1.28585 0.00023  1.28539-1.28631
1.28524-1.28646
    38     82      8199274| 1.2858 0.0003  1.2859 0.0002  1.2859 0.0005 |95/95/95| 1.28590 0.00023  1.28543-1.28636
1.28528-1.28651
    40     80      7998929| 1.2857 0.0003  1.2858 0.0002  1.2858 0.0005 |95/95/95| 1.28579 0.00022  1.28535-1.28623
1.28521-1.28637
 ------------------------------------------------------------------------------------------------------------------------
-----------
    42     78      7799091| 1.2857 0.0003  1.2859 0.0002  1.2858 0.0005 |95/95/95| 1.28580 0.00023  1.28535-1.28625
1.28521-1.28640
    44     76      7598413| 1.2856 0.0003  1.2858 0.0002  1.2858 0.0005 |95/95/95| 1.28578 0.00023  1.28532-1.28624
1.28517-1.28639
    46     74      7398657| 1.2856 0.0003  1.2858 0.0003  1.2857 0.0005 |95/95/95| 1.28575 0.00024  1.28528-1.28622
1.28513-1.28638
    48     72      7198395| 1.2856 0.0003  1.2858 0.0003  1.2858 0.0005 |95/95/95| 1.28572 0.00024  1.28525-1.28620
1.28509-1.28635
    50     70      6998546| 1.2856 0.0003  1.2858 0.0002  1.2857 0.0005 |95/95/95| 1.28576 0.00023  1.28530-1.28622
1.28515-1.28637
    52     68      6798747| 1.2856 0.0003  1.2858 0.0003  1.2856 0.0005 |95/95/95| 1.28572 0.00023  1.28525-1.28618
1.28510-1.28634
    54     66      6598554| 1.2856 0.0003  1.2858 0.0003  1.2857 0.0005 |95/95/95| 1.28578 0.00024  1.28530-1.28625
1.28515-1.28641
```

```
    56     64      6398776| 1.2856 0.0003  1.2859 0.0003  1.2856 0.0005 |95/95/95| 1.28577 0.00025  1.28528-1.28627
1.28512-1.28643
    58     62      6198804| 1.2857 0.0003  1.2859 0.0003  1.2855 0.0005 |95/95/95| 1.28577 0.00025  1.28528-1.28627
1.28512-1.28643
    60     60      5999461| 1.2858 0.0003  1.2860 0.0002  1.2856 0.0005 |95/95/95| 1.28589 0.00023  1.28543-1.28636
1.28527-1.28651
 ------------------------------------------------------------------------------------------------------------------------
-----------
    62     58      5799361| 1.2858 0.0003  1.2860 0.0002  1.2854 0.0005 |95/95/95| 1.28589 0.00024  1.28541-1.28637
1.28525-1.28653
    64     56      5599119| 1.2858 0.0003  1.2860 0.0003  1.2856 0.0005 |95/95/95| 1.28591 0.00025  1.28542-1.28640
1.28525-1.28657
    66     54      5398881| 1.2857 0.0003  1.2859 0.0003  1.2854 0.0006 |95/95/95| 1.28580 0.00024  1.28531-1.28628
1.28515-1.28645
    68     52      5199474| 1.2858 0.0003  1.2859 0.0003  1.2853 0.0005 |95/95/95| 1.28582 0.00025  1.28532-1.28631
1.28516-1.28647
    70     50      4999247| 1.2858 0.0003  1.2859 0.0003  1.2852 0.0006 |95/95/95| 1.28582 0.00026  1.28531-1.28634
1.28513-1.28651
    72     48      4799043| 1.2857 0.0003  1.2860 0.0003  1.2852 0.0006 |95/95/95| 1.28585 0.00027  1.28531-1.28639
1.28513-1.28657
    74     46      4599227| 1.2858 0.0003  1.2860 0.0003  1.2853 0.0006 |95/95/95| 1.28587 0.00028  1.28531-1.28643
1.28512-1.28661
    76     44      4399181| 1.2858 0.0003  1.2860 0.0003  1.2853 0.0006 |95/95/95| 1.28587 0.00029  1.28529-1.28644
1.28510-1.28664
    78     42      4199364| 1.2857 0.0003  1.2860 0.0003  1.2854 0.0006 |95/95/95| 1.28591 0.00029  1.28532-1.28651
1.28512-1.28671
    80     40      3999359| 1.2856 0.0003  1.2859 0.0003  1.2854 0.0006 |95/95/95| 1.28582 0.00030  1.28522-1.28643
1.28501-1.28663
 ------------------------------------------------------------------------------------------------------------------------
-----------
    82     38      3799466| 1.2856 0.0004  1.2859 0.0003  1.2855 0.0007 |95/95/95| 1.28583 0.00032  1.28519-1.28647
1.28497-1.28669
    84     36      3599608| 1.2856 0.0004  1.2860 0.0003  1.2854 0.0007 |95/95/95| 1.28587 0.00033  1.28519-1.28654
1.28496-1.28678
    86     34      3399812| 1.2856 0.0004  1.2859 0.0003  1.2854 0.0007 |95/95/95| 1.28583 0.00035  1.28512-1.28654
1.28487-1.28679
    88     32      3199405| 1.2854 0.0004  1.2858 0.0004  1.2852 0.0008 |95/95/95| 1.28569 0.00036  1.28494-1.28643
1.28468-1.28669
    90     30      2999456| 1.2855 0.0004  1.2858 0.0004  1.2852 0.0008 |95/95/95| 1.28568 0.00038  1.28489-1.28647
1.28461-1.28675
    92     28      2799375| 1.2855 0.0005  1.2857 0.0004  1.2852 0.0008 |95/95/95| 1.28563 0.00041  1.28478-1.28647
1.28449-1.28677
    94     26      2599755| 1.2855 0.0005  1.2858 0.0004  1.2851 0.0009 |95/95/95| 1.28566 0.00043  1.28476-1.28655
1.28444-1.28687
    96     24      2400109| 1.2857 0.0005  1.2859 0.0005  1.2847 0.0009 |95/95/95| 1.28576 0.00047  1.28479-1.28673
1.28444-1.28708
    98     22      2199803| 1.2857 0.0006  1.2857 0.0005  1.2849 0.0010 |95/95/95| 1.28567 0.00049  1.28464-1.28669
1.28426-1.28707
   100     20      1999867| 1.2857 0.0006  1.2857 0.0005  1.2851 0.0011 |95/95/95| 1.28563 0.00051  1.28456-1.28670
1.28416-1.28710
 ------------------------------------------------------------------------------------------------------------------------
-----------
   102     18      1800181| 1.2859 0.0006  1.2859 0.0005  1.2855 0.0012 |95/95/95| 1.28586 0.00052  1.28475-1.28697
1.28433-1.28740
   104     16      1599791| 1.2856 0.0007  1.2854 0.0004  1.2854 0.0013 |95/95/95| 1.28542 0.00047  1.28440-1.28643
1.28400-1.28683
   106     14      1400098| 1.2860 0.0007  1.2856 0.0005  1.2858 0.0014 |95/95/95| 1.28561 0.00054  1.28443-1.28679
1.28394-1.28727
   108     12      1199892| 1.2865 0.0006  1.2861 0.0004  1.2861 0.0014 |95/95/95| 1.28614 0.00048  1.28505-1.28723
1.28458-1.28771
   110     10       999626| 1.2862 0.0005  1.2861 0.0005  1.2873 0.0013 |95/95/95| 1.28624 0.00052  1.28501-1.28746
1.28443-1.28804
   112      8       799893| 1.2858 0.0004  1.2859 0.0005  1.2876 0.0016 |95/95/95| 1.28561 0.00053  1.28426-1.28697
1.28349-1.28774
   114      6       599625| 1.2855 0.0005  1.2856 0.0007  1.2872 0.0021 |95/95/95| 1.28536 0.00069  1.28316-1.28755
1.28133-1.28938
   116      4       399804| 1.2854 0.0008  1.2851 0.0008  1.2857 0.0029 |95/95/95| 1.28642 0.00152  1.26704-1.30580
1.18934-1.38349
   117      3       299833| 1.2847 0.0006  1.2844 0.0005  1.2853 0.0041 |
   118      2       199614| 1.2851 0.0007  1.2848 0.0004  1.2856 0.0071 |
 the minimum estimated standard deviation for the col/abs/tl keff estimator occurs with   7 inactive cycles and  113
active cycles.
 the first active half of the problem skips 20 cycles and uses  50 active cycles; the second half skips  70 and uses  50
cycles.
 the col/abs/trk-len keff, one standard deviation, and 68, 95, and 99 percent intervals for each active half of the
problem are:
```

```
             problem        keff     standard deviation       68% confidence         95% confidence         99%
confidence

            first half     1.28598         0.00033           1.28565 to 1.28630     1.28532 to 1.28663     1.28510 to
1.28685
           second half     1.28582         0.00026           1.28556 to 1.28608     1.28531 to 1.28634     1.28513 to
1.28651
          final result     1.28591         0.00020           1.28570 to 1.28611     1.28550 to 1.28631     1.28537 to
1.28644

 the first and second half values of k(collision/absorption/track length) appear to be the same at the 68 percent
confidence level.

1plot of estimated col/abs/track-length keff one-standard-deviation interval by active cycle number     print table 179
 | = final keff =  1.28591

 inactive   active 1.284               1.286                1.288                1.290                1.292
   cycles   cycles  |-------------------|--------------------|--------------------|--------------------|
        0      120  |                   |            (-----------------------------k----------------------|
        1      119  |                   |          (----------------k-----------------)                    |
        2      118  |                   |    (-------k--------)                                           |
        3      117  |                   |  (---k----)                                                     |
        4      116  |                   |(--k--)                                                          |
        5      115  |                   |-k--)                                                            |
        6      114  |                  (|-k-)                                                            |
        7      113  |                  (|k-)                                                             |
        8      112  |                 (-|k-)                                                            |
        9      111  +                 (-k--)                                                           +
       10      110  |                 (-k-)                                                            |
       11      109  |                 (-|k-)                                                           |
       12      108  |                 (-k--)                                                           |
       13      107  |                 (-k--)                                                           |
       14      106  |                 (-k--)                                                           |
       15      105  |                 (-k--)                                                           |
       16      104  |                 (-k-)                                                            |
       17      103  |                 (-k-)                                                            |
       18      102  |                 (-|k-)                                                           |
       19      101  +                 (-k-)                                                            +
       20      100  *                (--k-)                                                            *
       21       99  |                (--k-)                                                            |
       22       98  |                (-k|-)                                                           |
       23       97  |                (-k|-)                                                           |
       24       96  |                (-k|)                                                            |
       25       95  |               (--k|)                                                            |
       26       94  |               (--k|)                                                            |
       27       93  |               (--k|)                                                            |
       28       92  |               (--k|)                                                            |
       29       91  +               (--k|)                                                           +
       30       90  |               (--k|)                                                            |
       31       89  |               (--k|)                                                            |
       32       88  |               (--k|)                                                            |
       33       87  |               (--k|)                                                            |
       34       86  |               (--k|)                                                            |
       35       85  |                (-k|-)                                                           |
       36       84  |                (-k|-)                                                           |
       37       83  |                (--k-)                                                           |
       38       82  |                (--k-)                                                           |
       39       81  +                (-k|-)                                                           +
       40       80  |               (-k-|)                                                            |
       41       79  |               (-k-|)                                                            |
       42       78  |               (--k|)                                                            |
       43       77  |               (-k-|)                                                            |
       44       76  |               (-k-|)                                                            |
       45       75  |               (-k-|)                                                            |
       46       74  |              (--k-|)                                                            |
       47       73  |              (-k--|                                                             |
       48       72  |              (--k-|                                                             |
       49       71  +              (-k--|                                                            +
       50       70  |               (-k-|)                                                            |
       51       69  |              (--k-|                                                             |
       52       68  |              (--k-|                                                             |
       53       67  |              (--k-|)                                                            |
       54       66  |               (-k-|)                                                            |
       55       65  |              (--k-|)                                                            |
       56       64  |              (--k-|)                                                            |
       57       63  |              (--k-|)                                                            |
       58       62  |              (--k-|)                                                            |
       59       61  +              (--k-|)                                                           +
       60       60  |                (--k-)                                                           |
```

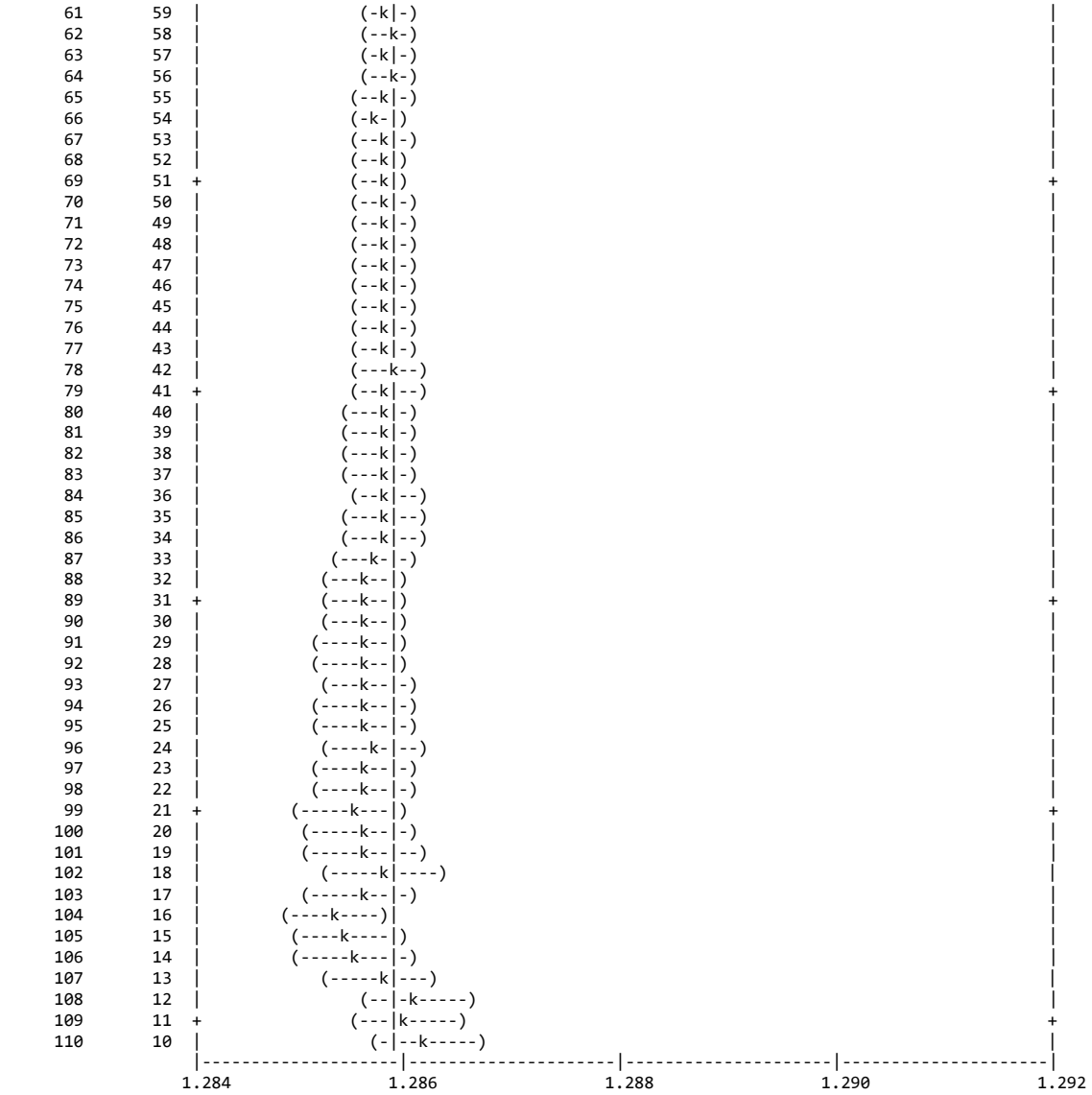

****

dump no. 3 on file runtpa nps = 12036217 coll = 1535340077 ctm = 387.69 nrn = 20710380932

13 warning messages so far.

run terminated when 120 KCODE cycles were done.

computer time = 387.77 minutes

mcnp version 6 05/08/13 11/22/17 20:59:01 probid = 11/22/17 20:34:42

APPENDIX B: SAMPLE WIMS-AECL CODE INPUT AND OUTPUT

This appendix presents the output file from one of the WIMS-AECL models in this research. In particular, the model is that of the OCSL core that was selected in Chapter 6 and the results of the simulation were presented in Table 11 in Section 7.9.

```
WIMS-AECL Release 3.1.2.1, 2006-03-30,  colin 2018-01-10 13:04:32

 Library   1 -- E70ACR: ACR-specific patch to E70LIB1 library, ENDF/B-VII.0, 2009-04-22
 Library   2 -- E70LIB1: 89-group library (Rev.1) based on ENDF/B-VII.0, 2008-10-30


 WIMS DATA LIBRARY PARAMETERS
 ----------------------------
          363 NUCLIDES                   89 ENERGY GROUPS
           47 FISSION GROUPS             22 FAST GROUPS
           25 RESONANCE GROUPS           42 THERMAL GROUPS
           50 FISSILE ISOTOPES          213 FISSION PRODUCT ISOTOPES
           24 RESONANCE NUCLIDES        363 P1 NUCLIDES


 2018-01-10 13:04:32   Starting  0 Prelude       WIMS-AECL Release 3.1.2.1, 2006-03-30,         CPU Time
0.016 Secs

 INPUT DATA SCAN - New Case
 ------------------------------------------
          Number of cells                 1
          Number of annuli               27
          Number of polygons              0
          Maximum number of sectors       0
          Number of rod arrays           16
          Maximum number of rod annuli    4
          Maximum number of rod sectors   2
          Number of materials used       95
          Number of materials defined    97
          Transport solution groups      89


 2018-01-10 13:04:32   Starting  1 Main Data     WIMS-AECL Release 3.1.2.1, 2006-03-30,         CPU Time
0.031 Secs
> * Test case C6
> * Cluster
> * E65LIB Rev6
> * Full PIJ
> * Burnup
>
> PRELUDE
> Title "OCSL CORE 21"
>
> plot
>
> SEQUENCE Pij
>
> CELL cluster
>
> lines  0.       27.00    300  7
>
> symmetry -12 0d 30d
>
> ANNULUS #   1.00  Cool
> ANNULUS #   2.00  Cool
> ANNULUS #   3.00  Cool
> ANNULUS #   4.00  Cool
> ANNULUS #   5.00  Cool
> ANNULUS #   6.00  Cool
```

```
> ANNULUS #   7.00  Cool
> ANNULUS #   8.00  Cool
> ANNULUS #   9.00  Cool
> ANNULUS #   10.00  Cool
> ANNULUS #   11.00  Cool
> ANNULUS #   12.00  Cool
> ANNULUS #   13.00  Cool
> ANNULUS #   14.00  Cool
> ANNULUS #   15.00  Cool
> ANNULUS #   16.00  Cool
> ANNULUS #   17.00  Cool
> ANNULUS #   18.00  Cool
> ANNULUS #   19.00  Cool
> ANNULUS #   20.00  Cool
> ANNULUS #   21.00  Cool
> ANNULUS #   22.00  Cool
> ANNULUS #   23.00  Cool
> ANNULUS #   24.00  Cool
> ANNULUS #   25.00  Cool
> ANNULUS #   26.00  Cool
> ANNULUS #   27.00  Cool
> NPIJAN #
>
> ARRAY # 1 1 0 0
> RODSUB # # 0.0708 Fuel1a
> RODSUB # # 0.1417 Fuel1b
> RODSUB # # 0.2125 Fuel1c
> RODSUB # # 0.2625 Clad
>
> ARRAY # 1 6 1.773 0
> RODSUB # # 0.0708 Fuel2a1 90d Fuel2a2 270d
> RODSUB # # 0.1417 Fuel2b1 90d Fuel2b2 270d
> RODSUB # # 0.2125 Fuel2c1 90d Fuel2c2 270d
> RODSUB # # 0.2625 Clad
>
> ARRAY # 1 12 3.547 0d
> RODSUB # # 0.0708 Fuel3a1 90d Fuel3a2 270d
> RODSUB # # 0.1417 Fuel3b1 90d Fuel3b2 270d
> RODSUB # # 0.2125 Fuel3c1 90d Fuel3c2 270d
> RODSUB # # 0.2625 Clad
>
> ARRAY # 1 18 5.32 0
> RODSUB # # 0.0708 Fuel4a1 90d Fuel4a2 270d
> RODSUB # # 0.1417 Fuel4b1 90d Fuel4b2 270d
> RODSUB # # 0.2125 Fuel4c1 90d Fuel4c2 270d
> RODSUB # # 0.2625 Clad
>
> ARRAY # 1 24 7.093 0
> RODSUB # # 0.0708 Fuel5a1 90d Fuel5a2 270d
> RODSUB # # 0.1417 Fuel5b1 90d Fuel5b2 270d
> RODSUB # # 0.2125 Fuel5c1 90d Fuel5c2 270d
> RODSUB # # 0.2625 Clad
>
> ARRAY # 1 30 8.867 0
> RODSUB # # 0.0708 Fuel6a1 90d Fuel6a2 270d
> RODSUB # # 0.1417 Fuel6b1 90d Fuel6b2 270d
> RODSUB # # 0.2125 Fuel6c1 90d Fuel6c2 270d
> RODSUB # # 0.2625 Clad
>
> ARRAY # 1 36 10.64 0
> RODSUB # # 0.0708 Fuel7a1 90d Fuel7a2 270d
> RODSUB # # 0.1417 Fuel7b1 90d Fuel7b2 270d
> RODSUB # # 0.2125 Fuel7c1 90d Fuel7c2 270d
> RODSUB # # 0.2625 Clad
>
> ARRAY # 1 42 12.413 0
> RODSUB # # 0.0708 Fuel8a1 90d Fuel8a2 270d
> RODSUB # # 0.1417 Fuel8b1 90d Fuel8b2 270d
> RODSUB # # 0.2125 Fuel8c1 90d Fuel8c2 270d
```

```
> RODSUB # # 0.2625 Clad
>
> ARRAY # 1 48 14.187 0
> RODSUB # # 0.0708 Fuel9a1 90d Fuel9a2 270d
> RODSUB # # 0.1417 Fuel9b1 90d Fuel9b2 270d
> RODSUB # # 0.2125 Fuel9c1 90d Fuel9c2 270d
> RODSUB # # 0.2625 Clad
>
> ARRAY # 1 54 15.96 0
> RODSUB # # 0.0708 Fuel10a1 90d Fuel10a2 270d
> RODSUB # # 0.1417 Fuel10b1 90d Fuel10b2 270d
> RODSUB # # 0.2125 Fuel10c1 90d Fuel10c2 270d
> RODSUB # # 0.2625 Clad
>
> ARRAY # 1 60 17.733 0
> RODSUB # # 0.0708 Fuel11a1 90d Fuel11a2 270d
> RODSUB # # 0.1417 Fuel11b1 90d Fuel11b2 270d
> RODSUB # # 0.2125 Fuel11c1 90d Fuel11c2 270d
> RODSUB # # 0.2625 Clad
>
> ARRAY # 1 66 19.506 0
> RODSUB # # 0.0708 Fuel12a1 90d Fuel12a2 270d
> RODSUB # # 0.1417 Fuel12b1 90d Fuel12b2 270d
> RODSUB # # 0.2125 Fuel12c1 90d Fuel12c2 270d
> RODSUB # # 0.2625 Clad
>
> ARRAY # 1 72 21.28 0
> RODSUB # # 0.0708 Fuel13a1 90d Fuel13a2 270d
> RODSUB # # 0.1417 Fuel13b1 90d Fuel13b2 270d
> RODSUB # # 0.2125 Fuel13c1 90d Fuel13c2 270d
> RODSUB # # 0.2625 Clad
>
> ARRAY # 1 78 23.053 0
> RODSUB # # 0.0708 Fuel14a1 90d Fuel14a2 270d
> RODSUB # # 0.1417 Fuel14b1 90d Fuel14b2 270d
> RODSUB # # 0.2125 Fuel14c1 90d Fuel14c2 270d
> RODSUB # # 0.2625 Clad
>
> ARRAY # 1 78 24.826 0
> RODSUB # # 0.0708 Fuel15a1 90d Fuel15a2 270d
> RODSUB # # 0.1417 Fuel15b1 90d Fuel15b2 270d
> RODSUB # # 0.2125 Fuel15c1 90d Fuel15c2 270d
> RODSUB # # 0.2625 Clad
>
> ARRAY # 1 60 26.6 0
> RODSUB # # 0.0708 Fuel16a1 90d Fuel16a2 270d
> RODSUB # # 0.1417 Fuel16b1 90d Fuel16b2 270d
> RODSUB # # 0.2125 Fuel16c1 90d Fuel16c2 270d
> RODSUB # # 0.2625 Clad
>
> newres   4  .1  -12  0d  30d
>
> TOLERANCE 1E-6
>
> material Cool   -1  588.15 CO  C=0.035922, H1=0.041668
>
> material Moder   -1  588.15 CO  C=0.035922, H1=0.041668
>
>
> MATERIAL  Gap     -1  400.00  MO $
>       O16     = 5.2695E-05
>
> material Clad   -1  610.15 CL  Zr90=0.022043, Zr91=0.004807, Zr92=0.007348, Zr94=0.007446, Zr96=0.0012
>
> MATERIAL  Fuel1a  -1  672.15 FU  U235 =0.004712, U238=0.018929, O16=0.47399
>
> MATERIAL Fuel1b  = Fuel1a
> MATERIAL Fuel1c  = Fuel1a
> MATERIAL Fuel2a1 = Fuel1a
```

```
> MATERIAL Fuel2a2 = Fuel1a
> MATERIAL Fuel2b1 = Fuel1a
> MATERIAL Fuel2b2 = Fuel1a
> MATERIAL Fuel2c1 = Fuel1a
> MATERIAL Fuel2c2 = Fuel1a
> MATERIAL Fuel3a1 = Fuel1a
> MATERIAL Fuel3a2 = Fuel1a
> MATERIAL Fuel3b1 = Fuel1a
> MATERIAL Fuel3b2 = Fuel1a
> MATERIAL Fuel3c1 = Fuel1a
> MATERIAL Fuel3c2 = Fuel1a
> MATERIAL Fuel4a1 = Fuel1a
> MATERIAL Fuel4a2 = Fuel1a
> MATERIAL Fuel4b1 = Fuel1a
> MATERIAL Fuel4b2 = Fuel1a
> MATERIAL Fuel4c1 = Fuel1a
> MATERIAL Fuel4c2 = Fuel1a
> MATERIAL Fuel5a1 = Fuel1a
> MATERIAL Fuel5a2 = Fuel1a
> MATERIAL Fuel5b1 = Fuel1a
> MATERIAL Fuel5b2 = Fuel1a
> MATERIAL Fuel5c1 = Fuel1a
> MATERIAL Fuel5c2 = Fuel1a
> MATERIAL Fuel6a1 = Fuel1a
> MATERIAL Fuel6a2 = Fuel1a
> MATERIAL Fuel6b1 = Fuel1a
> MATERIAL Fuel6b2 = Fuel1a
> MATERIAL Fuel6c1 = Fuel1a
> MATERIAL Fuel6c2 = Fuel1a
> MATERIAL Fuel7a1 = Fuel1a
> MATERIAL Fuel7a2 = Fuel1a
> MATERIAL Fuel7b1 = Fuel1a
> MATERIAL Fuel7b2 = Fuel1a
> MATERIAL Fuel7c1 = Fuel1a
> MATERIAL Fuel7c2 = Fuel1a
> MATERIAL Fuel8a1 = Fuel1a
> MATERIAL Fuel8a2 = Fuel1a
> MATERIAL Fuel8b1 = Fuel1a
> MATERIAL Fuel8b2 = Fuel1a
> MATERIAL Fuel8c1 = Fuel1a
> MATERIAL Fuel8c2 = Fuel1a
> MATERIAL Fuel9a1 = Fuel1a
> MATERIAL Fuel9a2 = Fuel1a
> MATERIAL Fuel9b1 = Fuel1a
> MATERIAL Fuel9b2 = Fuel1a
> MATERIAL Fuel9c1 = Fuel1a
> MATERIAL Fuel9c2 = Fuel1a
> MATERIAL Fuel10a1 = Fuel1a
> MATERIAL Fuel10a2 = Fuel1a
> MATERIAL Fuel10b1 = Fuel1a
> MATERIAL Fuel10b2 = Fuel1a
> MATERIAL Fuel10c1 = Fuel1a
> MATERIAL Fuel10c2 = Fuel1a
> MATERIAL Fuel11a1 = Fuel1a
> MATERIAL Fuel11a2 = Fuel1a
> MATERIAL Fuel11b1 = Fuel1a
> MATERIAL Fuel11b2 = Fuel1a
> MATERIAL Fuel11c1 = Fuel1a
> MATERIAL Fuel11c2 = Fuel1a
> MATERIAL Fuel12a1 = Fuel1a
> MATERIAL Fuel12a2 = Fuel1a
> MATERIAL Fuel12b1 = Fuel1a
> MATERIAL Fuel12b2 = Fuel1a
> MATERIAL Fuel12c1 = Fuel1a
> MATERIAL Fuel12c2 = Fuel1a
> MATERIAL Fuel13a1 = Fuel1a
> MATERIAL Fuel13a2 = Fuel1a
> MATERIAL Fuel13b1 = Fuel1a
> MATERIAL Fuel13b2 = Fuel1a
```

```
> MATERIAL Fuel13c1 = Fuel1a
> MATERIAL Fuel13c2 = Fuel1a
> MATERIAL Fuel14a1 = Fuel1a
> MATERIAL Fuel14a2 = Fuel1a
> MATERIAL Fuel14b1 = Fuel1a
> MATERIAL Fuel14b2 = Fuel1a
> MATERIAL Fuel14c1 = Fuel1a
> MATERIAL Fuel14c2 = Fuel1a
> MATERIAL Fuel15a1 = Fuel1a
> MATERIAL Fuel15a2 = Fuel1a
> MATERIAL Fuel15b1 = Fuel1a
> MATERIAL Fuel15b2 = Fuel1a
> MATERIAL Fuel15c1 = Fuel1a
> MATERIAL Fuel15c2 = Fuel1a
> MATERIAL Fuel16a1 = Fuel1a
> MATERIAL Fuel16a2 = Fuel1a
> MATERIAL Fuel16b1 = Fuel1a
> MATERIAL Fuel16b2 = Fuel1a
> MATERIAL Fuel16c1 = Fuel1a
> MATERIAL Fuel16c2 = Fuel1a
> SUPPRESS  1 1 1 1 1  1 1 1 1 1  1 1 1  -1  1 -1
>
>
> Power 8 20000 1 1 0.0001
> BEGIN

 2018-01-10 13:04:32   Starting  2 Cross SectionsWIMS-AECL Release 3.1.2.1, 2006-03-30,         CPU Time
0.203 Secs

 2018-01-10 13:04:33   Starting  3 Resonance     WIMS-AECL Release 3.1.2.1, 2006-03-30,         CPU Time
0.859 Secs

 2018-01-10 13:04:41   Starting  4 Spectrox      WIMS-AECL Release 3.1.2.1, 2006-03-30,         CPU Time
9.094 Secs

 2018-01-10 13:04:41   Starting  5 Condensation  WIMS-AECL Release 3.1.2.1, 2006-03-30,         CPU Time
9.094 Secs

 2018-01-10 13:04:41   Starting  7 Perseus       WIMS-AECL Release 3.1.2.1, 2006-03-30,         CPU Time
9.094 Secs

 Integration time of 2D collision probabilities:      3.172 CP seconds

 Elapsed  time for modification of Pij matrix:        0.281 CP seconds

 Iteration time of neutron transport equation:        1.672 CP seconds

 MAIN TRANSPORT SOLUTION, K-INFINITY = 1.665372

 2018-01-10 13:04:46   Starting 11 Unsmear       WIMS-AECL Release 3.1.2.1, 2006-03-30,         CPU Time
14.219 Secs

 2018-01-10 13:04:46   Starting 13 Edit          WIMS-AECL Release 3.1.2.1, 2006-03-30,         CPU Time
14.219 Secs

 DEFAULT IS 24 THERMAL GROUPS BELOW 6.2500E-01 EV

>
>
> BENOIST 0
>
> BEEONE  0
>
> BUCKLING  0.005639  0.0028057
> LEAKAGE -6
>
> PRINT  1 1 1 0 0 1
>
> REACTION ALL 0
```

```
>
> PARTITION 89
>
>
> BEGIN

 EDIT DATA READ BY CHN13

 2018-01-10 13:04:46   Starting 14 Leakage       WIMS-AECL Release 3.1.2.1, 2006-03-30,         CPU Time
14.234 Secs

 LEAKAGE EDIT: RADIAL BUCKLING    5.63900E-03
               AXIAL  BUCKLING    2.80570E-03
 DIFFUSION FLUX SOLUTION GIVEN BUCKLING AND DIFFUSION COEFFICIENTS
 TRANSPORT DIFFUSION COEFFICIENTS

 89 GROUPS.....  K-INFINITY   1.66537   K-EFFECTIVE   1.20585

  2 GROUPS.....  K-INFINITY   1.66537   K-EFFECTIVE   1.20585
                                                                                                  PARTIAL
FISSION
 GROUP      DIFFUSION    ABSORPTION   REMOVAL    NU-FISSION   FLUX-EFF    FLUX-INF      SLOWING DOWN
SPECTRUM    LEAKAGE
         RADIAL   AXIAL                                                                  RADIAL    AXIAL
   1      1.130   1.130  4.0784E-03  2.6865E-02  4.5182E-03  3.4321E+01  3.0888E+01    36.506    36.506
1.0000E+00  0.0000E+00
   2      0.379   0.379  5.5937E-02  8.3130E-04  9.7882E-02  1.5375E+01  1.5511E+01     6.679     6.679
0.0000E+00  0.0000E+00

                     BUCKLING SEARCH                                    NUMBER OF
 GIVEN     RADIAL         AXIAL         TOTAL         K-EFFECTIVE      ITERATIONS
 RATIO   9.249804E-03  4.602266E-03  1.385207E-02       1.00000             8

 2018-01-10 13:04:46   Starting 15 Reactions     WIMS-AECL Release 3.1.2.1, 2006-03-30,         CPU Time
14.234 Secs

 2018-01-10 13:04:46   Starting 16 Burnup        WIMS-AECL Release 3.1.2.1, 2006-03-30,         CPU Time
14.281 Secs
 ZERO LEAKAGE K-EFFECTIVE IS    1.665372

 K-EFFECTIVE  1.66537   INTEGRATED K-EFFECTIVE  1.66537          K-INFINITY  1.66537   INTEGRATED K-
INFINITY  1.66537
 TIME =    0.000 DAYS  BURNUP =      0.000 MWD/TE.INITIAL  IRRADIATION =   0.000 N/KB  THERMAL IRRADIATION
=   0.000 N/KB
 TOTAL FLUX = 1.830805E+13  THERMAL FLUX = 6.120189E+12  GROUP FLUX = 3.021324E+10
 POWER =   22.079   MW/TE.INITIAL  FISSION RATE = 6.167438E+14  REACTION RATE = 0.000000E+00 RATING =
2.000000E+04 W/CM
 ----------------------------------------------------------------------------------------------------------
--------------------

 TIME=         1.000 DAYS   IRRADIATION=   0.002 N/KB   BURNUP=     22.077 MWD/(T.INITIAL)

 BURNUPS (MWD/T.INITIAL)
 MATERIAL       FUEL1A     FUEL1B     FUEL1C       CLAD    FUEL2A1    FUEL2A2    FUEL2B1    FUEL2B2
FUEL2C1
               FUEL2C2    FUEL3A1    FUEL3A2    FUEL3B1    FUEL3B2    FUEL3C1    FUEL3C2    FUEL4A1
FUEL4A2
               FUEL4B1    FUEL4B2    FUEL4C1    FUEL4C2    FUEL5A1    FUEL5A2    FUEL5B1    FUEL5B2
FUEL5C1
               FUEL5C2    FUEL6A1    FUEL6A2    FUEL6B1    FUEL6B2    FUEL6C1    FUEL6C2    FUEL7A1
FUEL7A2
               FUEL7B1    FUEL7B2    FUEL7C1    FUEL7C2    FUEL8A1    FUEL8A2    FUEL8B1    FUEL8B2
FUEL8C1
               FUEL8C2    FUEL9A1    FUEL9A2    FUEL9B1    FUEL9B2    FUEL9C1    FUEL9C2   FUEL10A1
FUEL10A2
              FUEL10B1   FUEL10B2   FUEL10C1   FUEL10C2   FUEL11A1   FUEL11A2   FUEL11B1   FUEL11B2
FUEL11C1
              FUEL11C2   FUEL12A1   FUEL12A2   FUEL12B1   FUEL12B2   FUEL12C1   FUEL12C2   FUEL13A1
FUEL13A2
```

```
              FUEL13B1   FUEL13B2   FUEL13C1   FUEL13C2   FUEL14A1   FUEL14A2   FUEL14B1   FUEL14B2
FUEL14C1
              FUEL14C2   FUEL15A1   FUEL15A2   FUEL15B1   FUEL15B2   FUEL15C1   FUEL15C2   FUEL16A1
FUEL16A2
              FUEL16B1   FUEL16B2   FUEL16C1   FUEL16C2
                19.860     18.811     20.856      0.000     17.975     18.673     19.405     19.959
23.480
                22.904     18.955     18.125     19.856     19.848     23.754     23.084     18.615
18.694
                19.728     20.083     23.653     23.609     18.837     18.406     19.798     20.354
23.677
                23.893     18.533     18.384     20.129     20.083     23.811     23.696     18.532
18.433
                20.094     19.933     23.709     23.664     18.787     18.468     19.818     20.151
23.544
                23.627     18.343     18.626     20.103     20.174     23.812     23.725     18.753
18.439
                20.151     19.965     23.733     23.669     18.689     18.836     20.074     19.930
23.640
                23.587     18.572     18.643     20.118     20.007     23.583     23.710     19.069
18.741
                20.265     19.987     23.756     23.852     19.189     19.200     20.497     20.231
24.059
                24.136     19.420     19.512     20.726     20.616     24.478     24.406     19.143
19.393
                20.486     20.409     24.088     24.258

 2018-01-10 13:04:46   Starting  0 Prelude       WIMS-AECL Release 3.1.2.1, 2006-03-30,         CPU Time
14.703 Secs
 WIMS COMPLETED WITH     0 SEVERE ERRORS AND     0 WARNINGS
```

APPENDIX C: MATLAB® SCRIPTS

This appendix presents the MATLAB® scripts used throughout this research to accelerate computations. The scripts included are as follows:

- mincrit.m;
- hexcircle.m; and
- htfuelchannel.m.

mincrit.m

The MATLAB® script mincrit.m estimates the minimum critical dimensions of the reactor by assuming a homogenous mixture of fuel and moderator defined by the user. An expanded description of the calculations in mincrit.m is found in Section 7.3.

```
clear
dfuel = 0.425; %Enter the diameter of the fuel portion of element in cm. This calculation
neglects cladding and assumes negligible impact on diffusion.
dclad = 0.525; %Enter the outside diameter of cladding.
pitch = 1.95; %Enter the pitch in cm. The pitch in this calculation is the length of one side of
the parallelogram lattice cell.
densf = 10.6; %Enter the density of fuel in g/cm^3.
wff = 0.1735; %Enter weight fraction U-235 in fuel. This calculation only considers U-235 as a
fuel source.
densm = 0.785; %enter density of HB-40 in g/cm^3.
af = pi*dfuel^2/4;
am = sqrt(3)*pitch^2/2 - pi*dclad^2/4;
fuelmodratio = (wff*densf*af/235.0439231)/(densm*am/6.092645161); %Atomic mass of U-235 is taken
from atom.kaeri.re.kr. Molar masss of HB-40 computed from 46.297 at% Carbon and 53.703 at%
Hydrogen.
display('nf/nm is')
display(fuelmodratio)
Z = fuelmodratio*680.8/0.125365195; %Absorption cross section for HB-40 calculated by hand from
atomic composition and corrected to 300 oC.
f = Z/(Z+1);
display('Thermal Utilization is')
display(f)
kinf = 2.07*f; %Assume fast fission factor (epsilon) is equal to 1 since neglecting U-238 as
fuel. Neglect resonance capture so that p=1. Thermal fission factor (eta) is 2.07 for U-235 for
thermal neutrons.
buckle = (kinf-1)/(46+(1-f)*6.061); %This line computes B^2 in cm^2. The calculations for
diffusion length (L), slowing down length (tao), and migration length (M) were performed by hand
for HB-40.
adjust = input('adjust buckling for heterogenous lattice')
buckle = buckle*adjust;
h = input('reactor height')
r = input('reactor radius')
if h==0 && r==0 %If zero is input for h and r the minimum critical dimensions of the core will be
computed.
    display('mincrit dimensions')
    r = sqrt(8.763/buckle);
    h = 1.85*r;
    display('radius is')
    display(r)
    display('height is')
    display(h)
elseif h>0 && r==0
    display('height prescribed')
    r = 2.405/sqrt(buckle-(pi/h)^2);
    display('radius is')
    display(r)
    display('height is')
```

```
    display(h)
else
    display('error in dimensions input')
end
```

hexcircle.m

The MATLAB® script hexcircle.m computes the number of fuel pins in the reactor and their arrangement to approximate the cylinder defined by mincrit.m. The user inputs a particular lattice pitch for the triangular lattice and the critical radius from mincrit.m. A circle of the prescribed radius is superimposed over the lattice and a matrix is produced defining the arrangement of the fuel pins in the reactor according to the MCNP input structure.

```
clear
lx = 1.95; %user defines the lattice pitch of the triangular lattice
ly = 1.95*sqrt(3)/2; %the distance between rows of pins
a = input('matrix dimension'); %user defines the dimensions of the matrix to be filled.
b = input('core radius'); %user supplies the radius calculated by mincrit.m
A = zeros(a);
c = (a+1)/2;
text = '%g';
text2 = text;
for i=1:a %script evaluates whether a matrix entry falls within the prescribed radius
    for j=1:a
        x = j-c;
        y = c-i;
        r = sqrt(lx^2*(x-.5*y)^2+ly^2*(y)^2);%the radius calculation accounts for the geometrical
transform between the matrix and the actual lattice
        if r > b
            A(i,j) = 2; %entries outside the circle receive the number 2 in the matrix
designating them as surrounding moderator
        else
            A(i,j) = 1; %entries inside the circle receive the number 1 in the matrix designating
them as fuel pins
        end
    end
end
display(A)
pins = sum(sum(A))%note: to obtain total fuel pins line 16 must be edited to "A(i,j) = 0"
for i= 1:(a-1) %the matrix is written to text file for implementation in MCNP models
    text2 = [text2,' ',text];
end
text3 = ['           ',text2,'\r\n'];
fid=fopen('hexcircle.txt', 'w');
fprintf(fid, text3, A);
fclose(fid);
```

htfuelchannel.m

The MATLAB® script htfuelchannel.m estimates the thermal hydraulics of the reactor according to Newton's Law of Cooling. The user specifies the thermal power of the reactor, the inlet and outlet temperatures of the coolant, the number of fuel pins, and the core length. The script returns the coolant mass flow rate, the maximum cladding and fuel temperatures and a plot of the temperature distributions for the fuel, the cladding, and the coolant. An expanded description of the calculation is found in Section 7.4.

```
clear
pind = 0.00525; %Fuel element diameter in m.
pins = 660; %Total fuel elements.
Cp = 2622; %Heat capacity in J/kg/K. Calculated by HB-40 correlations for a mean coolant
temperature of 315 degC.
Q = 1000000; %Total energy to be transferred in watts.
channelQ = Q/pins; %Energy transferred per channel.
```

```
Tbo = 290; %Coolant inlet temperature in degC.
Tbmax = 340; %Coolant outlet temperature in degC. Selected to be 2 degrees under atmospheric
boiling point of HB-40.
display('Phase 1: Coolant Treatment - calculating coolant flowrate')
omega = channelQ/Cp/(Tbmax-Tbo);
pump = pins*omega; %total coolant flow rate.
if pump > 20 %Flowrate should be less than 20kg/s to avoid exeedingly large pumps.
    display('WARNING: FLOWRATE HAS EXCEEDED 20KG/S')
end
display('Coolant flow rate is')
display(omega)
display('pump size is')
display(pump)
display('Phase 2: Cladding Treatment - calculating max cladding temp')
h = 5000; %Heat transfer coefficient in w/m^2/K.
l = 0.5; %Core length in m.
a = Cp*omega/h/pind/l;
Tcmax = Tbo+channelQ/h/2/pind/l*(1+sqrt(1+a^2))/a;
if Tcmax > 435
    display('WARNING: CLADDING TEMP EXCEEDS 435oC - CORE LENGTH WILL BE INCREASED')
    dl = 0.01*l;
    for i = 1:100
        l = l + dl;
        Tcmax = Tbo+channelQ/h/2/pind/l*(1+sqrt(1+a^2))/a;
        if Tcmax <= 435
            break
        end
    end
end
display('Max Clad Temp is')
display(Tcmax)
display('Reactor length is')
display(l)
display('Phase 3: Fuel Treatment')
b = 0.002125; %Fuel radius in m.
c = 0.0005; %Cladding thickness in m.
kf = 4.67; %Thermal conductivity of fuel in W/m/K at approximately 399 oC.
kc = 18.6; %Thermal conductivity of cladding in W/m/K at approximately 337 oC.
R = b/(2*kf*pi*pind*l)+c/(kc*pi*pind*l)+1/(h*pi*pind*l);
beta = pi*omega*Cp*R;
Tmmax = Tbo+channelQ*pi/2*R*(1+sqrt(1+beta^2))/beta;
display('Max Fuel Temp is')
display(Tmmax)
display('Phase 4: Plot Temp Distribution')
xbounds = l/2;
x = linspace(-xbounds,xbounds);
Tb = Tbo+channelQ/2/Cp/omega*(1+sin(pi*x/l));
Tc = Tb + channelQ/h/pind/l/2*cos(pi*x/l);
Tm = Tb + pi*channelQ/2*R*(cos(pi*x/l));
figure
plot(x,Tb,x,Tc,x,Tm)
```